Climate Change Across The Macaronesian Geographical Region, 1850 - 2100

Thomas E. Cropper

Submitted in accordance with the requirements for the degree of Doctor of Philosophy from the University of Sheffield.

Supervisors:

Professor Edward Hanna

Professor Grant R Bigg

Examiners:

Dr Andrew Sole

Dr Dennis Wheeler

University of Sheffield
Department of Geography

April 2015

Tables of Contents i
Originality Declaration, Intellectual Property and Publication Statements iv
Acknowledgements v
Abstract vi
List of Tables viii
List of Figures ix
List of Equations xi
List of Abbreviations xiii
1. Introduction 1
1.1 Global Climate Change 2
1.2 Macaronesia – Geographical & Climatological Overview 5
1.3 Weather & Climatological Features across Macaronesia 14
1.3.1 The Azores High 14
1.3.2 The North Atlantic Oscillation 16
1.3.3 The Trade Winds 17
1.3.4 The Inter-Tropical Convergence Zone 19
1.3.5 The African Continental Thermal Low and Monsoon 20
1.3.6 African Easterly Jet/Waves 20
1.3.7 Saharan Dust Advection 21
1.3.8 Coastal Upwelling 23
1.3.9 Ocean Currents 23
1.3.10 Global and Regional Oscillatory Modes 25
1.4 Climate Change & Macaronesia 28
1.5 Thesis Structure & Aim / Objectives 32
2. Methods & Data 38
2.1 Standard Methods Overview 38
2.2 Linear-Least Squares Regression 43
2.2.1 Splicing 43
2.2.2 Trend Estimation & Significance 45
2.3 Theil-Sen Slope Estimator 46
2.3.1 Mann-Kendall trend test 47
2.4 Principal Component & Empirical Orthogonal Functions 49
2.5 Homogeneity Testing 52
2.6 Cubic Tension Spline 56
2.7 Probability Analyses 57
2.7.1 Monte Carlo 57
2.7.2 Hypergeometric Distribution 58
2.8 Climatological Extreme Indices 59

2.9 Ekman Transport & Coastal Upwelling 59
2.10 Dataset Overview 60

3. The North Atlantic Oscillation 62

3.1 Existing NAO Indices 62
3.2 A Daily NAO Index 64
3.2.1 Historical SLP Data 64

3.2.1.1 Time of Observation 64
3.2.1.2 Northern NAO node (Southwest Iceland) 65
3.2.1.3 Southern NAO node (Ponta Delgada, Azores) 66
3.2.1.4 Historical Azores SLP data (1872-1961) 67
3.2.1.5 Modern Azores SLP data (1944-2013) 67
3.2.2 Completing the Azores SLP Record 70
3.2.3 Normalisation of the Daily NAO 74
3.2.4 Difference between CH14 and CHVJ15 NAO 80
3.3 NAO Effects across Macaronesia 82

3.3.1 Spatial Relationships 82
3.3.2 Temporal evolution of the NAO 90
3.4 The Trade Wind Index 94
3.5 Chapter Summary 99

4. Macaronesia Climate Evolution (1865-2012) 100

4.1 Surface Air Temperature 100
4.2 Precipitation 114
4.3 Climate Extremes 122
4.4 Macaronesian Climate Change in Context 133
4.5 Chapter Summary 137

5. The Future Of Macaronesian Climate 138

5.1 Mean Future Response 139

5.1.1 Surface air temperature 139
5.1.2 Precipitation 142
5.2 Future Response in Extreme Conditions 145

5.2.1 Temperature Extremes 145
5.2.2 Precipitation Extremes 153
5.3 Changes in Climate Indices 158

5.3.1 North Atlantic Oscillation 158
5.3.2. Trade Wind Index 159
5.4 Physical Controls on Future Changes 160
5.5 Chapter Summary 165

6. NORTHWEST AFRICAN COASTAL UPWELLING 166

6.1 Coastal Upwelling Overview 166

6.2 The Upwelling Intensification Hypothesis across northwest Africa 169

6.3 Upwelling: Increase, Decrease or No Change? 173

6.3.1 Research Approach 173
6.3.2 Data & Methods 173
6.3.3 Results 179
6.3.3.1 Seasonal Upwelling Cycle 179
6.3.3.2 Interannual Upwelling Evolution 182
6.3.3.3 Upwelling Proxy Variables 188
6.3.4 Discussion 193

6.4 The Future of Coastal Upwelling 199

6.5 Chapter Summary 201

7. SYNTHESES & OUTLOOK 203

7.1 Thesis Summary & Conclusions 203

7.1.1 Highlights 205

7.2 Future Work Direction & Suggestions 209

8. REFERENCES 212

9. APPENDICES 238

A. Supplementary Material to Chapter 1 238

B. Supplementary Material to Chapter 2 243

C. Supplementary Material to Chapter 3 251

D. Supplementary Material to Chapter 4 257

E. Supplementary Material to Chapter 5 260

F. Supplementary Material to Chapter 6 261

G. Published Material from this Thesis. 267

Originality Declaration, Intellectual Property and Publication Statements

This thesis was written entirely by the candidate, T.E. Cropper. Chapter 1-2 and 7 are originally composed for the purpose of this thesis. Approximately 80% of the work in Chapters 3-6 is taken from published articles that have their content lifted and/or paraphrased or slightly altered (in terms of structure and 'linking in', with the overall thesis design). The five published articles of direct relevance are C13, CH14, CHB14, CHVJ15 and H15.

(C13) / (Cropper, 2013) – **Cropper TE**, (2013), The weather and climate of Macaronesia: past, present and future, *Weather*, **68(11)**, 300-307

(CH14) / (Cropper and Hanna, 2014) – **Cropper TE** and Hanna E, (2014), An analysis of the climate of Macaronesia, 1865-2012, *International Journal of Climatology*, **34**, 604-622

(CHB14) / (Cropper *et al.*, 2014) – **Cropper TE**, Hanna E and Bigg, GR, (2014), Spatial and temporal seasonal trends in coastal upwelling off northwest Africa, 1981–2012, Deep-Sea Research I, **86**, 94-111

(H15) / (Hanna *et al.*, 2015) – Hanna E, **Cropper TE**, Jones PD, Scaife AA and Allan R, (2015), Recent seasonal asymmetric changes in the NAO: a marked summer decline and increased winter variability, *Early Online View at International Journal of Climatology*

(CHVJ15) / (Cropper *et al.*, 2015) – **Cropper TE**, Hanna E, Valente MA and Jónsson T, (2015), A Daily Azores-Iceland North Atlantic Oscillation Index back to 1850, *Early Online View at Geoscience Data Journal*

Literature review aspects from CH14 are included in Chapter 1. CHVJ15 and the North Atlantic Oscillation and Trade Wind Index component of CH14 make up the bulk of Chapter 3. The meteorological-station analysis in C13 and CH14 contribute to Chapter 4. Future climate evolution from C13 contributes to Chapter 5. CHB14 is essentially Chapter 6. Additionally, some analysis from H15, dealing with the historical and future evolution of the North Atlantic Oscillation (where the candidate is the second author and contributed to the analysis of the paper) is included in Chapter 3 and 5. The Digital Object Identifiers of the papers are appended as supplementary material at the end of the thesis.

Acknowledgements

I would like to thank Professor Edward Hanna for his expert guidance and advice throughout the duration of my time spent studying at Sheffield. Edward's passion, enthusiasm and patience have been inspirational and it was an honour and privilege to be supervised by Edward. I would also like to thank Professor Grant Bigg for his advice, contributions and discussions in his role as secondary supervisor.

My thanks are extended to Edward, Grant, Maria Antonia Valente and Trausti Jónsson for their contributions as co-authors on the published papers that stem from this thesis.

Additional acknowledgements are due to the editors and reviewers from the *International Journal of Climatology*, *Weather*, *Geoscience Data Journal* and *Deep Sea Research: Part One*, for their time spent reviewing and assessing the manuscripts that were submitted to their journals.

I also wish to thank my father Paul, and mother Elaine, for their unwavering support and motivation.

Funding for undertaking the PhD research is acknowledged from NERC Doctoral Training Grant (NE/I528618/1) and from the Department of Geography, University of Sheffield.

Abstract

The Macaronesian geographical zone extends from 10-40°N, 325-355°E and primarily includes the island chains of the Azores, Madeira, the Canary Islands and Cape Verde. This thesis presents a wide-ranging analysis of the physical climate and oceanography of the region back to 1850, in order to place recent climate change within a historical context. Subsequently, this thesis presents the most complete documentation of the physical climate of Macaronesia in the English language literature. One of the main outputs of this thesis is the creation of a long-term, monthly surface air temperature record for each island chain (from 1865 for the Azores and Madeira, 1885 for the Canary Islands and 1895 for Cape Verde). These temperature records exhibit generally coherent patterns of variability, and a post-1976 increase in temperature - most probably reflecting an anthropogenic climate signal - is the most ubiquitous, significant rise (or fall) in the record. Precipitation variability is also analysed, although only trends from Cape Verde are particularly significant, where a slight precipitation recovery - after the turn of the Twenty-first Century since drought conditions in the mid-late Twentieth Century - is apparent. Climatological extreme indices, based on calculations that assimilate daily temperature and precipitation data, were also analysed for the recent past (1979-2011) and point towards warmer conditions. An assessment of potential future changes in the mean state and extreme indices of climate across the islands by the end of the Twenty-first Century is provided. Warming magnitudes for the 2071-2100 period range between 0.8-3.0°C above the 1976-2005 mean temperature. Precipitation is expected to decrease across the Canary Islands and Madeira, whereas the Azores is expected to experience more extreme precipitation events and precipitation changes across Cape Verde are uncertain.

In addition to the analysis of temperature and precipitation changes, a daily North Atlantic Oscillation index extending back to 1850 using historical sea-level pressure data from the Azores was constructed. The temporal length of this newly created index exceeds the length of any previously available long-running, daily-resolution series by a hundred years and should be of great value to researchers across multiple disciplines. The spatial and temporal variability of the North Atlantic Oscillation was analysed, finding an increase in post-2004 winter variability, alongside a post-1991 negative summer trend. A novel method to characterise the strength of the Trade Winds by using data from the Azores and Cape Verde was also developed. The newly-defined Trade Wind index has been steadily increasing since 1973.

An additional analysis was a comprehensive overview and reconciliation of multiple data sources to answer the question of whether coastal upwelling has been increasing across the Canary Upwelling Ecosystem along the northwest African coastline. This analysis determined that the Bakun upwelling intensification hypothesis developed in 1990 appears to be realised in the summertime coastal upwelling indices. The North Atlantic Oscillation was discovered to be strongly related to upwelling magnitudes for all seasons except summer, in addition to exerting a strong control on temperatures and precipitation across the three northernmost Macaronesian island chains. The small-scale features affecting island climates and the large-scale modes of variability that influence the Macaronesian region are also discussed.

List of Tables

(A prefix before the table number indicates the table can be found in the appendices. Appendix A is associated with Chapter 1, Appendix B with Chapter 2 and ... Appendix F with Chapter 6).

Table A1: Basic geographical information and island information for the Azores.
Table A2: Basic geographical information and island information for Madeira.
Table A3: Basic geographical information and island information for the Canary Islands
Table A4: Basic geographical information and island information for Cape Verde.

Table B1: Precipitation-based climate extreme indices.
Table B2: Temperature-based climate extreme indices.
Table B3: Meteorological-station archives.
Table B4: Climate Indices.
Table B5: Atmospheric and oceanic reanalyses datasets.
Table B6: Observationally-based datasets.

Table 3.1: Ponta Delgada regression splicing coefficients.
Table 3.2: Azores data-source percentages.
Table 3.3: NAO correlations.
Table C1: List of different NAO indices.
Table C2: Daily Ponta Delgada data source.

Table 4.1: Macaronesia monthly temperature data.
Table 4.2 and 4.4: Monthly temperature statistics.
Table 4.3 and 4.5: Seasonal and Annual temperature trend rates for various periods.
Table 4.6: Macaronesia monthly precipitation data.
Table 4.7: Monthly precipitation statistics.
Table 4.8: ETCCDI indices basic description and abbreviations.
Table 4.9: Annual trends in temperature and precipitation extremes.
Table 4.10: Temperature rend rates across comparable island regions.
Table D1: Seasonal precipitation statistics, trends and NAO-correlations.

Table 6.1: Homogeneity corrections applied to wind-speed data.
Table 6.2: List of climate indices used in Chapter 6.
Table 6.3: Seasonal trend rates in upwelling magnitudes.
Table F1: List of data sources used to create upwelling indices in Chapter 6.
Table F2-5: Seasonal correlation coefficients between climate and upwelling indices.

List of Figures

(A prefix before the figure number indicates the figure can be found in the appendices)

Figure 1.1: A map of the Macaronesia Islands
Figure 1.2: Example of a gridded dataset
Figure 1.3 – 1.5: The seasonal climatology of temperature, wind and precipitation
Figure 1.6: Winter and summer SLP climatology
Figure 1.7: Climatic impacts of the NAO
Figure 1.8: Trade Wind inversion example
Figure 1.9: West African Monsoon and African Easterly Jet
Figure 1.10: Atlantic Multidecadal Oscillation
Figure 1.11: Early data availability from CLIWOC and ICOADS

Figure 2.1: Regression splicing approach
Figure 2.2: TS and OLS comparison
Figure 2.3: EOF analysis example
Figure 2.4: Illustration of different smoothing methods
Figure B1: R-code for tension spline

Figure 3.1: NAO station locations
Figure 3.2: Daily data availability from the Azores
Figure 3.3: Contribution of data source to the final Azores record
Figure 3.4: Homogenised Azores SLP record.
Figure 3.5: Tension spline illustration
Figure 3.6: Monthly average of the normalised daily NAO
Figure 3.7: Monthly average of the natural daily NAO
Figure 3.8: Distribution of the winter NAO during certain periods.
Figure 3.9 – 3.11: Monthly correlation of the NAO with SAT, Precipitation and Z500
Figure 3.12: DJF and JJA correlation of the NAO with SAT and Precipitation
Figure 3.13: Temporal variability in the NAO correlation
Figure 3.14 – 3.15: Change in the December and DJF running-standard deviation
Figure 3.16: December daily-NAO variability trend.
Figure 3.17: Composite wind-speed maps
Figure 3.18: The Trade Wind Index
Figure 3.19: Ocean Heat Content
Figure 3.20: DJF and JJA correlations of climate variables with the TWI.
Figure C1: Maximum and minimum SLP values from the ERA-I reanalysis

Figure 4.1: Available Macaronesian raw temperature data
Figure 4.2: Location of meteorological-stations
Figure 4.3: Stratospheric Aerosol data
Figure 4.4 – 4.5: Long-term Macaronesia temperature records
Figure 4.6 – 4.7: Trends in Macaronesia temperature
Figure 4.8 – 4.9: Macaronesia precipitation evolution and trends
Figure 4.10 – 4.16: Evolution of ETCCDI-extreme indices across the Macaronesian region
Figure 4.17: Precipitation from Sal and the West African Monsoon Index

Figure 5.1: Future temperature evolution across Macaronesia
Figure 5.2 – 5.4: DJF and JJA precipitation evolution across Macaronesia
Figure 5.5 – 5.9: Future evolution of ETCCDI-extreme indices across Macaronesia
Figure 5.10: The difference between RCP2.6/8.5 and present day WSDI conditions
Figure 5.11: Difference between the historical and future CMIP5 precipitation indices
Figure 5.12. Difference between the CMIP5 and ERA-I precipitation indices
Figure 5.13. Station, reanalyses and CMIP5 annual precipitation cycle
Figure 5.14: The future evolution of the North Atlantic Oscillation
Figure 5.15: The future evolution of the Trade Wind Index
Figure 5.16: Example of variable future model evolution across Macaronesia

Figure 6.1: Geographical location of major coastal upwelling zones.
Figure 6.2: northwest Africa region, meteorological-station locations and upwelling zones
Figure 6.3 – 6.4: Monthly climatology of coastal upwelling
Figure 6.5: Temporal evolution of summer coastal upwelling
Figure 6.6: Spatial pattern of summer meridional wind-speed trends
Figure 6.7: Winter upwelling time series along with the NAO
Figure 6.8: Temporal evolution of wind-speed from coastal meteorological-stations
Figure 6.9: The spatial regression of the TWI and its temporal evolution
Figure 6.10: Trends in summer vertical water velocity from ocean reanalysis
Figure 6.11: Trends in summer SSH from ocean reanalysis
Figure 6.12: Comparison of satellite-derived and ship-derived wind-speeds
Figure 6.13: A modified upwelling intensification hypothesis for the NW Africa region
Figure 6.14: The potential future of coastal upwelling
Figure F1: Coastal upwelling and wind-stress curl induced upwelling difference.

List of Equations

2.1.1 – Arithmetic mean....38
2.1.2 – Standard Deviation....39
2.1.3 – Normalisation....39
2.1.4 – Covariance....39
2.1.5 – Pearson's Correlation Coefficient....39
2.1.6 – Spearman's Rank Correlation. 40
2.1.7 – Cross(Auto)-Correlation. 40
2.1.8 – Ordinary Least Squares Linear Regression (OLS)....41
2.1.9 – Residuals of the best fit line....41
2.1.10 – Sum of residuals....41
2.1.11 – T-test for significance of the Correlation Coefficient....42
2.1.12 – Standard error of the trend line....42
2.1.13 – T-test for significance of the trend line....42

2.2.1 – Adjusted Degrees of Freedom....45
2.2.2 – Number of data per effective Degrees of Freedom....45
2.2.3 – Adjusted Standard Error....45
2.2.4 – Modified Eq. 2.2.2 under ARIMA(1,1) process....46
2.2.5 – Modified autocorrelation under ARIMA(1,1) process....46

2.3.1 – Theil-Sen Slope Estimator....46
2.3.2 – Number of slopes....46
2.3.3 – Intercept of slope....46
2.3.4 – 2.3.5 – Mann-Kendall S statistic....48
2.3.6 – Variance of the S statistic....48
2.3.7 – Standardised Z score (MK Test) 48

2.4.1 – Empirical Orthogonal Function....49
2.4.2 – S-Mode Matrix....49
2.4.3 – Covariance Matrix....49
2.4.4 – Eigen element calculation....49

2.5.1 – 2.5.3 – SNHT Test....54
2.5.4 – Pettitt Test....54
2.5.5 – 2.5.6 – Buishand Range Test....54/55
2.5.7 – 2.5.11 – Penalised Maximal F-Test....55/56

2.7.1 – Hypergeometric Distribution.....58

2.8 – ETCCDI Extreme Indices (given in Table B1 and B2) 244-246

2.9.1 – Wind-stress (from wind-speed) 59
2.9.2 – Ekman Transport.....59
2.9.3 – Upwelling Index (UI^{W}) 60
2.9.4 – Upwelling Index ($UI^{\Delta SST}$) 60

List of Abbreviations

°C – Celsius (also given in degrees Celsius per decade as °C dec^{-1})

20CR – Twentieth Century reanalysis v2

AA – Arctic Amplification

ADVICE – Annual to Decadal Variability in Climate in Europe

AEJ/W – African Easterly Jet/Waves

AGW – Anthropogenic Global Warming

AMO – Atlantic Multidecadal Oscillation

AR5 – Fifth Assessment Report of the Intergovernmental Panel on Climate Change

AVISO – Archiving, Validation and Interpretation of Satellite Oceanographic Data

BP – Before Present

C13 – Cropper (2013) *Weather* article

CFSR – Climate Forecast System reanalysis

CH14 – Cropper and Hanna (2014) *International Journal of Climatology* article

CHB14 – Cropper *et al.* (2014) *Deep Sea Research I* article

CHVJ15 – Cropper *et al.* (2015) *Geoscience Data Journal* article

CLIWOC – Climatological Database for the Worlds' Oceans

CMIP5 – Coupled Model Intercomparison Project Phase 5

CO_2 – Carbon Dioxide

CPC – Climate Prediction Centre

CRU – Climatic Research Unit

CUE – Canary Upwelling Ecosystem

DTR – Diurnal Temperature Range

DJF – winter (December-February), this applies to months in general, i.e. JJASO would indicate the months June-October

EA – East Atlantic Pattern

ECA&D – European Climate Assessment and Dataset project

EMSLP– European Mean Sea Level Pressure dataset

ENSO – El Niño Southern Oscillation

EOF – Empirical Orthogonal Function

ERA-CLIM(2) – European Reanalysis of Global Climate Observations project 1/2

ERA-I – Era Interim reanalysis

ERA-SIGN – Signatures of Environmental Change in the Observations of the Geophysical Institutes

ETCCDI – Expert Team on Climate Change Detection and Indices

- CDD – Consecutive Dry Days
- CSDI – Cold Spell Duration Indicator
- CWD – Consecutive Wet Days

R1mm – Days when precipitation is greater than 1 mm

R10mm – Days when precipitation is greater than 10 mm

R20mm – Days when precipitation is greater than 20 mm

R95p / R99p – Precipitation amount that exceeds the 95^{th}/99^{th} percentile

R_X1Day / R_X5Day – Maximum 1 Day / consecutive 5 day precipitation

SDII – Simple Precipitation Intensity Index

TN_N – Minimum value of daily minimum temperature

TN_X – Minimum value of daily maximum temperature

TN10p – Percentage of days when TN is below the 10^{th} percentile

TN90p – Percentage of days when TN is above the 90^{th} percentile

TX_N – Maximum value of daily minimum temperature

TX_X – Maximum value of daily maximum temperature

TX10p – Percentage of days when TX is below the 10^{th} percentile

TX90p – Percentage of days when TX is above the 90^{th} percentile

WSDI – Warm Spell Duration Indicator

GISS – Goddard Institute for Space Sciences

GCM – Global Climate Model

GHCN – Global Historical Climatology Network

GMT – Greenwich Mean Time

GODAS – Global Ocean Data Assimilation System

GSOD – Global Summary of the Day database

H15 – Hanna et al. (2015) *International Journal of Climatology* article

HadISST – Met Office Hadley Centre SST dataset v1

hPa – Hectopascal

ICOADS – International Comprehensive Ocean-Atmosphere dataset v2.5

ISD – Integrated Surface Data archive

IPCC – Intergovernmental Panel on Climate Change

ITCZ – Inter-Tropical Convergence Zone

JA – high summer

JJA – summer

K – Kelvin

km – kilometre (m = metre, mm = millimetre)

LOESS – Locally-Weighted Regression

MAM – spring (March-May)

MERRA – Modern-Era Retrospective Analysis for Research and Applications reanalysis

MK – Mann Kendall Trend Test

NAO – North Atlantic Oscillation

NCEP-DOE – National Centre for Environmental Prediction reanalysis v2

NCEP-NCAR – National Centre for Environmental Prediction reanalysis v1

OHC – Ocean Heat Content

OISST – Reynolds Satellite SST Dataset

OLS – Ordinary Least Squares Linear Regression

ORSA4 – Operational Ocean System reanalysis 4

PC – Principal Component

PD – Ponta Delgada (always 'Ponta Delgada' in the main text, but PD in tables)

PFEL – Pacific Fisheries Environment Laboratory

PMF – Penalised Maximum F-Test

QBO – Quasi-Biennial Oscillation

RCP – Representative Concentration Pathway

SAT – Surface Air Temperature

SD – Standard Deviation

SeaWinds – Scatterometer-derived winds

SIGN – Signatures of Environmental Change in the Observations of the Geophysical Institutes project

SLP – Sea Level Pressure

SNHT – Standard Normal Homogeneity Test

SODA – Simple Ocean Data Analysis v2.1.6

SON – autumn

SSH – Sea Surface Height

SST(s) – Sea Surface Temperature(s)

STP – Station Pressure

TS – Theil-Sen Regression

TWI – Trade Wind Index

UI^{W} – Upwelling Index (Wind)

$UI^{\Delta SST}$ – Upwelling Index (Sea Surface Temperature)

UTC – Coordinated Universal Time

VWCV – Vertical Water Column Velocity

WAM – West African Monsoon

WASWind – Wave and Anemometer based Sea-Surface Wind

z – local time

1. INTRODUCTION

The layout of this thesis is as follows:

Chapter 1 provides a general overview and introduction to climate change and the Macaronesian geographical zone, around which the thesis is based. The major objectives of this thesis and the hypotheses being tested are introduced. **Chapter 2** outlines the various methodologies applied throughout the rest of the thesis, which are referred back to during the later chapters to conserve the flow of the thesis. **Chapter 3** deals mainly with the recovery and treatment of surface pressure observations across the Macaronesian Islands and their usage in the construction of an extended daily North Atlantic Oscillation index, which is of strong value in itself but used here to illustrate its influence across much of the Macaronesian region. The evolution of the North Atlantic Oscillation Index itself is also analysed, alongside the creation of a Trade Wind index, based on the difference between sea-level pressure values between the Azores and Cape Verde. **Chapter 4** deals with the analysis of temperature and precipitation time series from the various Macaronesian Islands. This includes the initial creation of the time series, by intuitive splicing together of long-term records, followed by an analysis of the temporal evolution of their series. Additional records from atmospheric reanalyses are analysed to reaffirm the initial findings. **Chapter 5** analyses the potential future evolution of Macaronesian climate up to 2100 using the same suite of climate models as the recent Fifth Assessment Report of the Intergovernmental Panel on Climate Change. **Chapter 6** slightly diverges from the main analyses undertaken in Chapters 4-5, and focuses on the oceanic climate evolution across the region, with a specific focus on the changes in coastal upwelling along the northwest African coastline. **Chapter 7** concludes the thesis and summarises the main scientific findings and the suggested future research direction that could be pursued by those interested in the climate of the region.

The layout of this chapter is as follows:

The objective of this chapter is to provide a broad introduction of global climate change (1.1), a basic description of the Macaronesian geographical region and its seasonal regional climate (1.2), an overview of the important climatological features and regimes that affect the Macaronesian region (1.3) and a summary of the published literature regarding climate change across Macaronesia (1.4). The main research questions that are addressed in this thesis are then examined, along with a structure of the rest of the thesis (1.5).

1.1 Global Climate Change

To begin this chapter, and thesis in general, it is prudent to define exactly what is meant by the terms 'Climate', 'Climate System' and 'Climate Change' from the Fifth Assessment Report (AR5) of Working Group One of the Intergovernmental Panel on Climate Change (IPCC) (Planton, 2013, p.1450-1451).

Climate – "*Climate in a narrow sense is usually defined as the average weather, or more rigorously, as the statistical description in terms of the mean and variability of relevant quantities over a period of time ranging from months to thousands or millions of years. The classical period for averaging these variables is 30 years, as defined by the World Meteorological Organization. The relevant quantities are most often surface variables such as temperature, precipitation and wind. Climate in a wider sense is the state, including a statistical description, of the climate system.*"

Climate System – "*The climate system is the highly complex system consisting of five major components: the atmosphere, the hydrosphere, the cryosphere, the lithosphere and the biosphere, and the interactions between them. The climate system evolves in time under the influence of its own internal dynamics and because of external forcings such as volcanic eruptions, solar variations and anthropogenic forcings such as the changing composition of the atmosphere and land use change.*"

Climate Change – "*Climate change refers to a change in the state of the climate that can be identified (e.g., by using statistical tests) by changes in the mean and/or the variability of its properties, and that persists for an extended period, typically decades or longer. Climate change may be due to natural internal processes or external forcings such as modulations of the solar cycles, volcanic eruptions and persistent anthropogenic changes in the composition of the atmosphere or in land use.*"

Throughout the history of the Earth, its climate and the climate system have undergone periods of dramatic climate changes and periods of lasting stability. The most commonly used metric in defining climate is the global average surface air temperature (SAT). This is due to the availability of instrumental records throughout the past two centuries and the comparative ease of retrieving SAT estimates (relative to other climate variables) from climate proxy records, which has enabled the extension of the SAT record over millions of years back in time (Hansen *et al.*, 2013a). The average annual global temperature across land and ocean based on instrumental records for the 1961-1990 base period is 14.0°C (Jones *et al.*, 1999a). Over the past 800,000 years, the global mean SAT has been estimated to have undergone fluctuations on the order of approximately -5°C

to +1.5°C, paced by the ~100,000 year glacial-interglacial 'saw-tooth' cycle that is currently recognised as being externally forced by changes in incoming solar radiation due to variations in the orbit of the earth around the sun (Masson-Delmotte *et al.*, 2013). The deviations in solar radiation are then amplified by internal climate system feedbacks; such as variations in oceanic heat transport and a change in the planetary albedo related (primarily) to variations in the sizes of large-scale ice sheets (Hansen *et al.*, 2013a; Abe-Ouchi *et al.*, 2013). The past ~11,700 years, otherwise known as the Holocene, are considered to be a relatively stable, interglacial period marked by a warm phase (~0.4°C above the 14.0°C 1961-1990 average) lasting between 9,500-5,500 years Before Present (BP, where 'present' is 1st January 1950) which gave way to a cooling trend of -0.7°C over the period ~5,500 to ~50 years BP (Marcott *et al.*, 2013). Most of the signal of this recent global decline comes from the Northern Hemisphere extra-tropical and polar regions (30-90°N), and is proposed to be due to a combination of reduced high-latitude summer solar insolation (Marcott *et al.*, 2013) and a reduction in northward heat transport by the Atlantic Meridional Overturning Circulation (Hoogakker *et al.*, 2011).

The above brief account of SAT changes highlights how, on geological timescales, the dominance of external (solar) forcing and internal dynamics have been crucial in pacing the slow transitions between climate regimes across timescales of 10^3-10^5 years. Throughout the Twentieth Century, the influence of anthropogenic forcing has emerged as the newly dominant and rapid forcer of global SAT changes. The IPCC AR5 reports that the global mean annual SAT has risen by 0.72 (0.49-0.89)°C over the period 1951–2012 and it is *extremely likely* (95-100% probability) that more than half of the observed temperature increase is due to anthropogenic activities (Stocker *et al.*, 2013). The fact that the ~5,400 year duration of the -0.7°C cooling since the mid-Holocene has been essentially cancelled out by the ~0.72°C of warming in just 100 years (a warming rate over 50 times faster than the late-Holocene cooling rate) has raised concerns that continued anthropogenic climate forcing will lead to global temperatures higher than the "safe[1]" limit of 2°C greater than pre-industrial times (Hansen *et al.*, 2013b, p.2).

Naturally, whilst global mean SAT on its own is an invaluable metric for assessing medium-long term global climate change, the regional responses to external and internal climate forcing will not be uniform across the Earth. Changes in the mean temperature of the planet can (either directly or via interactive feedbacks with different aspects of the

[1] The 2°C 'safe' limit is a commonly agreed value in science and policy that is deemed a maximum acceptable limit for avoiding the effects of dangerous climate change. Vautard *et al.* (2014) describe the evolution of the international agreement on limiting anthropogenic emissions to ensure that global SAT stays below the 2°C warming target since it was initially advocated at the *Scenario to Deduct CO_2 Reduction Targets and Implementation Strategies* conference in Berlin in 1995, based on the scientific evidence presented in the second IPCC Assessment Report.

climate system) drive changes in the (1) hydrological cycle, (2) atmospheric composition (and radiative forcing), (3) atmospheric circulation, (4) ocean circulation, (5) the physical global surface area and (6) changes in the frequency, intensity and duration of climate extremes - defined not just as significant weather events, such as hurricanes, heat waves and droughts, but also as the changes in predefined climate extreme indices that measure the shifts in the characteristics of the spatial and temporal evolution of daily temperature and precipitation (Hartmann *et al.*, 2013 and references therein). Coincidentally, whilst anthropogenic climate forcing may be the largest contributor to the warming trend in the global climate system over the past 60 years, natural oscillations and modes of internal variability remain essentially important in determining regional climate variability, especially across monthly-decadal timescales, where local or regional trends can diverge from the global mean climate trend.

A prime example of one of these natural oscillatory teleconnections[2] is the leading mode of atmospheric variability across the extra-tropical North Atlantic Ocean, which is the North Atlantic Oscillation (NAO, Hurrell, 1995; Jones *et al.*, 1997). The NAO is a pattern where changes in the nature of the oscillation re-distribute energy (via mid-latitude storm systems) across preferred locations, which can result in warming/cooling and wetting/drying across different regions, influencing regional climates but without significantly affecting global average temperatures. The leading coupled atmosphere-ocean interaction across the Pacific Ocean, the El Niño Southern Oscillation (ENSO), is a mode of variability that determines the amount of heat uptake/release from the ocean to the atmosphere. Given the large area across which the process occurs, the phase of the ENSO is sufficient to significantly impact not only regional, but global temperatures on monthly-decadal time scales (as the energy is not being redistributed across just the atmosphere, but between the atmosphere and the ocean). This has led to the ENSO, along with solar variability and volcanic aerosol amounts, being included in studies that attempt to separate natural and anthropogenic global temperature trends (Lean and Rind, 2008; Foster and Rahmstorf, 2011). Several important teleconnections have been identified across all regions of the Earth and knowledge of how these have changed in the past and are likely to change under anthropogenic forcing in the future, is essential in determining the potential regional impacts of climate change.

[2] 'Teleconnection', is defined by the Climate Prediction Centre as "a recurring and persistent, large-scale pattern of pressure and circulation anomalies that spans vast geographical areas" and by the American Meteorological Society as: (1) "a linkage between weather changes occurring in widely separated regions of the globe" and (2) "a significant positive or negative correlation in the fluctuations of a field at widely separated points". The temporal scales and persistence of teleconnection patterns can vary from weeks to years.

1.2 Macaronesia – Geographical & Climatological Overview

Macaronesia is the name given to the geographical region occupied by the volcanic island chains of the Azores, Madeira, the Savage Islands, the Canary Islands and Cape Verde throughout the eastern North Atlantic Ocean (10-40°N 5-35°W, Figure 1.1). The region has a strong biological affinity with the (near-)coastal regions of western Iberia and northwest Africa (Fernández-Palacios *et al.*, 2011), and as such, 'Macaronesia' arguably also encompasses these regions. The distance between the northern and southernmost archipelagos of the Azores and Cape Verde is approximately 2500 kilometres (km) and the eastern Canary Island of Fuerteventura is the island closest to a continental landmass (~100 km from northwest Africa), with Flores (Azores) the furthest away (~1850 km from Iberia). Islands within their respective archipelagos can be as close as five km or as far as 600 km apart, although the closest neighbouring island is most typically ~100 km apart. There are nine, three, seven and ten major islands comprising the Azores, Madeira, Canary Islands and Cape Verde respectively (along with numerous minor islands, seamounts and guyots). Tables A1-4 provide an overview of the basic geography of the islands. The Savage Islands are without any form of openly available long-term meteorological observations, so are excluded as an entity within Macaronesia hereafter.

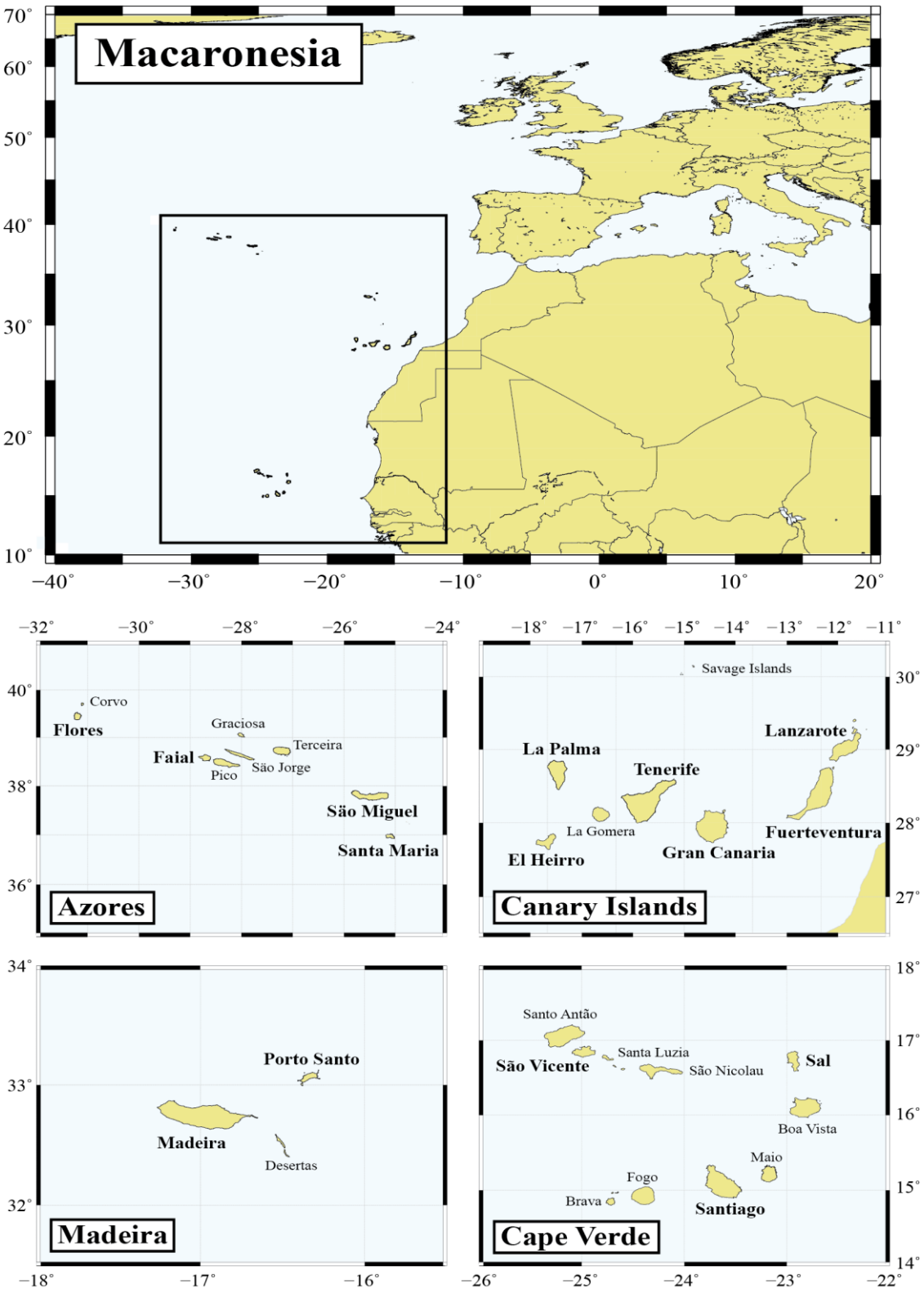

Figure 1.1. The Macaronesian geographical region and its location within the North Atlantic Ocean (Behrman Equal Area projection). Enhanced panels depicting the island chains of the Azores, Madeira, Canary Islands and Cape Verde are shown. Emboldened Island names highlight locations from where data are (freely and publically) available from at least one meteorological-station.

As illustrated in Figure 1.1 and Table A1, the Macaronesian region is a collection of mountainous islands ranging in altitude from 387 to 3,718 m. The four main factors that exert a significant control on mountain climatology are (Barry, 1992):

1. Altitude
2. Continentality
3. Latitude
4. Topography

An increase in altitude is generally associated with reduced air density, vapour pressure and temperatures, and an increase in incoming solar radiation. The relationship between altitude, wind-speed and precipitation is much less direct, but a gross approximation is that for regions in the mid-latitude westerly belt, wind-speed increases with altitude and decreases with altitude across the Trade Wind belt (Barry, 2008). The effect of altitude or rather more specifically, orography, serves to enhance precipitation on the windward side of mountains by forcing the uplift of air parcels, which undergo adiabatic cooling, condensation and then precipitation. The orographic uplift mechanism gives rise to significantly different climates on the windward (wetter) and leeward (drier) slopes of mountainous islands.

Continentality serves to modify the diurnal temperature range (DTR), cloud cover and precipitation regimes. Across Macaronesia, the greater heat capacity of the ocean relative to land reduces the DTR relative to continental environments. Due to their maritime position, the climate of the Macaronesian Islands have historically been thought of as very stable. Such 'stability' has been recognised for over 2000 years. The scholar Plutarch (46–120 AD), in his biography of notable Grecian individuals (Thayer, 2014) remarkably makes the first climatic observations of Macaronesia:

"These (islands) are two in number, separated by a very narrow strait; they are ten thousand furlongs **[just over 2000km – probably an exaggeration]** *distant from Africa...They enjoy moderate rains at long intervals, and winds which for the most part are soft and precipitate dews... Moreover, an air that is salubrious, owing to the climate and the moderate changes in the seasons, prevails on the islands. For the north and east winds which blow out from our part of the world plunge into fathomless space, and, owing to the distance, dissipate themselves and lose their power before they reach the islands; while the south and west winds that envelope the islands sometimes bring in their train soft and intermittent showers, but for the most part cool them with moist breezes".*

From his description, which would still be adequate today, it is most likely that the two islands which Plutarch refers to are Madeira and Porto Santo. This is because Madeira

has two major islands, in close proximity (~50 km), the Azores are believed to be uninhabited until the Fifteenth Century (Santos *et al.*, 2003) and it would be likely that historical discovery of the Canary Islands would not have been limited to two islands, although the description could potentially refer to Lanzarote and Fuerteventura. Interestingly, the difference between the prevailing southwesterly winds and northeasterly trades and their respective impacts on precipitation were well recognised, as well as the moderate changes in the seasons, reflecting the oceanic influence.

Given a continental and oceanic cloud, precipitation is (broadly) more likely to occur from the oceanic cloud, as there is greater moisture availability and there are typically less cloud-condensation nuclei over oceanic regions compared to land, so water droplets that form are fewer but larger (therefore more likely to precipitate and less likely to evaporate). Latitude modifies the seasonal solar radiation, length of day and temperature, and can significantly influence the mean weather and climate conditions that prevail across the islands, which are discussed later on in this section and Section 1.3. Topography can strongly influence island climatology by controlling spatial patterns of incident solar radiation, temperature regimes and precipitation as a result of general spatial heterogeneity, slope and aspect, and interaction of the larger scale weather regimes with these features. For example, the position and the dimensions of the orographic barrier and the average prevailing wind direction will likely be the major control on the island spatial precipitation pattern (Barry, 1992). There is a significantly greater annual temperature (range) and DTR at higher altitude locations than at locations close to sea level, where the maritime influence dominates. An exception to this could be within valley environments, where the DTR can be 2-3 times greater than surrounding regions (Barry, 2008).

The inter- and intra-island climatology across the archipelagos can be markedly similar or different dependent on several of the above factors. The most consistent constraint on intra-archipelago precipitation variability is the altitude of the island, with 'flatter' islands in the archipelagos (Graciosa and Santa Maria, Porto Santo and Fuerteventura and Lanzarote from the Azores, Madeira and Canary Islands respectively) predominantly drier than the 'higher' counterparts (C13). Latitude is the strongest control on inter-archipelago variability, with a general pattern of lower temperatures and greater precipitation across the higher latitude islands of Macaronesia (>35°N) and progressively warmer / drier conditions for the low-latitude islands (12-34°N). Topography regulates the topo- and micro- climatology of the islands, and the maritime stability persists across all four archipelagos. A strong example of the topographic climate influence can be taken from Tenerife. The island displays characteristics associated with five climatic zones as per the Köppen climate classifications (Peel *et al.*, 2007), which range from 'Boreal' at the peak of Mount Teide to 'Hot Desert' along the southern low altitude region of the

island, whereas the northern flanks are classed as 'Temperate, Dry summer' (Climate Atlas, 2012). Such changes purely as a function of latitude could conceivably occur over a range of 30-60°, highlighting the significance of the altitude effect. Coincidentally, the flatter Canary Islands, Fuerteventura and Lanzarote, (a few hundred km eastward) are purely 'Hot Desert' climates.

Without analysing any meteorological-station data from the islands, it is possible to derive how the regional climate changes throughout the seasons, across the region, by use of large-scale atmosphere-ocean observational and reanalysis products. Such products are provided in a gridded format, where the atmosphere and ocean are split into x, y, z (longitude, latitude, level) grid-boxes, with one data point at each time step (Figure 1.2). The time step can vary between datasets (usually any time between minutes to a year) as can the resolution (current global observational/reanalysis datasets vary in size between 0.3° and 2.5° grids). For example, the International Comprehensive Ocean-Atmosphere Dataset v2.5 (ICOADS, Woodruff *et al.*, 2011) offers surface marine data on a 1° grid resolution at a monthly time scale since 1960. For each 1° grid-box, any observations that were made (from ships, buoys and other platforms) during each time step are then assimilated and contribute to the value of the grid-box. Multiple observations for a specific grid-box at a specific time step are common (and are advantageous in eliminating bias due to local effects), as is the case of only one observation per grid-box per time step and also, unfortunately, no observations for a grid-box for long periods of time, particularly further back in time, and for the present day in data-sparse regions like Africa and Antarctica (Brohan *et al.*, 2006; Compo *et al.*, 2011). Purely 'observational' datasets will either leave data sparse regions empty (Woodruff *et al.*, 2011; Morice *et al.*, 2012) or interpolate the gaps using a variety of statistical methods (Hansen *et al.*, 2010; Cowtan and Way, 2014).

Atmospheric and oceanic reanalyses combine assimilated observational data with a forecast model that advances the state of the atmosphere and/or ocean a few time steps forward. At each time step, the previous forecast and current observations are assimilated and the cycle repeated (Dee *et al.*, 2011). Such a process has the advantage of, by use of the physically constrained equations in the forecast model, being able to interpolate over large distances and calculate values for unobserved parameters from local observational data, providing globally complete datasets of numerous climatological variables. Observationally-based and reanalysis data sets, in addition to meteorological station data, form the bulk of the data analysed in this thesis.

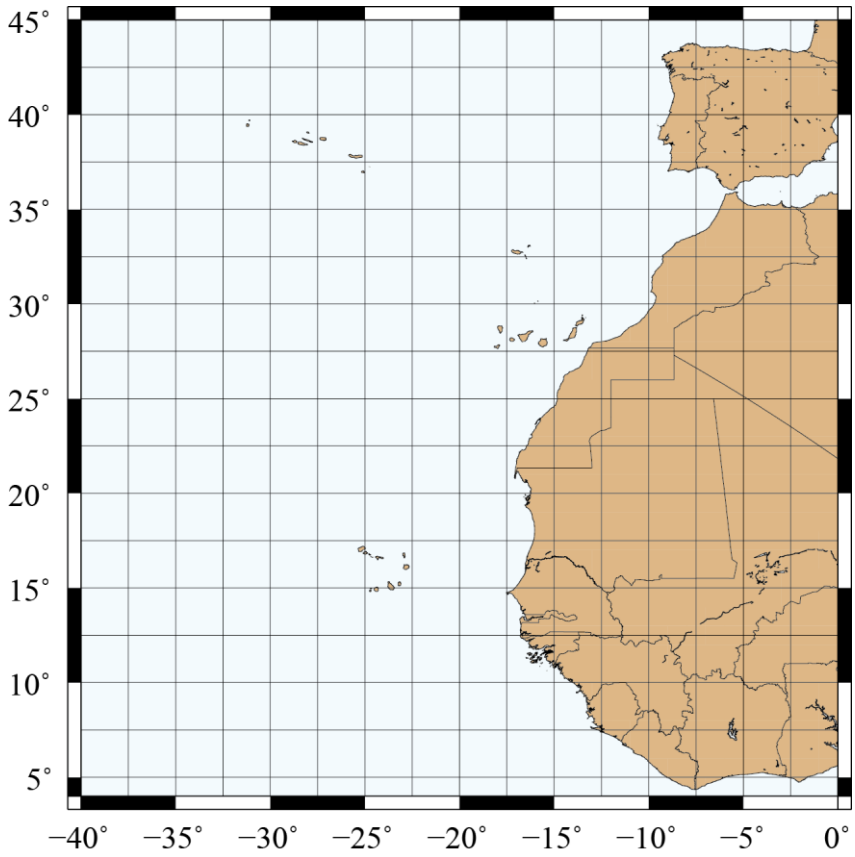

Figure 1.2. Using the Macaronesian region as an example, a regularly spaced (Cylindrical Equidistant projection) latitude by longitude grid at resolution 2.5° is shown. Throughout this thesis, unless otherwise stated, this is the projection that will be adopted for spatial maps.

For Macaronesia, gridded data at a scale of ~0.75° are sufficient to get roughly 'one island per grid-box', but this depends on the exact structure of the gridded dataset (for example, the Canary Islands are approximately centred on 28.5°N, placing them in the middle or at the boundary of a grid-box dependent on the dataset). Irrespective of this, a simple analysis of near-surface variables from a gridded atmospheric dataset allows for a basic analysis of the seasonal evolution of Macaronesian regional climate. Figures 1.3-5 display the seasonal climatology of 2 m SAT, precipitation and wind direction and magnitude from the ERA-Interim reanalysis (ERA-I, Dee *et al.*, 2011). Seasons are split accordingly into winter (December, January and February: DJF), spring (MAM), summer (JJA) and autumn (SON). Climatology is the mean of the selected variable across each season: in this case, the climatology is for the period 1979-2012, so the DJF SAT climatology is based on the seasonal value of SAT during 1979, 1980...2012.

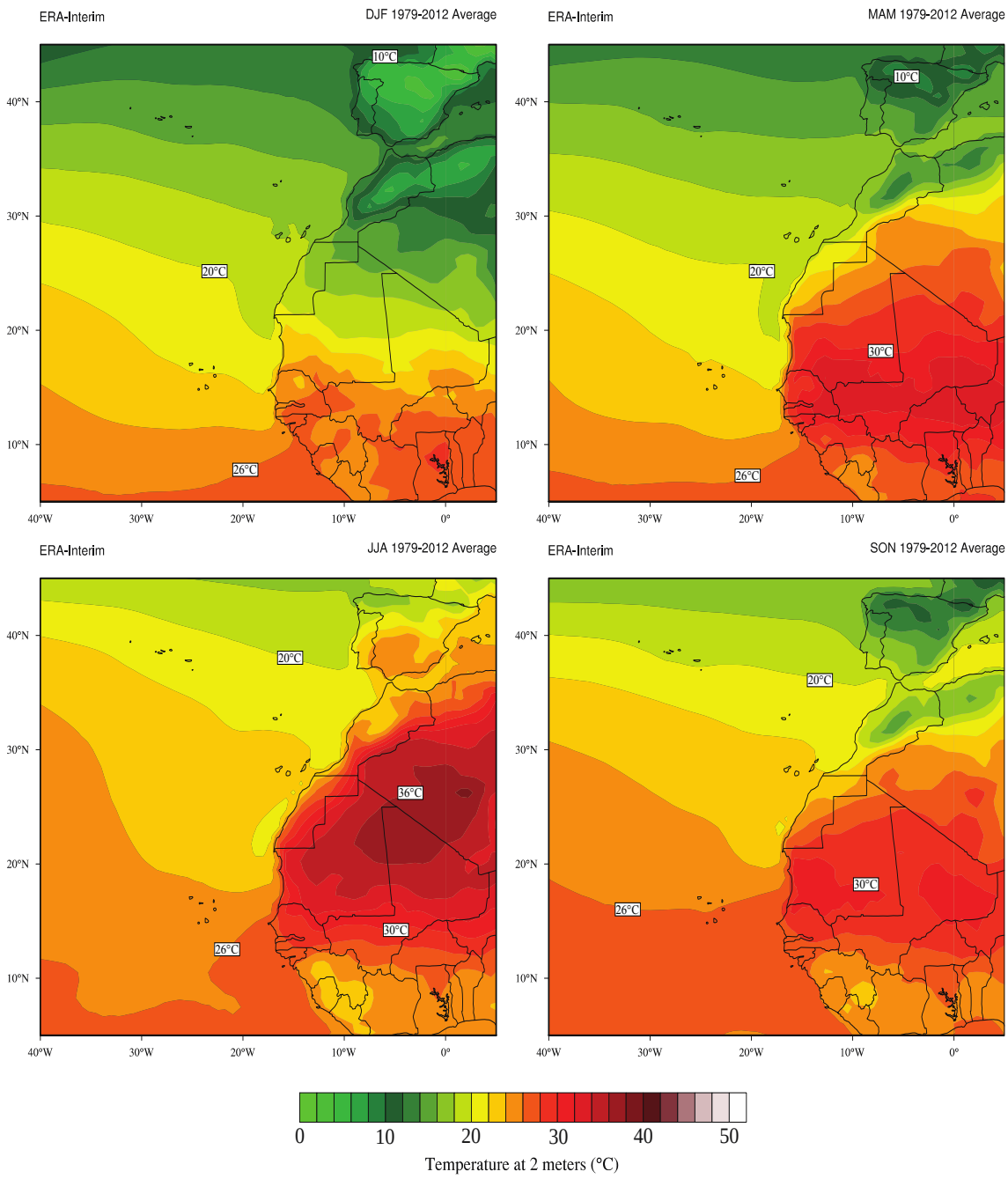

Figure 1.3. The seasonal climatology (1979-2012) of 2 m surface air temperature from the ERA-I reanalysis (Dee *et al.*, 2011).

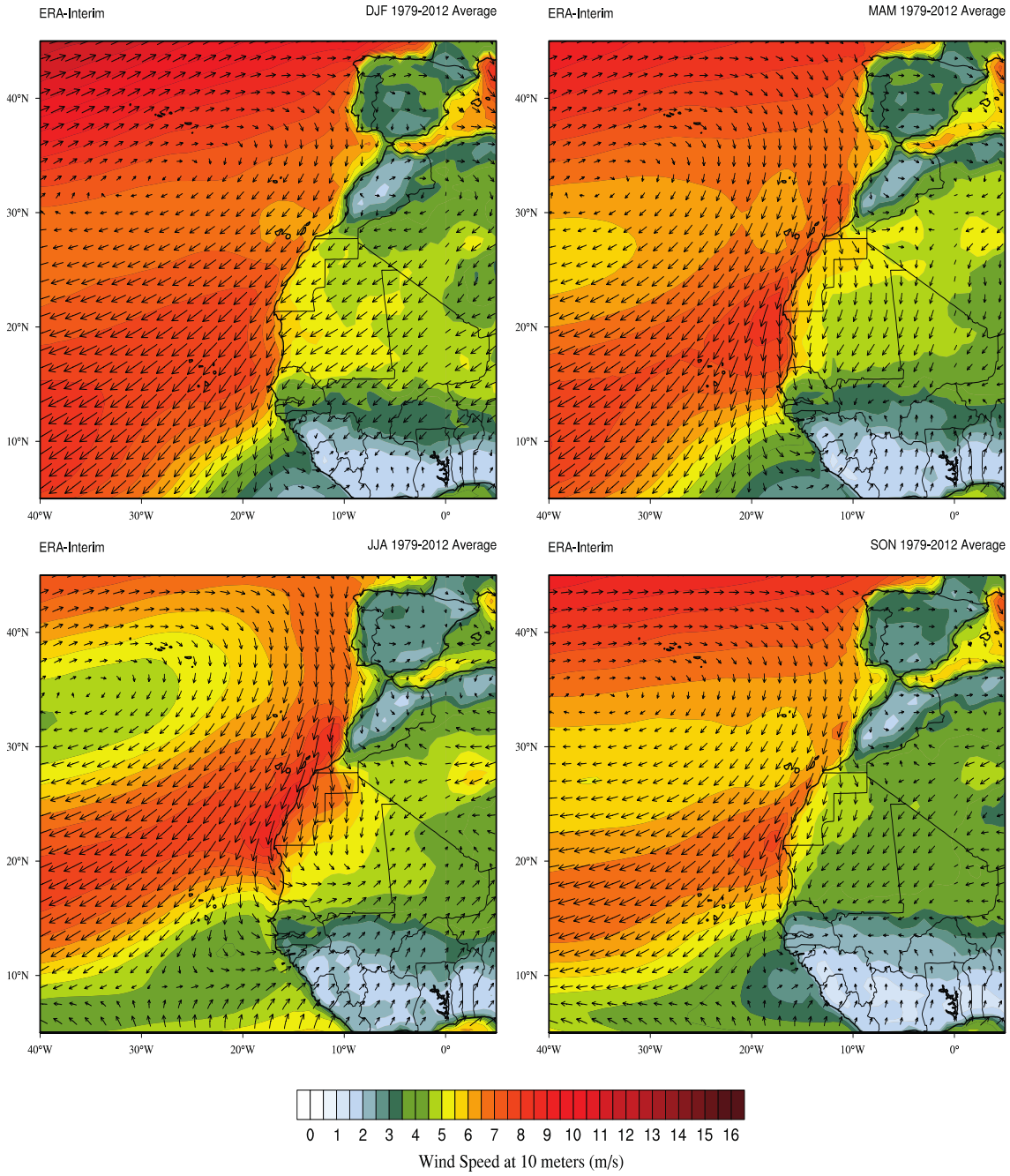

Figure 1.4. The seasonal climatology (1979-2012) of 10 m wind-speed and vector direction from the ERA-I reanalysis (Dee *et al.*, 2011).

A seasonal cycle is evident across all three variables (Figure 1.3 – 1.5). Beginning with SAT, winter and spring temperatures above the ocean show a markedly similar latitudinal distribution, as do the values for summer and autumn. Across northwest Africa and Iberia, spring and autumn show a similar latitudinal SAT distribution, with summer and winter temperatures greatly diverging as would be expected. The mid-latitude westerly winds that influence the Azores can be strongly seen across all seasons but are weaker in summer (Figure 1.4). The northeasterly Trade Winds can be seen to shift in their geographic distribution across the seasons and encompass the Macaronesian

Islands (except the Azores) during winter. During summer and autumn, the Trade Winds reach a southern extent of ~20°N next to the African coastline, where they are displaced by the southwesterly monsoon winds (introduced in section 1.3). An interesting feature is the strong summer wind-speeds along the northwest African coastline across 20-30°N: these correspond to a reduced SAT across the same region (Figure 1.3) and are related to coastal upwelling of cool subsurface waters (introduced in Section 1.3 and analysed in Chapter 6). Precipitation is expected during all seasons for the Azores and Madeira (Figure 1.5), with the greatest (least) amounts in autumn (summer). No precipitation is expected for Cape Verde during winter – spring or the Canary Islands during summer, with limited ($<$ 100 mm/season) amounts for these two archipelagos during their respective 'wetter' seasons.

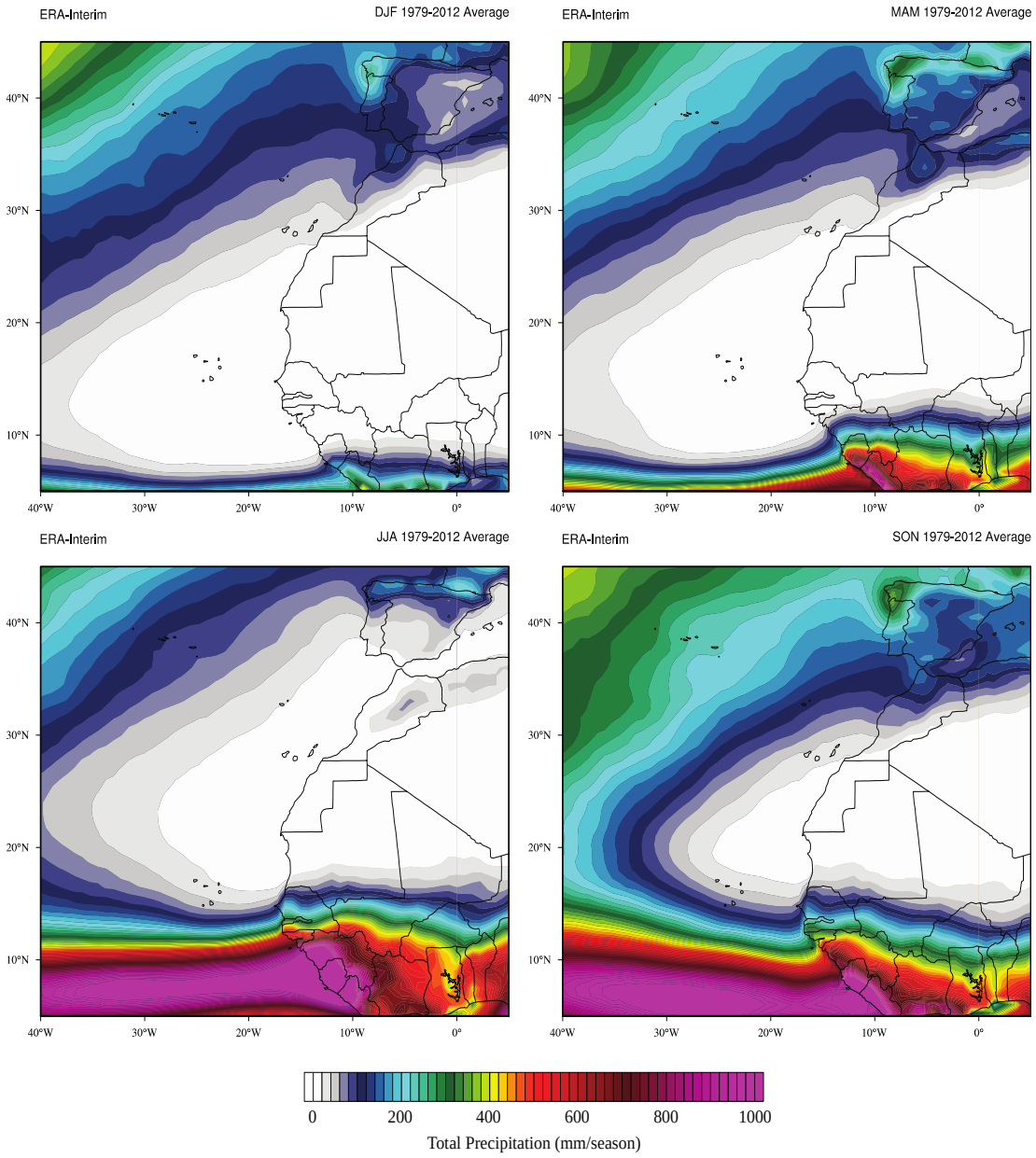

Figure 1.5. The seasonal climatology (1979-2012) of surface precipitation, based on the ERA-I reanalysis (Dee *et al.*, 2011).

It must be stressed that whilst reanalysis output is often treated as 'observational', there can be large discrepancies between reanalysis and reality in data-sparse regions. Comparing reanalysis output at the grid-box level to observational data from small islands is an analysis that has seldom been undertaken, only for Hawaii by Diaz *et al.*, (2011) and Elison-Timm *et al.* (2013) and for the Azores and Cape Verde by Bližňák *et al.* (2014) and is considered later in this thesis (Chapter 4).

1.3 Weather & Climatological Features across Macaronesia

Continuing from the broad description of the seasonal climate across the large-scale Macaronesian region as a whole in Section 1.2, here the discussion of several more specific weather and climate mechanisms that feature across the region are presented.

1.3.1 The Azores High

Atmospheric overturning circulation of the Hadley Cell results in the continuous downward subsidence of atmospheric mass from the tropopause (the boundary between the troposphere, where the Earth's weather occurs and the stratosphere, the atmospheric layer above the troposphere) to the surface at around ~30°N/S, resulting in 'semi-permanent' surface high-pressures systems around these latitudes. Continentality, seasonality, the influence of large mountain ranges and the state of the upper atmosphere additionally influence the preferred geographic location of the subtropical high-pressure systems. For the North Atlantic basin, the semi-permanent high-pressure system is most frequently centred above the Azores and known as the Azores High. From the sub-tropical surface highs, energy (heat, moisture and momentum) is transported polewards in the form of mid-latitude cyclonic low-pressure systems which are known as the mid-latitude westerlies. Some energy is conserved as part of the return equatorward flow of the Hadley Cell at the surface. The Azores High is more geographically widespread during winter (Figure 1.6) whereas during summer it is generally 'more focused' (only strong over the ocean), as continental regions experience thermally-induced lows (Figure 1.6).

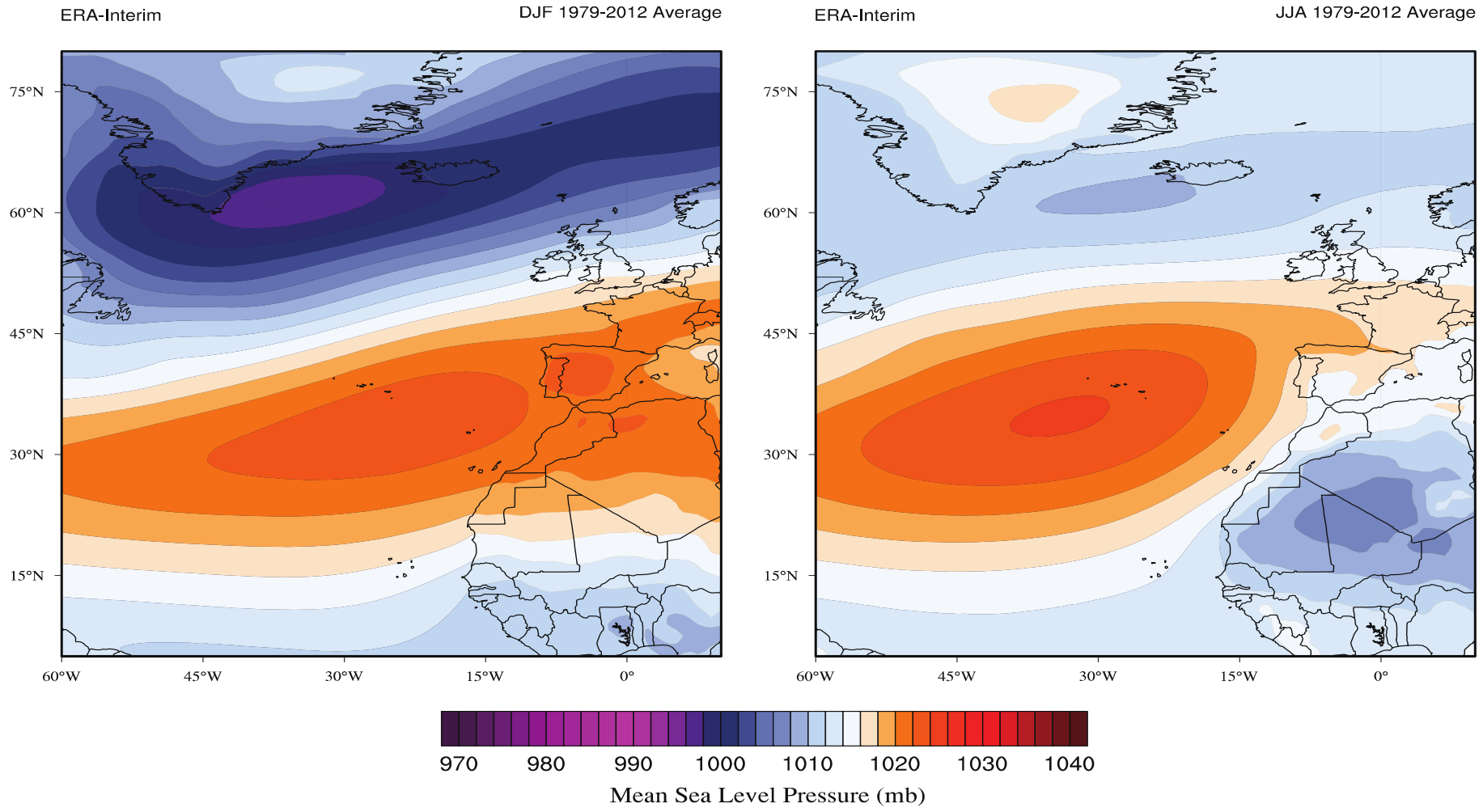

Figure 1.6. The climatology (1979-2012) of winter (DJF) and summer (JJA) sea-level pressure across the North Atlantic region from the ERA-I reanalysis (Dee *et al.*, 2011).

1.3.2 The North Atlantic Oscillation

The prominence of the Azores High displayed in Figure 1.6 is mirrored by the corresponding low-pressure system above Iceland: the Icelandic Low. Unlike the Azores High, the Icelandic Low isn't a semi-permanent weather feature, but represents the succession of low-pressure systems that pass through the region; so across a 'climatological' scale (~30 years) it appears as a semi-permanent feature (Serreze *et al.*, 1997), but on the 'weather' scale it is a dynamic, transient process. The difference in Sea Level Pressure (SLP) between the Azores and Iceland is the NAO, introduced in Section 1.1. The strength of the pressure difference between the high and low SLP centres of action exerts a strong control over the strength and direction of the mid-latitude westerly storm tracks. As such, the NAO has been linked to a variety of climatological, biological, hydrological and ecological variables across several locations (Ottersen *et al.*, 2001; Westgarth-Smith *et al.*, 2012), but is most frequently recognised as directly affecting the west of Europe (from Iberia to Scandinavia). A greater than normal pressure difference between the Azores and Iceland is a positive NAO (NAO+) and a weaker than normal pressure difference (not necessary a SLP reversal) is a negative NAO (NAO-). It is uncommon, but extremely negative NAO months can occur where the SLP oscillation is completely reversed and is higher at Iceland than the Azores (and the normal westerly flow is replaced by easterly flow from the Arctic or Central Europe).

During the winter months, the NAO+ is associated with warmer and wetter conditions across northwestern Europe and cooler and drier conditions across southern Europe (Figure 1.7) as the stronger pressure gradient between the Azores and Iceland drives the storm tracks poleward. The opposite is generally true for NAO- conditions as the weaker pressure gradient generally results in 'southward-shifted' storm tracks, and a SLP reversal will typically result in easterly conditions. As such, the NAO index is strongly related to favoured positions of the jet stream. The significantly negative NAO- events are probably the most influential across Macaronesia. As illustrated in Figure 1.7, weaker Trade Winds during NAO- events allow high subtropical sea-surface temperature (SST) anomalies to develop. During extreme NAO- events, it is likely that high-pressure anomalies near/around Iceland can 'block' the climatological path of storms, shifting storms southwards towards Macaronesia and Iberia (Fragoso *et al.*, 2012). The higher SSTs contribute to increased storm intensity and greater moisture availability (Ball, 2011).

The NAO is a more pervasive phenomenon during winter than summer. Figure 1.6 illustrates the stronger meridional pressure gradient in winter. The Azores High appears to have a more intense centre during summer, but the Icelandic Low is much weaker. The NAO remains an important mode of variability during transitional seasons (spring

and autumn) but it is far from a permanent feature, especially at the 'weather' temporal scale. It is believed that external (solar) and internal (Quasi-Biennial Oscillation) forcing can significantly affect the winter NAO, mainly by changes in the strength of the stratospheric polar vortex. These processes are explained in Section 1.3.10.

1.3.3 The Trade Winds

The Trade Winds are the near surface return flow component of the Hadley Cell. Figure 1.4 illustrates their seasonal evolution across the Macaronesian region. The northeasterly direction and the persistence of the Trade Winds ensure a consistent climatology across the Macaronesian Islands within the Trade Wind belt (Madeira, the Canary Islands and the northern Cape Verde Islands). The windward (northern) slopes of these islands receive much more precipitation than the leeward slopes. This is due to the orographic uplift of moist maritime air, which cools as it ascends (at a typical rate of -6.4°C km^{-1} (Glickman, 2000)) and condenses to form orographically-generated clouds, which precipitate out mostly on the northern slopes of the islands. The Trade Wind Inversion (Figure 1.8) exists whereby the typically dry and warm subsiding mass of the atmosphere (as part of the Hadley Cell circulation) meets generally cooling, moist, maritime air that rises from the surface of the Earth. Across the Macaronesian region this exerts an important control on the heights of clouds, as the height of the boundary of the intersection of these two air masses typically caps the altitudinal range of clouds between ~750-1500 m - so regions above the inversion can be very arid. This exerts an obvious environmental control on the islands, limiting the altitudinal range of the tropical laurel forests (Sperling *et al.*, 2004). In fact, the very first observations of the Trade Wind inversion were made (in Macaronesia) on Tenerife by Charles Piazzi-Smyth in 1856, who noted a temperature inversion not at the top of the Trade Wind flow (i.e. the boundary between the equatorward Trade Winds and the upper atmospheric poleward Hadley circulation) but halfway up Mount Teide and that the top of the cloud height corresponded with the base of the inversion (Oliver, 2005). The typical dryness of the atmosphere and cloud-free nature of the regions above the Trade Wind inversion make the peaks of Mount Teide (Tenerife) and Roque de los Muchachos (La Palmas) excellent sites for astronomical observatories.

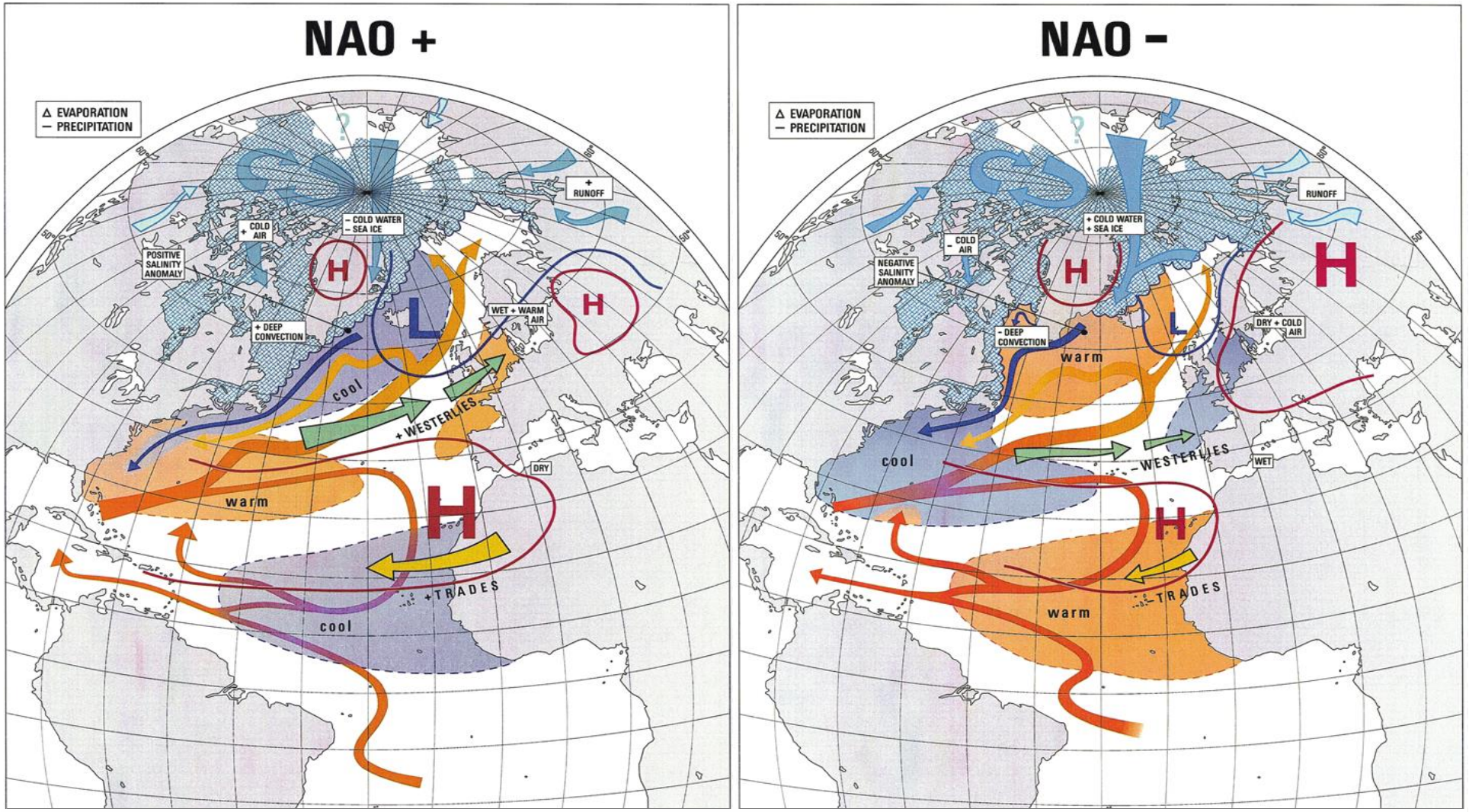

Figure 1.7. The climatic impacts associated with the positive and negative phase of the NAO (from Wanner *et al.* 2001).

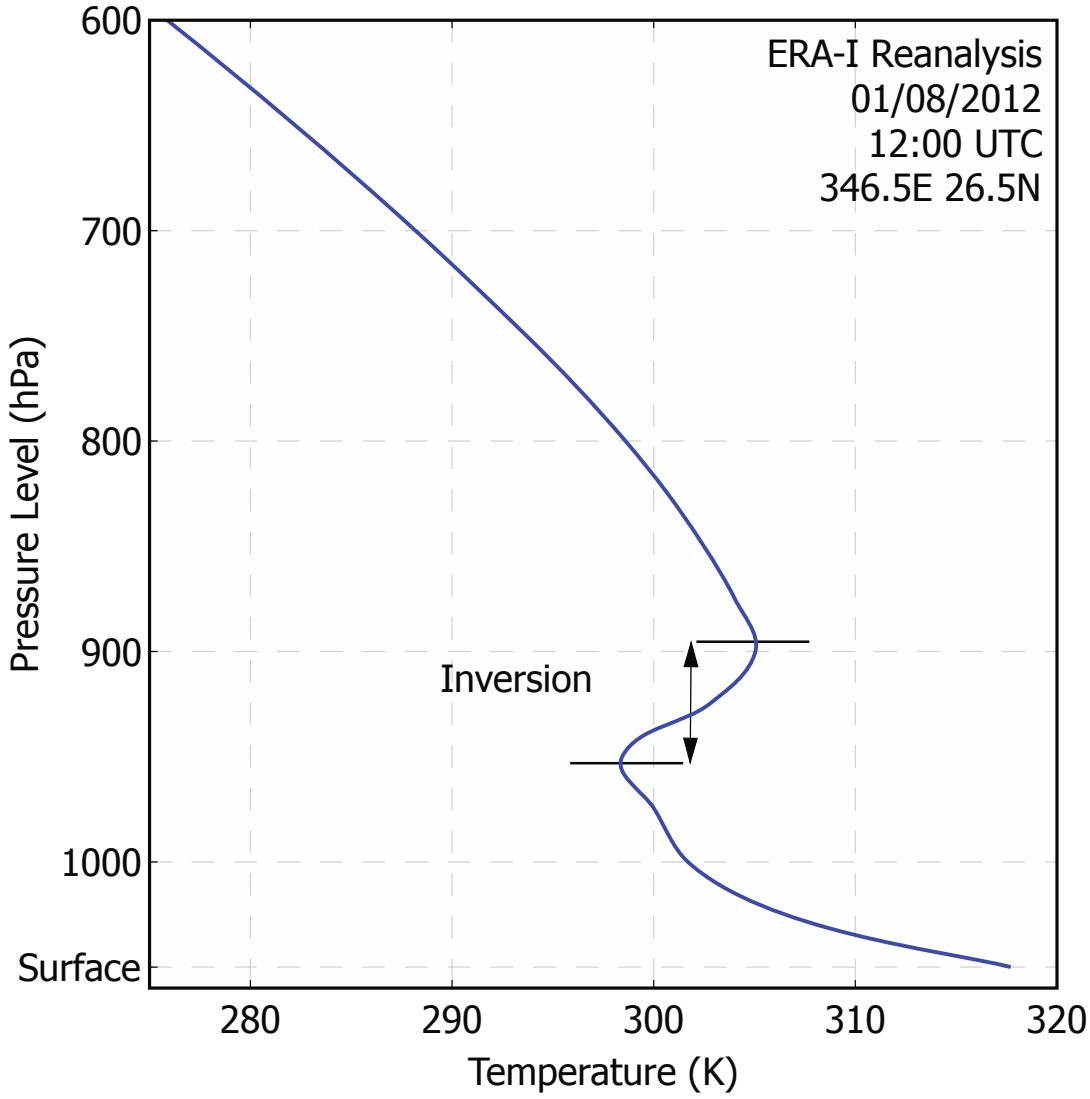

Figure 1.8. An example of the Trade Wind (temperature) inversion using temperature data from the ERA-I reanalysis on 01/08/2012 at 12:00 UTC from the grid-box located at 346.5E 26.5N (just south of the eastern Canary Islands).

1.3.4 The Inter-Tropical Convergence Zone

The Inter-Tropical Convergence Zone (ITCZ) ties in with the seasonal migration of the Azores High, Trade Wind, SAT and precipitation regimes. Loosely classified as the convergence zone between the northeasterly and southwesterly Trade Wind regimes, the ITCZ location roughly follows the seasonal shifts in the solar zenith path, occupying its northernmost (southernmost) latitudes during summer (winter). Most of Macaronesia (apart from Cape Verde) is not directly affected by the ITCZ, but the indirect consequences of the solar-induced changes throughout the seasons are felt across the region.

1.3.5 The African Continental Thermal Low and Monsoon

In summer, enhanced solar heating causes the continents to warm at a much greater rate than the ocean (Figure 1.2, 1.9a). Over land, this causes air to rapidly rise and produces a thermally-induced surface low-pressure. Across the Sahara desert this process is exacerbated by a lack of available moisture to provide evaporative cooling. Across the oceans during summer, SLP is higher (Figure 1.6, 1.9b), which draws airflow from ocean to land. The importance of this process across the Macaronesian region is threefold: firstly in initiating monsoonal circulation; secondly due to the links with the African Easterly Jet/Waves; and finally in potentially intensifying coastal upwelling (Section 1.3.8). Monsoonal circulation mostly affects northwestern Africa around the ~5°-15°N 'Sahel' region. The southwesterly airflow due to the land-sea pressure contrast provides an important seasonal (typically during months JJASON) rainfall source for many countries throughout this region, on the order of 100-600 mm per season, mainly depending on latitude (Nicholson, 2013).

1.3.6 African Easterly Jet/Waves

The African Easterly Jet (AEJ) is an easterly wind found at around ~4 km height in the atmosphere. The AEJ forms because of the surface conditions associated with the African continental thermal low and oceanic high. The thermal low itself, together with the confluence of the southwesterly monsoon winds and the northeasterly trades create ideal conditions for convection, with the convection predominantly 'dry' across the Sahara and 'wet' across the tropics (Nicholson, 2013). As such, this warm rising air gives rise to a higher thickness level across the Sahara at mid-altitudes relative to the surrounding ocean and tropical latitudes (Figure 1.9c). The centre of this process is around the 600 hectopascal (hPa) level (~4 km). At this level, equatorward flow occurs from the Saharan high, which is then deflected by the Coriolis effect and contributes to what is defined as the AEJ. The strong latitudinal pressure gradient is crucial in its formation, according to modelling work by Patricola and Cook (2007), who suggest that the AEJ was absent as a feature between 8000-6000 years ago, due to a reduced temperature gradient associated with a greener Sahara.

African Easterly Waves (AEW) are features that arise from AEJ flow. AEW propagation can directly affect Macaronesia, especially Cape Verde, where it influences storm activity and precipitation, and on rare occurrences, occasionally affect the other Macaronesian Islands. The storm events can vary in severity, ranging in scale from an initial low-pressure disturbance through tropical storm to hurricane-force winds. Historically, 'Cape-Verde Hurricanes' (so-named because of their geographical origin) are some of the

strongest and longest-lasting storms, as they have a large area of ocean over which to develop before encountering land. Recent examples are Hurricanes Ivan (2004) and Ike (2007) which are the sixth/third most damaging hurricanes of all time (updated from Blake *et al.*, 2011).

Normally, strong disturbances develop around 5-15°N latitude, so Cape Verde is frequently impacted, but not often by hurricane-force winds. If these disturbances develop into tropical storms then Hurricanes, their normal track is easterly, heading towards the Caribbean and eastern North America. On rare occasions, the storm track can propagate further north, as Tropical Storm Delta did in 2005 (Beven, 2006), when it crossed the Canary Islands, as a westerly storm, or as in 2012, when Hurricane Nadine initially propagated eastward but its path reverted poleward and it eventually ended up circling around the Azores twice, coincidentally becoming the third longest-lived named tropical storm on record at 20.5 (consecutive) days long (Brown, 2013). A higher level easterly jet (~14,000 m height), the 'equatorial or subtropical easterly jet' can migrate over Africa, usually during June-September, due to the large-scale process of the Asian monsoon (Hewitt and Jackson, 2009).

1.3.7 Saharan Dust Advection

The convection that occurs over the Sahara Desert results in ideal conditions for dust suspension. The amount can be on the order of 60 – 200 million tonnes per year (Prospero and Lamb, 2003). Typically this dust will travel west as part of the AEJ average flow and can end up in the western Atlantic; however, depending on weather patterns, it can also be dispersed into the Mediterranean region and across Europe. Significant dust events are linked to low activity hurricane seasons, as the dust can reflect incoming solar radiation, which lowers ocean temperatures. Additionally, the layer of dry air caused by the dust entrainment results in reduced upper-level moisture availability - damping the favoured 'ingredients' of hurricane formation (Lau and Kim, 2007). Dust outbreaks can frequently affect the Macaronesian Islands, particularly Madeira and the Canary Islands (Bergametti *et al.*, 1989).

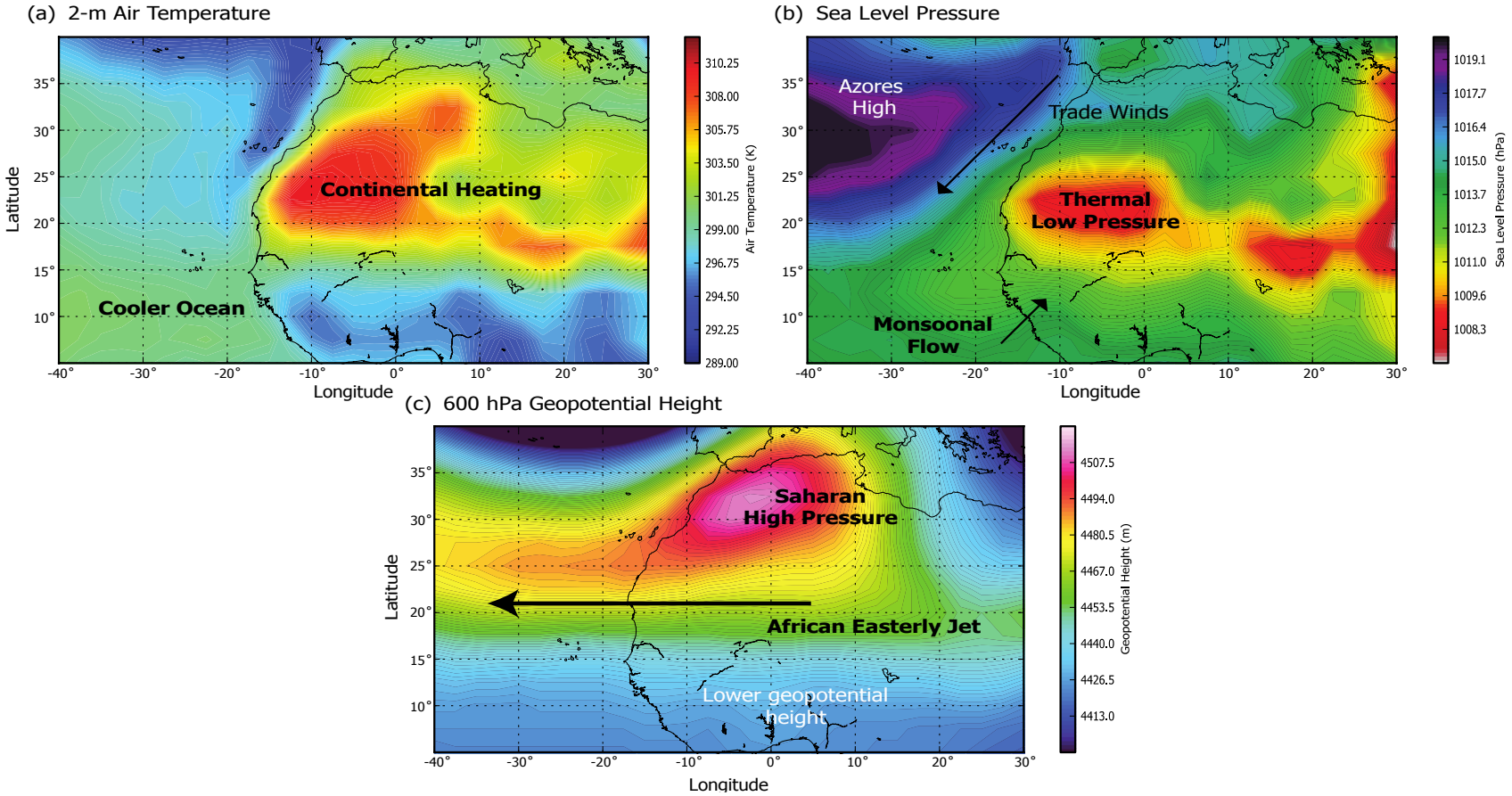

Figure 1.9. A composite of (a) 2 m Air Temperature, (b) SLP and (c) 600 hPa geopotential height from the National Centre for Environmental Prediction reanalysis (NCEP-NCAR, Kalnay *et al.*, 1996), 13-24th August 2012. Arrows indicate mean flow direction.

1.3.8 Coastal Upwelling

Coastal upwelling occurs along most of the northwest African coastline between 10°N to 35°N. Three factors are required for coastal upwelling to occur (Gómez-Gesteira *et al.*, 2008): (1) persistent winds, (2) a solid boundary, and (3) the Coriolis effect. The consistent along-shore, equatorward direction of the Trade Winds along the majority of the northwest African coastline results in the deflection of oceanic water to the right, away from the coast via Ekman Transport. When this transported water is forced offshore at sufficient rates, mass balance is maintained by the upwelling of subsurface water from below (Sverdrup, 1938). Upwelled water is typically denser, cooler and richer in nutrients than surface waters and has significant impacts on coastal climates and marine biology (Miranda *et al.*, 2012). As such, the two major effects of coastal upwelling across northwest Africa are a generalised reduction in coastal SST that can sometimes extend up to several hundred kilometres offshore, potentially influencing the land-ocean pressure gradients, and a dramatic increase in primary productivity and abundance of fish stocks across these upwelled regions. An introduction to the upwelling intensification hypothesis, first described by Bakun (1990) is given in Section 1.5. This forms the basis of the research undertaken in Chapter 6, which analyses changes in coastal upwelling intensity across the northwest African coastline.

1.3.9 Ocean Currents

The predominant surface ocean currents that influence Macaronesia are the Azores and Canary Currents which form part of the North Atlantic Gyre (Figure 1.10). The Azores Current flows in an easterly direction across the North Atlantic and meanders southwards as it approaches northwest Africa, joining the Canary Current which flows southwards along the African coastline until around 15°N – from where it flows outwards into the North Atlantic Ocean (Barton, 2001), The Canary Current is wide (1000 km) so extends some way offshore and encompasses the Canary Islands. The current often entrains upwelled waters from the northwest African coastline and can cause a widespread cooling effect. A third important current across the Macaronesia region is the (surface) eastward flow and (subsurface, ~100 m depth) westward outflow from the Mediterranean through the Strait of Gibraltar.

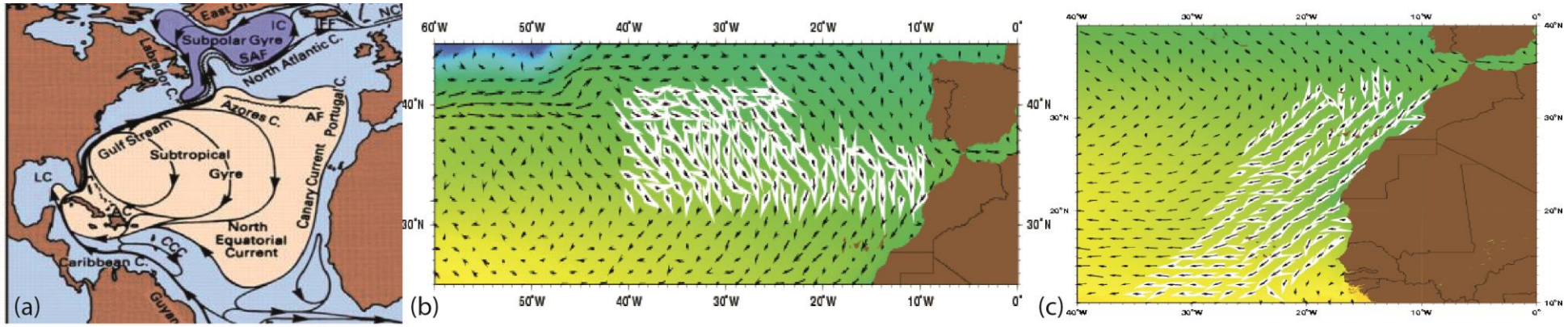

Figure 1.10. (a) The North Atlantic Ocean Currents, as displayed in Tomczak and Godfrey (2003), along with the highlighted (white arrows) (b) Azores and (c) Canary Current, as depicted by Gyory *et al.* (2014).

1.3.10 Global and Regional Oscillatory Modes

Several climatological and oceanographical modes exist which influence global and regional climates. Brief descriptions of the most important of these modes, regarding their potential effects on Macaronesian climate are presented here:

Solar

The amount of solar radiative energy that reaches the upper atmosphere of the Earth is the total solar irradiance. The total solar irradiance is independent of any lower atmosphere greenhouse effect (exogenous) and has a mean value of ~1366 watts per square meter (W/m^2), which varies by about ± 1 W/m^2 through an 11-year cycle (Fröhlich, 2000). Additionally, an ~87-year and ~210-year cycle are thought to contribute to long-term solar variability (Braun *et al.*, 2005). Satellite measurements of total solar irradiance go back to 1978, but sunspot numbers serve as a suitable proxy, allowing the record to be extended back to the Eighteenth Century and inferred back to the start of the Seventeenth Century (Vanlommel *et al.*, 2004). Typically, the changes in the 11-year solar cycle can account for -0.05 to +0.1 °C of global temperature anomaly variability. For comparison, on similar, decadal-scale time scales, ENSO (see below) and volcanic aerosols can shift global temperatures by around -0.2 to +0.3 °C and up to -0.5° respectively (Foster and Rahmstorf, 2011). Direct solar forcing is not expected to affect Macaronesian climate, other than through the small changes in global SAT and SST. Indirect effects, such as solar forcing modulating changes in the stratospheric vortex and driving NAO variability (De La Torre *et al.*, 2007; Scaife *et al.*, 2013; Gray *et al.*, 2013) cannot be discounted. Here, the basic mechanism is that reduced solar Ultraviolet Radiation during periods of solar minimum cools the stratosphere, which is balanced by an increase in easterly wind-speeds, which then propagate down towards the troposphere, favouring NAO- conditions (Ineson *et al.*, 2011).

El Niño Southern Oscillation

The ENSO is a coupled atmosphere-ocean feedback with a period of about two to eight years that controls the rate of ocean heat uptake/ release by changes in the strength of wind-speed and ocean circulation across the Pacific Ocean. As a consequence of the great area across which this process operates, it can significantly affect global climate and has a strong signal in the global SAT record (Lean and Rind, 2008; Foster and Rahmstorf, 2011). Direct links to Macaronesian climate are tentative, mainly because of the dominance of the NAO and the difficultly in attributing anomalous conditions directly to an ENSO influence. Some authors hint at a reasonably high-frequency, i.e. within

~three months response (e.g. Gouirand *et al.*, 2012). Enfield and Mayer (1997) illustrated that subtropical and mid-latitude SLP can decrease and equatorial SLP increase across the Atlantic following a winter El Niño peak, which results in a reversed pressure gradient, anomalous southwesterly winds and increased warming around western Africa (10-20°N). Conversely, Joly and Voldoire (2009) suggested an ENSO signal could be found in Sahelian rainfall only during the development phase of the oscillation or the decay phase of La Niña. Irrespective of the findings of the previous two papers, a long term low frequency connection generally appears lacking, leaving the general effect of ENSO on global temperatures and a possible tropical SST modulation as the main two effects across Macaronesia.

Atlantic Multidecadal Oscillation

The Atlantic Multidecadal Oscillation (AMO) is an apparent oceanic mode of variability occurring across the Atlantic Ocean. Its expression is mainly in the SST field, with a tripole pattern of SST anomalies (Figure 1.11). The AMO has been invoked as a primary driver in climate changes across a large spatial realm (Christensen *et al.*, 2013), noticeably with West African Monsoon (WAM) rainfall (Martin and Thorncroft, 2014). The AMO is thought to have a ~50-70 year cycle, but whether this remains constant or even present in the palaeo-record is ambiguous (Knudsen *et al.*, 2011). The proposed mechanism varies between different studies, with some invoking an atmospheric requirement (Dima and Lohmann, 2007) and others hinting at purely internal oceanic mode (Delworth *et al.*, 1993; Ba *et al.*, 2013). A general consensus is that variability in the regions of North Atlantic Deep Water formation as part of the global Thermohaline Circulation plays a strong role (Knight *et al.*, 2005). The degree to which the AMO signal is contaminated by the Anthropogenic Global Warming (AGW) signal is also open to debate as it is expressed in SST anomalies, which closely follow SAT variations. The AMO is responsible for one third of post 1975 global SAT rise according to Chylek *et al.* (2014), although disentangling the cause and effect of the AMO with respect to AGW remains controversial, as the AMO is essentially, just the linearly detrended regional North Atlantic SST (van Oldenborgh *et al.*, 2009).

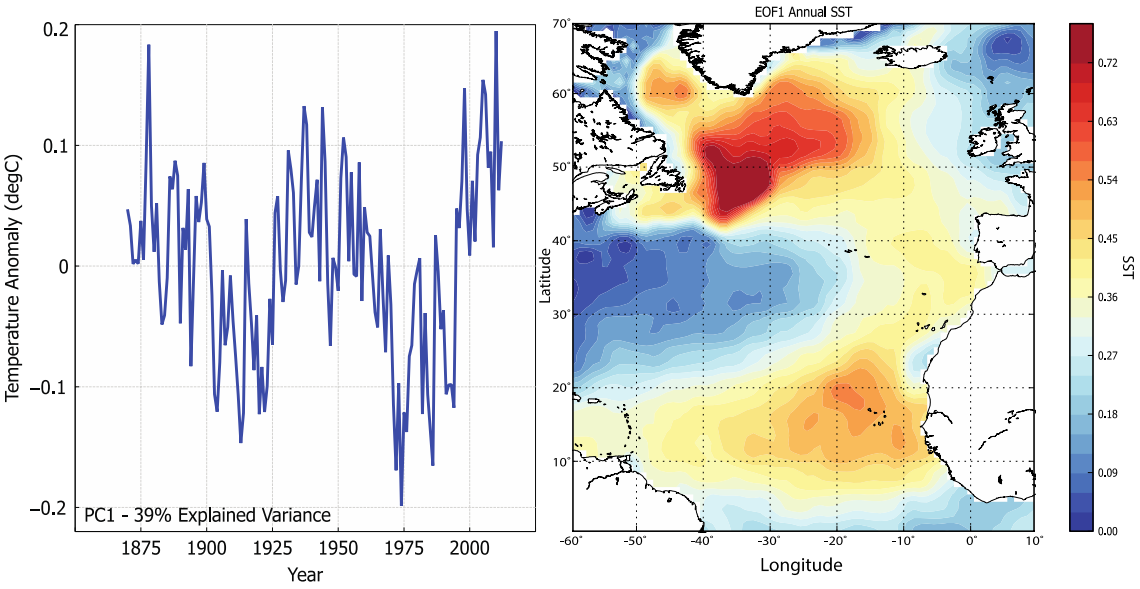

Figure 1.11. The temporal evolution and spatial pattern of the AMO derived from North Atlantic SSTs. SST data are from the Hadley Centre Sea Ice and Sea Surface Temperature dataset (Rayner *et al.*, 2003) and Principal Component analysis (introduced in Section 2.4) is the method used to generate the time series and its spatial pattern.

East Atlantic Pattern

The East Atlantic Pattern (EA) is the second leading mode of variability after the NAO across the North Atlantic basin. It has a similar structure, with a north-south dipole of anomalies shifted slightly southeastward with respect to the NAO centres of action (Barnston and Livezey, 1987). During winter, the EA accounts for 23% of the variance in the vertically integrated geopotential height field (relative to 39% for the NAO), so the pattern can be considered important for Macaronesia (Woollings and Blackburn, 2012). Like the NAO, the influence of EA pattern diminishes across summer.

Quasi-Biennial Oscillation

The Quasi-Biennial Oscillation (QBO) is a stratospheric phenomenon whereby above the equatorial latitudes, phases of easterly and westerly winds alternate in a quasi-periodic fashion and propagate downwards (from the top of the stratosphere) towards the tropopause where they dissipate (Baldwin *et al.*, 2001). The period of the oscillation is 27-29 months. There is a limited direct response at the surface to these winds, but an indirect response has been demonstrated via the QBO relationship with the stratospheric vortex, which can influence the NAO. During easterly QBO phases, easterly flow in the polar stratosphere is favoured; this gives rise to downward-propagating waves, which can influence the troposphere dramatically (NAO- conditions would be favoured in this scenario) (Anstey and Shepherd, 2014). A sinking, warming, polar stratosphere therefore ought to be a consistent response to an easterly QBO phase and also low solar activity

as previously mentioned. It has been suggested that in-phase solar/QBO cycles can significantly enhance NAO- events (Gray *et al.*, 2004), although not every single easterly QBO phase and solar low necessarily drive an NAO-, and surface conditions and internal variability remain important drivers (Manola *et al.*, 2013).

Volcanic Forcing

Aerosols can exert a significant cooling effect on global and regional temperatures by reflection of incident solar radiation and altering changes in clouds (particle size, reflectivity and height) (Boucher *et al.*, 2013). Aerosols have a resident time of ~one-two weeks in the troposphere and ~one year in the stratosphere. When significant volcanic eruptions occur in the tropics, a global climate impact, i.e. a lowering of surface temperature, is more likely, as (mainly sulphate) aerosols are more easily transferred to the stratosphere due to the convective nature of the atmosphere. Upper level winds will then disperse aerosols to achieve a large global coverage. Global cooling from large tropical eruptions can last ~one-to-three years. The potential effect of volcanic aerosols on Macaronesia depends on the distribution of aerosols and whether a direct (scattering or reflection of incident radiation 'above' the islands) or indirect effect (e.g. modification of large scale weather patterns, which then influence the islands) predominates.

1.4 Climate Change & Macaronesia

Given the interesting nature and relative importance of the climate of the Macaronesian region, it is surprising that there has been a relative paucity of literature concerning the region. This section summaries the full extent of the English language literature concerning Macaronesian climate and climate change throughout the instrumental (past few centuries) record. Only historical records that are either publically available or well described in the academic literature, that could conceivably constitute a 'climatic' time series, are discussed.

Currently, the earliest known weather observations (wind-speed and direction, pressure, SAT) recorded near the Macaronesian Islands have been archived from historical ship log books as part of the Climatological Database for the World's Oceans (CLIWOC) project (García-Herrera *et al.*, 2005). The data generated by the project are of good quality, but creating a long-term time series from the records for a specific region is difficult, owing to a lack of observations, unless large spatial scales (e.g. 8°x8° grid-boxes) are used (Gallego *et al.*, 2005). Figure 1.11 displays the annual count of SAT observations from ships in the CLIWOC archive (1750-1854) and the early part of the ICOADS

(Woodruff *et al.*, 2011) database that were taken within the region 10-40°N, 325-355°E. A similar number of readings are available for SLP and many more for just wind-speed and direction (from CLIWOC). Unfortunately, if the records are restricted to those taken within close proximity (within 1°) near the four island groups, then there are only a total of 306, 243, 139 and 309 SAT records from the Azores, Madeira, Canary Islands and Cape Verde respectively. The monthly median of these observations equates to ~two days per available month, so constructing a time series for a specific island chain is difficult. However, only 12% of logbooks available to the CLIWOC project (covering the period 1750-1854) were digitised by the end of the project, so there is the potential for many more records near the Macaronesia Islands to be analysed, especially given the important location of the islands with respect to historical shipping routes.

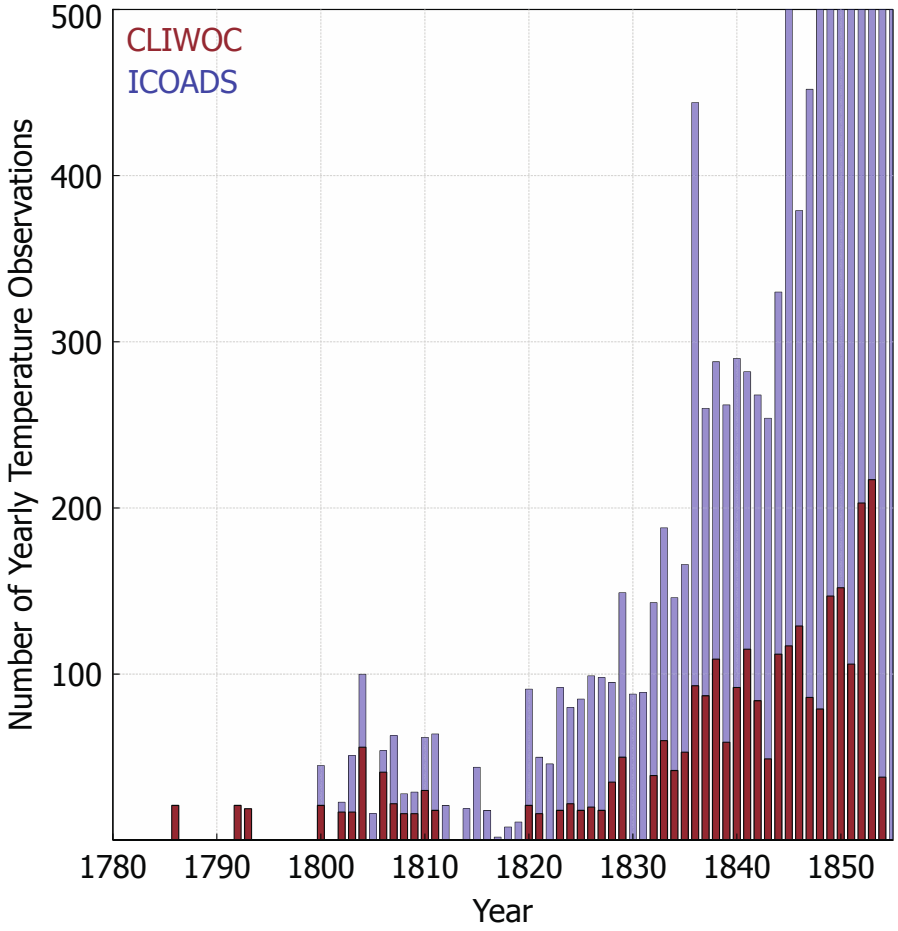

Figure 1.12. The annual count of SAT observations taken throughout the Macaronesian geographical zone (10-40°N, 325-355°E) from the CLIWOC and ICOADS archives (It is likely the ICOADS signals incorporate all of the CLIWOC data, as the CLIWOC archive is assimilated by ICOADS, Woodruff *et al.*, 2011).

The earliest documented observations taken from Madeira (in Funchal) were by Thomas Heberden (1747-1753) and James Murdock (1793-1802). Both authors recorded monthly temperature and pressure readings (Heberden also measured precipitation) and appeared

interested in the link between extreme heat/drought conditions and agricultural success (Alcoforado *et al.*, 2012). A direct comparison with modern values is difficult, owing to lack of metadata about instrumental observation. However, temperatures from 1747-1753 appear to have been 1-2°C higher than the recent past (1980-1994, although it is unclear which data Alcoforado *et al.* (2012) used) yet minimum temperatures compared well, hinting at a (probably) unventilated thermometer or unsuitable (by modern standards) observing location.

Meteorological observations by individuals were taken throughout the Eighteenth and early-mid Nineteenth Centuries across the Macaronesian Islands (Climate Atlas, 2012); however, these data are often short, fragmented series, of significant interest, but limited climatological use and they are difficult to obtain. Permanent observing sites, which constitute the main station-based climate data of this thesis, were set up at the Azores, Canary Islands and Madeira in 1865 (Climate Atlas, 2012). These data are analysed in Chapter 4.

The volume of published literature regarding the climate of the Macaronesian Islands during the last ~50 years is rather small. Harris *et al.* (1962) reported on the characteristics of semi-diurnal oscillations in temperature, wind and pressure at Terceira, Azores. After a ~40 year gap, Tomé and Miranda (2004) identified a 0.22°C dec^{-1} increase of maximum December temperature from 1960 to 2002 at Angra do Heroismo, Azores, with Santos *et al.* (2004) reporting a 0.30°C dec^{-1} increase in maximum annual temperature at the same location for 1963 – 2003. The latter study also identified a significant increase in maximum (0.53°C dec^{-1}) and minimum (0.66°C dec^{-1}) temperatures at Funchal, Madeira, for 1973–2003. Sperling *et al.* (2004) observed a significant summer (JJA) temperature increase of 0.16°C dec^{-1} at Izaña, Canary Islands, for 1950 – 1999 (rising to 0.45°C dec^{-1} for 1970 – 1999) in addition to significant summer temperature trends at La Laguna and Santa Cruz, which were all located on the central island of Tenerife. More recently, Martín *et al.* (2012) used an aggregate of 28 stations and observed a 0.17°C dec^{-1} mean temperature rise for 1970 – 2010 across Tenerife, mainly due to increasing minimum temperatures. winter precipitation values across the western and central Canary Islands are negatively linked with the NAO (García-Herrera *et al.*, 2001), whilst a decreasing trend in Canary Island precipitation during the second half of the Twentieth Century is related to a reduction in the occurrence and intensity of extreme precipitation events (García-Herrera *et al.*, 2003).

Ball (2011) and Levizzani *et al.* (2013) discuss the highly anomalous conditions (large NAO- and relatively high Macaronesian SSTs) that led to significant flooding in February 2010 across the Macaronesian Islands. Madeira was most directly impacted. The heavy precipitation on 20 February 2010 led to damaging flash floods and mudslides, killing 45

people and injuring over 100 (Levizzani *et al.*, 2013). The total storm precipitation of 147 mm (recorded at Funchal) corresponded to a 290-year return period (Fragoso *et al.*, 2012). The transformation of high-atmospheric water vapour content into heavy precipitation was significantly enhanced by orographic uplift (Luna *et al.*, 2011). In a globally warming world, a moister atmosphere is expected (Stocker *et al.*, 2013), suggesting future storms could be equally, if not more, destructive.

Fründt *et al.* (2013) analysed data from a deep-sea mooring just east of Madeira (33°N, 338°E) at depths of 240 m and 500 m and found warming magnitudes of 1.4 and 1.0°C respectively, over the period 1980-2009, which seemed to be accelerating over the last 5 years of the time series. The NAO was suggested as a strong driver of changes in sub-surface current strength and direction (also seen by Siedler *et al.*, 2005) and as a potential moderator of temperature rises and plateaus against the backdrop of a progressively increasing global warming signal.

For Cape Verde, McSweeney *et al.* (2010) identified a mean annual temperature increase of 0.14°C dec^{-1}, with a greater increase of 0.23°C dec^{-1} present during the wet (ASO) season. Significant precipitation trends were absent, although the authors noted a recent increase in precipitation during the drier (NDJ) season, in particular, the high values displayed in 1999, 2000 and 2002. Mannaerts and Gabriels (2000) estimated, from three stations of seven years length, that an individual precipitation event of ~100 mm had a five-year return period on the island of Santiago and the maximum precipitation in a 24 hour period could potentially account for 45% of the total annual precipitation. An analysis of precipitation from Santiago Island during 1981-2010 identified a strong elevation control on low precipitation amounts but not on significant large precipitation events, which suggests a greater importance of convection/frontal activity (likely related to the AEJ/AEW, Section 1.3) (Sanchez-Moreno *et al.*, 2014).

Additional significant weather events have affected the Macaronesian Islands in recent years. The driest hydro-meteorological year on record from the Izaña Observatory on Tenerife was during 2011-2012 (AEMET[3], 2014a), which preceded significant wildfires across the Canary Islands and Madeira during summer 2012. However no published study exists confirming a link between the winter/early year dryness and the extended summer fires. It is assumed the area burned in 2012 is significantly greater than the ~17,000 ha (on Tenerife) during the last significant fire season in 2007 (Neris *et al.*, 2013). The total annual precipitation at Izaña has decreased during the second half of the Twentieth Century (AEMET, 2014a) and wildfires across the Mediterranean basin have increased

[3] AEMET (Agencia Estatal de Meteorología) is the meteorological institute of Spain. The AEMET (2014) reference refers to news articles posted on the Izaña Observatory webpage (http://izana.aemet.es). Full links to specific webpages are provided in the reference list.

(Garzón-Machado *et al.*, 2012), hinting at a potentially causal link. After significant fire events/seasons, the following flood events (if they occur) can display marked increases in runoff and erosion potential (Moody and Ebel, 2012), which could increase the destruction from the events like the Madeira 2010 floods. Uncertainties in the latitudinal displacement of the jet stream (i.e. NAO/EA, Woollings *et al.*, 2012) make it difficult to assess if such events are more likely or not to occur in the future. However a small shift to more NAO+ like conditions (in winter) is apparent in future Global Climate Model (GCM) predictions (H15), suggesting a potential drying of the Macaronesian region. Conversely, on 15 February 2014, a storm caused rime damage (potentially the most adverse in ~18 years) to meteorological equipment at the Izaña observatory (AEMET, 2014b), highlighting recent increased variability across the region.

1.5 Thesis Structure & Aim / Objectives

The background information provided about the Macaronesian region in this chapter conveys a strong understanding of the basic climatological features that characterise the region. However, as noted from the literature review in Section 1.4, simple statistics ranging from a mean climatology of the islands and a long-term climate change record are lacking, whereas studies concerning individual weather events are more prevalent. Historical meteorological data are available for Macaronesia in several archives and have hitherto been underexplored, yet the individual records are often incomplete, fractured or inhomogeneous. It is of critical importance to build long-term, homogenous climate records for under-observed regions of the globe, as surface observations are the fundamental records that underpin many regional and global climate datasets and studies. Filling in spatial and temporal gaps helps to 'complete the global picture' of climate change. Therefore, the first objective of this thesis is to:

1. Create a climate record that will allow analysis of long-term changes in Macaronesian climate

This will be accomplished by focusing primarily on monthly-resolution temperature and precipitation data. Temperature and precipitation are chosen as the primary physical climate system measurements to assess due to their importance in assessing long-term climate change and the greater and longer-term availability of these variables relative to other metrics. From review of the Macaronesian climate literature (Section 1.4), it is apparent that (in terms of openly and freely available climate data) a meteorological-station density of greater than one per island is rarely exceeded and not every island within each island chain has data available. However, monthly-resolution observations

back to 1865 are available, even if the 'major'/longest-running record, seldom runs from this time until the second decade of the Twenty-first Century. Data from stations within the same island chain often fortuitously cover the gaps in the major records, which enables use of these complementary records to fill the gaps. Application of this process to the major record from each island chain would then result in a much more useable and valuable long-term climate record for each of the Azores, Canary Islands, Madeira and Cape Verde. These records can then be analysed individually to assess climate change across each island chain and be compared against other regions and globally to place these local to regional changes in a broad-scale climate context.

In addition to the major monthly-resolution climate records, there are gridded observational, reanalysis or climate model outputs of variable temporal and spatial resolution that encompass the Macaronesian Islands (which are documented in Section 2.10). These products are heavily used in climate science and form the basis for many of the conclusions of the recent IPCC AR5 (Stocker *et al.*, 2013). As such, it was determined that use of these independent data sources would be beneficial with regards to the analysis of the climate of Macaronesia, in terms of reinforcing the findings from the major climate records and potentially offering new insights. Consequently, the second objective of this thesis is to:

2. Determine if additional climate data support the conclusions drawn from the main climate records

Use of these additional data sources will allow direct comparisons with the major Macaronesian records to be made. This includes comparison of trend rates and correlation values from observational/reanalysis/model sources with the major records. Alternative regions (e.g. Europe or globally) can be extracted from these archives, which will allow comparison between Macaronesian and other regional climates. It is also possible to analyse climate 'extremes' using daily-resolution data sources, which can be referenced and compared with the major records. Here, the definition of climate extreme refers to a set of pre-defined indices documented by the Expert Team on Climate Change Detection and Indices (ETCCDI). These indices include threshold-based measures (e.g. >25°C), percentile-based measures (e.g. number of days per year where temperature falls below the 10^{th} percentile) and duration-based indices (e.g. consecutive days with precipitation <1mm) which are most suitable for picking out 'moderate' extreme events with return times typically on the order of one year or less. This approach is favoured for a few reasons. Firstly, analysis of individual extreme events, such as the 2010 floods discussed by Levizzani *et al.* (2013) and Fragoso *et al.* (2012), is more feasible when an entire island network of observational data are available - which in terms of freely-available data - is rarely the case. Secondly, there is an abundance of studies employing the ETCCDI

methods as the global standard for climate-extreme analysis (e.g. Alexander *et al.*, 2006; Donat *et al.*, 2013), including the IPCC AR5 (Stocker *et al.*, 2013). The indices can be applied to station and gridded data (so individual extreme events won't be missed by this approach) which result in monthly/seasonal values of the indices which can then be directly analysed or compared with other climate variables. Fulfilling the criteria for objectives one and two will result in the most complete, and also, the only full characterisation (which includes all four island groups) of Macaronesian climate in the published English language literature.

Sections 1.3.1 and 1.3.2 discussed the Azores High and NAO and illustrated how the NAO is an important feature across Macaronesia. Several different ways to characterise the NAO exist and therefore, there are several different versions of the NAO Index. These are covered in detail in Section 3.1. Some station-based NAO indices at the monthly-resolution can extend back to the 1820s (Jones *et al.*, 1997). However, when Gibraltar or Lisbon are used as the southern node rather than the Azores, the index is unsuitable for characterising the NAO across all but the winter months. Pozo-Vázquez *et al.* (2000) suggest that the Azores is the most suitable location for the southern node of the station-based NAO, as it tracks the location of the Azores High throughout the year more adequately than at Lisbon/Gibraltar. The Azores-based monthly NAO extends back to 1865. Additionally, the longest-running daily NAO index, provided by the Climate Prediction Centre (CPC) extends only to 1950. Early pressure readings from the Azores are available back to 1872 and continue to the present day (albeit through numerous fragmented sources), and a gridded SLP dataset at a daily-resolution is available back to 1850 (Ansell *et al.,* 2006). Combining these multiple data sources presents an opportunity to extend the Azores SLP time series back to 1850, which could be combined with the southwest Iceland SLP series which extends back to 1823 (Jónsson and Garðarsson, 2001; Jónsson and Miles 2001; Jónsson and Hanna, 2007) to create a daily-resolution NAO index that extends the length of the previous longest (daily-resolution) index by 100 years. As such, the third objective of this thesis is to:

3. Conduct a detailed analysis of the North Atlantic Oscillation, including extending the daily-resolution index back to 1850

Following the creation of the new daily NAO index, it can be analysed to assess the temporal changes, trends and variability. Changes in the index itself are of importance not just to Macaronesia, but also to a much wider region, given the large-scale influence of the NAO. The spatial correlations of the NAO across Macaronesia and how these change through time will also be discussed. The Azores SLP time series can also be combined with SLP data from Cape Verde to create a measure of Trade Wind strength and variability across Macaronesia.

Once the historical-present climate of Macaronesia has been analysed, and variability in the NAO considered, attention can be turned towards the potential influence of AGW on the climate across the islands. The IPCC AR5 reports an expected global mean SAT rise by 2081-2100 (relative to 1986-2005) of 0.3°C-1.7°C under the 'peak and decline' Representative Concentration Pathway[4] 2.6 emissions scenario (RCP2.6) and 2.6°C-4.8°C under the 'business as usual' RCP8.5 emissions scenario. Naturally, regional climates are not expected to track the global mean so regional assessments of future climate change are important. Unsurprisingly, given the paucity of published research on the contemporary and historical climatology of Macaronesia (Section 1.4) there is currently no published research on the potential future climate changes across the region. Therefore, the fourth objective of this thesis is to:

4. Deliver estimates of future climate change at the end of the Twenty-first Century across Macaronesia

As with the first stated objective, temperature and precipitation will be the variables assessed. Changes in the mean state and variability, together with changes in extreme values will be analysed. The potential future evolution of the NAO will be discussed and the results will be analysed in the context of the physical constraints on the climate system – essentially, what is more 'expected' due to thermodynamics and what is 'uncertain' due to dynamics (circulation variability). The temperature and precipitation constraints will provide the first assessment of future Macaronesian climate, addressing an important knowledge gap.

Within the Macaronesia biogeographical zone (Figure 1.1) is the northwest African coastline. This region is of particular interest because it is one of the four major Eastern Boundary Upwelling Ecosystems along with the California, Humboldt and Benguela zones. Coastal upwelling is an important biological process, as the water that is brought to the surface is nutrient rich - potentially in excess of 1000 parts per million carbon dioxide (CO_2) content - which acts a photosynthetic carbon source for phytoplankton: the primary producer in the coastal food chain (Capone and Hutchins, 2013). Coastal upwelling regions are among some of the most biologically-productive regions in the world, covering approximately 1% of the total ocean surface but accounting for over 20%

[4] The Representative Concentration Pathways are four Greenhouse Gas concentration trajectories which were chosen as forcing scenarios for the Global Climate Model runs as part of the Coupled Model Intercomparison Project Phase for the IPCC AR5. The four scenarios vary, with RCP2.6 the least severe scenario with (theoretical) emissions peaking in the 2040s. Greenhouse Gas concentrations in the RCP4.5, RCP6.0 and RCP8.5 scenarios all continue to increase throughout the Twenty-First Century.

of the global fish catch (Pauly and Christensen, 1995), and this makes monitoring of their evolution an important requirement.

It has been identified that AGW may lead to an intensification of coastal upwelling due to an increase in along-shore coastal wind-speeds (Bakun, 1990). Research since the original hypothesis has identified that winds have increased in all major coastal upwelling zones except the northwest African region, where there are many contrasting studies suggesting either an increase, a decrease or no significant change in upwelling intensity across northwest Africa (Sydeman *et al.*, 2014). Many of the research papers (that are discussed in Section 6.2) have conclusions based on only one or two primary data sources and specific spatial and temporal limits. Due to the limitation of the wider literature, it was identified that there was an opportunity, by using as many available data sources as possible and carefully considering the temporal period to analyse, to reduce the uncertainty regarding changes in coastal upwelling across northwest Africa, such that the final research objective of this thesis is to:

5. Test whether the Upwelling Intensification Hypothesis can be verified across northwest Africa

Chapter 6 describes in detail the approach taken, which is essentially the use of seven primary wind-speed datasets, supported by analysis of SSTs, meteorological-station data and oceanic-reanalysis in order to determine seasonal-scale changes in coastal upwelling across northwest Africa since 1981. The findings of this chapter results in a modification of the 'upwelling intensification hypothesis' for northwest Africa.

The overriding aim of this thesis, which binds the above objectives together, is to gain a greater understanding of the climate of the Macaronesian geographical region. Consistent with the research aims described above are the contributions of this thesis to the wider climatological literature, which are as follows:

1) The creation of a daily-resolution NAO back to 1850 (Chapter 3) (CHVJ15)
2) An analysis of the temporal variability of the winter NAO, highlighting recent dramatic changes. (Chapter 3) (H15)
3) An analysis of the spatial relationship of NAO and Macaronesian climate. (Chapter 3)
4) The creation of long-term monthly-resolution Macaronesian time series and an analysis into the current and historical climate of the Macaronesian Islands. (Chapter 4) (CH14)
5) A summary of potential future climate change scenarios across the Macaronesian Islands. (Chapter 5) (C13)

6) Characterisation of the spatial-temporal trends in coastal upwelling across the northwest African coastline. (Chapter 6) (CHB14)

In summary, the structure of the research component of this thesis, after the introductory chapter is as follows:

Chapter 2: Description of data and methods used throughout this thesis.
Chapter 3: North Atlantic Oscillation and Trade Wind Index
Chapter 4: Historical/modern climate of Macaronesia
Chapter 5: Future climate of Macaronesia
Chapter 6: Coastal Upwelling across northwest Africa
Chapter 7: Conclusions and suggestions for future research

The structure was chosen, primarily based on the optimal way to separate different aspects of the physical climate system that were analysed. Essentially, the climate system can be deconstructed into two major mechanics: thermodynamics and dynamics (circulation). Many expected or robust changes in climate science are based upon the thermodynamic component, e.g. increasing global temperatures as AGW alters the planetary energy balance, whilst many of the unknowns are based on the circulation-based aspects, e.g. 'weather' in general and modes of circulation variability such as the NAO (Shepherd, 2014). As the NAO is fundamentally a circulation-based phenomenon, and also a critical climate phenomenon endemic to and strongly influencing Macaronesia, it is logical to begin the thesis with the major research chapter on the NAO. The analysis of the main climate variables, temperature and precipitation, which reflect the climate of Macaronesia, follow the NAO chapter, so that the discussed relationships in Macaronesian climate relative to the NAO can be more naturally connected. The analysis of climate model output and the projected changes across Macaronesia by the end of the Twenty-first Century logically follow the analysis of the previous chapter. The final research chapter analyses air-sea interaction eastward of the Macaronesian Islands by testing the coastal upwelling intensification hypothesis along the northwest African coastline. The concluding chapter offers an overall summary of the thesis and suggests potential directions for future work.

2. Methods & Data

This chapter explores the data sources and methods used in this thesis. Throughout the various sections, several statistical methods are illustrated. Symbols and notation should be thought of as 'carrying through' to the next equation, unless otherwise stated. Unless clearly stated, the listed methods assume central limit theorem (i.e. an approximate Gaussian / 'normal' distribution of data). Some methods or modes of analysis in the thesis that don't require a significant mathematical explanation are introduced in the text as they are referred to, but most analyses are discussed below. During subsequent chapters, all methodological and data source comments relate back to the contents of this chapter.

2.1 Standard Methods Overview

Below are a collection of standard methods used in the atmospheric sciences that are applied in this thesis, the variable notation carries through and most formulae are described as in Wilks (2011).

Mean

Any reference to the 'mean' refers to the arithmetic mean, which is defined as:

$$\overline{x} = \frac{1}{n}\sum_{i=1}^{n} x_i, \qquad \text{Eq. } \mathbf{2.1.1}$$

where $\overline{x}$ is the arithmetic mean and n is the number of x values. For this thesis and climate science in general, the mean is used to define the climatology, which is typically the mean value of a meteorological variable across x amount of years (usually 30). The deviations from $\overline{x}$ at x_n are known as anomalies (see normalisation). Climatological time series are frequently displayed as anomalies, rather than absolute values, to allow a clearer interpretation of time series evolution.

Standard Deviation

The Standard Deviation σ (referred to as SD in the text hereafter) measures the dispersion of values around the mean. It is sensitive to outliers, and under the assumption

of normality, 68/95/99.7% of data values are expected to be inside ±1/2/3 SD's of the mean.

$$\sigma = \sqrt{\frac{1}{n-1}\sum_{i=1}^{n}(x_i - \overline{x})} \qquad \text{Eq. } \mathbf{2.1.2}$$

Normalisation

Normalisation (also known as the standardised anomaly) is the process of dividing anomalies by the SD. This process is used, for example, when it is desirable to compare two time series that have a different mean and SD.

$$z = \frac{x - \overline{x}}{\sigma_x} = \frac{x'}{\sigma_x}, \qquad \text{Eq. } \mathbf{2.1.3}$$

where x' is the anomaly and z is the standardised anomaly. The NAO index, when calculated using meteorological-station data, uses normalised values to prevent the larger variability from the Icelandic node dominating the index.

Covariance and Correlation

If there are two different variables, x and y, for which observations were made at the same time, these variables are classed as 'paired' and it is possible to examine the association between these two series (i.e. if changes in x are related to changes in y) by analysing the covariance of the two series:

$$Cov(x,y) = \frac{1}{n}\sum_{i=1}^{n}(x'y'), \qquad \text{Eq. } \mathbf{2.1.4}$$

where *Cov(x,y)* is the covariance and x'/y' are the anomalies of x and y. The value of the covariance will be dependent on the magnitude of values in the raw data, so typically, the correlation is preferred to the covariance in climate science as the correlation coefficient r_{xy} is bounded between $-1 \leq r_{xy} \leq 1$. The first way to determine the correlation between two variables (Pearson Correlation) is:

$$r_{xy} = \frac{Cov(x,y)}{\sigma_x \sigma_y}, \qquad \text{Eq. } \mathbf{2.1.5}$$

the main limitations of Pearson Correlation are the influence of outliers, trends and the assumption of linearity. The correlation coefficient squared r^2_{xy} is known as the coefficient of determination and describes the proportion of variability of y that is linearly accounted for by x. Often the r^2_{xy} (hereafter, r^2) value is cited as the amount that 'x explains y', but care is needed in interpreting the 'explanation' and should be linked to the physical mechanisms at work (inferred from what the time series x and y are measuring). An alternative way to calculate the correlation coefficient is the Spearman Rank Correlation r_{rank}, where the x and y values are replaced by the rank of the values:

$$r_{rank} = 1 - \frac{6\sum_{i=1}^{n} D_i^2}{n(n^2-1)}, \qquad \text{Eq. } \mathbf{2.1.6}$$

where D_i is the difference in ranks between the *ith* pair of x and y values. This approach is non-parametric (does not assume a normal distribution), does not assume linearity and is less sensitive to outliers. Throughout this thesis, correlation values are reported as the Pearson Correlation Coefficient r_{xy}, and time series are always detrended (Section 2.2) before calculating r-values unless otherwise stated (which removes the linear component of a change over time that can bias the correlation towards stronger values). Whilst not reported, any correlation analysis is also repeated using Eq. 2.1.6 to verify that the r-values do not change significantly as a result of methodology.

Cross Correlation

Cross correlation allows the examination of r_{xy} when one of either x or y is shifted by k time steps forwards or back in time i.e. for testing for a 'leading' or 'lagged' relationship (for example, to compare January temperature with February precipitation). Additionally, the cross correlation of a time series with itself allows one to determine its persistence characteristics (i.e. its autocorrelation) which is important to know when determining the significance of temporal trends (Section 2.2.2). The autocorrelation (presented here for x, but this is also applicable as the cross correlation for x and y) r_k at lag k is given as:

$$r_k = \frac{\sum_{i=1}^{n-k}((x_i - \overline{x}_-)(x_{i+k} - \overline{x}_+)}{(\sum_{i=1}^{n-k}(x_i - \overline{x}_-)^2)^{1/2}(\sum_{j=k+1}^{n}(x_i - \overline{x}_+)^2)^{1/2}}, \qquad \text{Eq. } \mathbf{2.1.7}$$

where $-$ and $+$ subscripts are the sample means across $n - k$ values (as shifting the time series by the *kth* step results in k fewer paired data points). For assessing autocorrelation, r_0 always =1, and the lag-1 autocorrelation is the most frequently used statistic ($k = 1$), but the first few values are also of interest as these values provide important information regarding a time series persistence. A series is typically classified as 'white-noise' in the

absence of autocorrelation or 'red-noise' when autocorrelation is present. When interpreting the cross correlation between two paired series, as before, care must be taken in assigning a realistic physical mechanism to any observed strong lead/lag relationships, as shifting a time series will invariably lead to spuriously high r-values.

Linear Regression

Linear regression models the relationship between a dependent variable y and one or more independent variables x (i.e. regression allows the user to determine an approximate value of y, given x). Given the paired dataset (x, y) (least-squares- or 'ordinary'- linear) regression aims to create the line that best fits the data by minimising the sum of the squared errors (i.e. limiting the overall deviation from the line) such that:

$$\hat{y} = a + bx, \qquad \text{Eq. } \mathbf{2.1.8}$$

where $\hat{y}$ is the predicted value of y given the constant (intercept) a and parameter vector (slope) b. The divergences of the real y values from the best fit line are defined as residuals, where:

$$e_i = y_i - \hat{y}(x_i), \qquad \text{Eq. } \mathbf{2.1.9}$$

and,

$$\sum_{i=1}^{n} e_i = 0, \qquad \text{Eq. } \mathbf{2.1.10}$$

so that there is a residual e_i for each data pair and the sum of all the residuals is equal to zero. Linear regression in this format (hereafter, OLS) assumes linearity, no error in x and residuals that have a constant variance (homoscedastic) and are independent (i.e. not autocorrelated). In climate science these assumptions are often invalidated. Using precipitation as an example, it is unlikely that the SD of a monthly 20 mm precipitation total will be similar to a month where the mean precipitation is 200 mm (i.e. heteroscedastic variance). Furthermore, monthly temperatures often display strong traits of autocorrelation, which results in unevenly distributed (autocorrelated) residuals. Heteroscedasticity in the above example can be countered by drawing on populations with a similar distribution (i.e. examining seasonal instead of monthly values) or transforming the data so that they better resemble the normal distribution. Autocorrelation does not affect the value of the line of best fit, but does affect how the significance of the regression is assessed, which is introduced below and discussed further

in section 2.3.2. OLS is used throughout this thesis to detrend time series (i.e. subtracting the calculated trend from the time series, so that the overall trend of the new series will = 0), which is a necessary preliminary approach before certain analyses.

Assessing Significance – Correlation

The correlation coefficient (r) is determined to be statistically significant if the r-value exceeds what one would expect 'by chance' or 'within the realms of natural variability', given n samples. This is commonly computed using the Student's T-Test. Where the (two-tailed) t-statistic (t) is given by:

$$t = r\sqrt{\frac{(n-2)}{(1-r^2)}} \qquad \text{Eq. } \mathbf{2.1.11}$$

The result is then compared against values from standard t-tables to determine if t exceeds the critical t value, given the number of degrees of freedom (DF) minus two (n - 2) and required likelihood of the event not occurring by chance (i.e. significance level). The normal benchmark for statistical significance is a 95% chance the relationship cannot occur naturally (written as $p < 0.05$), with 90% ($p < 0.1$) as the minimally accepted requirement and above 99% ($p < 0.01$) as a high level of significance.

Assessing Significance – Linear Regression

For assessing the significance of a regression relationship, it needs to be determined if the slope (b) of the best fit line is significantly different from zero. Again, this draws upon the t-statistic, but in a slightly different form (the t-statistic in its various forms is usually a ratio, dividing the 'hypothesis value' by a scaling parameter). Firstly, the standard error SE of the regression line SE_y needs to be known:

$$SE_y = \sqrt{\sum_{i=1}^{n}(e_i)^2/n-2,} \qquad \text{Eq. } \mathbf{2.1.12}$$

and the t-statistic is given by

$$t = b/SE_y, \qquad \text{Eq. } \mathbf{2.1.13}$$

and the same procedure as before is used to determine if a statistically significant value has been obtained.

2.2 Linear-Least Squares Regression

Linear regression was introduced in the previous section. In this thesis, the method is used for three different purposes: for splicing together of overlapping time series (Hanna *et al.*, 2006), for detrending time series prior to subsequent analysis and for trend estimation and significance. In this section it is documented how the method allows the construction of a single time series from many fractured records (regression splicing) followed by a closer look at the significance of linear regression for climatological time series, given that not all data satisfy the basic assumptions of OLS.

2.2.1 Splicing

Envisage a location where a continuous record of climate data (e.g. monthly temperature) does not exist; assessing modern climate change relative to the recent past would be quite challenging, as a consistent record is necessary to examine change in a time series. However, if at that location, two or more records exist that (taken together) do cover the entire required observing period (e.g. 1900-2012), then it would be possible to combine these records to create a consistent long term time series. For example, at a specific location, taking two hypothetical time series, the first from meteorological-station A has a record (e.g. temperature) running from 1900-1970 and meteorological-station B started recording in 1950 and ends in 2012. These two stations that recorded temperature were quite close (e.g. $<$ 50 km apart) and within a similar altitudinal band (so there is likely to be a strong linear relationship between them). Given their close proximity and the 21 years of overlap, it is possible to use OLS to splice together the records and create a continuous time series. In this case the dependent (y) variable is meteorological-station B and the independent (x) variable is meteorological-station A. This then allows the relationship between meteorological-station A and B to be established, so that the two records can be seamlessly joined together and a continuous time series (with all measurements scaled to station B) to be created. This process is illustrated in Figure 2.1.

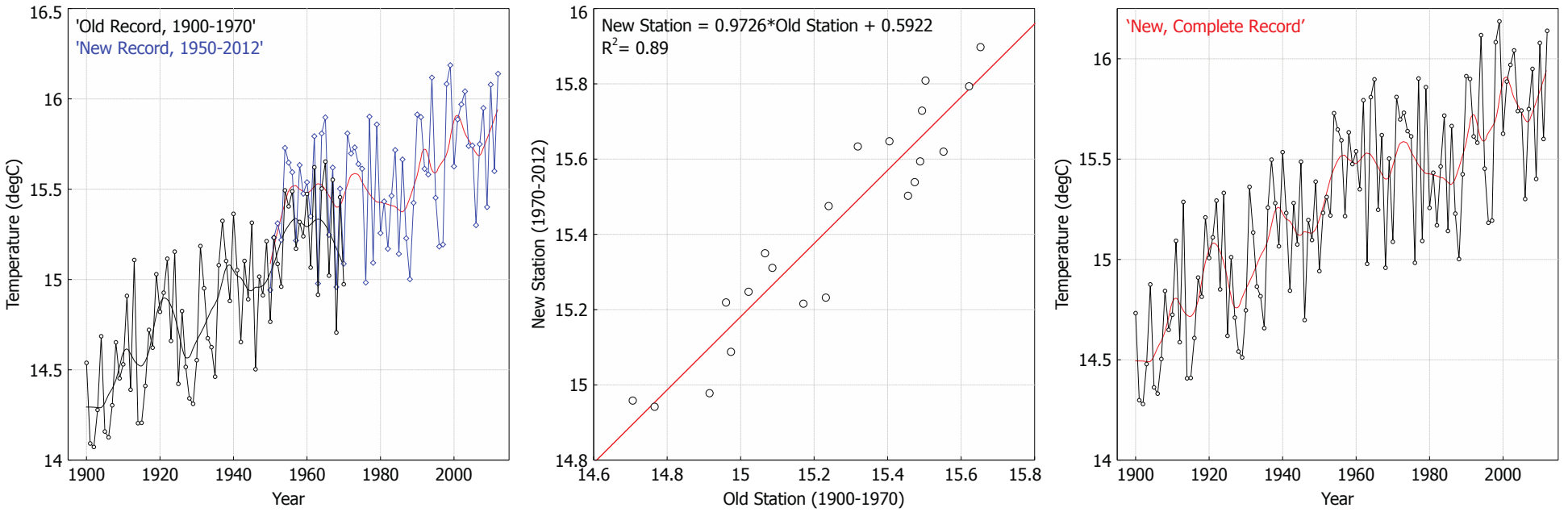

Figure 2.1. Graphical representation of the regression splicing process adopted to two artificially generated time series. The strong relationship between the separate 'Old' and 'New' record across their common overlap period allows a continuous record to be created that is unaffected by any systematic difference between the previous two records.

2.2.2 Trend Estimation & Significance

OLS trend estimation and significance were introduced in Section 2.1. This section documents how revised estimates of trend and significance are produced, given the nature of many climatological time series to display strong traits of autocorrelation. Autocorrelation is the cross correlation of a time series with itself, and the presence of autocorrelation can invalidate the t-statistic for significance of the regression slope - making the significance values 'too conservative' (Santer *et al.*, 2000). To overcome the problem, for each time series analysed using OLS in this thesis, the autocorrelation (ϕ) of the residuals (e_i) of the trend estimate are examined. If the time series are significantly autocorrelated, corrections to the SE_y and effective degrees of freedom $DF_{adjusted}$ based on the structure of the autocorrelogram are applied.

If, at lag-1, the residuals display no significant autocorrelation then no adjustments to the SE and DF are made (and the 'normal' procedure described in Section 2.1 is adopted); however if the lag-1 autocorrelation (r_1) is significant, it is assumed that the data follow a first order autoregressive AR(1) structure. To account for this, firstly the $DF_{adjusted}$ is calculated, based on the number of data points n:

$$DF_{adjusted} = n\left(\frac{1 - r_1}{1 + r_1}\right), \qquad \text{Eq. } \mathbf{2.2.1}$$

then the standard error is adjusted by assuming a number of data per effective degree of freedom k under an AR(1) process (as in Foster and Rahmstorf (2011)), which is given as:

$$k = \left(\frac{1 + \phi}{1 - \phi}\right), \qquad \text{Eq. } \mathbf{2.2.2}$$

here (ϕ) is the lag-1 value of the time series autocorrelation (r_1). Then, the square root of k is then multiplied by the original standard error to give the adjusted standard error:

$$SE_{adjusted} = SE\sqrt{k}, \qquad \text{Eq. } \mathbf{2.2.3}$$

The $SE_{adjusted}$ then replaces the original SE in the Student's t-test, and the $DF_{adjusted}$ taken into account when determining significance. However, sometimes the autocorrelation structure is more pronounced, i.e., it differs from a typical AR(1) process (which assumes an exponential decay) and there is still significant autocorrelation in the residuals of the trend estimate at or beyond lag-2. When this occurs, corrections are

applied to the SE as if the residuals are structured as an ARIMA(1,1) process (AutoRegressIve Moving Average), which changes the estimated number of data per effective degrees of freedom to:

$$k = 1 + \frac{2r_1}{(1-\phi)}, \qquad \text{Eq. } \mathbf{2.2.4}$$

where the autocorrelation (ϕ) is taken as:

$$\phi = \frac{r_2}{r_1} \qquad \text{Eq. } \mathbf{2.2.5}$$

and ϕ from Eq. 2.2.5 replaces r_1 in Eq. 2.2.2. A broad generalisation can be made of certain types of climatological time series. Higher resolution (i.e. daily / monthly) series display traits of autocorrelation more frequently than seasonally or annually sampled time series, with certain variables (e.g. SAT, SST) more frequently displaying traits of serial dependence than others (e.g. precipitation and climate indices). Confidence intervals (when given) around the trendline are given as $\pm SE_{adjusted}$ (so intuitively, will be wider around 'red' time series).

2.3 Theil-Sen Slope Estimator

The Theil-Sen (TS) slope estimator serves as an alternative regression method to OLS (Theil, 1950; Sen, 1968). The approach is non-parametric (does not assume a normal distribution) and less sensitive to outliers as it is based on the median value of all data pairs. The regression equation is the same as Eq. 2.1.8 and the median slope b_{ij} is defined as (Jain and Kumar, 2012):

$$b_{ij} = \frac{(y_j - y_i)}{(x_j - x_i)} \; for\; i = 1\; to\; n-1\; and\; j = 2\; to\; n, \qquad \text{Eq. } \mathbf{2.3.1}$$

where the total number of possible slopes N_p is given as:

$$N_p = \frac{n \times (n-1)}{2}, \qquad \text{Eq. } \mathbf{2.3.2}$$

and the slopes are ranked and the median value taken as b. The intercept a is given as (Conover, 1980):

$$a = y_{median} - (b \times x_{median}) \qquad \text{Eq. } \mathbf{2.3.3}$$

according to Granato (2006), the TS regression test underperforms OLS when all the assumptions of OLS are satisfied (but TS regression is 'almost as efficient'). However, TS regression out-performs OLS when the basic OLS assumptions are falsified (Vannest *et al.*, 2011) with an example of this displayed in Figure 2.2. TS regression is used in this thesis as the principal method of regression for data that do not meet the standard OLS criteria (Section 2.1), with the main application being precipitation time series. It is additionally calculated for any time OLS is used as an extra quality control check on trend results, but only reported if there is a significant difference between the two methods.

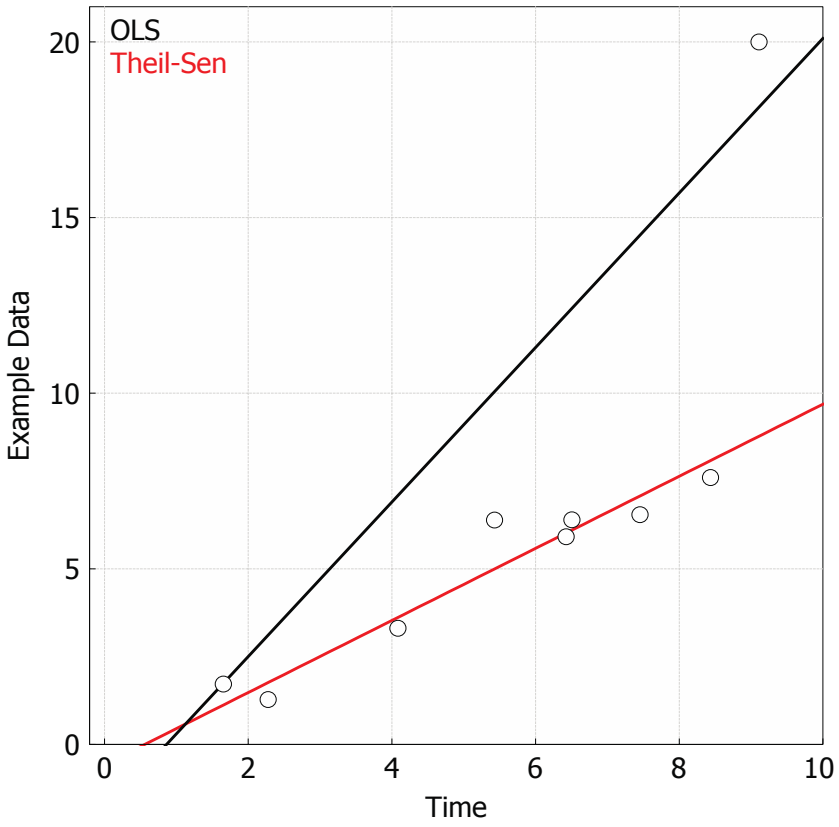

Figure 2.2. Graphical illustration of the difference between OLS and TS regression given a significant outlier in a short time series.

2.3.1 Mann-Kendall trend test

The significance test associated with TS regression is the Mann-Kendall (MK) trend test (Kendall, 1938; Mann, 1945). This is because all the possible data pairs are considered in the calculation and like the Spearman correlation, data are ranked (so the test is non-parametric), with the test statistic S given as:

$$S = \sum_{i=1}^{n-1} \sum_{j=i+1}^{n} sgn(x_{i+1} - x_i), \qquad \text{Eq. } \mathbf{2.3.4}$$

with,

$$sgn(x_j - x_i) = \begin{cases} +1, if\ x_j - x_i > 0 \\ 0, if\ x_j - x_i = 0 \\ -1, if\ x_j - x_i < 0 \end{cases}, \qquad \text{Eq. } \mathbf{2.3.5}$$

so, if an (example) annual climate time series x are ordered by the yearly values i and the difference between each data pair (i, j) is given a value of 1 if j is greater than i, 0 if the same and -1 if lower. Therefore, in the case of no trend, we would expect the mean of equation 2.3.5 to be zero. The variance of the S-statistic σ_S is given as:

$$\sigma_S = \frac{n(n-1)(2n-5) - \sum_{k=1}^{K} t_k(t_k-1)(2t_k+5)}{18}, \qquad \text{Eq. } \mathbf{2.3.6}$$

where K indicates the number of groups of repeated values and t_k is the number of repeated values in the *kth* group (this is to adjust the variance estimate for the times when $x_j - x_i = 0$, i.e. when the data pairs are tied). Subsequently, the significance of the test is evaluated against standard z-tables, where the z-score is:

$$z = \begin{cases} \frac{S-1}{\sqrt{\sigma_S}}, S > 0 \\ 0\ if\ S = 0 \\ \frac{S+1}{\sqrt{\sigma_S}}, S < 0 \end{cases}, \qquad \text{Eq. } \mathbf{2.3.7}$$

as with the t-test of the slope in OLS, autocorrelated residuals can affect the significance estimate of the trend using the MK approach. Two methods are additionally applied throughout the thesis (calculated alongside the original MK test) that deal with the serially dependent distribution of residuals as described in Hamed and Rao (1998) and Yue and Wang (2002). The two methods apply a different way of parameterising the variance dependent on the degree of autocorrelation that modifies the resulting z values and gives less conservative significance estimates. Typically, the Hamed and Rao (1998) methodology returns fewer results where a significant value is obtained.

2.4 Principal Component & Empirical Orthogonal Functions

So far, the methods illustrated have been primarily for 'univariate' one-dimensional time series. As mentioned in Section 1.2, climate data often exist in the x, y, z, t format. It is possible to analyse their temporal and spatial evolution by applying simple univariate statistics at the grid-box scale and gain a significant amount of insight (into the nature of the evolution of the 3- or 4- dimensional field). Frequently, more 'advanced' methods suitable for application on gridded datasets are employed in the climate sciences. Principal Component (PC) and Empirical Orthogonal Function analysis (EOF) (named interchangeably but essentially representing the same calculations) are a multipurpose tool, designed to break a three-dimensional space-time field $X(t,s)$ down into a number of (static) spatial patterns $U_k(s)$, classified here as the 'EOF's that are each associated with a temporal expansion $C_k(t)$, classified here as the 'PC's. So the M modes of variability in field X are summarised as:

$$X(t,s) = \sum_{k=1}^{M} C_k(t) U_k(s), \qquad \text{Eq. } \mathbf{2.4.1}$$

where the first mode corresponds to the first spatial pattern (EOF1) and its temporal expansion (PC1). In practice, this is achieved using the S-Mode analysis method described by Björnsson and Venegas (1997), where a 3-dimensional space-time field X is displayed as:

$$X = \begin{bmatrix} x_{11} & x_{12} & \dots & x_{1p} \\ x_{21} & x_{22} & \dots & \dots \\ \vdots & \vdots & \ddots & \vdots \\ x_{n1} & \dots & \dots & x_{np} \end{bmatrix}, \qquad \text{Eq. } \mathbf{2.4.2}$$

where X is the matrix (n x p) of n columns by p rows. Here, row p is the 'map' (i.e. a latitude-longitude field of climate data) and column n is a time series of p by location (i.e. grid-box). Throughout this thesis, the matrix X is formed using anomalies (Eq. 2.1.1) that are linearly detrended (Section 2.1). Then, the covariance matrix (Eq. 2.1.4) of X is taken as:

$$S = \frac{1}{n} X^t X, \qquad \text{Eq. } \mathbf{2.4.3}$$

(where X^t is the transpose of X) then, S is decomposed such that:

$$SC = C\Lambda, \qquad \text{Eq. } \mathbf{2.4.4}$$

where Lambda is the static spatial pattern $U_k(s)$ (known as 'eigenvalues', here representing the 'EOF's) and C is the expansion coefficient $C_k(t)$ (known as eigenvectors, here representing the 'PC's). Each eigenvalue λ_i corresponds to a measure of the fraction of the total variance in S (given in percentage as the value of each eigenvalue divided by the sum of all eigenvalues). So once all the eigen-elements are determined (Eq. 2.4.4), the eigenvalues are sorted in order $(\lambda_1, \lambda_2, \ldots \lambda_p)$, so that λ_1 (EOF1) explains the greatest source of variance in the field, and how it evolves over time is given by c_1 (PC1). The eigenvalues are the (linear) attempt to find the maximum variance in the field and are uncorrelated with each other in space (Hannachi *et al.*, 2007). If the goal of EOF analysis was to utilise many EOFs, then this would pose a problem (as climatic processes are often correlated in space and time) and more advanced methods would have to be applied, however the use of EOF analysis in this thesis is to characterise only the leading mode of variability in SST and SLP across the Atlantic (the AMO and NAO), so 'normal' EOFs are sufficient.

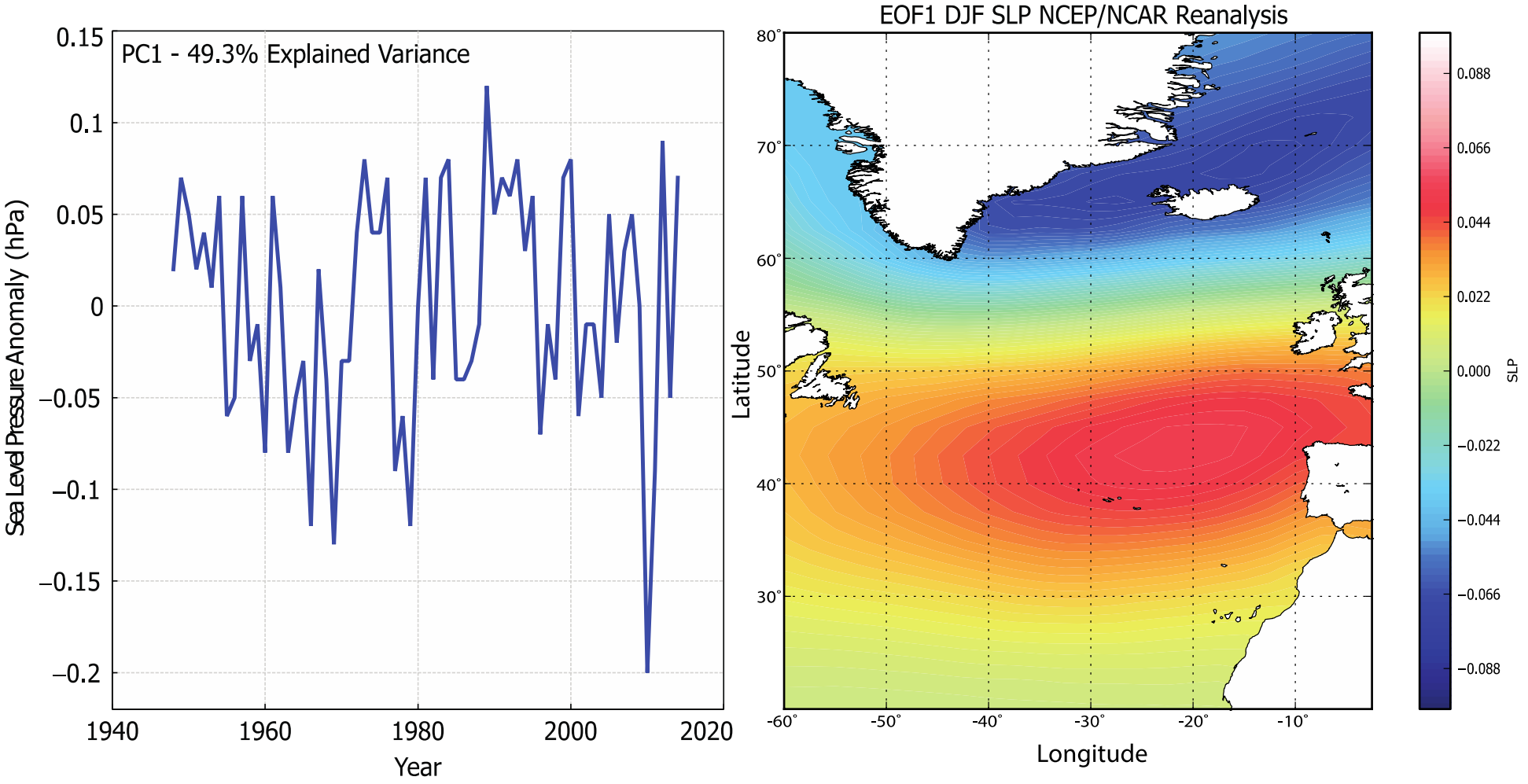

Figure 2.3. The leading (PC1 and EOF1) PC and EOF of SLP (detrended anomalies, weighted by the cosine of the latitude) from the NCEP/NCAR reanalysis for winter (DJF) 1948-2012. This spatial pattern and corresponding time series reflects the NAO (Section 1.3.2).

2.5 Homogeneity Testing

This section presents the various homogeneity tests used in this thesis in order to ensure that changes in climatic time series are not due to any form of bias that would reflect non-climatic changes. Conrad and Pollack (1962) define homogeneity as:

"A numerical series representing the variations of a climatological element is called 'homogeneous' if the variations are caused only by variations of weather and climate"

Non-climatic changes can be due to instrument degradation and replacement, a change in location of the observing station, changes in the surrounding conditions of the observation location (as rapid changes or slow processes over time), changes in observation practises and post-observation data degradation/corruption and how it is post-processed (Aguilar *et al.*, 2003). A logical first step when analysing a new climate time series for the first time is to plot the data and undertake a basic quality control analysis. This enables the user to initially subjectively assess the time series (large discontinuities will stand out) and eliminate or identify errors or issues due to factors such as changing units, unrealistic values and missing data. Once the basic quality control is completed, tests should then be run to determine any potential inhomogeneities (Costa and Soares, 2009). An overview of the available tests widely used in homogenising time series and best-practice advice is given by Peterson *et al.*, (1998), Aguilar *et al.*, (2003) and Reeves *et al.*, (2007). Convention would dictate that application of multiple tests is the most prudent method. A popular choice (e.g. Morozova and Valente, 2012; Kang and Yusof, 2012) is to apply the Standard Normal Homogeneity Test, the Pettitt Test, the Buishand Range Test and the Von Neumann Ratio to each series being tested (Buishand, 1982; Pettitt, 1979; Alexanderson, 1986). This thesis follows a similar approach and also makes use of the Penalised Maximum F-Test (Wang, 2008a, b; Wang *et al.*, 2010; Wang and Feng, 2013).

A problem that became evident quite early on from analysing the available climatological data for Macaronesia (sources listed in Section 2.10) was a lack of 'metadata' – information regarding any significant (non-climatic) changes in the station. When metadata are available, assessing potential changes in a climatological time series is more straight-forward (e.g. if a station is known to have changed in altitude by 200 m, and suddenly its pressure values are a few hPa lower, one may more confidently assume that this difference is due to the altitude shift rather than a real climatological change). Without metadata, assessing whether or not identified change points are real is a greater challenge. Certain elements that are included can help ease assessment of whether

changes need to be made. For example a gap of over a few months in the historical record is a likely indicator of some form of change. If a station record contains more than one variable, one can see if gaps or obvious changes in the variables are synchronous (potentially indicative of a shift in station location, although if only present in one variable it could be just a single instrument change). Knowledge of the general historical global and regional climate is also advantageous. For example, some test statistics may identify elements of natural variability that can cause sharp rises or falls in a time series. Strong El Niño years such as 1998, which lead to a large positive (global) SAT anomaly and volcanic eruptions such as Agung, El Chichón or Pinatubo which cause negative anomalies may trigger false positive test results. As such, knowing when not to apply corrections is just as important as knowing when to apply them.

Homogeneity testing is typically achieved by either the 'relative' or 'absolute' method. The relative method uses a nearby station with a record that is deemed 'homogenous' as a baseline for implementing changes in the candidate record. Given how climatic zones can change quite variably on an individual Macaronesian Island or between Islands (Section 1.2), it becomes quite obvious that finding ideal stations for the relative method would be difficult, given a typical density of one to two stations per island (Chapter 4) – although this can depend on the variable analysed – SLP will typically have quite a large decorrelation scale (up to hundreds of kilometres (Cornes, 2010)), followed by temperature, whereas precipitation can be highly variable across a few kilometres. Suitable candidate series do indeed turn out to be rare for the Macaronesian Islands; therefore, the absolute method of testing for homogeneity is favoured throughout this thesis. The absolute method has a test hypothesis H_A of a significant change or break in the time series at point i in time and a H_0 of an independent, identical distribution, i.e. no significant inhomogeneity (Wijngaard *et al.*, 2003).

In addition to the test statistics described below, tested time series were always subjected to more 'simple' analyses, including running-variance (of different window lengths) and visual analyses. The tests and 'simple' analyses are repeated at various scales (daily, monthly, seasonally and annually) to help identify potentially robust changes (only at the daily resolution for the Penalised Maximum F-Test, as the 'traditional tests' are sub-optimal at below monthly scales). Ultimately the goal of homogeneity is to attain the 'real' (or as close as possible) climate record, but unless it appeared that altering a time series was necessary, then adjusting the raw data as little as possible was favoured throughout.

Notation and critical values are derived from Wijngaard *et al.* (2003), unless otherwise stated.

Standard Normal Homogeneity Test

The Standard Normal Homogeneity Test (SNHT) is essentially the 'normalised score' test. It assumes a normal distribution and is more sensitive to breaks at the start or end of a series. The statistic *T(k)* compares the means of the first k years of the record with the last $n - k$ years such that:

$$T(k) = kz_1^{-2} + (n-k)z_2^{-2}, k = 1, \dots, n, \qquad \text{Eq. } \mathbf{2.5.1}$$

where,

$$\bar{z_1} = \frac{1}{k}\sum_{i=1}^{k}(Y_i - \bar{Y})/\sigma \; and \; \bar{z_2} = \frac{1}{n-k}\sum_{i=k+1}^{n}(Y_i - \bar{Y})/\sigma. \qquad \text{Eq. } \mathbf{2.5.2}$$

When a break is located at time step K, *T(k)* reaches a maximum near $k = K$. With the test statistic T_0 defined as:

$$T_0 = \max_{1 \le k < n} T(k) \qquad \text{Eq. } \mathbf{2.5.3}$$

If T_0 exceeds the critical value (that is dependent on n), then H_0 is rejected and the break is assumed significant. This process is then repeated on the fragmented time series until $T_0 <$ the critical test value.

Pettitt Test

Like Spearman's rank correlation, the Pettitt test is rank $(r_1, \dots, r_n)$ based (and does not assume a normal distribution), where the statistic X is given as:

$$X_k = 2\sum_{i=1}^{k} r_i - k(n+1), k = 1, \dots, n, \qquad \text{Eq. } \mathbf{2.5.4}$$

and as for the SNHT, the test statistic is maximum near time step K, and compared to critical values and reapplied on the fragmented time series as before.

Buisand's Range Test

The Buishand test is a variant of 'cumulative sums from the mean', with the test statistic S^* defined as:

$$S_k^* = \sum_{i=1}^{k}(Y_i - \bar{y}), k = 1, \dots, n, \qquad \text{Eq. } \mathbf{2.5.5}$$

and,

$$R = (\max_{0 \le k \le n} S_k^* - \min_{0 \le k \le n} S_k^*)/s. \qquad \text{Eq. } \mathbf{2.5.6}$$

The Von Neumann ratio was also applied to each series along with the SNHT, Pettitt and Buishand tests, but the test is not location specific (does not indicate where the break occurs) and returned a positive result for nearly tested time series (false positive) so was not relied upon as a decision-making test statistic.

Penalised Maximum F-Test

The Penalised Maximum F-Test (PMF) is based on a two-phase linear regression model where each regression line is set to meet at each point in a time series and the year with the lowest residual sum of squares is identified as a discontinuity. The process is repeated on the sub-series until all discontinuities are realised (Costa and Soares, 2009). Wang (2008a, b) defines the H_0 of the test as:

$$H_0: X_t = \mu + \beta t + \varepsilon_t, t = 1, \dots, N, \qquad \text{Eq. } \mathbf{2.5.7}$$

where time series X_t has mean μ, trend β and zero-mean randomly distributed error ε. The H_A of the test is that at time t=k a break point c exists because $\mu_1 \neq \mu_2$ as:

$$H_A: \begin{cases} X_t = \mu_2 + \beta t + \varepsilon_t, t \le k \\ X_t = \mu_2 + \beta t + \varepsilon_t, k - 1 \le t \le N \end{cases}, \qquad \text{Eq. } \mathbf{2.5.8}$$

and the significance of the test (whether or not to adopt an identified break point) is assessed by the F statistic:

$$F_c(k) = \frac{SSE_0 - SSE_A}{SSE_A/(n-3)}, \qquad \text{Eq. } \mathbf{2.5.9}$$

where the sum of squared residuals SSE_0 is given as:

$$SSE_0 = \sum_{t=1}^{N} (X_t - \hat{\mu}_0 - \hat{\beta}_0 t)^2, \qquad \text{Eq. } \mathbf{2.5.10}$$

and,

$$SSE_A = \sum_{t=1}^{N}(X_t - \hat{\mu}_1 - \hat{\beta}t)^2 + SSE_0 = \sum_{t=k+1}^{N}(X_t - \hat{\mu}_2 - \hat{\beta}t)^2. \qquad \text{Eq. } \mathbf{2.5.11}$$

The F statistic is evaluated against a critical value table (Wang, 2008a). Subsequent moderations (Wang, 2008b) take into account autocorrelation and the algorithm (provided as an R package, RHTests v3) identifies all potential breakpoints and allows the users to select which ones are implemented (Wang and Feng, 2013).

2.6 Cubic Tension Spline

A spline is an interpolation function that fits a curve around a series of 'knots' (specified points in the series). A cubic spline with tension is used in this thesis as a means of creating a daily annual cycle from monthly data. A cubic tension spline is chosen because when interpolating down to the daily scale from monthly values, the value of the curve is such that for each individual month, the mean of the newly created daily data points are equal to the monthly value of the original data (Tveito *et al.*, 2001; Henriksen, 2003; Björnsson *et al.*, 2007; Björnsson 2013). This characteristic, which retains compatibility between monthly and daily time series, makes the cubic tension spline a valued interpolation method. Henriksen (2003) provides a detailed mathematical description of the tension spline methodology. Rather than repeat this across several pages here, the calculation code is included in the appendices (Figure B1). A brief example of the smoothing method is shown (Figure 2.4) and application of the tension spline is discussed in detail with respect to the daily NAO in Section 3.3.

The tension spline (Figure 2.4c) applied to the annual SLP cycle follows the low frequency variation in the data. The value of the curve for the 31 days in January is, when averaged, the same as the displayed January monthly value (and continues this way throughout the year). The 15-day running-mean and Locally-Weighted Regression (LOESS) trends generally appear to also fit the annual cycle well, but their daily averages for the month do not equal the monthly mean. The running-mean suffers from edge-effect degradation and the LOESS trends displays (arguably) too much high frequency variation. Of course the sliding parameter can be changed to higher-frequency values, but the ability of these two methods to accurately model the low frequency cycle degrades as this increases, highlighting the usefulness of the tension spline method.

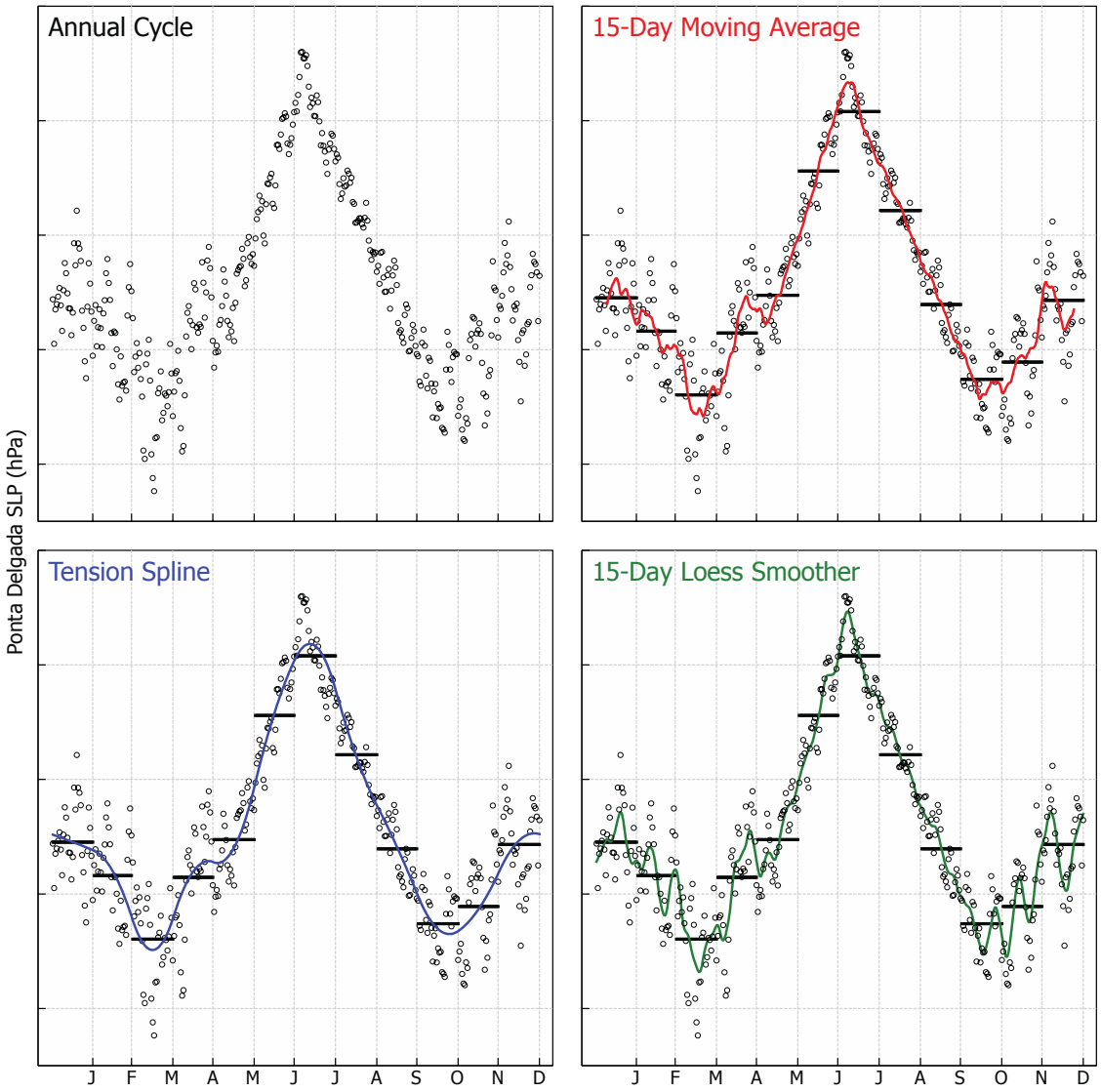

Figure 2.4. The (a) annual cycle of SLP data from Ponta Delgada, Azores (Chapter 3), with a (b) 15-day moving average (running-mean), (c) tension spline and (d) 15-day LOESS trend applied. Black horizontal lines indicate monthly means.

2.7 Probability Analyses

In this thesis, two types of probability analysis are used to determine the likelihood of a specific number of events occurring in a limited period of a time series that is due to chance (e.g. x above average precipitation seasons in a row, given n length time series and knowledge of the distribution of the data).

2.7.1 Monte Carlo

Suppose an approximately normally distributed, white noise time series. In the real series, there is a situation where seven of the highest ten values occur in a 15-year period. The

length of the series is known ($n = 100$ years) and the mean and variance of the series can be determined. It is then possible to randomly generate k series of n length of known mean $\overline{x}$ and variance σ^2, typically $k = 10{,}000$. From these randomly generated series, one can work out the number of times in each (sliding)-15-year period that seven of the top ten values occur. The ratio (probability) and/or percentage chance of the positive occurrences (seven of the top ten values do occur in the 15-year window) compared to the negative occurrences (less than seven of the top ten values occur in the 15-year window) can then be determined, and this information used to assess the probability of occurrence of extreme events in the original time series.

2.7.2 Hypergeometric Distribution

The Hypergeometric distribution is a discrete distribution with four properties.

N – the population size
K – the number of 'success-states' in the population
n – the number of draws made from the population
k ¬– the number of successful draws

such that the Hypergeometric probability P is given as:

$$P(X = k) = \frac{\binom{K}{k}\binom{N-K}{n-k}}{\binom{N}{n}} \qquad \text{Eq. } \mathbf{2.7.1}$$

Returning to the imaginary dataset as above, N would remain as 100, K would be ten (representing the ten highest values), n would be 15 (the number of years in which the high values occurred as from before) and k would be 7. After each (imaginary) draw, N decreases by one and k changes based on whether or not a success occurred. Using the example above, the probability of seven out of 10 high events occurring in a 15 year period is:

$$P(X = 7) = f(7; 100,10,15) = \frac{\binom{10}{7}\binom{90}{8}}{\binom{100}{15}} = 0.0000367$$

giving a 1 in ~27,000 chance of random occurrence, which would (in a real time series) merit further investigation. Realistically, the chance of getting eight, nine and ten out of ten high values should also be included in the probability estimate (the cumulative Hypergeometric probability), which reduces P to 0.0000381 or 1 in ~26,000. All

probability estimates are reported as the cumulative version throughout (including the Monte Carlo method).

2.8 Climatological Extreme Indices

The ETCCDI have developed a suite of temperature and precipitation-based indices to facilitate international collaboration with regards to analysis of extreme weather and climate events (http://etccdi.pacificclimate.org/). The indices are designed to be applied to daily temperature and precipitation (Table B1, B2). Such analyses have been undertaken for various individual countries or regions and a global dataset on a 5° resolution exists (Alexander *et al.*, 2006; Donat *et al.*, 2013). The Macaronesian Islands have not been included in any analyses, so a primary analyses is presented here, along with how the indices compare when calculated using reanalysis and model output from grid-boxes that override the islands (Chapter 4 and 5).

2.9 Ekman Transport & Coastal Upwelling

Chapter 6 of this thesis deals with the evolution of coastal upwelling across the NW Africa coastline in the Macaronesian region. No direct measurements of coastal upwelling exist, so it has to be estimated from variables (typically wind and SSTs, but it is also possible to 'infer' upwelling from chlorophyll concentrations and sea levels, which is an approach attempted in Chapter 6). A discussion of upwelling indices is provided in Section 6.2. Here, the index initially developed by Bakun (1973) is used. To calculate the upwelling index (Borja *et al.*, 1996; Gómez-Gesteria *et al.*, 2006; Santos *et al.*, 2012) the Ekman transport (Q) is derived from the wind-stress (τ) fields. Firstly, the zonal (τx) and meridional (τy) components of wind-stress are calculated from the wind-speeds (W = (Wx, Wy)), as:

$$\tau_x = \rho_a C_d \left(W_x^2 + W_y^2\right)^{0.5} W_x \; and \; \tau_y = \rho_a C_d \left(W_x^2 + W_y^2\right)^{0.5} W_y \qquad \text{Eq. } \mathbf{2.9.1}$$

then,

$$Q_x = \frac{\tau_y}{\rho_w f} \; and \; Q_y = \frac{-\tau_x}{\rho_w f} \qquad \text{Eq. } \mathbf{2.9.2}$$

where ϱ_a is the air density (1.22 kg m-3), ϱ_w the sea water density (1025 kg m^{-3}) and Cd the dimensionless drag coefficient, typically 1.3 x 10-3 (Schwing *et al.*, 1996). The Coriolis parameter, *f*, is defined as twice the component of the angular velocity of the Earth, Ω,

at latitude ϑ ($f = 2\Omega\sin(\vartheta)$, where $\Omega = 7.292 \times 10^{-5}$ s^{-1}). In turn, the UI^{W} can then be calculated as:

$$UI^{W} = -(\sin(\varphi - \pi/2)Q_x + \cos(\varphi - \pi/2)Q_y) \qquad \text{Eq. } \mathbf{2.9.3}$$

where φ is the mean angle between the shoreline and the equator. Using this index, positive (negative) values correspond to upwelling (downwelling) favourable conditions. The units of this index are $m^3 s^{-1} 100 m^{-1}$. A second commonly used method to derive coastal upwelling is based on the SST (along the same longitude) at the coast, compared to the SST across the open ocean. The SST upwelling index $UI^{\Delta SST}$ is defined as:

$$UI^{\Delta SST} = SST_{coast} - SST_{ocean} \qquad \text{Eq. } \mathbf{2.9.4}$$

where the SST_{coast} value is taken from the grid-box that is closest to the coastline and the SST_{ocean} is taken from the grid-box that is 5° west along the same latitude. With this index, a decrease (increase) in the $UI^{\Delta SST}$ is equivalent to an increase (decrease) in upwelling intensity. The assumptions and caveats of both UI are discussed in Section 6.2.

2.10 Dataset Overview

The data used in this thesis can be described in two simple categories:

1. Univariate time series data, such as a temperature record from a meteorological-station or a climate index, and
2. Gridded 'observational' or 'reanalysis' datasets, as introduced in Section 1.2.

Historical climate data from across Macaronesia are sourced from several international sources (all the data are publically, freely available). Studies such as Martín *et al.* (2012) and Sanchez-Moreno *et al.* (2014) indicate that there are high-density meteorological-station networks available for some of the individual Macaronesian Islands, but these data are not publically available (and rarely of sufficient temporal extent for analysis of long term climate). The Global Historical Climatology Network (GHCN) is a global database of land surface meteorological observations at a monthly and daily scale, providing raw and homogenised station time series (Lawrimore *et al.*, 2011). Temperature and precipitation data from all four Macaronesian archipelagos were extracted from the GHCN-Monthly archive (raw data were favoured so the homogeneity methods in Section 2.5 could be applied). Daily temperature, precipitation, SLP and wind-speed data are taken from the Global Summary of the Day archive (GSOD, http://www.ncdc.noaa.gov/), which is preferred to the GHCN-Daily as the GSOD

records are more temporally complete (updating only a few days after the observations are made). Extra (daily) records covering the European Islands (Azores, Madeira, Canary Islands) are taken from the European Climate Assessment and Dataset project (ECA&D, Klein-Tank *et al.* 2002) and monthly SLP records for the Azores from the Annual-to-Decadal Variability in Climate over Europe archive (ADVICE, Jones *et al.* 1999b). Additional daily SLP for the Azores that have been recently digitised as part of projects ERA-CLIM (European Reanalysis of Global Climate Observations) and SIGN (Signatures of Environmental Change in the Observations of the Geophysical Institutes) were provided by M.A. Valente (Valente *et al.*, 2008; 2013), but will also be archived in the International Surface Pressure Databank (Yin *et al.* 2008).

As well as the NAO index developed in this thesis (Chapter 3), several widely used NAO indices are used for comparative purposes (mainly to check the validity of the new reconstruction) in addition to other climate indices from online sources. These alternate indices are listed, along with a description in Table B4 and C1. Several observational and reanalysis gridded data sources are used in this thesis, an overview is provided in Tables B5 and B6. For analysis of the potential future evolution of Macaronesian climate (Chapter 5), model runs depicting future climate scenarios from the Coupled Model Intercomparison Project Phase 5 are used (CMIP5, Taylor *et al.*, 2012). An ensemble of models from the archive is used for analysis of mean changes in the state of temperature and precipitation in addition to the ensemble taken from the CMIP5 Extreme Indices archive (Sillmann *et al.*, 2013a; 2013b), which have the ETCCDI extreme indices equations applied at the grid-box scale. Further details of the CMIP5 models are given in Chapter 5.

3. The North Atlantic Oscillation

The third major objective of this thesis was to, *"Conduct a detailed analysis of the North Atlantic Oscillation, including extending the daily-resolution index back to 1850"*. As such, the initial focus of this chapter is the documentation of the process involved in the assembly and collation of SLP data from the Azores Islands across Macaronesia. The data from the Azores (and also from Iceland) allowed for a historical reconstruction of the NAO at a daily temporal-resolution back to 1850. Additionally, a new, unique measure to characterise the strength of the Trade Winds across Macaronesia – the Trade Wind Index (TWI) – was developed using data from the Azores and Cape Verde. Also, the 'traditional' monthly-resolution NAO index used in CH14 is briefly discussed along with new insights into changes in the NAO from H15. The effects of the NAO and TWI across Macaronesia are then explored. The chapter is structured as follows: (3.1) firstly, a detailed overview and background of the available measures of NAO are given (a basic introduction was given in Sections 1.3.2 and 1.5), (3.2) the construction of a daily, ~09:00 UTC NAO Index back to 1850 is documented, along with the monthly NAO used in CH14, (3.3) the NAO effects across Macaronesia and the temporal evolution of the NAO index are explored and (3.4) the TWI is introduced and analysed and (3.5) the chapter is concluded and summarised.

3.1 Existing NAO Indices

(Much of the text from the following two sections, 3.1-3.2, is taken from CHVJ15)

The NAO represents the principal mode of annual variability across much of the Atlantic sector of the Northern Hemisphere (Visbeck *et al.*, 2001; Osborn, 2011). The NAO is traditionally defined as the difference in normalised SLP anomalies between a southern node, located in continental Iberia or the Azores, and a northern node, usually southwest Iceland (Hurrell, 1995; Jones *et al.*, 1997), which is hereafter referred to as the 'station-based' method. Alternatively, the NAO can be calculated from gridded climate datasets using EOF or similar methods (Thompson and Wallace, 1998; Folland *et al.*, 2009), hereafter, the PC-based method. The advantage of the station-based methodology is the extension back to the mid-Nineteenth Century and a continuous temporal record from each node, allowing a consistent methodology for deriving the NAO. The shortcomings of the station-based NAO are: (1) the fixed spatial location of the weather stations and (2) noise due to transient and local meteorological events and, as discussed below,

inhomogeneity of the southern station pressure series. The PC-based NAO better captures the annual migration of the centres of action of the NAO dipole, which is particularly important during the boreal high-summer months (July and August (Folland *et al.*, 2009)), when the pattern typically reverts to a 'Greenland-British Isles seesaw', instead of the usual 'Azores-Iceland' pattern. The PC-based indices are limited by the accuracy of the reanalysis products from which they are derived and the non-stationarity of the EOF pattern (Wang *et al.*, 2014).

The station-based NAO almost always use the southwest Iceland SLP time series as the northern node, which is a well-documented daily SLP record extending back to 1823 (Jónsson and Garđarsson, 2001; Jónsson and Miles 2001; Jónsson and Hanna, 2007). Three commonly used southern station nodes are Ponta Delgada (Azores, Portugal), Gibraltar (British Overseas Territory) and Lisbon (Portugal). The two continental locations are generally accepted as ideally located for representing the winter NAO (DJF), adequate for spring and autumn (MAM and SON respectively) and unsuitable for summer (Jones *et al.*, 1997; Hurrell and van Loon, 1997). Pozo-Vázquez *et al.* (2000) emphasised the importance of using the Azores station as the southern node if using a monthly or seasonal station-based NAO. The main reason the continent-based locations are unsuitable during the summer is due to strong continental warming during these months, which leads to developments of continental thermal low-pressures, preventing the Azores High from covering the Iberian Peninsula (Figure 1.6). Monthly SLP records from Gibraltar, Lisbon and the Azores extend back to 1821, 1864 and 1865 respectively. Several studies have sought to extend the temporal length of the NAO further back in time by the use of proxy-based reconstructions but these are usually winter-based and/or based on potentially non-stationary assumptions about the proxy-NAO relationship (Luterbacher *et al.*, 1999; Cullen *et al.*, 2001; Schöne *et al.*, 2003; Lehner *et al.*, 2012). A recent reconstruction of the monthly NAO back to 1692 using London and Paris as the northern and southern nodes highlights the value in using recently digitised historical data (Cornes *et al.*, 2013).

For all the potential caveats mentioned above, the different NAO series, especially during winter, generally display the same temporal evolution and trends/magnitudes and are highly correlated (this is explored further in Section 3.2). The different measures of NAO used in this thesis are given in Table C1. With the exception of the CPC NAO index in Table C1 and the daily NAO developed as part of this thesis, all of the indices are produced at a monthly scale. Section 3.2 documents the reconstruction of the new, daily temporal-resolution NAO back to 1850, using mainly station-based data from the traditional centres of action, the Azores and Iceland.

3.2 A Daily NAO Index

The focus of the research in CHVJ15 was to increase the temporal-resolution of the NAO index in the form of a continuous, daily ≅09:00 UTC index extending back to 1871, and back to 1850 with mean daily data. The reason for this was twofold. Firstly, it is apparent that the index, in winter but particularly in December, is undergoing a significant change in its variability towards more extreme values (H15, also discussed in Section 3.3) and, in contrast to global climate model simulations (Folland *et al.*, 2009; H15), there has been a significant recent (since ~1991) negative trend in the summer NAO (H15). Secondly, the consistency in the publication of Azores SLP values since 2003 has become increasingly sporadic (CH14). Also, it has recently become apparent that the published monthly SLP values from Lisbon in several meteorological archives are inhomogeneous (Bethke and Valente, 2012), which may propagate as errors into the NAO (as the index is normalised, the errors will be small, but improvements should be made where necessary). Furthermore, use of a consistent observing time where possible should minimise the effect of diurnal pressure tides (Dai and Wang, 1999). Typically, the diurnal pressure cycle for the Azores and Iceland peaks at ~05-6:00/17-18:00 UTC (minimum) and 23-00:00/11-13:00 (maximum) – with a (max-min) diurnal SLP range of ~2.0 and ~0.7 hPa respectively (not shown). The only widely available, consistently updated daily NAO index is provided by the CPC, who construct a daily index using a PC-based method (Barnston and Livezey, 1987) which extends from 1950 to present. Previously, several studies have made use of daily NAO indices (Jónsson and Miles, 2001; Blessing *et al.*, 2005; Philipp *et al.*, 2007; Folland *et al.*, 2009; Woollings *et al.*, 2010), displaying the usefulness of an enhanced temporal scale in analysing the predictability, persistence characteristics and evolution of the NAO. As such, a quality-controlled daily NAO index that can be easily updated should be of great value to researchers across multiple disciplines.

3.2.1 Historical SLP Data

3.2.1.1 Time of Observation

The following information regarding the time zone history of Iceland and the Azores is taken from the latest release of the Internet Assigned Numbers Authority Time Zone Database (Olsen and Eggert, 2013). Coordinated Universal Time (UTC) was introduced on January 1st, 1972, which superseded Greenwich Mean Time (GMT) (established 1st November 1884) as the international standard time. Throughout the chapter, 'z' refers to local time and UTC is the primary time standard (GMT from 1884-1971 and UTC 1972-onwards). The time zone of Iceland is UT0 (i.e. the same as Greenwich, UK), but

Iceland did not adopt the global time zone until January 1908, when GMT-1 was adopted. As such, based on the longitude of Reykjavik (338.11E), the local time of Iceland pre-1908 is approximately 90 minutes behind GMT (so 09:00UTC for Iceland pre-1908 is ~07:30z). Iceland invariably observed daylight saving time between March/April and the end of October during 1917-19 and 1939-67 (http://www.almanak.hi.is/klukkan.html) and from 1968 Iceland has been on UT0 with no summertime observed.

Portugal adopted GMT in 1912 and it is assumed, but not certain, that GMT was adhered to for meteorological observations across Portugal from 1912, but it may also not have been until 1947, when the Institute of Meteorology was formed. Based on the longitude of Ponta Delgada (334.32E), the pre-1912 local times from the Azores are ~110 minutes behind GMT (so 09:00 UTC for Portugal pre-1912 is ~07:10z). The Azores adopted GMT-2 in January 1912 and changed from GMT-2 to its current UTC-1 around September 1983. Daylight saving was introduced in 1916, and varied in when/if it was applied throughout the year until late in the Twentieth Century. The Azores and Iceland stations that are discussed below document how changes in the observation time vary between 06:00z and 12:00z in the early parts of the records (essentially, 08:00-1400 UTC), but this will introduce a minimal amount of bias into the time series given the small range of the diurnal pressure tides.

3.2.1.2 Northern NAO node (Southwest Iceland)

The southwest Iceland pressure series is a composite of fixed-time, usually at 09:00 UTC daily readings from Stykkishólmur and Reykjavík since March 1822 (Figure 3.1). Jones *et al.* (1997) and Jónsson and Garðarsson (2001) describe the sources of the early Icelandic pressure data and Jónsson and Miles (2001) applied additional homogenisation to the time series. The time of observation is usually around 07:00-08:00z pre-1920, and 07.30z/09:00 UTC post-1920 (Jónsson and Hanna, 2007). The southwest Iceland pressure series is extended to December 2013 with data from the Icelandic Meteorological Office.

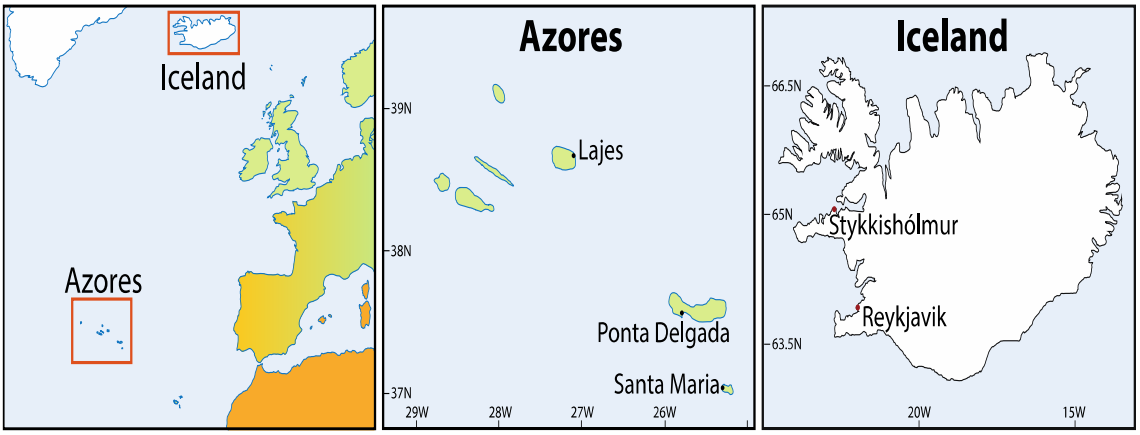

Figure 3.1. Location of the Azores and Iceland within the North Atlantic basin and the location of the specific stations used in construction of the daily Azores and Iceland SLP time series.

3.2.1.3 Southern NAO node (Ponta Delgada, Azores)

Monthly data from Ponta Delgada (1865-2000) are readily available (e.g. the ADVICE SLP archive (Jones *et al.*, 1999b)). However, (sub-)daily data have historically been difficult to acquire and this station has reported unreliably since 2003 (CH14). The 'historical' station which reported for ~140 years since 1865 has ceased operation and been replaced by a site at Nordela Airport since 1973 (Table C2). Sub-daily data from the Integrated Surface Data (ISD, http://www7.ncdc.noaa.gov/-CDO/cdo) have been made recently available for several Azores stations, most noticeably from 1931-1961 for Ponta Delgada. Additionally, data from Ponta Delgada extending back to December 1872 have been recently digitised (Table C2). Together, these new Ponta Delgada data have a long gap from 1888-1906 and shorter one from December 1939-1941, but otherwise run relatively uninterrupted until 1961, which overlaps with alternative Azores pressure records (from Santa Maria and Lajes) and allows for a continuous time series to be constructed. It is advantageous that many of the early records have pressure data at fixed daily readings, usually within ±2 hours of 09:00 UTC (Table C2), which is consistent with the southwest Iceland data. The following two sections (3.2.1.4 and 3.2.1.5) deal with the construction of two segments of the Ponta Delgada time series (1872-1961 and 1944-2013), and (Section 3.2.2) the filling in of gaps using Twentieth Century reanalysis (20CR) data (Compo *et al.*, 2011) and extension of the record back to 1850 with European Mean Sea Level Pressure (EMSLP) data (Ansell *et al.*, 2006). The final result is a continuous, homogenised Azores daily SLP record extending back to 1850.

3.2.1.4 Historical Azores SLP data (1872-1961)

Recently digitised Ponta Delgada, Azores data (Table C2) run from 1872-1887, 1906-1930, 1932-1935 and 1942-1946. The Nineteenth Century data for 1872-1887 were digitised through project SIGN (Valente *et al.*, 2008) and the early Twentieth Century (1906-1946) by project ERA-CLIM (Bethke and Valente, 2012; Valente *et al.*, 2013). During 1872-1887 and 1906-1921, pressure readings were taken at 09:00z (local time, equivalent to ~10:50 UTC). The location of the station slightly changes from an altitude of 20 m (37.74N, 334.32E) before 1888 to 17 m between 1906 and 1914 and to 22 m (37.73N, 334.33E) from 1915 onwards. During 1922-1930 and 1932-1935 pressure readings were taken at 11:00z. During 1942-1944 and 1945-1946 pressure readings were taken at 06:00z and 07:00z respectively. All data were digitised as station pressure (STP) and converted to SLP after applying corrections for gravity, temperature and altitude. Observational temperature data were not yet available, so a set value of 289.15 K was used, which corresponds to an expected average indoor Azores temperature at ~09:00z (personal communication from M.A. Valente). After conversion to SLP, the digitised Ponta Delgada data were treated as a continuous series.

Ponta Delgada data from the ISD archive were provided directly as SLP. Daily readings at 06:00 UTC run from 1931-1939 and 1953-1961 and at 12:00 UTC from 1931-1939 and 1948-1953. When possible, a 09:00 time for each day is created by taking the average of the 06:00 UTC and 12:00 UTC reading. A historical Ponta Delgada record is spliced together by least-squares linear regression of the ISD data against the digitised Azores data (based on the 1932-1935 overlap period), which creates a historical Ponta Delgada time series from 1872-1961 without any large gaps (>1 year) between 1906-1939 and 1942-1961. Preference is given to 09:00/06:00UTC ISD data when gap-filling. The regression splicing served as a basic quality control for identifying and removing significant outliers (with regression coefficients being recalculated after outlier removal). Obvious incorrect SLP values (below/above 950/1050 hPa) were also removed as these values are unrealistic across the Azores (Figure C1).

3.2.1.5 Modern Azores SLP data (1944-2013)

09:00 UTC data from the ISD Ponta Delgada station run uninterrupted from 1973-1992 and 2002-2013, with significant gaps present between 1992-1996 and 1999-2002. 06:00 UTC and 12:00 UTC data adequately cover the 1999-2002 gap and provide somewhat limited coverage between 1992-1995. This Ponta Delgada record is extended as before by OLS regression against the 09:00/06:00/12:00 UTC ISD data (based on the long-term 1973-2013 overlap period). However, this does not cover all of the gaps in the time series

or extend the data back to a period where it can be spliced against the old Ponta Delgada record to form a continuous series. To do this, 09:00 UTC data from two nearby stations were used from Santa Maria (the island 80 km to the southwest of São Miguel) and Lajes Air Base (on Terceira, 170 km to the northwest), which report back to August 1944 and January 1947 respectively (Table C2). 09:00 UTC data from Santa Maria were provided directly as SLP values and run from August 1944 – September 1946, 1951-1955 and 1973-present. 09:00 UTC readings from Lajes were incompletely provided as SLP, with the period March 1966 – January 1973 only provided as STP (a significant period given the gaps in the Ponta Delgada records, Table C2). STP values were corrected to SLP as before, with use of 09:00 UTC temperature data when available or 289.15 K when a temperature reading is unavailable. The calculated SLP values were also checked for consistency with the given SLP values on days where both were available. Figure 3.2 displays the time series of all the individual Azores station data sources. The Santa Maria and Lajes records (using Santa Maria with priority due to its closer proximity) were regressed against the 1973-2013 Ponta Delgada record, which extends the modern 09:00 UTC daily Ponta Delgada pressure record back to August 1944 (with only ten missing days up to present).

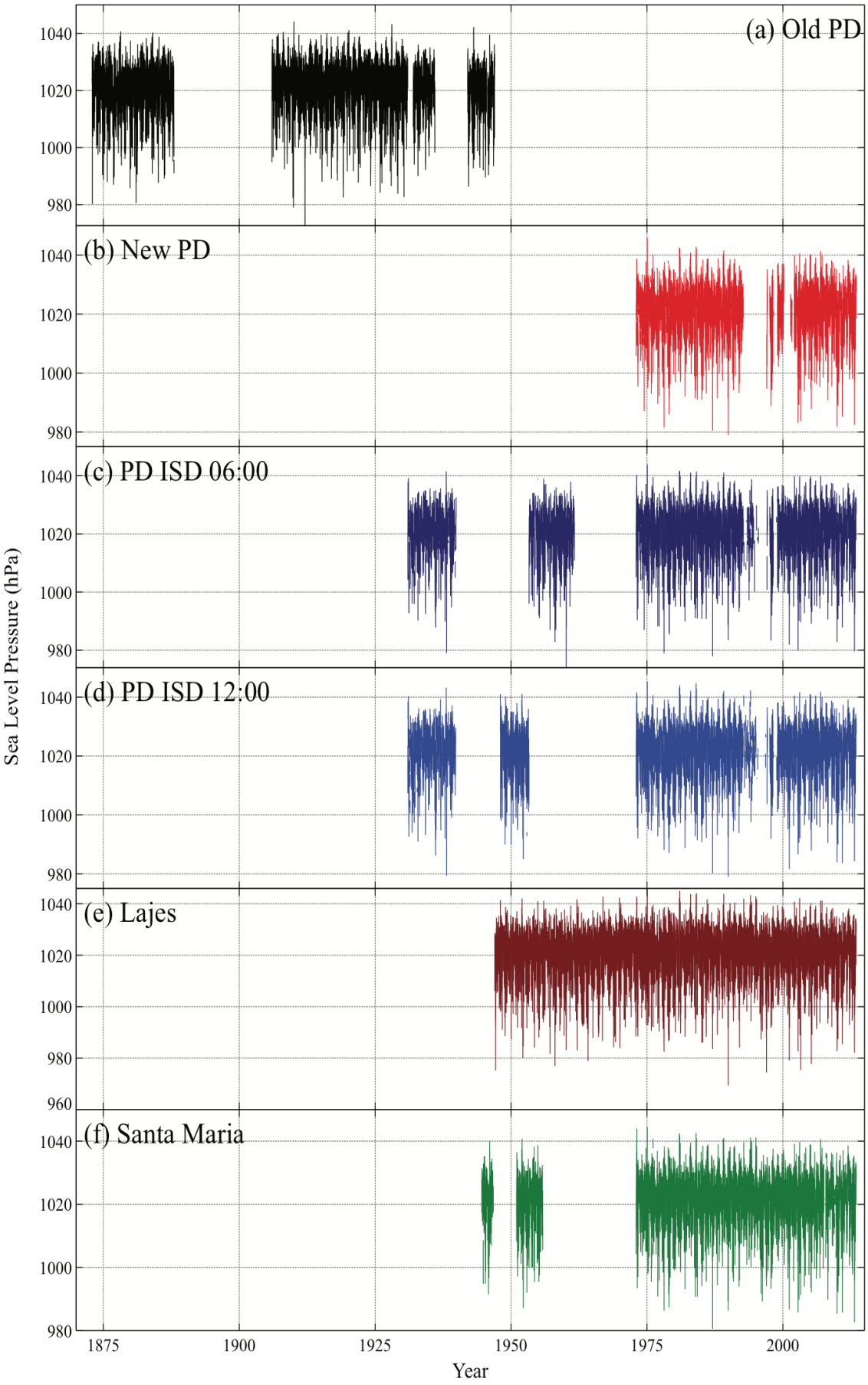

Figure 3.2. Daily time series of all the currently available raw (unhomogenised) meteorological-station SLP data from the Azores.

3.2.2 Completing the Azores SLP Record

The fully extended 'historical' (1872-1961) Ponta Delgada record is regressed against the 'modern' (1944-2013) record to create a long-term Ponta Delgada time series (December 1872-October 2013). The main gaps in this record are 1888-1905 and December 1939-1941, with only 135 single days missing outside of these periods. To create a fully complete, continuous record, the grid-box that overrides São Miguel from the 20CR dataset is used ((Compo *et al.*, 2011), Table C2). The 20CR has a 4x daily resolution for SLP, so the average of the 06:00 UTC and 12:00 UTC daily values were used as a proxy for 09:00 UTC, which is then regressed against the long-term Ponta Delgada series. The linear relationship between the 20CR and observational data (Table 3.1) is strong (r^2 = 0.931). The 20CR-filled Ponta Delgada time series runs continuously from 1st January 1871 – present. An extension of the Ponta Delgada record back to 1850 is calculated by using additional daily data from the EMSLP project (Ansell *et al.*, 2006); however, the EMSLP readings are daily averages, which differ from the typical ~09:00 UTC readings (the number of daily observations that create the daily average do vary temporarily and are a potential source of bias). The EMSLP output is on a 5x5-degrees grid and during 1850-1880, 85-90% of the daily grid cells have missing data, so a large fraction of the SLP values were constructed based on the reduced-space optimal interpolation procedure used. As such, one might expect large uncertainties in the early record, although Ansell *et al.* (2006) showed that the winter (DJF) NAO constructed from EMSLP fields shows almost perfect correlation (correlation coefficient = 0.97 and 0.98) with those derived from the Historical Gridded Mean Sea Level Pressure Dataset (Allen and Ansell, 2006) and Jones *et al.* (1997). Furthermore, the correlation between the EMSLP data and the 20CR-filled Ponta Delgada record is still remarkably high (r^2 = 0.810). Figure 3.3 graphically illustrates how the input data in the creation of the Ponta Delgada SLP record varies with time. All of the regression relationships in Table C2 that were used to create the Azores SLP time series were based on annual data, r^2 values show no improvement and sometimes worsen when seasonal/monthly/daily regressions were attempted.

Dependent	Predictor	Regression	r^2
Old PD (1872-1946)	OPD(ISD)0600	HistPD = -1.615+1.001*ISD0600	0.995
Old PD (1872-1946)	OPD(ISD)1200	HistPD = 10.072+0.989*ISD1200	0.968
Old PD (1872-1946)	OPD(ISD)0900	HistPD = -3.120+1.002*ISD0900	0.991
After all the possible gaps were filled, this became the 'complete', historical PD time series (1872-1961) [Section 3.2.1.4]			
Modern PD (1973-2013)	NPD(ISD)0600	ModernPD = 5.677+0.995*ISD0600	0.989
Modern PD (1973-2013)	NPD(ISD)1200	ModernPD = -0.286+1.000*ISD1200	0.989
Modern PD (1973-2013)	NPD(ISD)0900	ModernPD = -5.950+1.005*ISD0900	0.997
After all the possible gaps were filled, this became the 'complete', New PD time series (1973-2013) [Section 3.2.1.5]			
New PD (1973-2013)	Lajes	NewPD = 100.048+0.902*Lajes	0.949
New PD (1973-2013)	SantaMaria	NewPD = -48.751+1.047*Santa Maria	0.982
This extended the New PD record back to August 1944 and fills in almost all daily gaps since then (1944-2013) [Section 3.2.1.5]			
New PD (1944-2013)	HistPD (1872-1961)	NewPD = 39.662+0.962*HistPD	0.940
This resulted in a long-term PD record, with only 145 missing days from December 1872 onwards (excluding the long-term gaps of 1888-1905 and December 1939-1941) (1872-2013) [Section 3.2.2]			
PD (1872-2013)	20CR (1871-2011)	PD = 47.347+0.954*20CR	0.931
This filled in every gap from Jan 1st 1871 to present day (July 2013), creating a continuous, unbroken time series (1871-2013) [Section 3.2.2]			
PD (1871-2013)	EMSLP (1850-2003)	PD = -52.650+1.053*EMSLP	0.810
Optionally extends the PD record back to 1850 using EMSLP data (1850-2013) [Section 3.2.2]			

Table 3.1. The regression coefficients used to splice together the Ponta Delgada record. The regression relationships were calculated using data up until July 2013. Updating the record with new values (i.e. to present day) simply requires addition of updated SLP data from the Ponta Delgada (Azores) and Reykjavik (Iceland) records from the ISD. PD = Ponta Delgada.

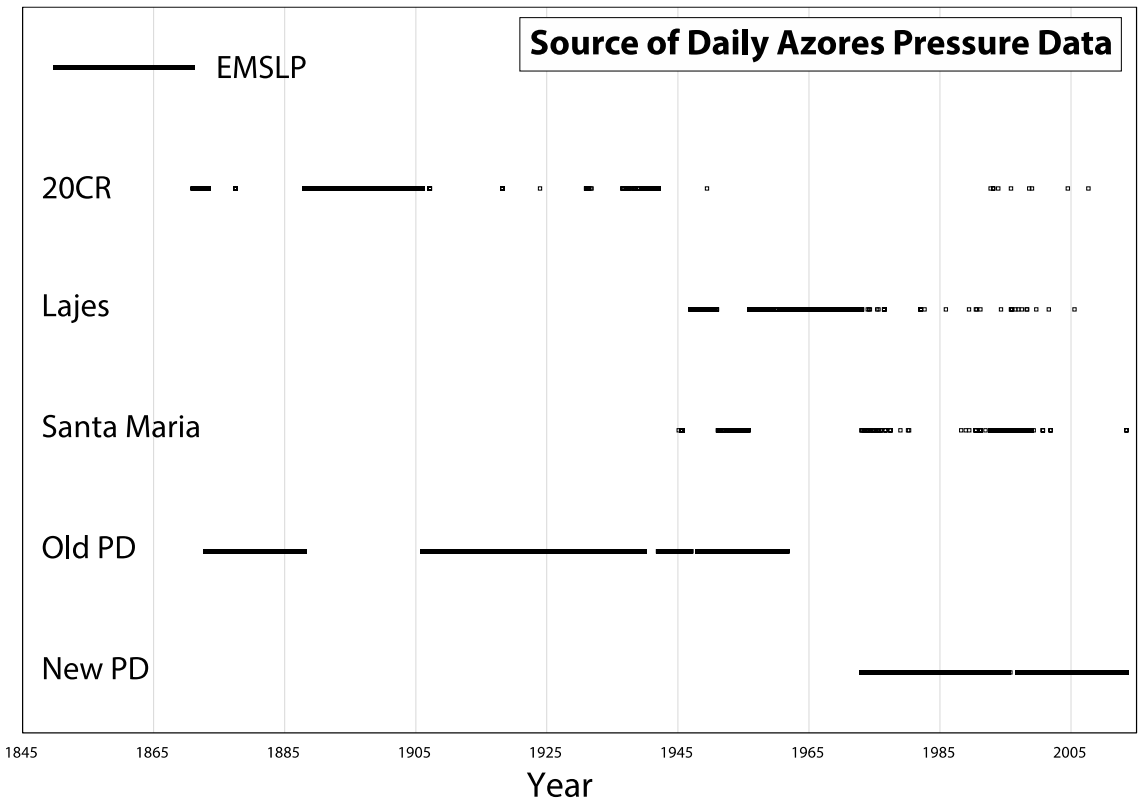

Figure 3.3. The source of daily pressure data used in the creation of the finalised daily Azores/Ponta Delgada time series.

Homogeneity tests were applied to the Ponta Delgada time series, with no 'reference' series to compare against and an assumption of no known documented shifts (even though it is known when source data changes occur), the PMF (Section 2.5) was run to detect any significant ($p < 0.05$) change points. This was also repeated using the SNHT, Buishand Range Test and the Pettitt Test, finding very similar results. Typically, when the extra 21 years of data back to 1850 were included, two break points (1853 and 1936) were found and when testing just the 1871-2013 period, break points at 1903 and 1931 were found. As there were changes in data source at 1906 (from 20CR back to the historical Ponta Delgada station) and at 1931 (ISD data, Table C2), slight homogeneity corrections were applied at these times (Figure 3.4). There is also a change in the data source around 1936 (Table C2), but when the correction at 1931 is applied, correcting the 'shift' at 1936 becomes unnecessary. When the Ponta Delgada time series is extended back to 1850 with the EMSLP data, the pre-April 1853 data were adjusted upwards (a known low bias is present in 1850s EMSLP data (Ansell *et al.*, 2006)), as there is a strongly visible ~3 hPa shift.

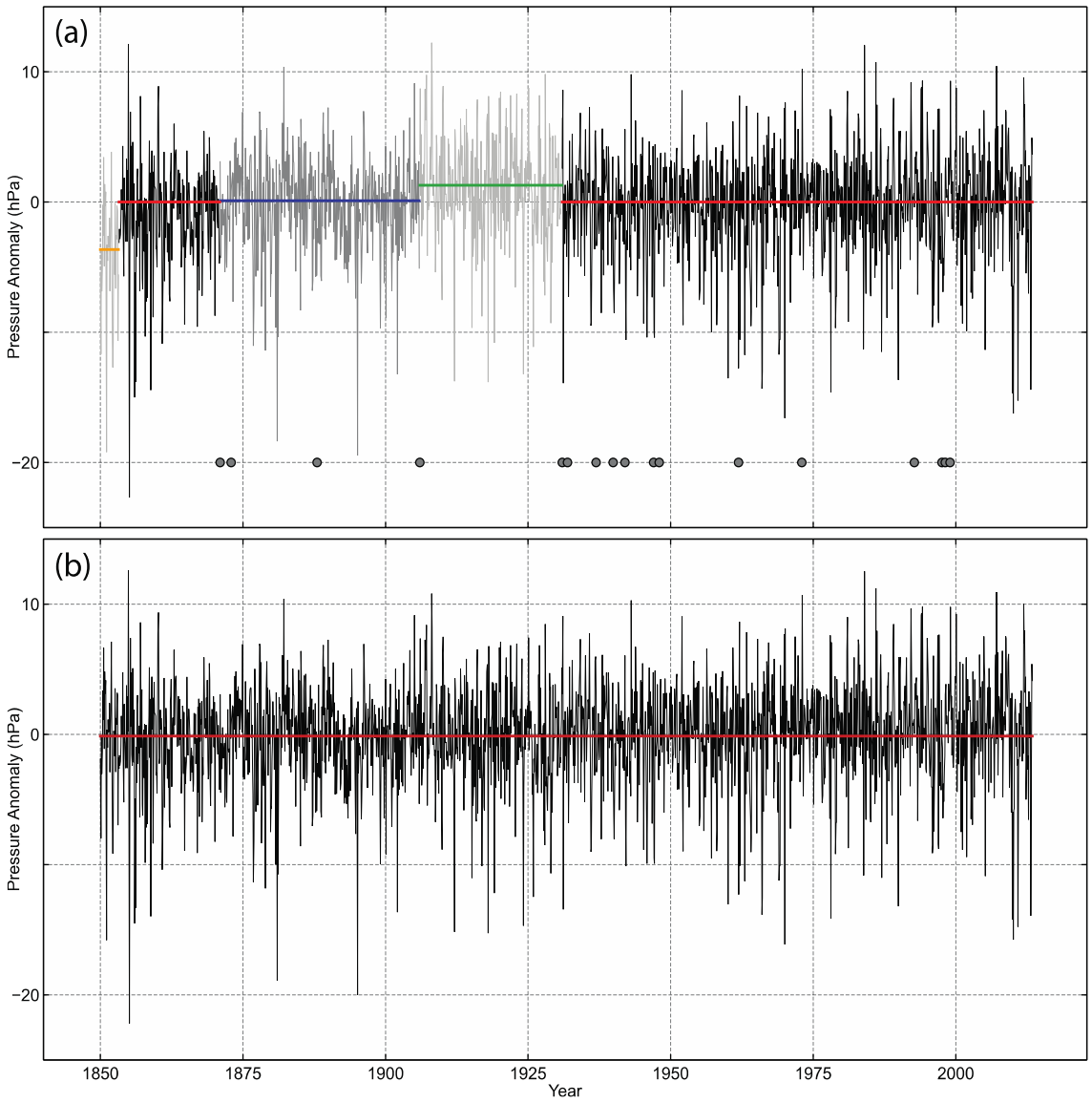

Figure 3.4. (a) Ponta Delgada monthly SLP time series (as anomalies relative to 1901-2000) before homogenisation procedures applied. Solid lines indicate the difference in means between the three periods (Jan 1850 - Mar 1853, Jan 1871 - Dec 1905, Jan 1906 - Dec 1930) that underwent homogeneity adjustments. Circles along the -20 hPa axis indicate a change in a dominant data source. (b) Finalised Ponta Delgada SLP (anomaly) time series.

Table 3.2 indicates the percentage of the Ponta Delgada record made up from the constituent data sources (up to October 2013). Nearly ~72% of the 1871-2013 record is directly from a station located in Ponta Delgada, with ~12% of the record contributed from the stations on other Azores Islands and ~16% from 20CR data.

Station	Number of Days	Percentage of Record (1871-2013)	Percentage of Record (1850-2013)
New Ponta Delgada (1973-2013)	13376	25.64	22.35
Historical Ponta Delgada (1872-1961)	24129	46.25	40.32
Santa Maria (1944-2013)	1730	3.32	2.89
Lajes (1947-2013)	4753	9.11	7.94
20CR (1871-2011)	8181	15.68	13.67
EMSLP (1850-2003)	7670	0	12.82

Table 3.2. The proportion of the Azores record made up by the different data sources (data up to October 2013).

3.2.3 Normalisation of the Daily NAO

The standard method to calculate the monthly NAO is to subtract the normalised monthly value of SLP at Iceland from the Azores. The normalisation is done by subtracting the monthly SLP value at each station from its long term mean and then dividing by its long term SD. Replicating this approach at the daily scale is problematic because even with >160 yearlong records, the annual mean cycles of SLP (or SD) as calculated by daily values were irregular (some of these noise features, especially across Iceland, are likely to be real climatological features (Jónsson and Miles, 2001), but such a discussion is beyond the scope of this thesis). A smooth annual mean and SD cycle were required for normalisation to avoid step changes in the NAO calculation due to day-to-day pressure variability. Therefore, the tension spline method (Section 2.6) is applied, where a daily annual cycle (of mean SLP and the SLP SD) is interpolated from monthly values and forced so that the average of the daily values of the curve for each month is equal to the monthly means (Figure 3.5). Ideally, it would have been preferred to use this method on both the monthly mean and SD fields (where the monthly SLP mean and SD were calculated from daily data beforehand) for Iceland and the Azores. However, while this works for the mean SLP, the variability of the monthly SLP SD is problematic (when comparing the annual evolution of the monthly SLP SD with monthly means of the daily SLP SD). Regardless of the base period used (here 1901-2000 is used), this issue arises because of the 'order' in which the SD is calculated. For example, if the SD of January 1st is taken (over the 1901-2000 base period) from Iceland, a value of 16.95 hPa is found. Repeating this across the rest of January and then taking the mean of these 31 values gives a January mean SD of 18.13 hPa. If the raw daily data for January 1901,

1902...2000, were first aggregated to a monthly mean January time series and then the SD of this monthly series (for the same years) is taken, a January mean SD of 9.63 hPa is obtained (the same 'order' of calculation has no effect on the mean). This disparity in SD is simply due to the fact that the spread of pressure values for the same day over a large number of years will be greater than the variability of a monthly pressure series. The difference varies disproportionately throughout the year (Figure 3.5e-f), and is strongest (weakest) during JFM (MJJASO).

Figure 3.5a and 3.5b illustrate the good fit of the tension spline procedure to monthly mean SLP values when compared to the daily annual SLP cycle for the Azores and Iceland. If a normalised NAO is created using the mean SLP splines from Figures 3.5a-b and the 'monthly'-derived SD splines from Figure 3.5e-f, the monthly average of this daily NAO is exactly equal to the monthly NAO (as if it were derived traditionally by converting all daily data to monthly first and applying monthly normalisation). This is obviously advantageous, however, due to the (relative) overestimation of the daily SD at each node by use of the 'monthly'-derived SD splines during the first ~90 days of the year, the SD of the daily NAO index is suppressed during the first ~90 days of the year (inset box on Figure 3.5e).

To counter this, the daily SD was taken and then the monthly mean SD was calculated from the daily SD. The daily cycle is then 'interpolated-back' (based on the new monthly SD) using the tension spline methodology, which results in a better fit to the daily annual SD cycle (Figure 3.5c-d). The resulting variability of the NAO index calculated using the SD splines from Figures 3.5c-d is consistent throughout the year (shown by the inset on Figures 3.5d). The only disadvantage of this method is that the monthly average of the daily NAO values is not exactly the same as the monthly NAO values calculated from daily pressure data that were averaged to the monthly scale beforehand (i.e. the 'traditional' method). However, from a theoretical and statistical viewpoint, it is clear that the 'adjusted' daily NAO is a more suitable way to calculate the index as the annual cycle is adequately preserved.

The difficulty in creating a suitable NAO index at the daily scale highlights the potential hazard of normalisation. As such, a 'natural' NAO index is also produced (Jónsson and Miles, 2001; Björnsson, 2013), which is simply the daily Azores SLP anomaly minus the Iceland SLP anomaly. This index retains the natural annual pressure cycle, so may be more useful for certain climatological applications. The temporal evolution closely matches the normalised NAO (Figure 3.6 and 3.7).

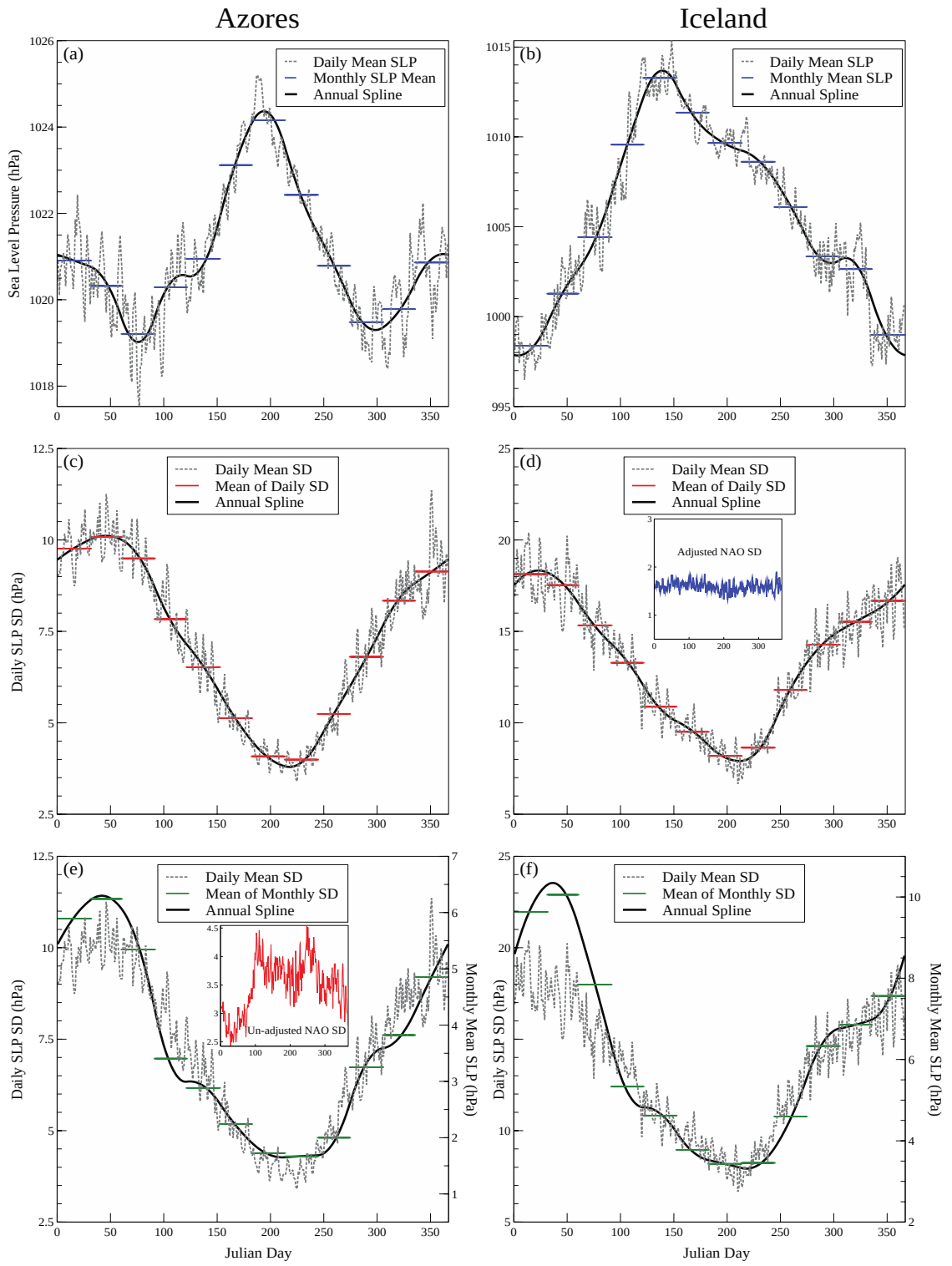

Figure 3.5. Application of the tension spline method to (a) Azores and (b) Iceland monthly mean (1901-2000 base) SLP pressure, (c) Azores and (d) Iceland monthly SLP SD (where the monthly value is the mean of the daily SLP SD (1901-2000) for each month) and (e) Azores and (f) Iceland monthly SLP SD (where the monthly SD is calculated using monthly SLP data that were aggregated from daily data beforehand). The inset graphs on (d) and (e) display the daily cycle of the SD of the NAO (1850-2013) calculated by using the different annual splines. This illustrates the impact of the normalisation procedure when calculating the daily NAO. If 'normal' monthly SLP SD values (i.e. from Figure (e and f)) were used, then the normalisation overly suppressed winter variability (e). If the modified monthly SLP SD values (c and d) were used, then a smooth annual cycle in the NAO index was preserved (d). Note the variable Y-axis for the Azores/Iceland and two NAO inset plots.

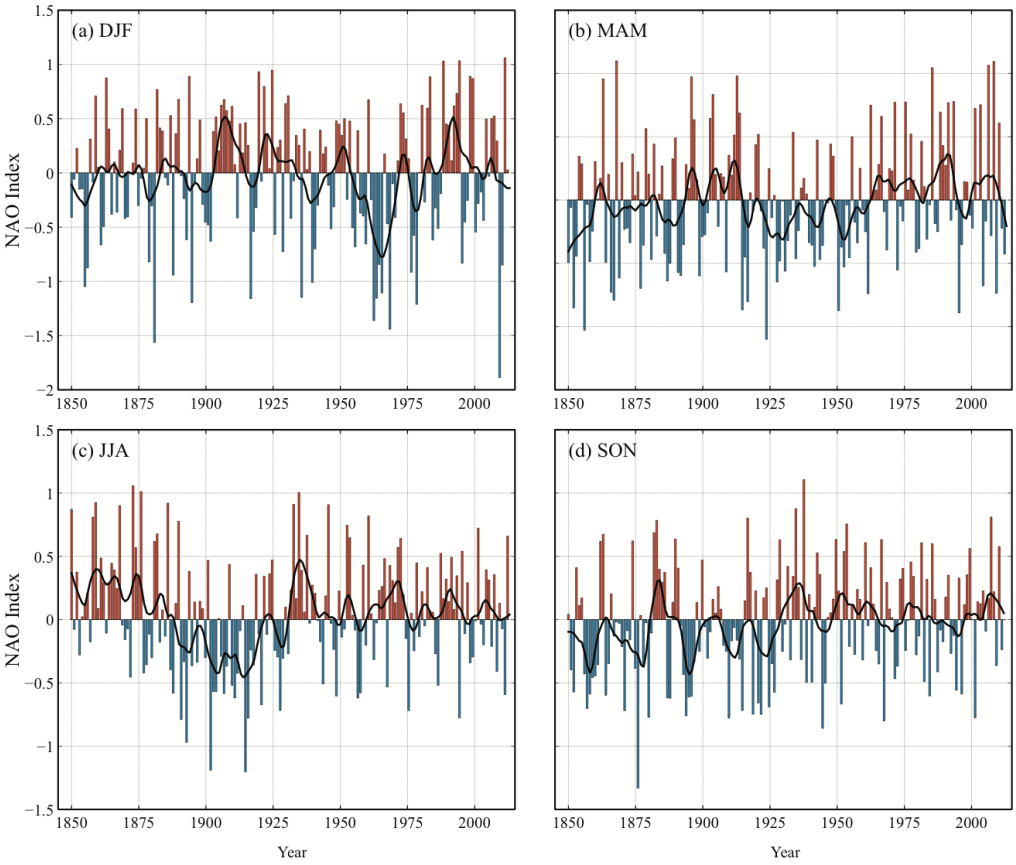

Figure 3.6. The seasonal NAOI, with an 11-year LOESS regression line.

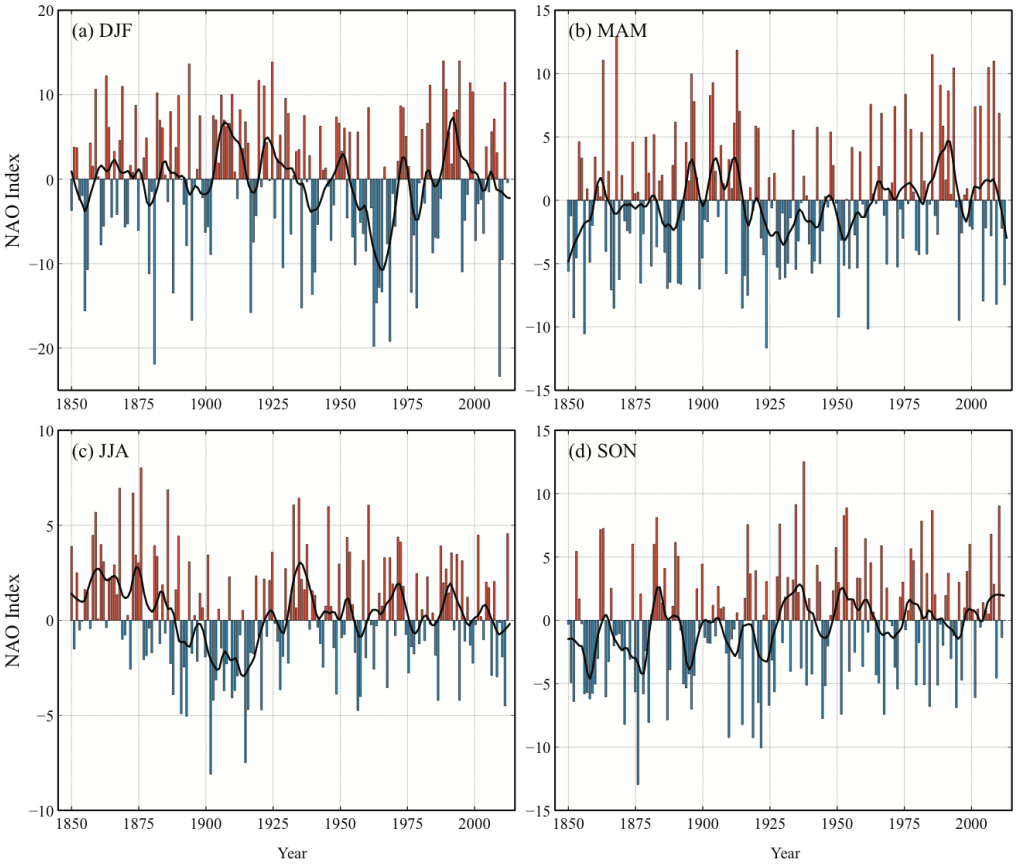

Figure 3.7. The seasonal Natural NAO, with an 11-year LOESS regression line.

To check the robustness of the reconstruction, the monthly average of the newly created daily NAO is compared against five alternative realisations of the NAO (Table 3.3). Monthly correlations with the Hurrell Station index (Hurrell, 1995) and updated Climatic Research Unit (CRU) index (http://www.cru.uea.ac.uk/cru/data/nao/), which both use Iceland as the northern node and Lisbon (Hurrell) and the Azores (CRU) as the southern node, remain above 0.90 all year round. A more pronounced seasonal variation is displayed between the Jones *et al.* (1997), Hurrell PC and the CPC indices, due to use of Gibraltar as the southern station and the PC-based method respectively. The difference between the strength of the summer correlation between the two PC-based indices is most likely a function of how they were calculated – the CPC index uses daily 500 hPa height anomalies across 20°-90°N (projected onto a fixed loading pattern) and the Hurrell index uses SLP data across 20°-80°N, 90°W-40°E. As such, the higher correlation values with the Hurrell index were unsurprising, as the spatial domain is restricted to the North Atlantic region and SLP is used as opposed to 500 hPa height anomalies. The generally reduced summer correlation across the Gibraltar and PC-based indices compared to the winter months represents the slight northerly shift in the centres' of action of the NAO during summer. The temporal difference between the new (monthly) NAO and the CRU Azores-Iceland NAO was examined and there is no evidence of any significant systematic bias. However, during 1921-1923, the daily NAO shows much lower values than the CRU version. This arises mainly from the Icelandic node (the early 1920s are a known period of uncertainty in the Icelandic record) and is due to higher SLP values in the version of the southwest Iceland SLP series used here, compared to the monthly values archived online at CRU.

Month	Hurrell PC (1899-2013)	Hurrell NAO (1865-2013)	CRU Jones-Azores (1865-2010)	CRU Gibraltar (1850-2013)	CPC (1950-2013)
Jan	0.89	0.99	0.99	0.83	0.91
Feb	0.91	0.99	0.99	0.86	0.93
Mar	0.92	0.99	0.99	0.85	0.87
Apr	0.80	0.98	0.98	0.74	0.64
May	0.83	0.97	0.97	0.67	0.66
Jun	0.83	0.96	0.96	0.70	0.71
Jul	0.69	0.90	0.90	0.54	0.35
Aug	0.66	0.94	0.93	0.52	0.34
Sep	0.76	0.95	0.95	0.67	0.52
Oct	0.82	0.97	0.98	0.75	0.72
Nov	0.82	0.99	0.99	0.78	0.71
Dec	0.88	0.99	0.99	0.81	0.87

Table 3.3. The (Pearson) correlation coefficient between the reconstructed NAO presented here (using the monthly average of the daily NAO) with five widely used alternative indices; the updated Hurrell (1995) Lisbon-Iceland station and Principal Component-based indices (https://climatedataguide.ucar.edu), the CRU Azores- and Gibraltar-Iceland indices (Jones *et al.*, 1997) and the CPC NAO index. The time periods the correlation coefficients were calculated across are indicated. All values are significant ($p < 0.05$).

The result of this chapter so far is the production of a daily NAO, which is presented as a data paper in *Geoscience Data Journal* (CHVJ2015). The index represents the best efforts with currently available data to construct an accurate, continuous, daily NAO index. It is anticipated that as data are recovered from global meteorological archives in the future, this index, and similar historical climatic records, can be further refined. Whilst there are numerous monthly versions of the NAO index available, the high value of this index is: (1) the importance of the approximately consistent 09:00 UTC observation time, (2) the daily temporal resolution and (3) the >160 year length of the time series. The index length doubles that of previously available equivalent (daily) datasets and provides a 'normal' (normalised) and 'natural' (not normalised) version. No attempts were made, other than the pre-April 1853 homogeneity adjustment, to remove any outliers in the EMSLP data that contributed to the Azores record during the 1850-1871 period. Pre-December 1872 values in the NAO indices and the periods 1887-1906 and 1940-1941 should be treated with caution as reanalysis output dominates the signal

from the southern node, although there is a strong agreement between station- and reanalysis-based SLP for common overlap periods.

3.2.4 Difference between CH14 and CHVJ15 NAO

Before the daily NAO index was created, an initial version of the NAO index was produced as a part of CH14, which was created using monthly resolution data from the Azores and Iceland, and solved the problem of data consistency from the Azores by splicing a recently-available daily record onto the end of the traditional monthly Ponta Delgada time series (at the time of writing the CH14 article, the Hurrell and CRU Azores-based NAOs were not frequently updated). This daily series ran from 1973 as part of the GSOD archive (Table B3) and was most probably the same station from which hourly data were derived as part of the 'Modern Ponta Delgada' record that makes up the daily NAO. The monthly Azores SLP data from 1865-2000 were taken from the Annual to Decadal Variability in Climate in Europe (ADVICE) archive (Jones *et al.*, 1999b). The historical daily Azores SLP pressure data, which make up the daily NAO presented earlier in this chapter, were only recently released (mid-2013) and can be thought of as a succession to the index published in CH14.

The publication of the daily NAO index as a data paper in *Geoscience Data Journal* (CHJV2015) has made the index freely available to researchers in climate science and other disciplines. The most likely and potentially strongest uses of the index will be in analysis of events across the 'weather' timescale of days to weeks, something which use of monthly indices precludes. A prime example of this would be the NAO relationship with atmospheric blocking events above the Greenland Ice Sheet (Hanna *et al.*, 2014, 2015), as the NAO and blocking events across Greenland are known to show a significant negative correlation. An analysis of the daily variability of European 'westerly indices' by Yan *et al.* (2001) indicated significant variations around the ~16 day timescale and Cassou (2008) identified the potential predictability in daily NAO probabilities when the lagged relationship between the NAO and the Madden-Jullian Oscillation was considered. Both these studies highlight the benefit of an enhanced temporal resolution of the NAO. Finally, Dippner *et al.* (2014) identified that biological regime shifts towards loss of species predictability and increased variability in benthic macrofauna in the North Sea coincided with periods when the winter NAO changed from consistent year-to-year values (consistently positive or negative) to more variable yearly changes. Their analysis used a monthly version of the NAO (the Hurrell PC index). Application of the daily NAO may assist in similar studies conducted in the future – where persistence could be analysed at a higher resolution.

To begin the initial analysis of the (normalised) daily-NAO, first the probability density functions of the wintertime (DJF) NAO index for four periods are displayed (Figure 3.8). A common characteristic is a negative skew, and this feature is present regardless of the selected time period. The two most recent periods (1971-2000 and 1991-2013) are virtually identical in their distribution. The most marked deviation from 'normal' conditions (i.e. relative to the 1850-2013 period) is during 1951-1980, where a greater occurrence of negative values is observed. This is coherent with the large negative deviation of the index during the 1960s (Figure 3.6), which is one of the most pronounced sustained shifts in the series.

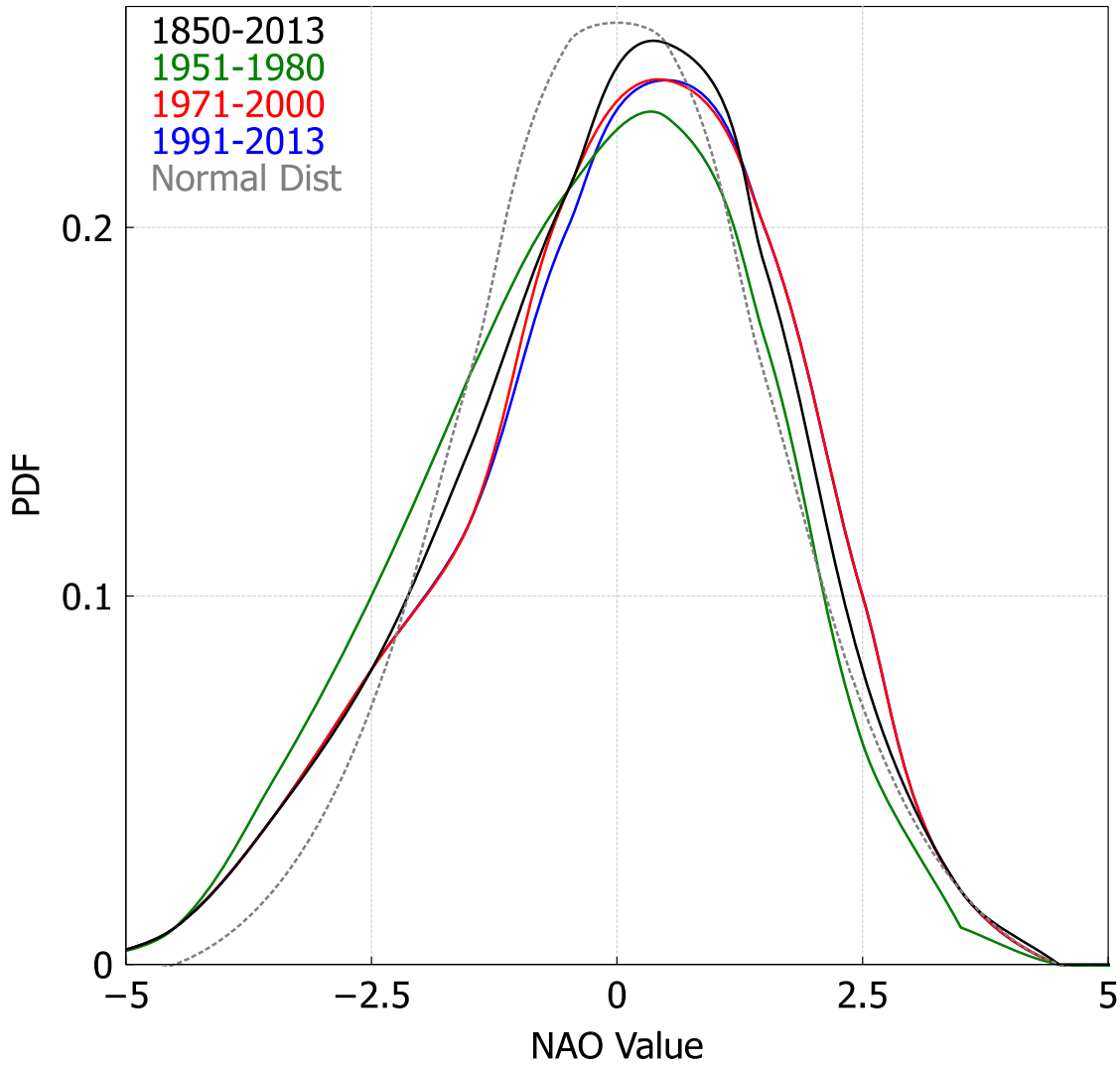

Figure 3.8. The probability distribution curves of the winter NAO for different periods.

The absolute lowest value (-6.74) occurs on the 2nd October, 1880, and the highest (6.15) on the 20th September, 1900. Overall, the NAO exceeds <-5 and >5 a total of 83 and 10 times respectively. An effort was made to replicate the approach of Woollings *et al.* (2010), who characterised the 'event duration' of positive and negative NAO events and found a tendency for an increased residence time of negative NAO events in the 5-20 day

period (An event was defined as when the index exceeds >1 SD and persists until a sign change). They concluded that sustained NAO- events were significantly different from a typical autoregressive process, which aided their analysis in inferring that the NAO was a manifestation of two distinct regimes; 1) 'normal' (NAO+) jet stream conditions and 2) 'blocking' (NAO-) conditions centred around Greenland. The departure of weak NAO- events (-2 < 0) below the normal distribution and above departure of strong NAO- events (<2) above the normal distribution (Figure 3.8) offers tentative support of strong NAO- events representing a different 'regime'. Here, replication of the event duration methodology yielded opposite results to Woollings *et al.* (2010), but will be the subject of future research as the method was applied to annual data here, rather than just winter data, which will likely alter the results obtained.

Interestingly, four out of the longest thirteen NAO- events have been since 2010 (based on analysis of all ~60000 days since 1850). The 2009/10 winter has two events of 37 and 42 days length (ending on 15th January and 19th March), which were only interspaced by a few days departure from negative conditions in the 3rd week of January. Winter 2010/11 has the single longest event at 54 days long (ended on 13th January), and the extreme negative conditions that characterised March 2013 totalled 52 days, ending on the 13th April, which is the second longest NAO- event in the record. Correspondingly only (1/79) of the longest NAO+ events have occurred since 2010 (a 32 day event ending January 11th, 2012). There appears to be no significant trend in seasonal/annual 'event duration'. The temporal evolution of the NAO is further discussed in Section 3.3.2.

For the following section regarding the NAO and its effects across Macaronesia, the monthly averages of the newly created NAO and the NAO from CH14 were used. The monthly NAO from CH14 and the monthly average of the daily NAO from CHVJ15 are statistically similar (r^2 of monthly values = 0.91), so at the greater than monthly timescale it is unlikely that any significant difference would arise from using the different indices. As previously mentioned, the strength of the daily NAO is likely to lie in its ability to depict the 'weather' timescale of days to weeks.

3.3 NAO Effects across Macaronesia

3.3.1 Spatial Relationships

Figures 3.9-3.11 illustrate the relationship between the monthly average of the daily NAO described earlier and the monthly 2 m minimum temperature, precipitation and horizontal wind at 500 hPa height (u500) from the ERA-I reanalysis across the period 1979-2013. The NAO is positively correlated with Azores minimum temperatures and

negatively correlated with Madeira, Canary Island and Cape Verde temperatures all year round (with stronger Trade Winds under a stronger Azores High as the basic physical mechanism). This pattern is reasonably consistent (February and September slightly differ), but only significant ($p < 0.05$) across the Macaronesian Islands during sporadic months (strongest in December). The structure of the pattern shifts seasonally, but the 'core' base pattern of orthogonal anomalies centred over the UK/ eastern America and southern Greenland/ Africa can be followed throughout the annual cycle. The NAO correlation with the large-scale minimum 2 m temperature field is generally strongest during autumn-winter and weakest during high summer (JA).

The NAO-precipitation pattern is distinctly more meridional in nature. The Azores are under a significant area of negative NAO/precipitation correlation all year round. This reflects the subsidence regime of the semi-permanent Azores High, which extends to include Madeira and the Canary Islands during the autumn and winter months. Cape Verde is generally unaffected by the NAO. As discussed in Chapter 1, the temperature and precipitation patterns are the direct consequence of the poleward transfer of energy by mid-latitude storm systems. NAO+ reflects a northerly storm track, NAO- a more southerly path and extreme NAO- events as a breakdown in the climatological conditions and replacement via easterly flow. Such regimes correspond strongly with upper level atmospheric flow patterns. Figure 3.11 illustrates the close relationship of the NAO and upper level zonal winds (with u500 serving as a basic proxy for the jet stream). The links between the NAO and jet stream are becoming increasingly more apparent; i.e. the NAO is strongly seen as the surface manifestation of the sub-polar Atlantic Jet Stream (Vallis and Gerber, 2008). In Figure 3.11 a clear separation of the sub-polar and sub-tropical jet can be seen during November-April and a weaker 'merged' (essentially equatorward shifted sub-polar jet) regime during summer. Both jet streams are weaker during summer due to a reduced latitudinal temperature gradient (Galvin, 2007) (easterly flow replaces westerly flow across regions of Africa as described in Sections 1.3.5-6).

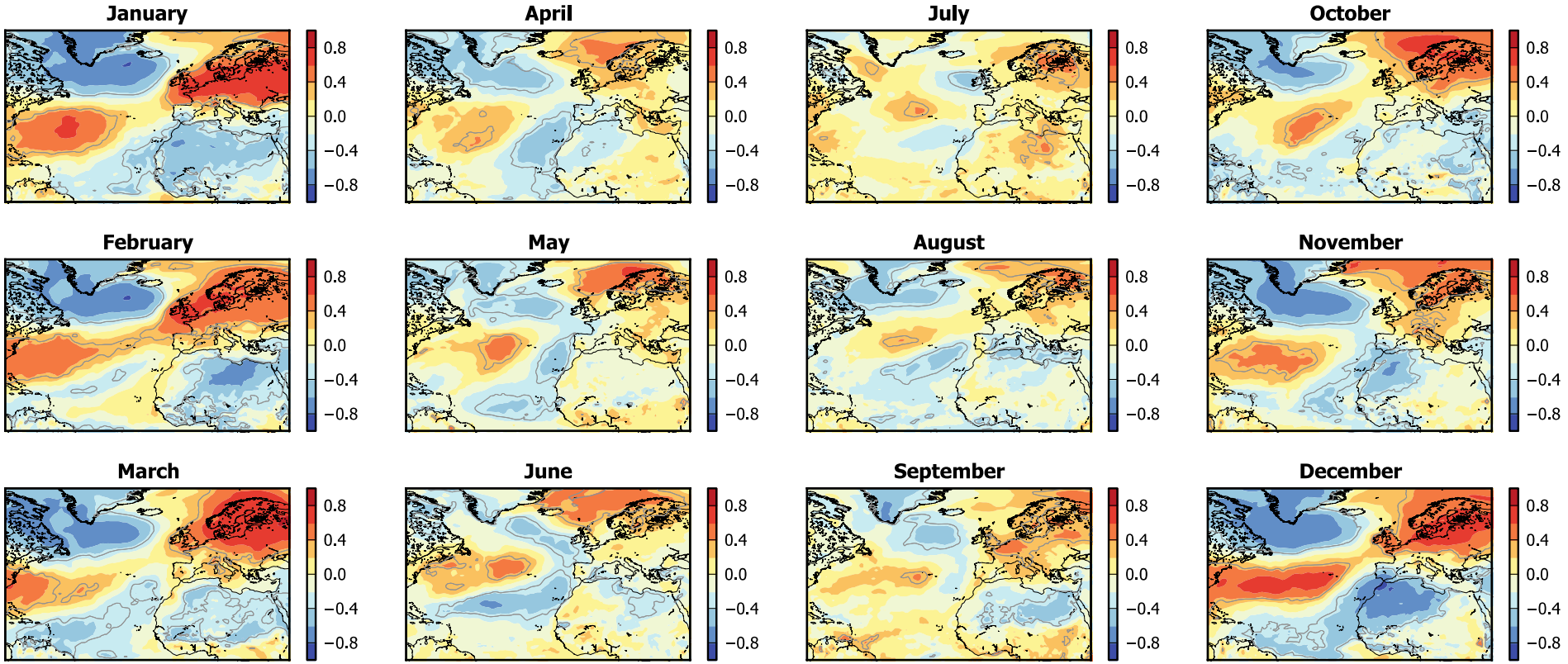

Figure 3.9. The correlation coefficient between the detrended anomalies of ERA-I 2 m minimum temperature and the CHVJ15 NAO (1979-2013). Grey lines bound areas of significance ($p < 0.05$).

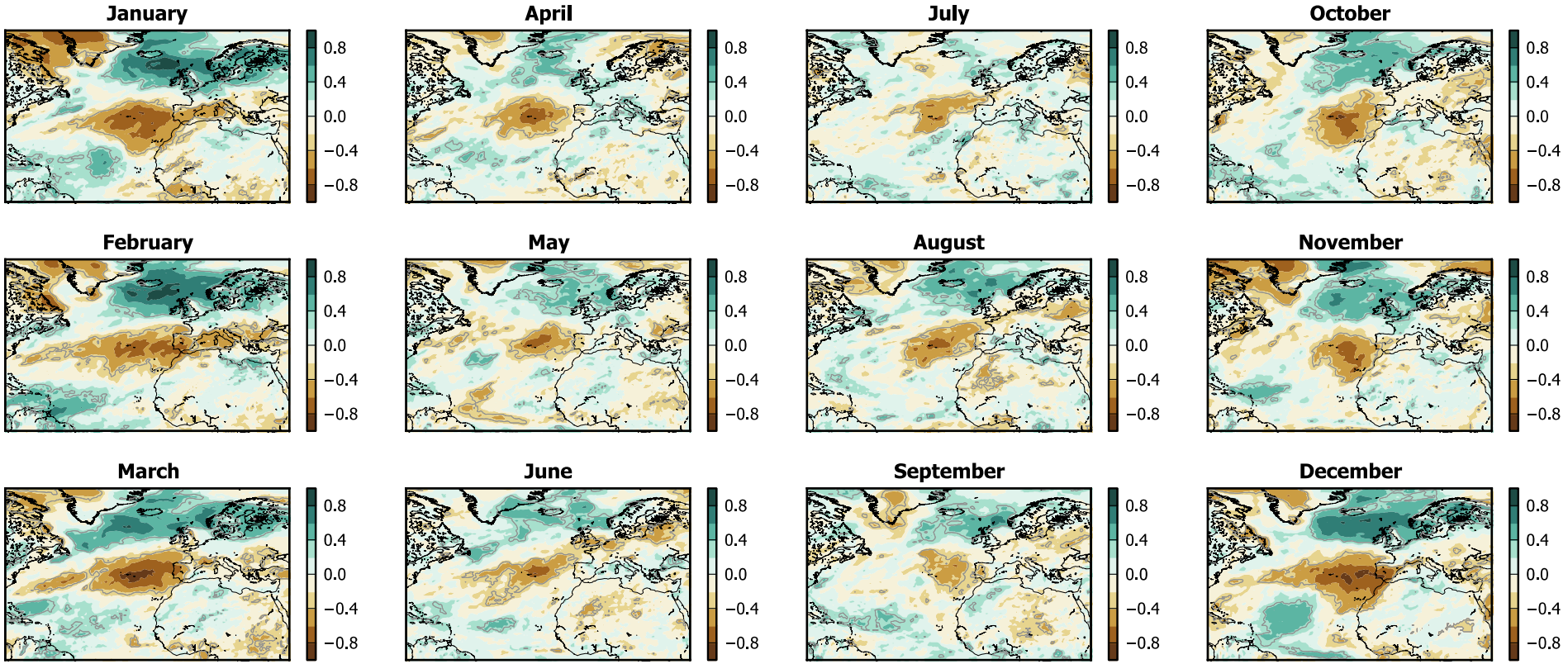

Figure 3.10. The (rank) correlation coefficient between the detrended anomalies of ERA-I precipitation and the CHVJ15 NAO (1979-2013). Grey lines bound areas of significance ($p < 0.05$). Rank correlation is used as opposed to standard correlation as precipitation values do not generally adhere to the normal distribution.

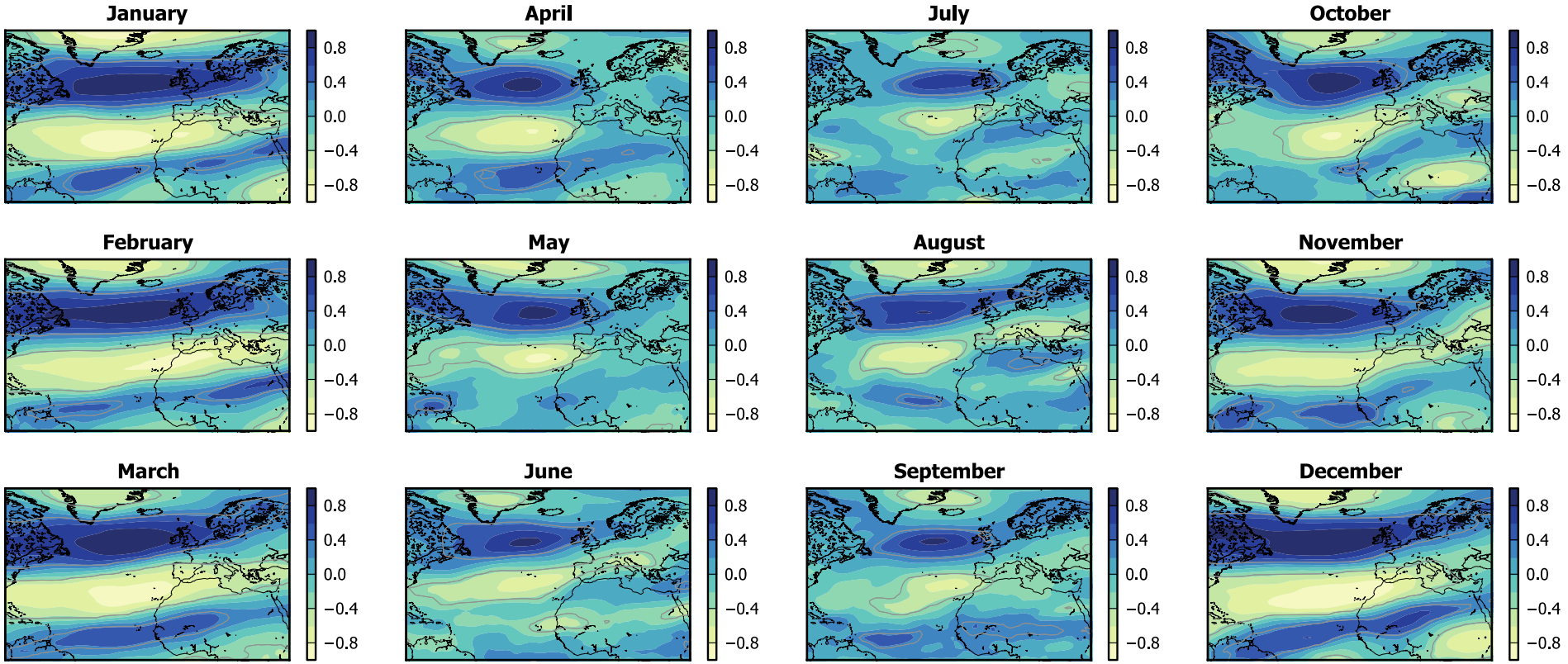

Figure 3.11. The correlation coefficient between the detrended anomalies of ERA-I 500 hPa zonal (u) winds and the CHVJ15 NAO (1979-2013). Positive (blue colour) indicates westerly (from the west) winds. Grey lines bound areas of significance ($p < 0.05$).

In CH14 the early version of the NAO based on purely monthly data was compared to 2 m mean temperature and precipitation from ERA-I across Macaronesia in winter and summer. The seasonal correlation patterns (Figure 3.12) are very similar to the corresponding months (Figure 3.9, 3.10). The relationship appears stronger, with greater correlation values and some of the Macaronesian Islands within the regions of significance, which would be expected by using seasonal instead of monthly values, as the signal-to-noise ratio is higher.

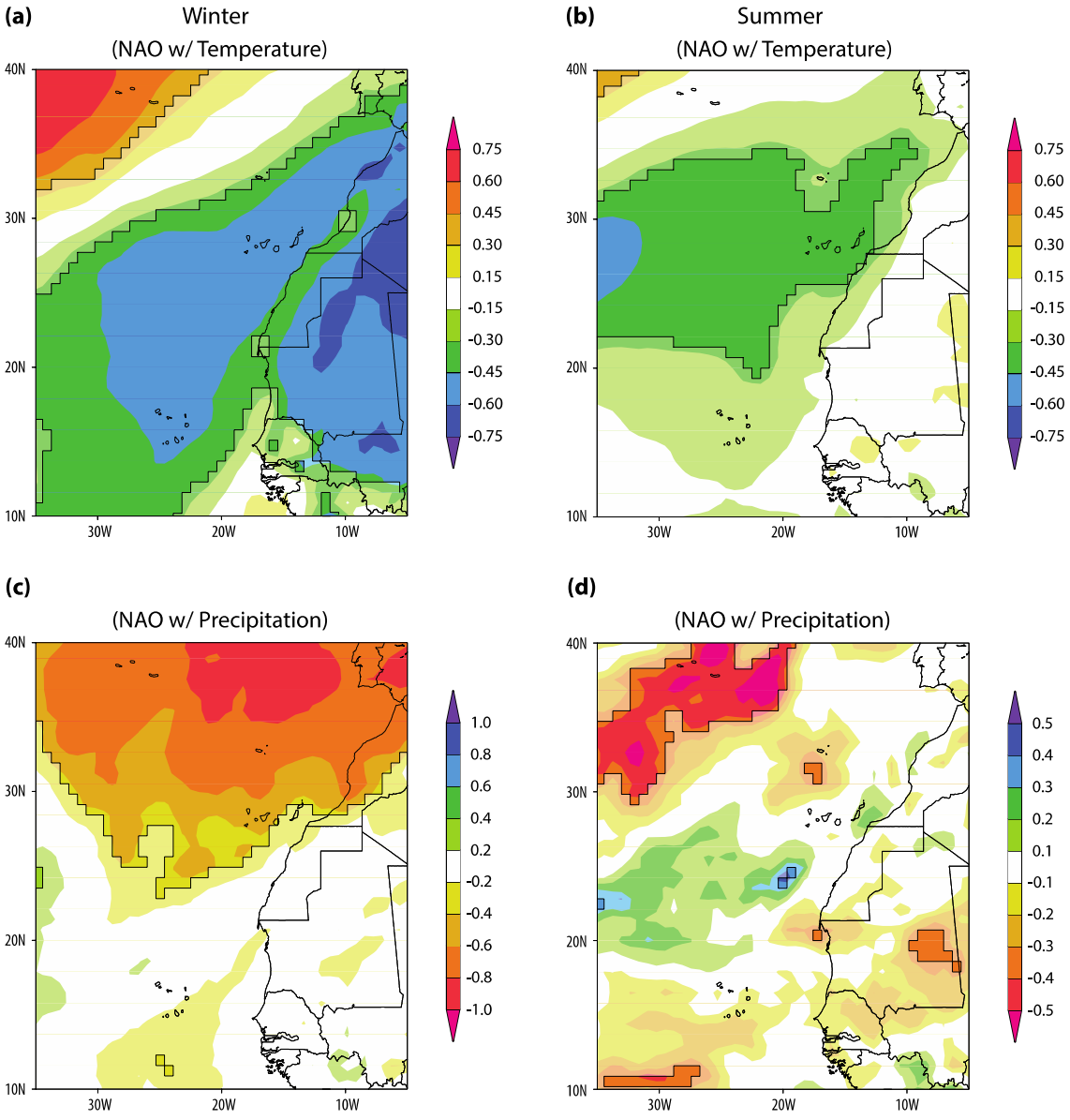

Figure 3.12. The correlation coefficient between the detrended anomalies of the station-based NAO and (a, b) 2 m SAT and (c, d) surface precipitation during winter and summer (1979-2011/12) from the ERA-I reanalysis. Solid black lines surround significant regions ($p < 0.10$).

The spatial correlation patterns have focused on the recent past (since 1979/1981). This is due to the temporal limit of the ERA-I dataset; however, other datasets exist that go further back in time (Table B5, B6). An analysis by Polyakova *et al.* (2006) suggests that the NAO relationship with the large-scale Atlantic SAT, SST and SLP fields is not constant in time. These authors found a varying spatial structure in the correlation pattern between the NAO and their analysed fields across different time periods, with 1910-1936 and 1937-1963 displaying markedly different conditions. Coincidentally, Walter and Graf (2002) noted that during the first three decades of the Twentieth Century and since 1975, the NAO and North Atlantic SSTs were strongly coupled (coinciding with generally NAO+ and AMO- years). However during the 1930s-1960s (AMO+ years) the SST-SLP relationship was weaker/absent. Eden and Jung (2001) also highlighted how the evolution of North Atlantic SST anomalies (JFM) during 5-year periods was tied in to different circulation regimes (and that a full switch in the sign of the SST anomalies took ~25 years). Periods of variability lasting ~25-30 years correspond with the approximate half cycle of the AMO, hinting at a suggested 'pacing' of natural North Atlantic climate variability. The ~60-70 year climate 'cycle' appears in numerous climate indices and observations (Wyatt and Curry, 2014) although pinning down robust physical mechanisms to explain the prominence, phase, lag and spatial connectivity of the cycle across multiple features of the climate system remains elusive.

Slight longitudinal and/or latitudinal shits in the correlation patterns depicted in Figures 3.9-3.11 would potentially result in different NAO-relationships with the Macaronesian Islands. Figure 3.13 illustrates the running correlation between the wintertime NAO and SAT from the Macaronesian Islands, which were constructed in Chapter 4. The (monthly) correlation between Macaronesian SATs and the NAO exhibits characteristics of a long-term climate cycle, with periods of negative NAO/SAT correlation during ~1895-1920 and ~1975-present and positive correlation between 1930-1960 (Figure 3.13a). Whilst the correlation values do invariably extend beyond the 95% significant line, the results are unlikely to be significant in reality, as the 19-year window removes a large amount of variation (the effective degrees of freedom were not adjusted in Figure 3.13a). The purpose of the plot is to highlight the time-variant NAO relationship with the Macaronesian Islands temperature, which strongly suggests the centres of action of the NAO shift through time. Figure 3.13b offers a 'proxy' view for the SAT across the Azores displaying a global warming/emergence from natural variability signal. Typically the Azores-NAO winter correlation and Azores winter temperatures were out of phase until ~1976. That is, a negative winter NAO implies weaker westerly flow across the mid-latitude North Atlantic region; the Trade Winds will be correspondingly weaker, allowing higher SSTs to develop across the sub-tropics which enhances the likelihood of higher temperatures across the Macaronesia region. Since the 1970s, the Azores/NAO

relationship has remained positive, yet temperatures increase rather than decrease, suggesting the emergence of a global warming signal in the SAT record.

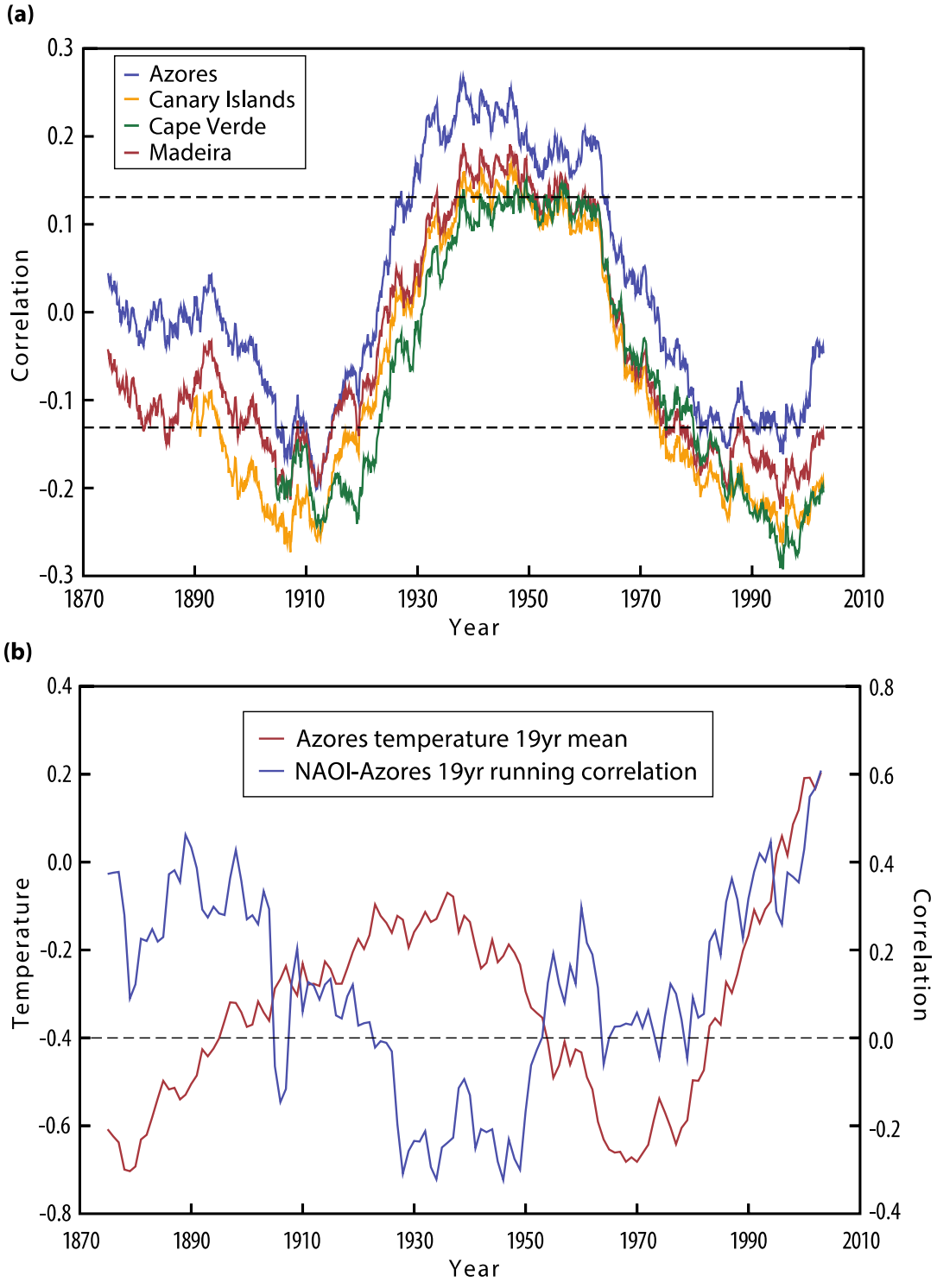

Figure 3.13. (a) The running correlation (19-year sliding window) between detrended monthly Macaronesian temperature anomalies and the monthly NAOI. Dashed lines indicate the boundaries of statistical significance ($p < 0.05$) for the correlations and (b) the running correlation (19-year sliding window) between the detrended Azores winter temperature anomalies and detrended winter NAOI in addition to the 19-year running mean of the Azores winter temperature anomalies.

3.3.2 Temporal evolution of the NAO

Historical NAO literature during the late 1990s/early 2000s cites the 1980s and 1990s as a period of strongly positive (winter) NAO values that were potentially an early signal of AGW (Gillet *et al.*, 2003). However the trend does not appear to continue throughout the 2000s (regardless of which version of the NAO is used) and the trend is in fact strongly negative (during winter) throughout the recent 1991-2013 period, with the trend magnitude exceeding the SD of the series (H15). This trend is likely exacerbated by the positive values of the early 1990s and strong negative events of winter 2009 and 2010, but highlights the strong decadal variability of the oscillation. In the CHVJ15 NAO index, the 1980-1990s positive period is less pronounced than the negative excursions of the index during the 1960s. The NAO displays no significant long-term trends during the transitionary seasons, spring and autumn (Figure 3.6, 3.7). The summer NAO has three distinct phases: (1) a marked decline from strong, consistent, positive values in the early 1850s-1880s, to a predominantly negative phase from the 1890s-1920s, (2) a return to strongly positive values during the 1930s and, (3) a weak negative trend/oscillation around neutral values since (Figure 3.6, 3.7). Trend analysis of the Hurrell NAO (which correlates above 0.90 all year-round with the CHVJ15 NAO) in H15 indicates that the centennial-scale summer trend (1900-2013) is significantly positive and recent decadal-scale trend (1991-2013) is significantly negative. The recent negative trend in the summer NAO and its associated atmospheric anomalies (Figure 3.9-3.11) has also been identified by other authors (Fettweis *et al.*, 2012; Bellflamme *et al.*, 2015), although the variation in the summer NAO from the CHVJ15 index (Figure 3.6, 3.7) appears within the realms of the longer-term natural variability (given the more extreme excursions at the start of the record).

Irrespective of the trend across certain periods in the NAO, there is an apparent shift towards a more variable pattern in the winter, and particularly, the December index. Figure 3.14 highlights the long-term trend in the running-SD of the winter NAO (using the Hurrell PC index) and Figure 3.15 in the December index (using seven monthly indices). January does not follow the same pattern, whereas February does, but weakly (not shown). In the Hurrell PC index, five out of the ten most extreme December values were in the last nine years from 2004-2013: 2010 and 2009 have the two lowest December NAO values, whereas 2011 and 2006 have the two highest December NAO values and 2004 has the fourth highest December NAO value (H15). In a 114-year long record, the likelihood of this occurring by chance is ~0.035% (1 in ~3000), based on the hypergeometric distribution and Monte Carlo sampling (Section 2.7).

The Monte Carlo test was done by generating 10,000 random time series with the same statistical properties as the December NAO series (n = 114, mean = 0 and variance = 1.59). The numbers were generated according to the normal distribution – to which the December NAO broadly approximates (the series were generated as 'white-noise', with no traits of autocorrelation, as the December NAO series is not significantly autocorrelated). Then for each time series, the number of times that five extreme NAO events occurred in 9-year windows was counted and the probability of these compared to non-occurrences of the same number of extreme NAO events was determined.

For the hypergeometric distribution (as used to analyse extreme precipitation events in Wigley and Jones (1987)), the population size is set to 114 and the 'number of events' to ten (mimicking the five top and bottom NAO extremes). Then the sample size was set to nine (to represent the 2004-2012 period) and the number of successes in the sample to five (representing the five extreme NAO values since 2004). Both methods resulted in the same answer of a ~0.035% expected chance of the values occurring naturally.

A further test of the robustness of the increased variability of the winter and December NAO was carried out by using the daily index. The mean of each calendar day was taken from 1961-1990, then for each day in each year, the squared difference between every calendar day and the mean of the calendar day was taken; the squared differences were then summed across each calendar month, allowing a monthly time series to be produced. A clear pattern, similar to the trend identified in Figure 3.14 was found, although the linear trends are non-significant (Figure 3.16). Repeating the procedure with the CPC NAO index gave a similar positive trend although the signal was smaller.

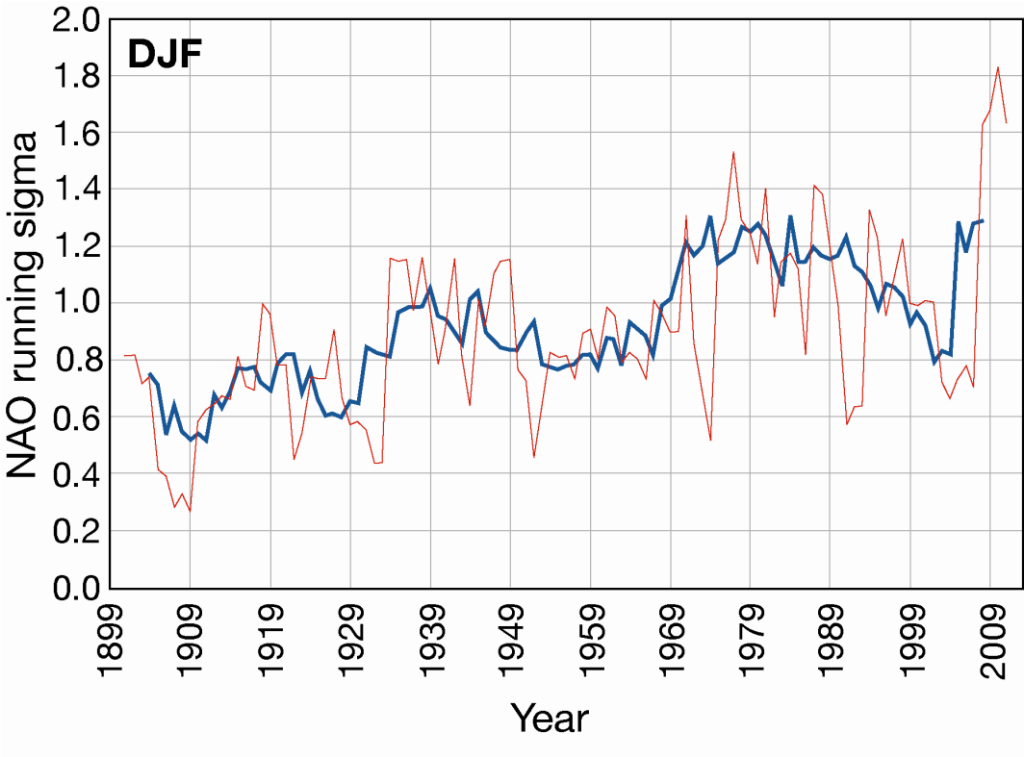

Figure 3.14. Running SD of seasonal NAO values from 1899-winter 2013. Faint red lines (bold blue lines) show the data plotted using a 5-(11-) year running sigma. NAO data are from the Hurrell PC Index.

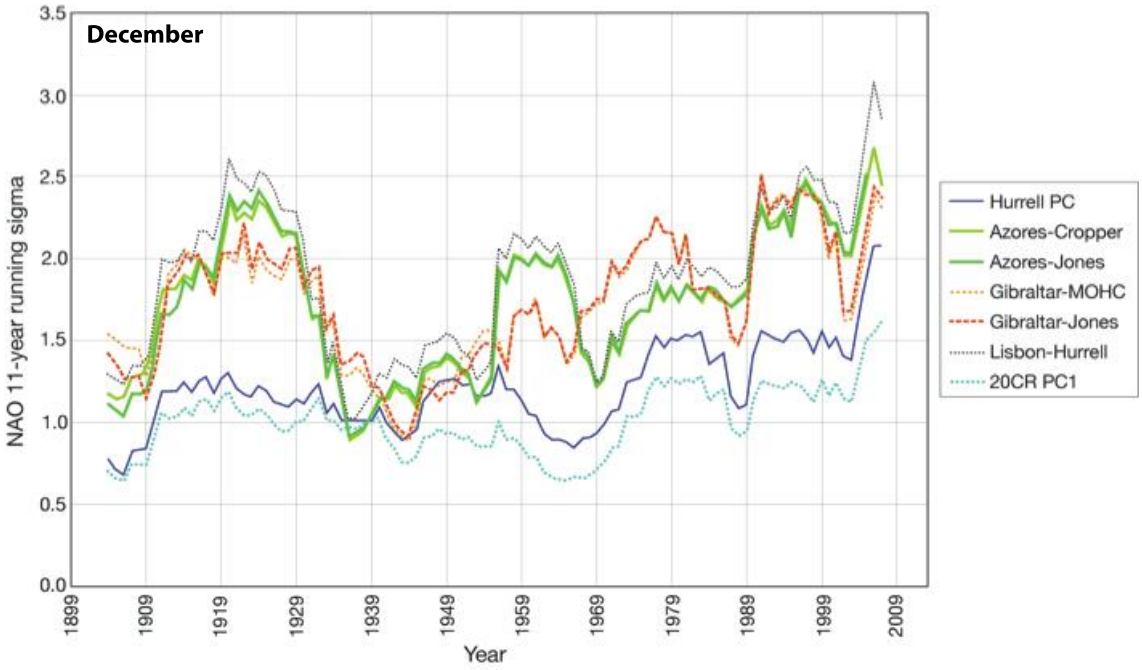

Figure 3.15. 11-year running SD of December NAO values from seven different monthly indices. Abbreviation definition can be found in Table C1.

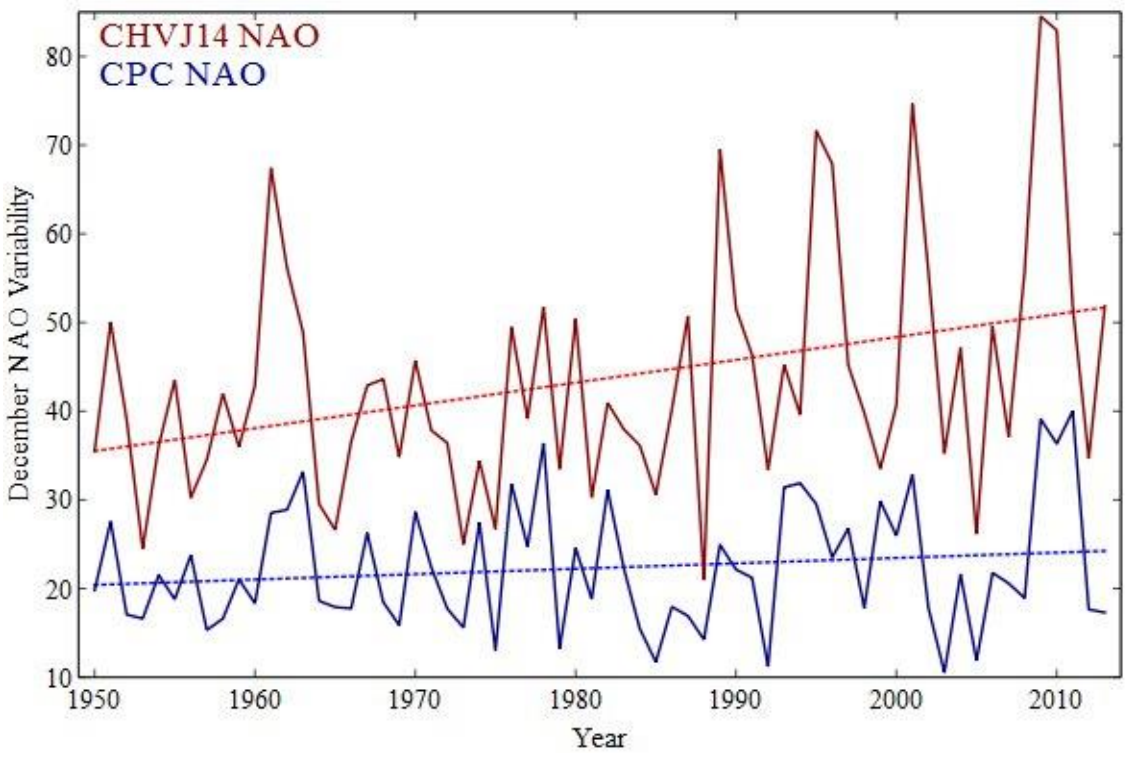

Figure 3.16. Measure of the daily NAO December variability for the CHVJ15 (red line) and CPC NAO (blue line) indices. Variability is taken as the monthly sum of the daily squared difference between each daily value and the long-term (1950-2013) daily mean. OLS trendlines are shown for each series.

What might cause the increased variability in DJF and particularly, the December NAO? The trend appears to be long term, so an immediate candidate is AGW; however, a plausible physical mechanism would need to be identified for this link to be confirmed. The NAO is potentially influenced by changes in the Arctic (snow cover, sea ice), the stratosphere, SST anomalies and deeper ocean mechanics, 'upstream' atmospheric mechanics and the jet stream, solar forcing and internal variability (Ineson *et al.*, 2011; Sutton and Dong, 2012; Fereday *et al.*, 2012). Disentangling true 'cause and effect' remains challenging. A potential feature that could contribute towards the variability 'spike' at the end of the record and ~1925-1949 is 'Arctic Amplification' (AA). When AA conditions are favoured, as has been apparent during the Twenty-first Century and ~1910-1940, the temperature gradient between the Arctic and the mid-latitudes is decreased. This decrease in temperature gradient then causes a slower, eastward propagation of planetary waves / the jet stream (Francis and Vavrus, 2012; Overland *et al.*, 2012). This is reflected in slower zonal winds and a larger wave amplitude (i.e. a more elongated, wavy jet stream, rather than a 'streamlined', pronounced jet). These slower weather patterns increase the chance of more persistent weather, which can lead to more extreme events, such as an increased incidence of atmospheric blocking which leads to a reversal of climatological pressure patterns, with downstream changes in temperature and precipitation. Of course, the conditions would not persist every year, so a more variable

year to year climate (i.e. which would be reflected in a running-average of a monthly SD time series) is found where conditions switch between 'normal' and 'strongly-AA-influenced'. The increased variability could also come from persistent AA conditions alone, although certain features are likely to be favoured. One of these is enhanced blocking conditions over Greenland (Hanna *et al.*, 2013; 2014), which when set up, can persist for weeks and steer weather patterns. A support for AA conditions driving the winter NAO increased variability would be that under the more consistent NAO+ conditions of the 1980-90s, in which there was a colder Arctic, there was less extreme weather than since the turn of the Twenty-first Century (Francis and Vavrus, 2012; Overland *et al.*, 2012). The pronounced positive NAO phase of the 1980-90s reflects this, shown by the temporary negative trend in 5/11-year SD during the 1980s until the mid-2000s in Figure 3.14 (i.e. consistently positive values = less variability).

The above scenario represents the 'tropospheric' influence school of thought. As previously mentioned, it is likely the interplay of numerous effects contribute to the variability changes. For example, if the 'stratospheric school of thought' is considered, Lu *et al.* (2014) suggest that the mechanism that connects the phase of the QBO with the stratospheric polar vortex (and indirectly the NAO) was disrupted during 1978-1997, coincident with the temporary variability decrease in the NAO index seen in Figure 3.14. The QBO has significant power in the 26-29 month period, so this period of ~2 year variability could further contribute to NAO running-SD in 5 and 11-year window lengths. H15 also identified a significant long term increase in the summer 'Greenland Blocking Index', which represents the strength of high-pressure through a deep layer of the atmosphere above Greenland. When large high-pressure systems 'set up' above Greenland, the resultant effect is close to an NAO- pattern (H15 identifies a significant negative correlation with the NAO, r = -0.84 over 1948-2012 for JJA on average). Hanna *et al.* (2012) suggest that the changes in the GBI may be a function of natural variability or potentially, as an initial global warming response, seeing as the proportion of high Greenland-blocking events were more common since the start of the Twenty-first Century.

3.4 The Trade Wind Index

As shown in Figure 1.7, the NAO is strongly related to the Trade Winds. This is mainly through modification of the Azores High. A stronger subtropical high relative to the equatorial low-pressure is likely to result in stronger winds (and vice-versa). However the NAO centres of action are more fixed toward the mid-latitudes (as displayed in Figure 2.3 – the stronger EOF values in the spatial field are equal to the areas where the greatest

amount of variability is explained by the analysis). The design purpose of the TWI was to take advantage of the position of the Azores, located in the subtropics, and the Cape Verde Islands, located just north of the equatorial low, by using a normalised station-based index between the two islands as a measure of the Trade Wind intensity. A positive value (stronger SLP difference than normal between the Azores and Cape Verde) implies stronger Trade Winds and a negative value suggests weaker Trade Wind strength. The data used were the GSOD stations from Ponta Delgada and Sal (Table B3, 4.1), which were aggregated to the monthly resolution (and also pass homogeneity tests). A daily TWI can be made the same way as the daily NAO discussed in Section 3.2, but limited station-data availability from Sal before 1973 limits the potential length of the reconstruction, unless reanalysis data are used.

The composite wind vectors of the climatological mean, five highest and five lowest summer TWI years (Figure 3.17) illustrate that the TWI may be of some use in determining Trade Wind strength. Figure 3.17a shows the climatological mean wind vector and Figure 3.17b illustrates the effects of highly positive TWI years, which is an enhanced Trade Wind pattern (wind-speeds increased by ~5–25%), greatest to the west of the Canary Islands above 25°N. Figure 3.16c illustrates the effects of highly negative TWI years, when between approximately 20 and 40°N the strength of the Trade Winds are reduced (note that the direction of the Trade Winds does not reverse, rather the strength of the north-easterly winds is being reduced, again by about ~5–25%). The TWI shows an increasing trend across all seasons from 1973 to 2012 (Figure 3.18), suggesting that Trade Wind strength, across the eastern boundary of the North Atlantic Ocean from 35 to 20°N, has significantly increased during the last 40 years (monthly and seasonally statistically significant, 1973–2012, with p values all <0.1).

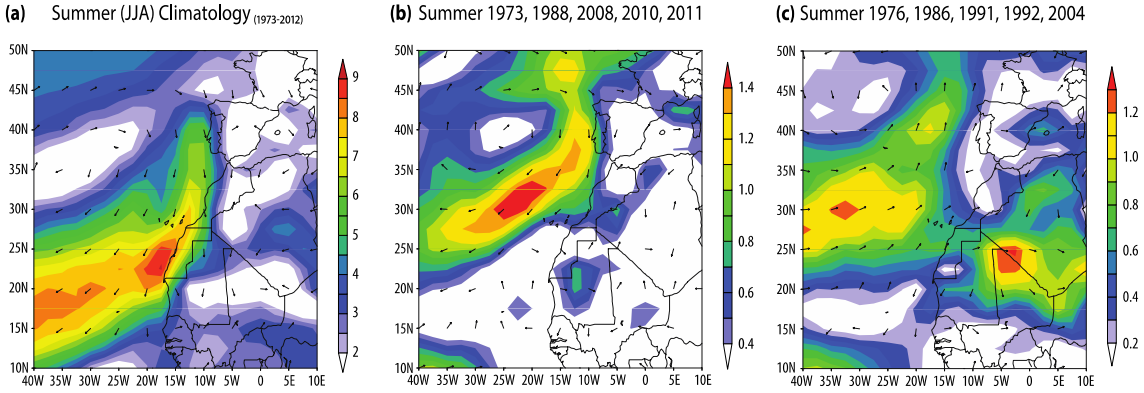

Figure 3.17. (a) The summer (JJA) climatological mean wind-speed (m/s) and vectors across the Macaronesian region for 1973–2010 (from the NCEP/NCAR reanalysis) and the composite anomaly of the five (b) most positive and (c) negative years for the summer TWI.

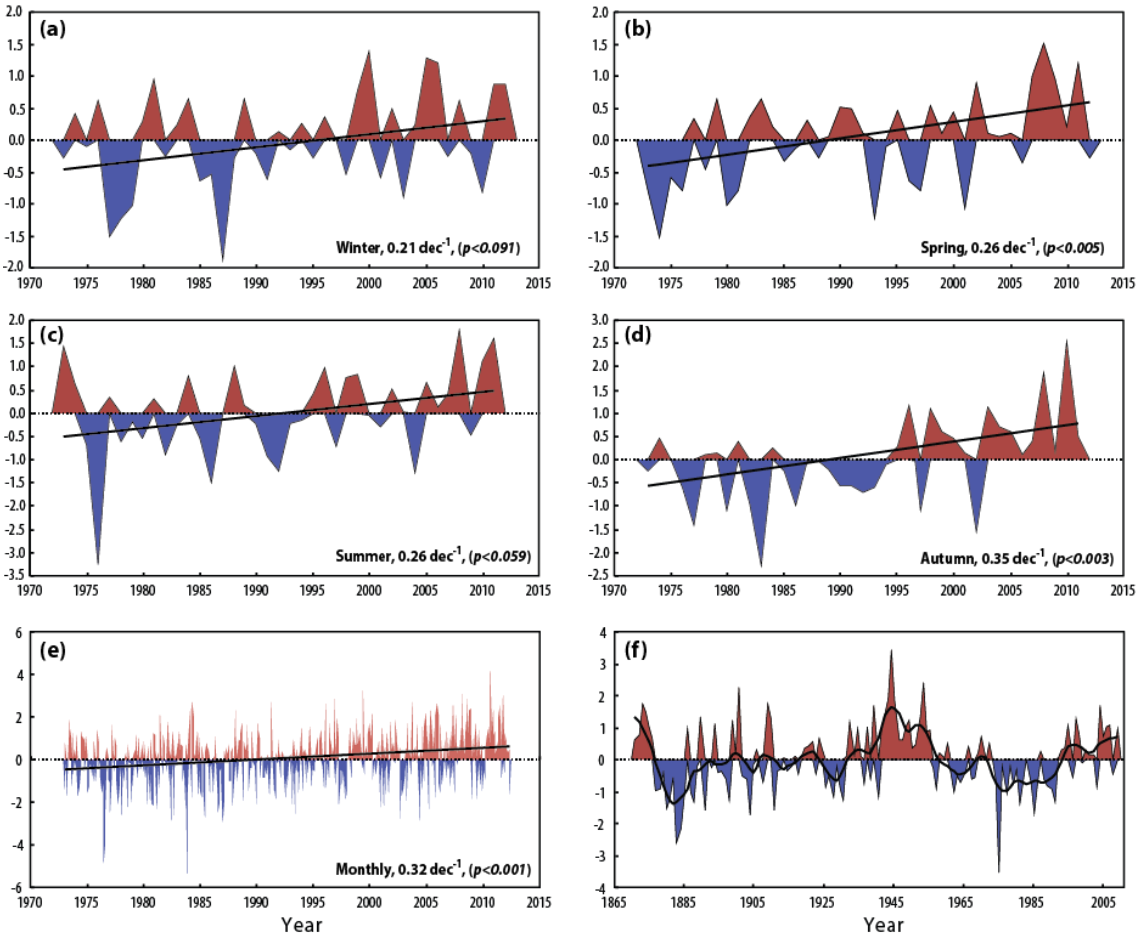

Figure 3.18. (a) The station-based seasonal (a–d) and monthly (e) Trade Wind index, 1973–2012 and (f) the extended summer (JJA) Trade Wind index, 1871–2010. The northern station is the SLP record from Ponta Delgada, and the southern station is the SLP record from Sal. The extended index is created by splicing the record at Sal with SLP data from the overriding grid-box from the 20CR reanalysis. The black lines (a–e) represent the 1973–2011/2012 TS trends and (f) an 11-year LOESS trend.

Such consistent trends across all seasons raises potential concerns that inhomogeneities may not have been identified in the earlier meteorological-station homogeneity testing. However, a logical test can be found by analysing ocean heat content (OHC) data from Levitus *et al.* (2012), under the rationale of stronger Trade Winds driving a surface cooling and greater uptake of upper level (0-700m depth) ocean heat. Such a mechanism has been invoked to occur in the Pacific Ocean, where stronger Trade Winds during the past two decades relate to a semi-permanent La Niña state (England *et al.*, 2014) that has had a strong cooling effect on global SATs (given the large area of the Pacific Ocean).

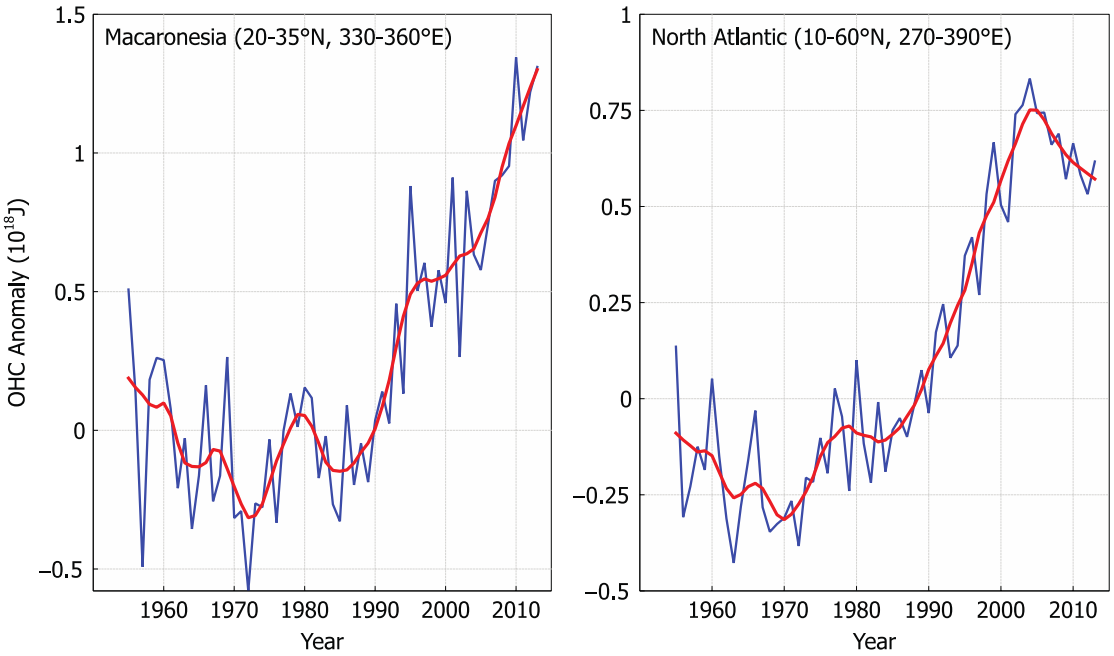

Figure 3.19. Ocean Heat Content data (Levitus *et al.*, 2012) through 0-700 m depth across (a) Macaronesia and (b) the wider North Atlantic region.

Here, restricting the spatial region to the northeast Atlantic region of 20-35°N, 330-360°E, it can be seen that OHC has risen almost linearly in line with the increasing Trade Winds, supporting the positive TWI increase (Figure 3.18, 3.19). Extending the spatial region of OHC trends to encompass the wider Atlantic basin indicates a peak at, and decline since, 2003. Potentially, since the shift to the positive regime of the AMO (or high Atlantic SSTs in general across the last 15 years), OHC uptake will have decreased across the wider-Atlantic, in line with higher SSTs.

It is possible to extend the TWI back to 1871 using the nearest 20CR reanalysis grid-box to Sal (with the regression splicing approach documented in Section 2.2.1 between the Sal station and the 20CR data). Doing so indicates a previous rise from around 1910–1945, followed by a decline from 1945–1975 (Figure 3.18f). Further analysis regarding the historical accuracy of the reconstruction and mechanisms behind these changes goes beyond the scope of this thesis; however, spectral analysis reveals an interesting ~70-year cycle in the long-term record (Figure 3.18f). Observed widening of the Hadley Cell along with a poleward migrating ITCZ, is thought to be a potential response to AGW, although the exact physical mechanisms are yet to be fully understood (Johanson and Fu, 2009; Schneider *et al.*, 2014). This shift could conceivably alter the SLP pressure patterns above the Azores (increase in SLP) and across Cape Verde (decrease in SLP as the ITCZ moves closer) and is suggested as a potential mechanism for the post-1973 increase in the TWI.

The winter temperature correlations with the TWI were identified as being very similar to the winter NAOI induced patterns (Figure 3.12, 3.20), due largely in part to the overriding influence of the strength of the Azores High and its more fixed winter location. The summer TWI index is observed to correlate strongly with wind-speeds across the Azores-Canary Islands region of Macaronesia (Figure 3.20). These conditions favour evaporation and reduced temperatures (due to transfer of colder water from higher latitudes, entrainment of cold Canary Current water and evaporative cooling) (Figure 3.20). It is assumed that the TWI is indirectly related to the northwest African Monsoon, as positive correlations with SAT and precipitation were observed below 20°N (which merits further investigation).

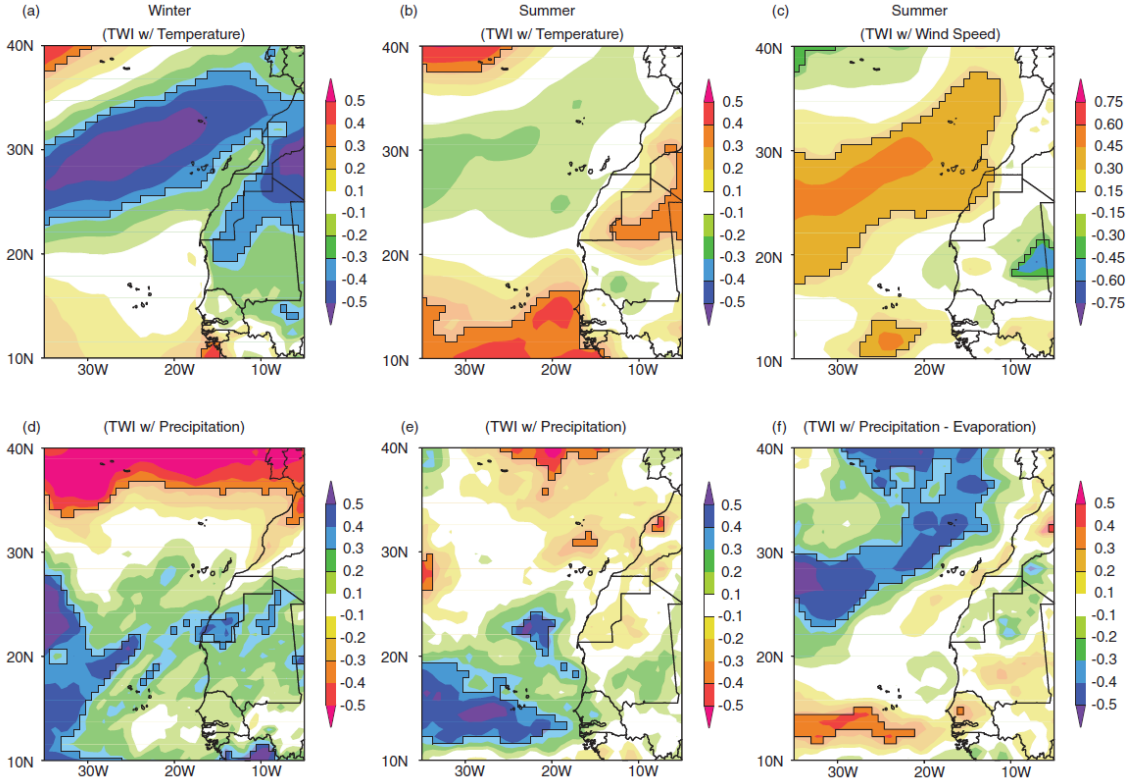

Figure 3.20. The correlation coefficient between the detrended anomalies of the TWI with 2 m SAT (a, b), wind-speed anomalies (c), surface precipitation (d, e), and P–E (f) from the ERA-I reanalysis across 1979–2011/2012 during winter (only for temperature and precipitation) and summer. Black lines enclose statistically significant areas ($p < 0.1$).

3.5 Chapter Summary

A daily/09:00 UTC station-based NAO running from 1850/1871 to present has been created by reconstructing a new SLP record from the Azores combined with the existing southwest Iceland SLP series. This extends the previous maximum extent (of the CPC daily indices which begins in 1950) by up to 100 years. A novel approach to normalise the daily indices has been implemented, using a tension spline method. The resulting monthly average of the daily NAO corresponds well with existing monthly-only NAO indices and should be of great use in future studies concerning Northern Hemisphere weather and climate variability. The new daily NAO index is archived at the Zenodo online repository (https://zenodo.org/record/9979).

The NAO exerts a significant control on temperature and precipitation values across the Macaronesian region. The relationship is strongest during winter, persists during spring and autumn and is weaker during the high summer months. Under current climate conditions, the NAO positively correlates with Azores temperatures and negatively correlates with Canary Island, Madeira and Cape Verde temperatures during winter. Winter precipitation negatively correlates with the NAO across most of the three northernmost island chains. It is unlikely that the spatial pattern of NAO correlations has remained constant in time. Changes in the centres of action of the NAO would potentially result in different effects across Macaronesia.

There were some recent dramatic changes in the NAO index itself; these were a marked increase in winter (particularly December) variability – i.e. the index is switching between more extreme values more frequently – and interesting long-term variations in the summer NAO, with a recent (1991-2013) trend towards more negative values of the index. AA conditions have been favoured since the turn of the Twentyfirst Century (Overland *et al.*, 2012; Francis and Vavrus, 2012), and cause a reduction in the mid-latitude to pole temperature gradient. This may affect the zonal propagation and the amplitude of the jet stream and atmospheric circulation across the Northern Hemisphere, and is potentially linked to both the increase in winter variability and negative summer trend in the NAO, although natural variability cannot be discounted.

A novel method to characterise the Trade Winds across the Macaronesian geographical zone, based on the SLP difference between the Azores and Madeira, has been created. This index shows a significant increase across all seasons since 1973. This is considered to be a robust feature; logical connections with observed patterns or changes in temperatures, wind-speeds, precipitation and OHC have been observed.

4. Macaronesia Climate Evolution (1865-2012)

(Much of the work, analysis and discussion from the following chapter was taken from C13 and CH14)

4.1 Surface Air Temperature

The primary objective of this thesis was to '*Create a climate record that will allow analysis of long-term changes in Macaronesian Climate'*. The following two sections present how this was objective was accomplished by creating a major long-term temperature and precipitation time series for each of the four Macaronesian Island chains. The data used in this chapter were primarily sourced from multiple freely available online sources (Table 4.1, B3) of daily-monthly data archived from weather stations across the Macaronesian Islands. The major archives were the GHCN, ECA&D and the GSOD databases. Initial analysis of long-term monthly temperature data from the four islands revealed that the most complete record was from Funchal, Madeira, which runs from 1865-2012 with limited gaps. Records from Ponta Delgada (Azores), Las Palmas (Canary Islands) and Mindelo (Cape Verde) start in 1865, 1885 and 1884 respectively. These were the most complete record for each island chain but the records did not extend up to the present (except Las Palmas) and were plagued by considerable gaps. As such, it was determined the best way to establish a long term temperature time series for each island was to apply the regression splicing method as in Hanna *et al.* (2006) (Section 2.2.1). Complementary temperature records for each island were required to either fill gaps in historical records and/or extend the record to present: these are listed in Table 4.1. Supplementary stations were needed to complete the 'major' records, which are shown as a Gantt chart in Figure 4.1. The locations of all stations used in this section are indicated in Figure 4.2.

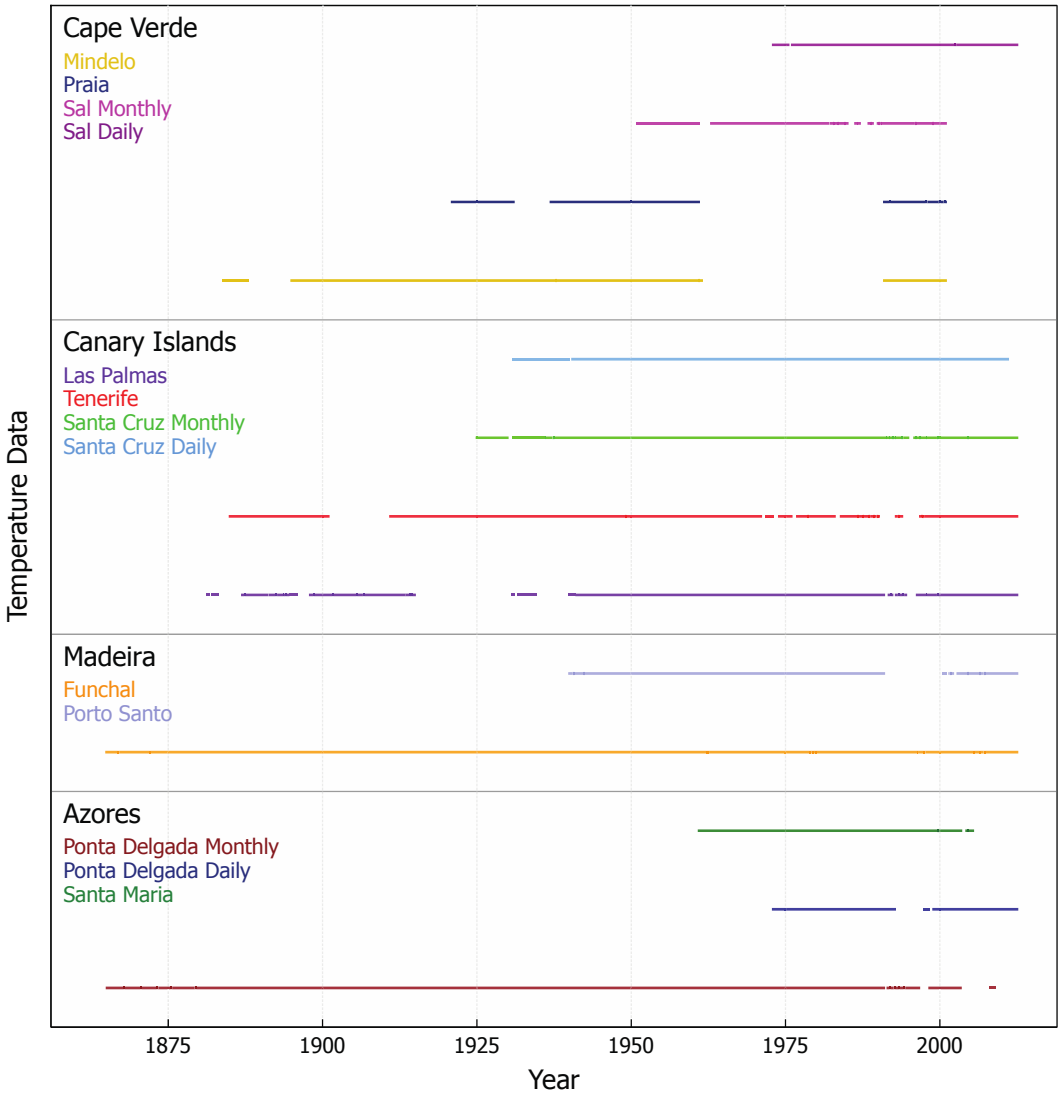

Figure 4.1. Gantt chart depicting the temporal availability of raw temperature data from 13 meteorological stations across the four Macaronesian Islands.

Station	Identification	Latitude (°North)	Longitude (°East)	Altitude (m)	Highest Island Elevation (m)	Start	End	Source
				Azores				
Ponta Delgada	PD	37.70	334.30	67	1105	1865	2003	GHCN
Ponta Delgada Daily	P2	37.73	334.30	71	1105	1973	2012	GSOD
Santa Maria	SM	37.00	334.88	100	587	1944	2005	GHCN, GSOD
				Canary Islands				
Tenerife	*TE*	28.47	343.68	617	3718	1885	2012	GHCN
Santa Cruz De Tenerife	*SC*	28.45	343.75	36	3718	1881	2012	GHCN
Santa Cruz De Tenerife	*SC*	28.45	343.75	36	3718	1938	2012	ECA&D
Las Palmas	*LP*	28.10	344.58	25	1949	1887	2012	GHCN
				Cape Verde				
Sal	*SA*	16.73	337.05	55	406	1951	1996	GHCN
Sal Daily	*S2*	16.73	337.43	54	406	1973	2012	GSOD
Mindelo	*MI*	16.88	335.00	63	725	1884	1961	GHCN
Praia	*PR*	14.90	336.48	35	1394	1921	1960	GHCN
				Madeira				
Funchal	*FC*	32.63	343.10	50	1862	1865	2012	GHCN
Funchal Daily	*F2*	32.68	343.23	49	1862	1973	2012	GSOD
Porto Santo	*PS*	33.07	343.65	82	402	1940	2004	GHCN

Table 4.1. Summary of meteorological-stations and data products utilised in this study. Refer to main text for dataset descriptions and reference. The identification column indicates the labels used in Figure 4.2.

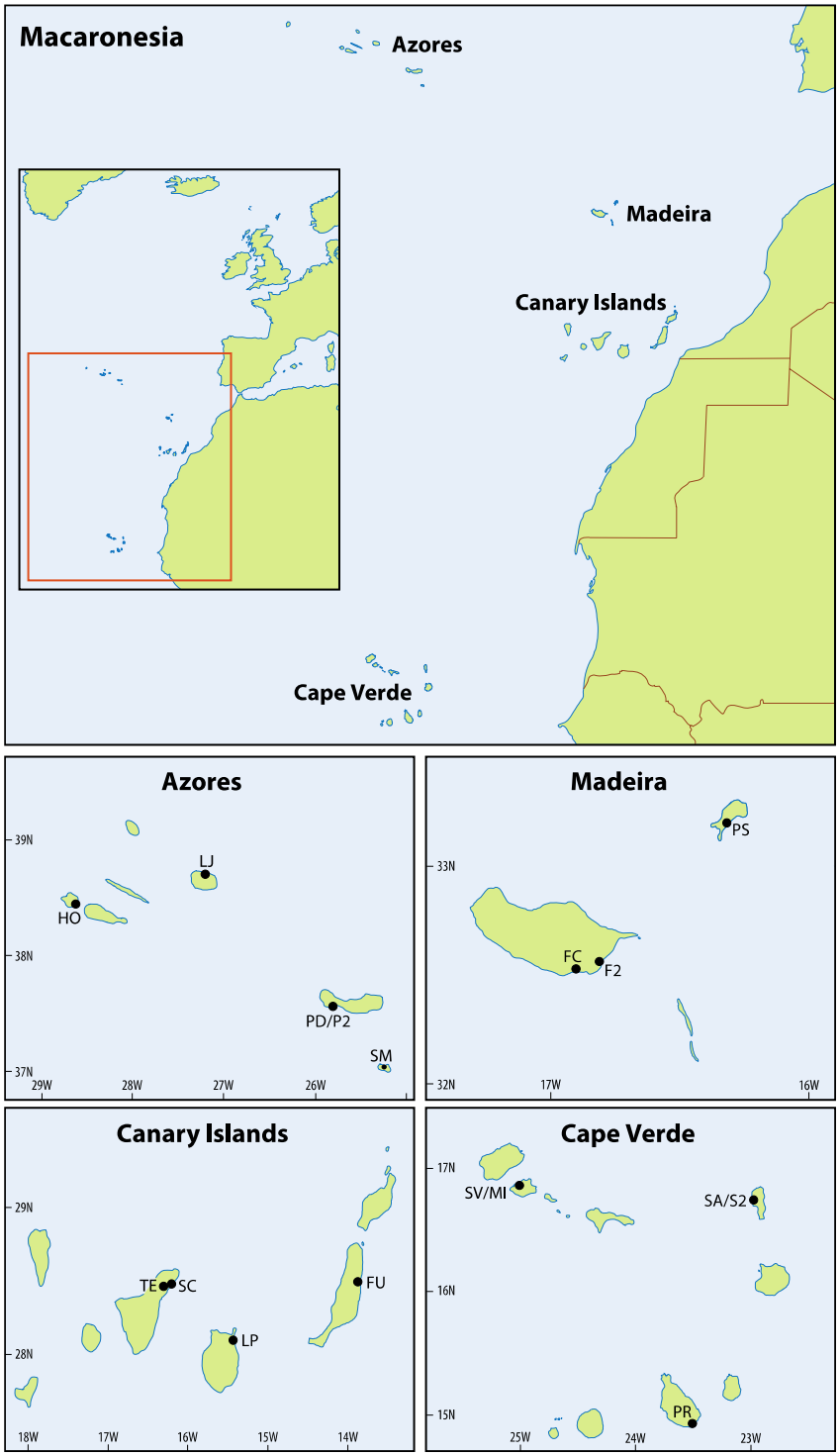

Figure 4.2. The Macaronesian region, marked with the meteorological-station positions used in Chapter 4 (Identification tags can be found in Table 4.1 and 4.6).

The reference stations for which the regression relationships were based on for each of the four island chains are: Ponta Delgada (Azores), Santa Cruz De Tenerife Daily (Canary Islands), Sal (Cape Verde) and Funchal (Madeira). Ponta Delgada passed all three location specific tests for homogeneity (SNHT, Pettitt and Buishand, the PMF test was not used in the CH14 paper) (Section 2.5). Funchal failed the SNHT and Buishand tests at 1986 and 1976 respectively. With no sign of any abrupt shifts and no obvious

outliers after visual observation and running variance analysis, these breakpoints were attributed to gradual climate change -or potentially a function of the well-known climate 'shift' that occurred in 1976–1977 (Overland *et al.*, 2008) - as opposed to a physical inhomogeneity. The Santa Cruz and Sal records both failed the SNHT test at a similar time (1994 and 1995 respectively). It was identified that the Santa Cruz record failed the homogeneity test because of a rapid (1.5–2°C) temperature swing between 1994–1995 and 1996–1997. Martín *et al.* (2012) attributed an early 1990s cooling to the effects of atmospheric dimming from the Mount Pinatubo eruption which, superimposed on the general 1990s warming trend, might explain the apparent sudden shift in temperatures - given the temporary cooling effect of volcanic aerosols. Figure 4.3 highlights the intense dispersion of stratospheric aerosols following the Pinatubo eruption. The Pinatubo eruption cooled Northern Hemisphere temperatures by ~-0.5°C (Foster and Rahmstorf, 2011), so Macaronesia was likely affected.

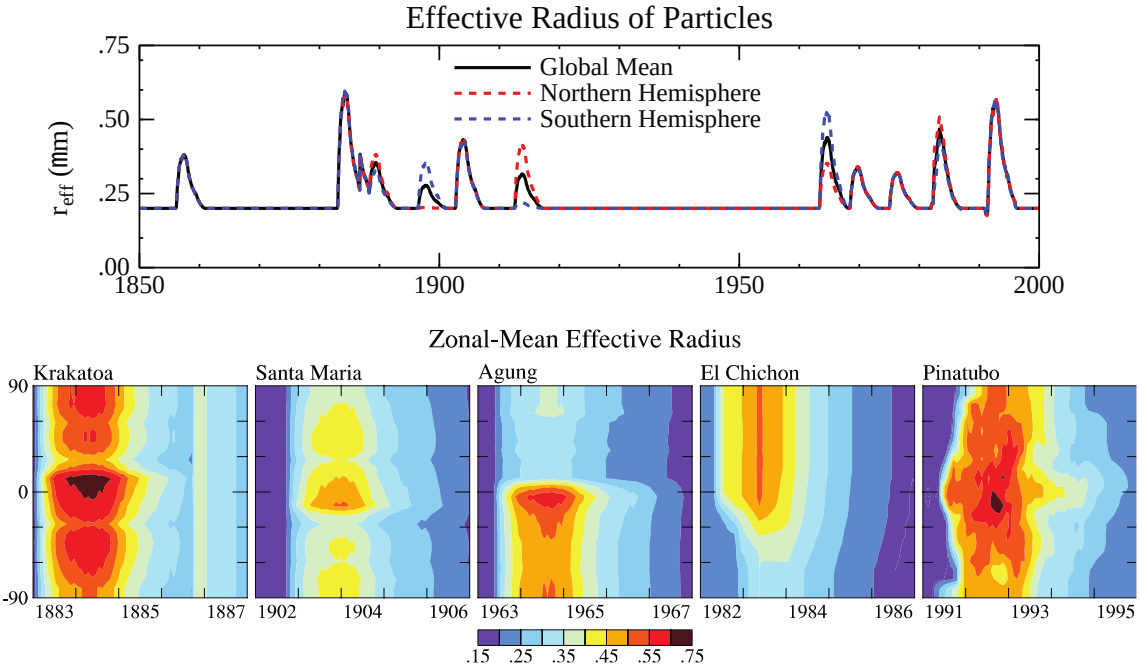

Figure 4.3. (http://data.giss.nasa.gov/modelforce/strataer/) Stratospheric aerosol optical thickness data at 550 nm from the NASA Goddard Institute for Space Studies archive.

The shift is also apparent in temperature records from the other Canary Island stations and the nearest grid-boxes from the ERA-I (Dee *et al.*, 2011) and NCEP/NCAR (Kalnay *et al.*, 1996) reanalyses, so this was accepted as a natural variation rather than an inhomogeneity requiring adjustment. A similar pattern is seen in the Sal record from 1994 to 1997 (and also across the three other Cape Verde stations) so likewise, no action was taken to alter the record. The early 1990s shift was also apparent in the Azores and Madeira records but was not as pronounced. Relative homogeneity corrections (shifts in the mean but not in trend) were applied to the following stations (Table 4.1): Ponta

Delgada Daily (January 1973 to July 1988), Santa Maria (May 1964 to September 1981), Las Palmas (December 1889 to January 1983), Porto Santo (January 1940 to April 1949; June 2000 to July 2012) and Sal (January 1973 to December 1981). The regression splicing between stations resulted in a continuous monthly temperature record from 1865 for the Azores and Madeira, 1884 for the Canary Islands and 1895 for Cape Verde (Figure 4.4).

Unfortunately, a few small gaps remained across the records (6/1770 monthly cases for the Azores record and 4/1531, 19/1459 and 6/1772 for the Canary Islands, Cape Verde and Madeira records respectively). Single months were filled using the mean of the adjacent two months, while longer gaps were set to the average monthly value of the previous and subsequent five years for each month. This caused minimal disturbances to the long-term trend and was only used to fill a small minority of gaps. Descriptive statistics and trends for climatological 'normal' periods are given (Tables 4.2 and 4.3).

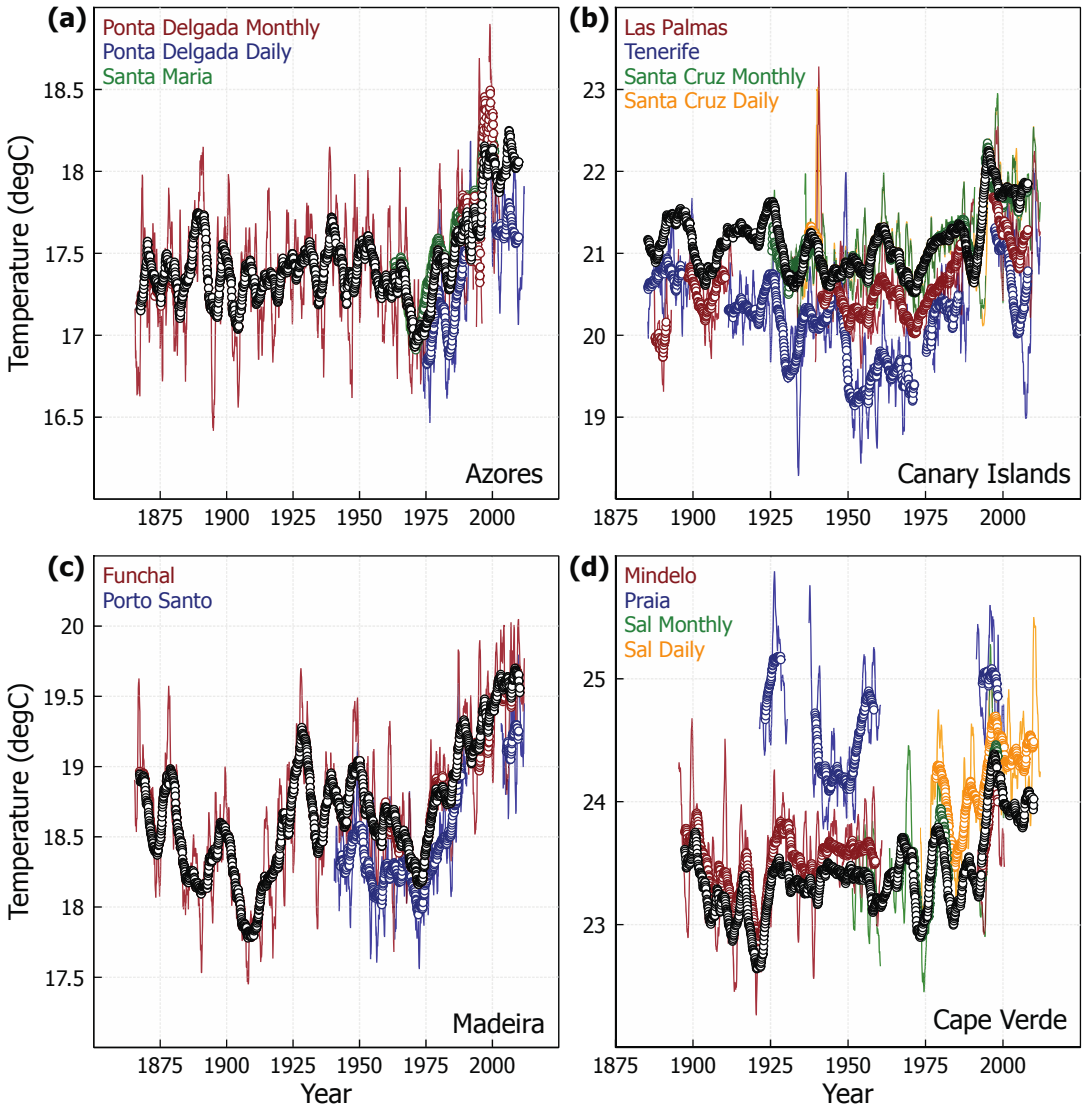

Figure 4.4. (Figure 5 from CH14) The reconstructed monthly SAT time series of (a) the Azores, (b) the Canary Islands, (c) Madeira and (d) Cape Verde. The 12-month running means of each station used in the reconstruction (as lines) and the 60-month running means of the stations (as circles, black circles indicate the 60-month running mean of the final island time series) are displayed.

Annual interquartile range across the entire time period is 5.2°C for the Azores, 3.4°C for Cape Verde and 4.8°C and 4.6°C for the Canary Islands and Madeira respectively. Annual temperatures increase for the islands that are progressively closer to the equator. The modulating effect on the islands' temperature due to the ocean is evidenced by the similarity of the SD for all months across all locations (Table 4.2). Generally, the four island temperature records display coherent variability (Figure 4.4, 4.5). The exception is the early part of the Madeira record (1865–1915), where a cooling trend that is strongest in winter (Table 4.3) results in lower temperatures than for the other three islands. Warm peaks were centred around 1900, 1927 and 1939, with a synchronous cool trough in the early 1970s, which is followed by a rapid warming phase continuing until the present (Figure 4.5). The trends for the entire time period (1865–2011/2) and the

standard century (1901–2000) are characterised by warming throughout (with the exception of Azores winter, Table 4.3), although generally these trends were not significant and there was little sustained change before the late Twentieth Century temperature rise. The magnitude of the 1981–2010 temperature increase surpasses most previous temperature variability (the only exception to this is Madeiran winter temperature during 1911–1940). Recently, summer is the season with the most prominent temperature increase (Table 4.3) with trends in the range of 0.32–0.46°C dec^{-1}. Accordingly, the first decade of the Twenty-first Century was the warmest decade on record for all the island chains. Meanwhile, 1971–1980 was the coldest decade for the Azores, 1951–1960 and 1971–1980 the joint coldest for the Canary Islands, 1941–1950 for Cape Verde and 1901–1910 for Madeira. Additionally, the Twenty-first Century contains seven of the warmest ten years on record for Madeira, and three out of ten for the other island chains. Using the bias adjusted GHCN v3 global average as a base (0.91°C per century, Lawrimore *et al.*, 2011) for 1901–2010 (annually), the Azores, Canary Islands and Cape Verde warmed at ratios of 0.57, 0.67 and 0.95 of the global average for this period, with Madeira exceeding the global average, warming at a rate of 1.37 times greater (a component of this greater increase was due to the aforementioned cooler early Twentieth Century temperatures). For 1981–2010, all four island chains exhibit warming rates greater than the global average of 0.27°C dec^{-1} at a ratio of 1.21, 1.11, 1.22 and 1.40 times greater for the Azores, Canary Islands, Madeira and Cape Verde respectively. The prominence of the late Twentieth Century temperature rise is further highlighted by the fact that these island stations in the middle of the North Atlantic Ocean exhibit typically clearer signal-to-noise ratios due to the stability of the surrounding maritime environment.

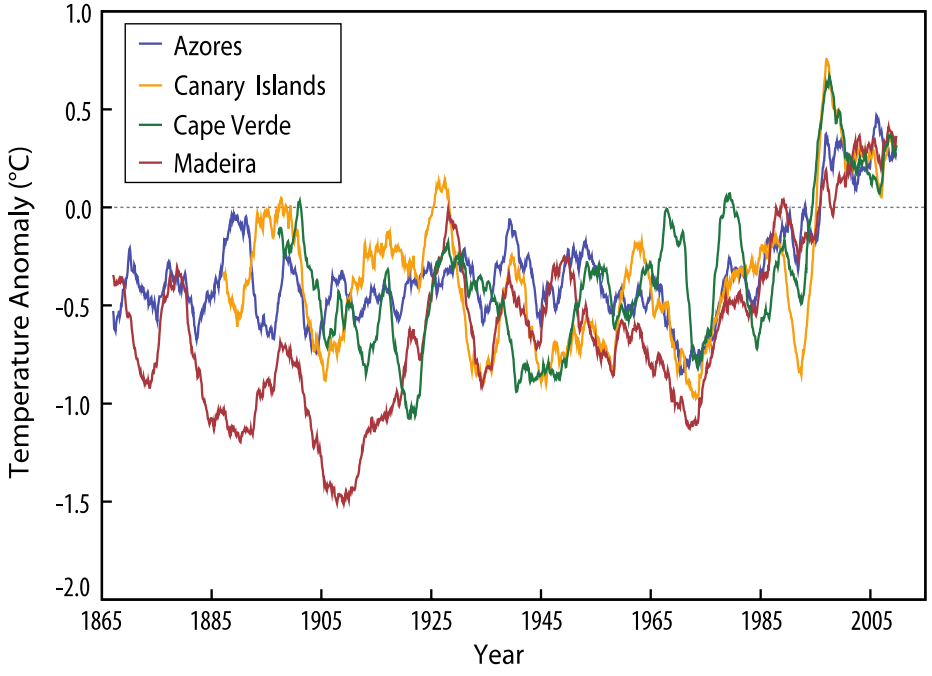

Figure 4.5. 11-year LOESS trends of the reconstructed Macaronesian SAT anomalies.

Location	Mean Temperature (°C)												
	Annual	**Jan**	**Feb**	**Mar**	**Apr**	**May**	**Jun**	**Jul**	**Aug**	**Sep**	**Oct**	**Nov**	**Dec**
Azores	17.4	14.5	14.1	14.4	15.2	16.6	18.9	21.0	22.1	21.1	19.1	16.9	15.4
	(2.9)	(0.8)	(0.7)	(0.7)	(0.7)	(0.7)	(0.7)	(0.7)	(0.7)	(0.7)	(0.8)	(0.8)	(0.7)
Canary Islands	21.1	17.9	18.0	18.6	19.3	20.6	22.5	24.4	25.2	24.5	23.1	20.8	18.8
	(2.7)	(0.7)	(0.9)	(0.9)	(0.8)	(0.8)	(0.8)	(0.9)	(1.0)	(0.8)	(0.8)	(0.8)	(0.8)
Cape Verde	23.4	21.3	20.9	21.3	21.7	22.4	23.4	24.4	25.7	26.4	25.9	24.5	22.5
	(2.0)	(0.7)	(0.9)	(1.0)	(0.8)	(0.7)	(0.7)	(0.7)	(0.7)	(0.7)	(0.7)	(0.7)	(0.8)
Madeira	18.7	15.8	15.7	16.1	16.7	17.9	19.7	21.4	22.4	22.2	20.8	18.6	16.8
	(2.6)	(0.8)	(0.8)	(0.9)	(0.8)	(0.7)	(0.7)	(0.7)	(0.8)	(0.7)	(0.7)	(0.8)	(0.8)

Table 4.2. Macaronesian annual and monthly average temperatures (SD in parentheses) for 1865-2011 (1885-2011 and 1895-2011 for the Canary Islands and Cape Verde respectively).

Location	ANN	DJF	MAM	JJA	SON
	Trend (°C dec^{-1})				
1865-2011/12					
Azores	**0.03**	0.03	0.03	0.01	0.05
Canary Islands (1885-)	0.02	0.03	0.03	0.04	0.01
Madeira	**0.06**	**0.09**	**0.06**	0.01	0.08
Cape Verde (1895-)	**0.07**	**0.06**	**0.06**	**0.08**	**0.05**
1865-1910					
Azores	0.01	0.11	0	-0.02	-0.03
Madeira	**-0.20**	**-0.24**	**-0.18**	**-0.18**	**-0.20**
1901-2000					
Azores	0.02	-0.02	0.03	0.02	0.06
Canary Islands	0.02	0.00	0.02	0.05	0.00
Madeira	**0.09**	**0.10**	0.08	0.04	**0.11**
Cape Verde	0.05	0.05	0.06	0.06	0.04
1911-1940					
Azores	0.10	0.06	0.21	0.06	0.05
Canary Islands	-0.15	-0.19	-0.05	-0.15	-0.14
Madeira	**0.31**	**0.33**	**0.41**	0.18	0.18
Cape Verde	0.17	0.15	0.18	0.20	0.18
1931-1960					
Azores	-0.04	-0.18	-0.08	0.04	0.06
Canary Islands	-0.05	-0.05	-0.11	0.07	0.04
Madeira	-0.03	0	-0.16	-0.13	0.15
Cape Verde	-0.02	0	-0.18	0.01	0.07
1981-2010					
Azores	**0.33**	0.27	0.28	0.32	0.23
Canary Islands	0.30	0.27	0.25	**0.40**	0.25
Madeira	**0.33**	0.24	**0.41**	**0.46**	0.16
Cape Verde	**0.38**	0.32	0.27	**0.41**	**0.38**

Table 4.3. Macaronesian seasonal and annual temperature trends over selected and standard periods. All trends are reported in degrees Celsius per decade (°C dec^{-1}). Bold indicates significant trends ($p < 0.1$) where the data passed both the standard and modified MK tests for significance.

Correlation coefficients between monthly temperature anomalies (1981–2010 base) and the monthly station-based NAOI across the longest possible temporal periods based on the island temperature records and using the CH14 NAO were 0.08, -0.27, -0.16 and -0.23 for the Azores, Canary Islands, Madeira and Cape Verde respectively. Seasonally,

the relationships were stronger, particularly in winter (DJF), where the long-term correlations were (again for the Azores-Cape Verde) r = 0.21, -0.38, -0.19 and -0.44 (all significant ($p < 0.01$)). Removing the long-term linear trend from both records does not significantly change the relationship.

The positive Azores correlation and negative correlation for the other islands were as expected, given the typical NAO-SAT relationship (Figure 3.9). For the Macaronesian Island chain, it is simple to think of this increasing negative correlation with decreasing latitude as a result of the distance–decay relationship between the islands and the Azores High-pressure system. More simply, the Azores will usually be close to the centre of action of the semi-permanent high-pressure system, so changes in its strength and location will not have as great an effect on Azores temperature (but have a greater control on precipitation (e.g. Figure 3.10)), whereas the islands further south will be more sensitive to changes in the semi-permanent high-pressure system. Theoretically, a stronger Azores High would result in stronger Trade Winds due to the enhanced subtropical-tropic pressure gradient, resulting in decreased temperatures due to the more intense Trade Winds bringing cool oceanic air and potentially intensifying coastal upwelling (Chapter 6). In contrast, a weaker Azores High would diminish the Trade Wind strength, allowing high sea-surface temperature anomalies to develop: this was the case during the exceptionally low NAOI of winter 2009/2010. A weaker Azores High also allows less dominant (i.e. non-NAO type structures) modes of variability to dominate. The strength of the NAO-temperature relationship changes seasonally (Figure 3.12), with summer correlation patterns displaying a weaker, less spatially defined relationship than in winter.

To reinforce the strong warming signal identified from ~1976 onwards in CH14, sixteen stations across Macaronesia were taken from the GSOD archive (Table 4.4) as part of the analysis in C13. The station time series mostly begin in 1973 and there were a few years with missing gaps (no attempt was made to gap fill these stations). Monthly mean temperatures are given along with recent winter, summer and annual trend rates (Table 4.4, 4.5; Figure 4.6). Additionally, the spatial patterns of the winter, summer and annual 2 m SAT trend from the ERA-I reanalysis are shown (Figure 4.7). The absolute range of trends from the GSOD stations, 0.26-0.50°C dec^{-1}, from 1973-2012 is comparable to the 0.30-0.38 °C dec^{-1} (1981-2010) range from the previous monthly time series from CH14 (Table 4.3). The higher-altitude stations at Tenerife Los Rodeos and Izaña display similar trends to near-sea-level stations (Figure 4.6). Summer trends were typically greater than winter trends and pass significance tests more often (Table 4.5). The warming rate from 1973-2000 is greater than the rate from 1973-2012 at (10/16) stations (Figure 4.6) and the annual trend is significant at (13/16) stations (Table 4.5). This fits in with the general global / Northern Hemisphere pattern illustrated in Cohen *et al.* (2012), who noted a

lack of significant trend direction in winter temperatures across the Northern Hemisphere poleward of 20°N (marked by negative trends across most of Europe) and with the slightly reduced rate in global SAT rise since ~2000 (Stocker *et al.*, 2013).

Spatially (using the ERA-I dataset) southern Iberia and the Sahara appear to be the two most rapidly warming regions during summer from 1981-2013 (Figure 4.7). All the Macaronesian Islands appear to be within large-scale regions where the warming trend is separable from natural variability (i.e. exceeds 1 SD). This holds true when annual values were considered as well (noticeable regions of cooling include upwelling zones along the northwest African coastline, which is discussed in Chapter 6). In winter, a strong cooling is displayed in the ocean around the Iberian region and western Mediterranean (no direct reference explaining this was found). This 'zone' of cooling and trends that were $<\pm$ 1 SD of variability, extend to encompass the Sahara, southwestern Europe and the Macaronesian Islands (except Cape Verde, as below 25°N across the Atlantic shows a strong warming trend).

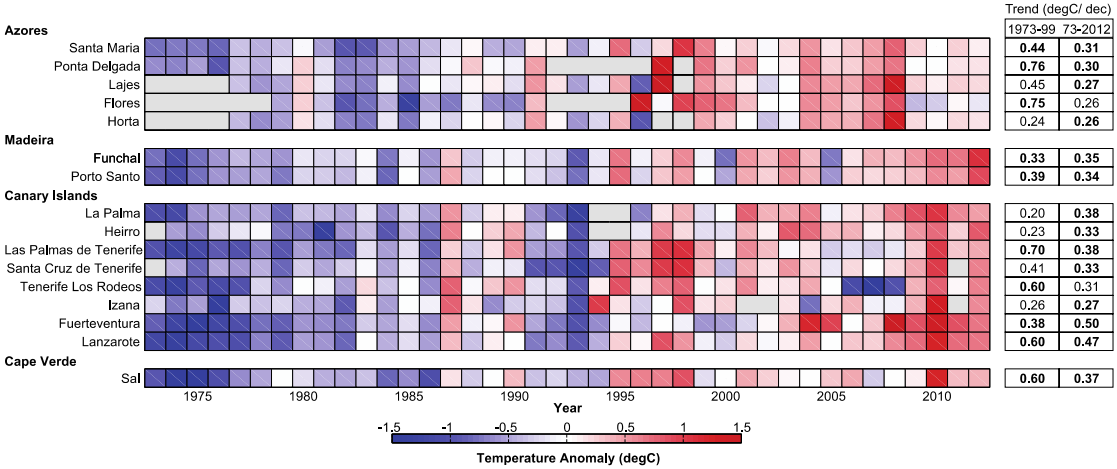

Figure 4.6. The annual temperature anomaly (relative to the 1981–2010 base period) for the sixteen Macaronesia stations listed in Table 4.4. Grey shading indicates no data. The table shows the linear trends of temperature against time (°C dec^{-1}) for 1973–1999 and 1973–2012. Bold values indicate significant trends ($p < 0.05$) calculated using the modified MK test.

Station	Altitude (m)	Location	Jan	Feb	Mar	Apr	May	Jun	Jul	Aug	Sep	Oct	Nov	Dec
Santa Maria	100	36.97N 25.17W	14.7	14.4	15.0	15.6	17.1	19.2	21.5	22.7	21.9	19.8	17.4	15.8
Ponta Delgada	36	37.75N 25.70W	14.4	14.1	14.3	14.8	16.3	18.5	20.7	22.0	21.2	19.0	16.7	15.3
Lajes	55	38.76N 27.10W	14.4	14.0	14.4	15.2	16.7	18.9	21.1	22.2	21.3	19.0	16.7	15.2
Flores	29	39.45N 31.13W	14.6	14.3	14.7	15.5	16.9	19.1	21.8	22.9	21.7	19.3	17.0	15.4
Horta	41	38.52N 28.71W	15.0	14.6	14.9	15.5	16.9	19.1	21.6	22.8	22.0	19.6	17.2	15.8
Funchal	56	32.63N 16.90W	16.4	16.1	16.5	17.0	18.4	20.4	22.2	23.2	22.9	21.2	19.1	17.5
Porto Santo	82	33.07N 16.35W	15.8	15.7	16.1	16.7	18.1	20.0	21.6	22.8	22.6	20.9	18.7	16.9
La Palma	31	28.62N 17.75W	18.0	17.8	18.4	18.8	19.9	21.5	23.0	23.9	24.0	22.8	20.9	19.2
El Hierro	32	27.81N 17.88W	18.8	18.5	18.8	19.1	20.2	21.6	22.6	23.5	24.0	23.2	21.5	19.9
Las Palmas de Gran Canaria	47	27.93N 15.38W	17.8	18.0	18.8	19.3	20.3	22.0	23.7	24.4	24.2	23.0	21.0	19.0
Santa Cruz De Tenerife	36	28.45N 16.25W	18.1	18.2	19.0	19.5	20.8	22.7	24.8	25.4	24.8	23.3	21.2	19.3
Tenerife Los Rodeos	617	28.47N 16.31W	13.0	13.3	14.2	14.6	16.0	17.9	20.2	21.1	20.7	18.8	16.4	14.2
Izaña	2862	16.50N 23.68W	4.2	4.4	6.0	7.2	9.8	13.7	17.8	17.8	14.0	10.2	7.1	4.9
Fuerteventura	30	28.45N 13.87W	17.6	17.8	18.6	19.3	20.4	22.2	23.9	24.4	24.2	22.8	20.8	18.8
Lanzarote	21	28.95N 13.60W	17.4	17.7	18.8	19.4	20.6	22.4	24.1	25.0	24.6	22.9	20.6	18.4
Sal	53	16.73N 22.95W	20.9	21.2	21.8	21.7	22.7	23.5	23.6	24.8	25.6	25.4	23.6	21.9

Table 4.4. Average monthly mean temperature (°C) from sixteen Macaronesia meteorological-stations from the Global Summary of the Day (http://www7.ncdc.noaa.gov/CDO/cdo) and European Climate Data Assessment archive (Klein-Tank *et al.*, 2002).

Station	DJF	JJA	ANN
	Azores		
Santa Maria	**0.45**	**0.45**	**0.41**
Ponta Delgada	0.26	0.14	**0.24**
Lajes	0.36	0.27	**0.32**
Flores	0.33	0.40	**0.45**
Horta	0.38	0.30	**0.35**
	Madeira		
Funchal	0.22	**0.36**	**0.28**
Porto Santo	0.07	**0.38**	**0.19**
	Canary Islands		
La Palma	0.24	**0.47**	**0.43**
El Hierro	0.37	0.27	**0.32**
Las Palmas de Gran Canaria	0.27	0.31	0.26
Santa Cruz De Tenerife	0.33	**0.46**	0.32
Tenerife Los Rodeos	0.00	0.05	0.11
Izaña	0.10	0.22	**0.16**
Fuerteventura	0.33	**0.44**	**0.45**
Lanzarote	0.27	**0.54**	**0.40**
	Cape Verde		
Sal	0.40	0.37	**0.40**

Table 4.5. Decadal trends (°C dec^{-1}) of winter, summer and annual temperatures from the 16 Macaronesia stations listed in Table 4.4 for the period 1981-2010. Bold indicates statistical significance ($p < 0.1$) where trends pass the modified MK trend test (Section 2.3.1).

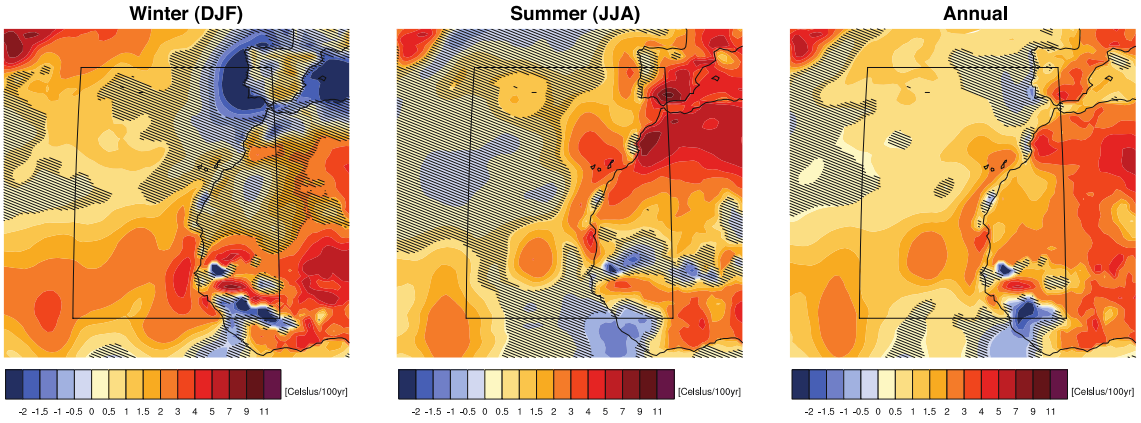

Figure 4.7. The 2 m SAT trend from 1981-2013 from the ERA-I reanalysis for winter, summer and yearly values. Hatching indicates where a trend does not exceed ±1SD (equivalent to ~$p < 0.32$).

4.2 Precipitation

Table 4.6 lists the eleven precipitation stations from the Macaronesian Islands for which long-term monthly precipitation records were available from the GHCN, GSOD and ECA&D archives. Precipitation is far more variable across islands than temperature, i.e. there is a distinct contrast between western and eastern Canary Island precipitation regimes (García-Herrera *et al.*, 2003) and the differences between the higher Madeira (island) and flatter Porto Santo in the Madeiran Island chain were pronounced. This is because precipitation has a much shorter decorrelation scale than temperature, as the processes governing precipitation are more variable than temperature. Precipitation forming processes are strongly circulation-based, which is a difficult process to replicate in models and reanalysis, and to forecast accurately further than ~15 days out (Stern and Davidson, 2015). Additionally, controls on precipitation are further complicated by the island climatology (altitude etc...) as discussed in Chapter 1. The general aim, as with the temperature time series was to disturb the historical precipitation records as little as possible after tests for normality, with monthly gaps set to the long-term average for the month of the same name. This method has been used previously (Zhang *et al.* 2011a; 2011b) and whilst it does not impact the overall long-term trends, it potentially leads to increased precipitation amounts for certain islands that typically have no precipitation across a number of months: in particular for Porto Santo (Madeira) and the Canary Islands and Cape Verde. Therefore, for gap-filling across typically 'dry' months, e.g. March to July for Cape Verde stations, where the average monthly values are below 1 mm, the value was set to 0 mm.

The only station to fail homogeneity tests was Ponta Delgada (pre-September 1939 values in the record were increased). For the Canary Islands, missing values at the selected GHCN stations were directly replaced with the station of the same name in the ECA&D dataset, as the monthly values were identical across the overlapping periods. The two stations for Madeira required minimal monthly gap filling. The records for the three Azores stations all stop reporting in the early 2000s, and were extended using regression with either a nearby daily station (Ponta Delgada from the GSOD archive) or the nearest ERA-I grid-box (Horta, Santa Maria). Because precipitation across the Azores at the monthly scale broadly resembles the normal distribution throughout the year, the regression relationships provided a reasonably accurate way to fill the gaps (the Azores records follow a more 'normal' distribution than the other islands). The reanalysis and nearby station values were very similar and the monthly correlations high (r^2 = ~0.9). Unfortunately this was not the case for the three Cape Verde stations, two of which (Saint Vincent and Praia) stopped reporting in the 1970s. There were no suitable stations for comparison, and regression with the nearest reanalysis grid-box (NCEP-NCAR as

opposed to ERA-I due to the temporal coverage) was unsuitable, as precipitation events are inconsistent, and typically confined to the wet (ASO) season. The nearest reanalysis grid-box for the Cape Verde stations tended to overestimate the lower magnitude events and underestimate the significant precipitation events, unlike for the Azores where the magnitudes were very similar. This appears to be a general reanalysis issue, with the equivalent ERA-I grid-boxes illustrating the same over/underestimations. It can be speculated that this is be a function of the typical precipitation generation mechanisms that operate across the different island chains, i.e. the Azores are more influenced by synoptic-scale depressions, while Cape Verde is predominantly influenced by the propagation of AEWs and the seasonal ITCZ migration (Section 1.3.4-1.3.6). Therefore, for Saint Vincent and Praia, the records were presented for the station from the 1880s to 1970s and for the nearest NCEP/NCAR grid-box from 1948 to 2012. The trends across the common time periods were in the same direction, but their magnitudes differ because of the aforementioned under/overestimation problem. Long-term temporal changes are depicted in Figure 4.8. Additionally, mean monthly and annual rainfall totals from the sixteen meteorological-stations from C13 are given (Table 4.7), along with seasonal summary values, seasonal trends and correlation coefficients with the NAO from the eleven stations initially mentioned (Table D1).

Station	Identification	Latitude (North)	Longitude (East)	Altitude (m)	Highest Island Elevation (m)	Start	End	Source
			Azores					
Ponta Delgada	PD	37°70'	334°30'	67	1105	1865	2003	GHCN
Santa Maria	SM	37°00'	334°88'	100	587	1944	2005	GHCN, GSOD
Horta	HO	38°50'	331°40'	62	1043	1902	2008	GHCN. GSOD
			Canary Islands					
Santa Cruz De Tenerife	*SC*	28°45'	343°75'	36	3718	1881	2012	GHCN
Las Palmas	*LP*	28°10'	344°58'	25	1949	1887	2012	GHCN
Fuerteventura	*FU*	28°44'	346°14'	25	807	1970	2012	ECA&D
			Cape Verde					
Sal Daily	*S2*	16°73'	337°43'	54	406	1973	2012	GSOD
Saint Vincent	*SV*	16°85'	335°00'	2	725	1883	1976	GHCN
Praia	*PR*	14°90'	336°48'	35	1394	1921	1960	GHCN
			Madeira					
Funchal	*FC*	32°63'	343°10'	50	1862	1865	2012	GHCN
Porto Santo	*PS*	33°07'	343°65'	82	402	1940	2004	GHCN

Table 4.6. Summary of meteorological-stations with precipitation records used in Chapter 4.

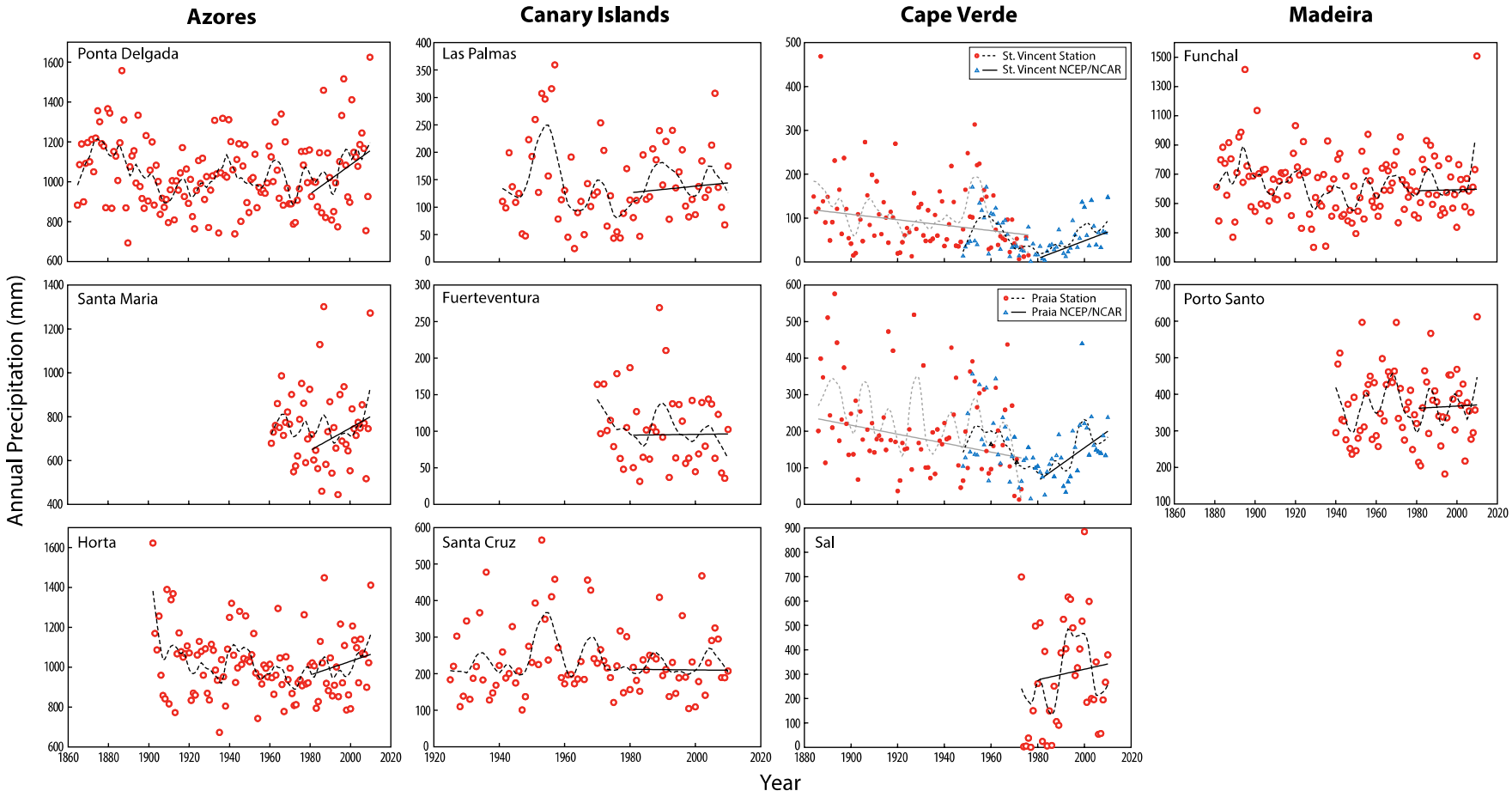

Figure 4.8. Annual precipitation (mm) records from various Macaronesian sites with their 1981–2010 TS trend line and long-term 11-year trends.

Station	Jan	Feb	Mar	Apr	May	Jun	Jul	Aug	Sep	Oct	Nov	Dec	ANN
Santa Maria	75	76	65	57	45	50	22	34	59	71	88	106	749
Ponta Delgada	79	76	82	69	53	32	23	42	79	87	99	109	829
Lajes	116	136	116	75	61	51	49	57	97	128	139	159	1184
Flores	170	146	134	99	97	88	49	72	118	159	168	211	1512
Horta	87	91	82	58	64	53	30	50	78	96	100	102	891
Funchal	97	78	61	46	33	15	10	6	40	84	95	121	686
Porto Santo	49	40	37	27	18	7	4	5	27	45	56	62	376
La Palma	44	56	26	21	7	2	1	2	9	33	60	65	328
El Hierro	20	29	19	12	2	1	0	1	5	11	28	39	166
Las Palmas de Gran Canaria	24	20	13	6	3	1	1	0	10	14	22	25	139
Santa Cruz De Tenerife	30	28	23	10	4	1	1	2	9	18	30	34	190
Tenerife Los Rodeos	77	53	50	32	19	9	5	5	22	44	68	71	457
Izaña	73	61	45	27	11	1	0	3	14	44	93	76	449
Fuerteventura	17	15	11	18	1	1	4	0	6	10	17	21	123
Lanzarote	21	14	12	4	2	0	2	0	2	8	12	21	100
Sal	12	15	4	6	5	1	6	12	36	15	5	9	125

Table 4.7. Monthly and annual precipitation totals from selected Macaronesia stations (1973-2012 climatology).

Precipitation decreases with decreasing latitude. The Azores and Madeira have precipitation all year round, although the summer magnitudes were much smaller. The greatest precipitation amounts were seen on the westernmost island of the Azores (Flores). The stations from 'flat' islands, such as Santa Maria, Porto Santo and Fuerteventura all have lower precipitation values than associated islands in their group that are more mountainous. Summer precipitation is rare for the Canary Islands and for Cape Verde from December to May. Significant negative correlations with the NAOI are displayed for the Azores across all seasons and Madeira for winter (Table D1).

Masking the NAO[5] makes no significant change to the correlation values. The coefficient of variation of annual monthly precipitation ranges from 16 to 24% for the Azores, 26 to 33% for Madeira, 40 to 52% for the Canary Islands and 77 to 108% for Cape Verde. This indicates the high degree of precipitation variability across Macaronesia, which again, changes as a function of latitude. For example, it would be 'normal' for one year in the Canary Islands to have 40–52% more or less rainfall than the year before, without this being a function of any secular change.

Recent increases in Cape Verde wet season (ASO) precipitation were evident in all three records from the 1980s onwards (statistically significant for Saint Vincent and Praia (Table D1)) although this trend appears to have reversed at Sal during the last 10 years (Figure 4.8). All three stations are situated at sea level (Table 4.6), although they have contrasting locations on their respective islands, and the orography of each island also differs markedly. Santiago (the island where the station at Praia is located) has the highest peak, with Saint Vincent and Sal significantly lower (1394, 725 and 406 m respectively). However, all three sites (the Sal Station and nearest grid-boxes for Saint Vincent and Praia) show similar precipitation increases in the late Twentieth Century. This increase corresponds with the recent 'recovery' of Sahel precipitation (Hoerling *et al.*, 2010). General consensus on the drivers of inter-annual Sahel precipitation variability have yet to be reached, although changes in tropical SSTs across the Atlantic, Pacific and Indian Oceans (Lu and Delworth, 2005) in addition to changes in North Atlantic oceanic heat transport (Baines and Folland, 2007) have been shown to display potential relationships. Factors influencing Cape Verde precipitation are: (1) seasonal migration of the Azores High and Equatorial Low and the resultant effect on Trade Wind and Canary Current strength (Mannaerts and Gabriels, 2000) and (2) the WAM, which brings south-westerlies, easterly waves and isolated convection events. Given the lack of significant rainfall increase elsewhere across the Macaronesian archipelago, it would seem that changes in the WAM may represent a significant factor in recent changes, potentially

[5] Masking the NAO here means that the correlation calculations are calculated an additional two times, one time with all the paired values associated with NAO > 0 removed and again with all values of NAO < 0 removed.

owing to an increased maritime-continental temperature gradient associated with general global warming. Bielli *et al.* (2010) indicate that both the AEJ (Section 1.3.6) and the WAM have been increasing since the early 1980s, although the WAM has not yet fully recovered since its abrupt decease around 1967 (Li and Zeng, 2002). Therefore it is likely that Cape Verde precipitation and the WAM are related.

The spatial NAOI with ERA-I rainfall correlation pattern in winter displays a strong negative correlation across the Azores, Madeira and the western and central Canary Islands (Figure 3.10, 3.12). A weaker NAO will result in more southerly-displaced storm tracks, and therefore more precipitation, explaining the observed pattern well. Correlations between the individual Canary Island stations (Table D1) and precipitation do not support such a relation, but this can be explained by lack of the eastern islands precipitation correlation with the NAO (García-Herrera *et al.*, 2001) and the location of the stations at Santa Cruz and Las Palmas in the rain shadow regions (eastern sides) of their respective islands. The summer pattern (Figure 3.12) shows a much weaker, northwestward shifted connection than in winter, due to the aforementioned weaker and more northeasterly-displaced Azores High and also the fact that precipitation amounts across Madeira and the Canary Islands were very low / close to 0 mm during summer anyway.

Positive trends can be seen towards the end of the records for the Azores stations (Table D1, Figure 4.8) although these were not significant and similar rise and falls were evident in the longer-term records (i.e. Horta and Ponta Delgada). There were no apparent precipitation trends in the central, more mountainous Canary Island stations (Santa Cruz and Las Palmas), whereas on the eastern, flatter island at Fuerteventura, precipitation appears to be decreasing. Coincidentally, whilst not analysed here, the meteorological-station from the ECA&D database at Izaña, Tenerife, (2371 m altitude) experienced its driest hydrometeorological year (September to August) and winter (DJF) season during 2011–2012 (AEMET, 2014a). The spatial pattern of precipitation trends during DJF and JJA are displayed in Figure 4.9.

An interesting feature of the higher altitudes across the Macaronesian Islands that will not be picked up by normal modes of analysis is the water that is captured as a result of 'fog-precipitation'. A newly-installed sensor next to the precipitation gauge at Izaña, on Mount Teide on Tenerife has suggested that the relative amount of available water that is captured around ~2500 m height due to fog, is between 4-7 times larger than that measured by a conventional rain-gauge (AEMET, 2014c). Only four years of data are available at present, which limits what conclusions can be drawn from the data; however, the fog-precipitation volume compared to the water amount in the normal precipitation

gauge was 14 times larger during the exceptionally dry 2011-12 hydrometeorological year (AEMET, 2014b).

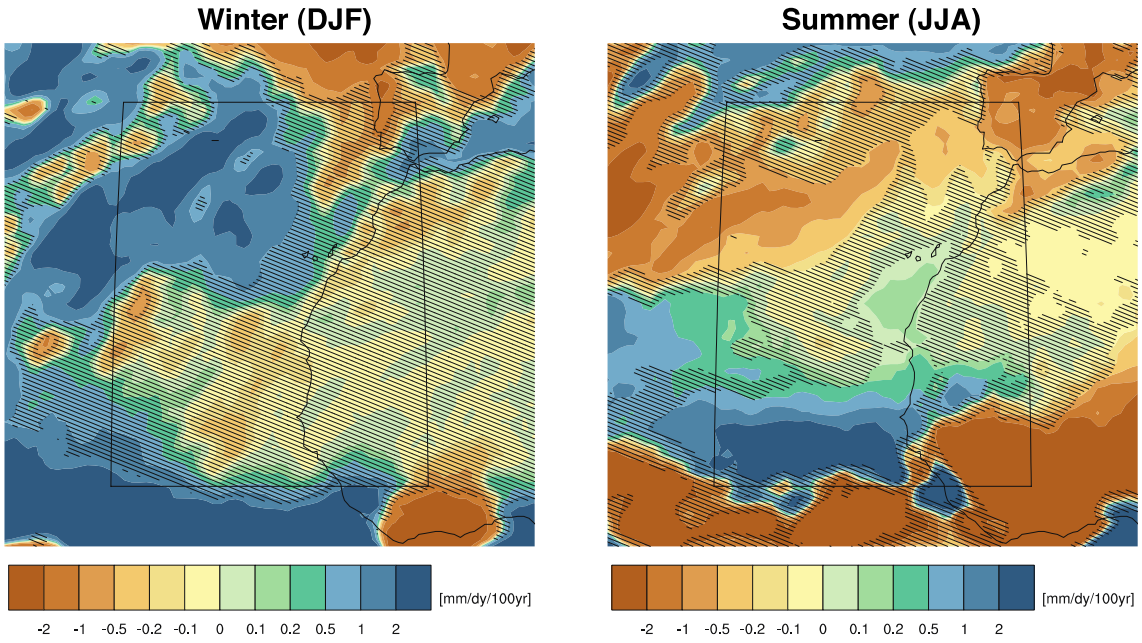

Figure 4.9. The linear trends of winter and summer surface precipitation from the ERA-I reanalysis (1981-2013). Hatched regions indicate where the trend is not greater than ±1SD.

4.3 Climate Extremes

The second major objective of this thesis was to "*Determine if additional climate data support the conclusions drawn from the main climate records*". This section will focus on this objective by analysing climate extremes. Changes in the mean state of climate variables provide an important metric for assessing decadal scale climate changes but changes in 'extreme' values, i.e. the significant flooding events, droughts and storms that have a more immediate, direct impact on humans and ecosystems are important metrics that require monitoring, analysis and advance planning for (Alexander *et al.* 2006; Donat *et al.*, 2013). There are numerous ways to assess the impact of extreme indices that make use of a variety of climatological data. The two most widely-used approaches are to focus analysis on the tail of the distribution (generally referred to as extreme value theory) or to create indices based on thresholds, percentiles and duration values[6] that describe the evolution of 'moderate' extreme events that generally have a return period of <1 year. Alternatively, individual events can be the focus of entire studies: for example, a strong focus on the February 2010 flooding events across Macaronesia was discussed in Chapter 1.

The approach favoured here is to use the threshold/percentile extreme indices methods, due to the development of a suite of extreme indices that were designed to be applied specifically to daily temperature and precipitation data by the ETCCDI indices (http://etccdi.pacificclimate.org/). A total of 27 'core' indices are suggested by the ETCCDI. A basic description of the indices used in this thesis and their abbreviations are given in Table 4.8 and a fuller description in Tables B1 and B2. These indices have been applied in global and regional studies by numerous authors (Alexander *et al.* 2006; Donat *et al.*, 2013). Typically, there appears a global tendency towards significant trends in extreme temperature indices (towards warmer conditions), whereas trends in extreme precipitation indices were often variable, non-existent, or not significant due to the temporal and spatial variability of precipitation across all scales.

[6] 'Threshold', 'percentile' and 'duration values' refer to the three major types of ETCCDI indices outlined in Tables B1 and B2. Threshold indices typically count the number of days in a year when a daily value exceeds or falls below a specific limit, e.g. days where the maximum temperature >25°C. Percentile values are based on the number of days when a daily value exceeds its *n*th percentile, and could be reported as the number of times when the *n*th percentile is exceeded (as a proportion of the total number of days in the year), e.g. percentage of days per year where the minimum temperature < 10^{th} percentile minimum temperature or as the total sum of values when the percentile range was exceeded, e.g. amount of precipitation that fell in the year due to events when the daily precipitation amount was greater than the 95^{th} percentile. Duration value indices typically count the number of days in a row when certain conditions are met, e.g. precipitation > 1 mm.

ETCCDI Index Abbreviation	Description
CDD	Consecutive Dry Days
CSDI	Cold Spell Duration Indicator
CWD	Consecutive Wet Days
R1mm	Days when precipitation is greater than 1 mm
R10mm	Days when precipitation is greater than 10 mm
R20mm	Days when precipitation is greater than 20 mm
R95p / R99p	Precipitation amount that exceeds the 95^{th}/99^{th} percentile
R_X1Day / R_X5Day	Maximum 1 Day / consecutive 5 day precipitation
SDII	Simple Precipitation Intensity Index
TN_N	Minimum value of daily minimum temperature
TN_X	Minimum value of daily maximum temperature
TN10p	Percentage of days when TN is below the 10^{th} percentile
TN90p	Percentage of days when TN is above the 90^{th} percentile
TX_N	Maximum value of daily minimum temperature
TX_X	Maximum value of daily maximum temperature
TX10p	Percentage of days when TX is below the 10^{th} percentile
TX90p	Percentage of days when TX is above the 90^{th} percentile
WSDI	Warm Spell Duration Indicator

Table 4.8. A summary of the ETCCDI extreme indices that were applied to daily temporal resolution ERA-I data in Sillmann *et al.* (2013a), the output of which is analysed in this thesis. Table B1 and B2 in the appendix list the full formulae of the indices.

Ideally, the ETCCDI indices would be applied to the daily Macaronesian meteorological-stations listed in Section 4.1-2. As the series were previously aggregated to the monthly scale, occasional missing days and periods with long gaps (Figure 4.6) were not generally an issue. However, gaps in daily series, when each day contributes to the annual total/value, were more problematic. As temperature has a relatively high autocorrelation, short gaps (1-2 days) can usually be linearly interpolated between surrounding days and longer gaps (several days) can usually be set to a climatological value without drastically altering the time series. This is not the case for precipitation, particularly across island locations, where typical gap-filling methods such as nearest-neighbour or correlation/regression based methods also perform poorly. A method using Singular Spectrum Analysis was used to attempt to fill gaps of days-weeks in the Macaronesian

precipitation time series (Kondrashov and Ghil, 2006). This approach was chosen, not to determine the exact amount of precipitation on the exact day that it fell (as if the record were fully complete), but so that for the gaps that were filled, that the data 'fit' the expected distribution of the precipitation time series. Setting missing values to the climatology or linearly interpolating would artificially increase the total precipitation amount and skew the ETCCDI indices (e.g. R1mm, RX1/5Day would increase, R95/99p and SDII would decrease). Normally, only the low-frequency periodicities are retained in the analysis; the intent here was to use the higher frequency 'noise' periodicities as the 'gap-fillers' (whilst the low-frequency cycles pick out the correct annual/semi-annual cycles). Application of the Singular Spectrum Analysis method, which utilises temporal periodicities in the time series to fill gaps, proved initially unpromising when applied at the annual (daily) scale. This was mainly because any significant precipitation event caused a 'downstream' effect of subsequent above-average precipitation values.

Given the time-consuming nature of the Singular Spectrum Analysis method approach, it was decided the best way to characterise the evolution of extreme indices was to use those as calculated from daily ERA-I fields from Sillmann *et al.* (2013a). Use of real-station data has not been discarded completely; future attempts could be made to adequately fill the gaps (discussed in Section 7.2) but for now the ERA-I daily fields were treated as the best indicators of changes in the extreme indices across Macaronesia. Figures 4.10-4.16 display the time series evolution of the grid-box over each Macaronesian Island and the spatial trend pattern for eleven temperature- and ten precipitation-based indices (Table B1, B2).

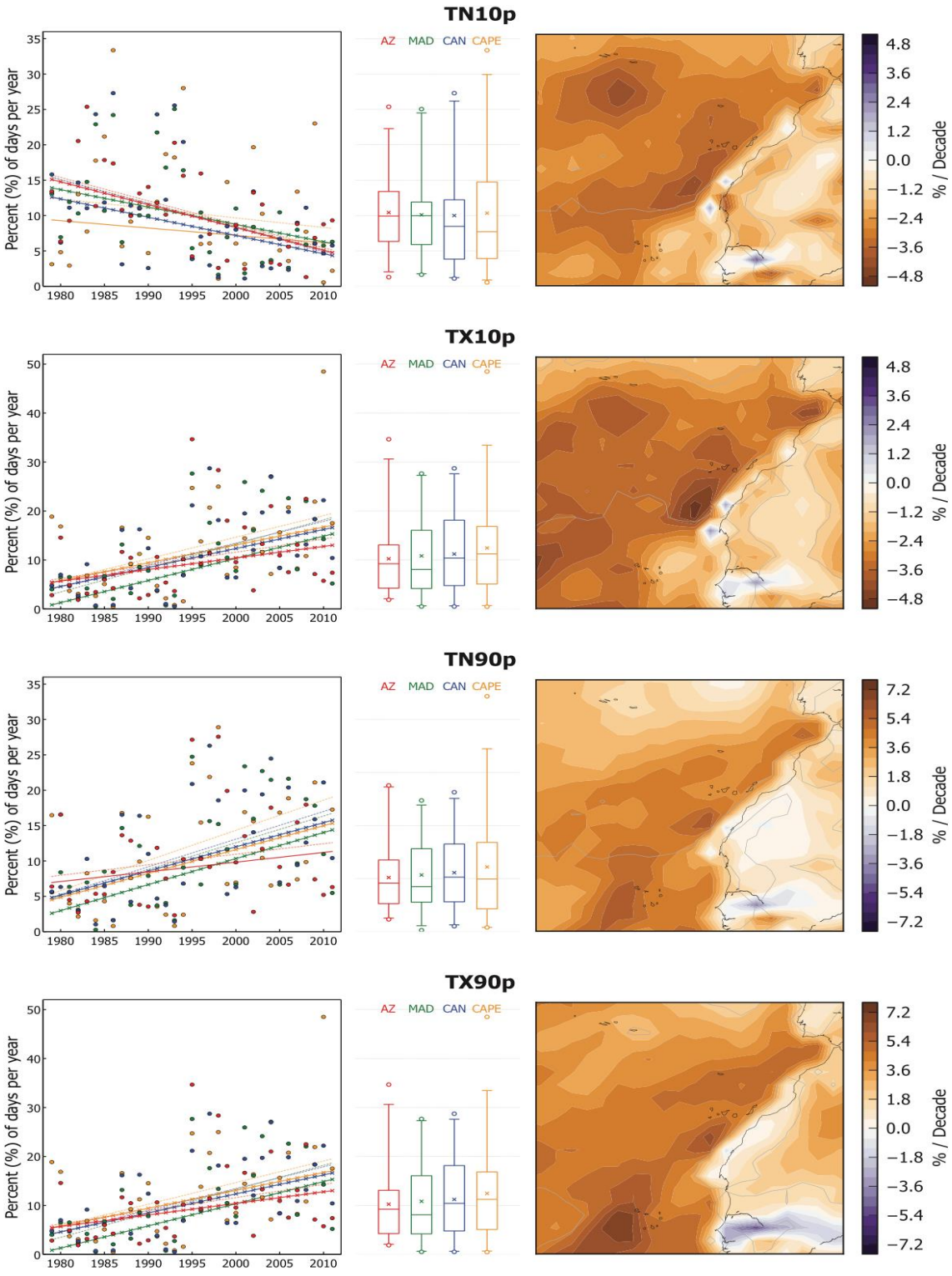

Figure 4.10. (Left Panels) The time series for TN10p, TX10p, TN90p and TX90p, along with OLS (dashed lines) and TS trends (solid lines), for the grid cells overriding the Azores (red), Madeira (green), Canary Islands (blue) and Cape Verde (tan) from the ERA-I reanalysis, 1979-2011. Crossed lines indicate significant (after autocorrelation accounted for) trends ($p < 0.05$). The middle panels display box and whisker plots of the data for each island (the whiskers mark the 2nd and 98th percentile). The right panel displays the spatial OLS trend from the ERA-I reanalysis (1971-2011) with significant regions ($p < 0.05$) bounded by grey lines. The base period used for the calculations was 1979-2008 (Sillmann *et al.*, 2013a).

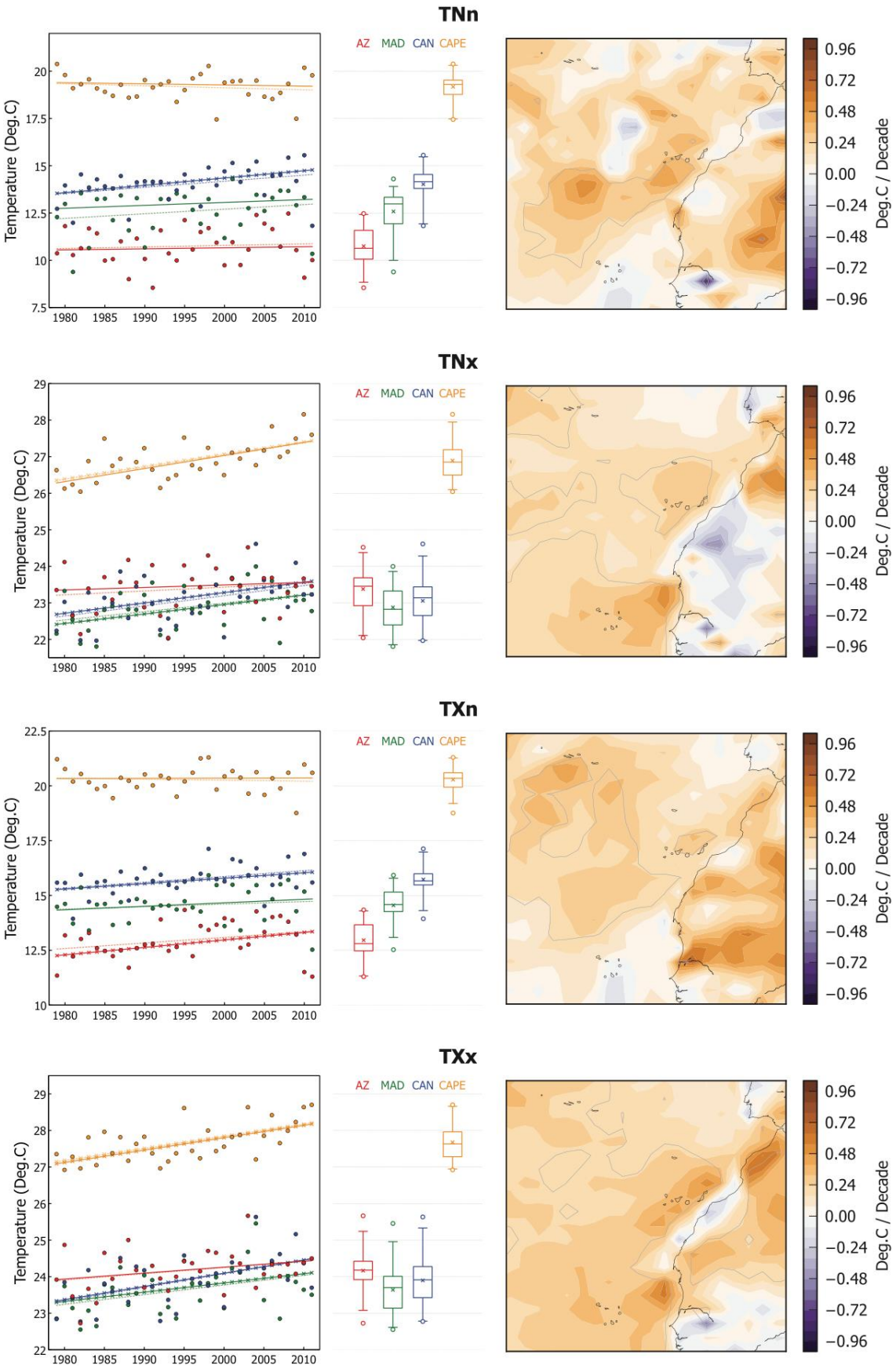

Figure 4.11. As for Figure 4.10 but for TNn, TNx, TXn and TXx.

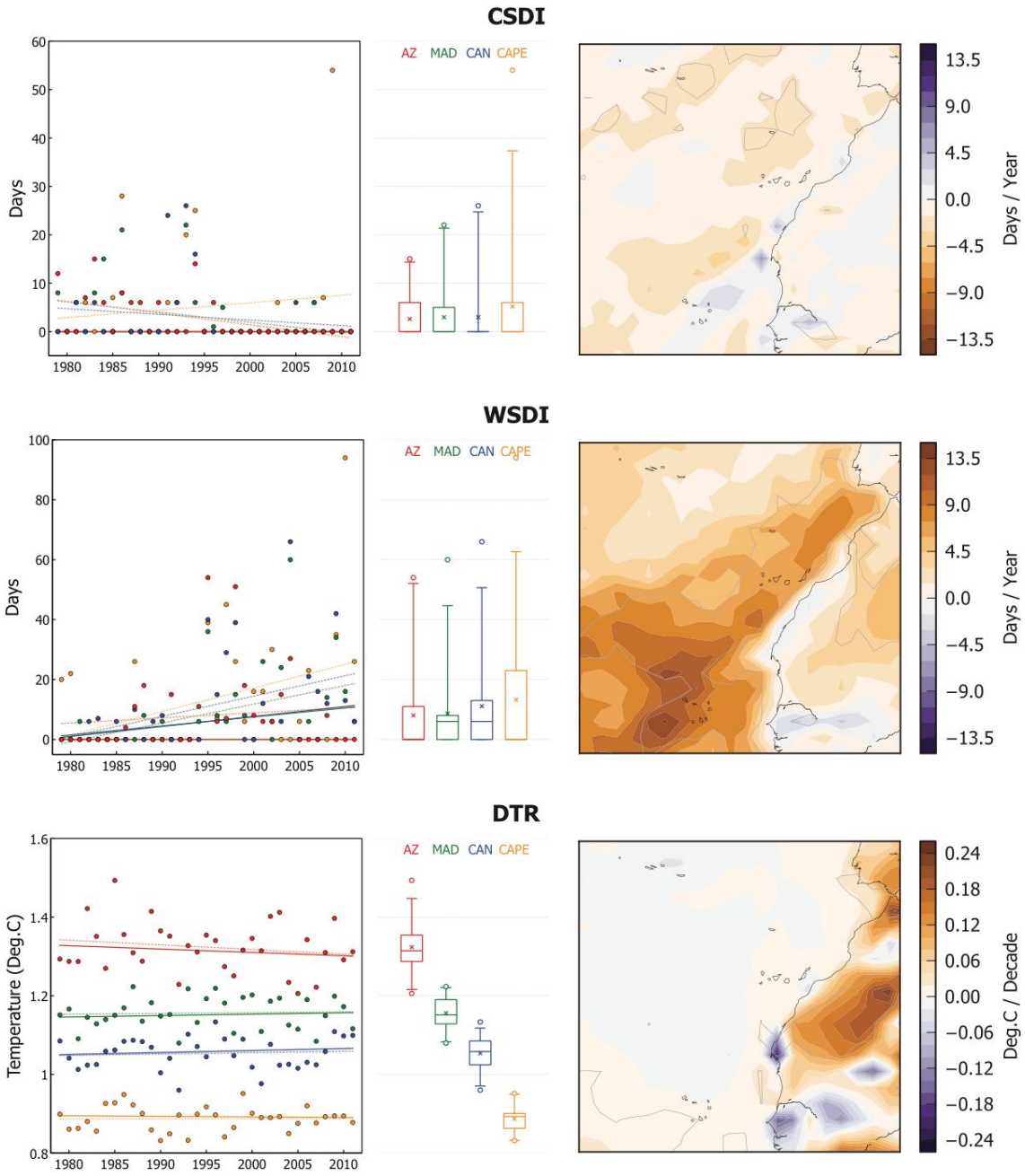

Figure 4.12. As for Figure 4.10 but for CSDI, WSDI and DTR.

Starting with the percentile-based indices, TN10/90p and TX10/90p (Figure 4.10, Table B2), it can be seen that the general trend direction ubiquitously points towards a warmer climate across the region, with the exception of coastal northwest Africa and a small region across the Sahel. Trends were often significant and were generally in the magnitude of 2-5% dec^{-1} across the islands (where % is the annual number of days in the top/bottom 10th percentile with respect to the 1979-2008 base period).

The four indices shown in Figure 4.11, TNn, TNx, TXn and TXx are 'absolute' indices, based on the actual maximum and minimum temperature during the year, rather than the values relative to a set percentage. The only significant increase in TNn (Figure 4.11,

Table B2) is across the Canary Islands, with little long-term change is apparent across the other islands, and even a slight cooling trend across Cape Verde. TXn also displays less striking increases, although the rates were significant across the Canary Islands and Azores. Trends in TNx and TXx (Figure 4.11) across the four islands were always positive, but not always significant. There is generally a slight decrease in the CSDI across the Macaronesian Islands, although such occurrences (six consecutive days <10th percentile temperature) appeared to be already unlikely (Figure 4.12). The WSDI (Figure 4.12) index appears to be slightly increasing, symptomatic of a warming climate, and variability in DTR outweighs any changes.

No statistically significant signal emerges from analysis of the ten precipitation-based extreme indices across the Macaronesian Islands (Table 4.9, Figure 4.13-16).

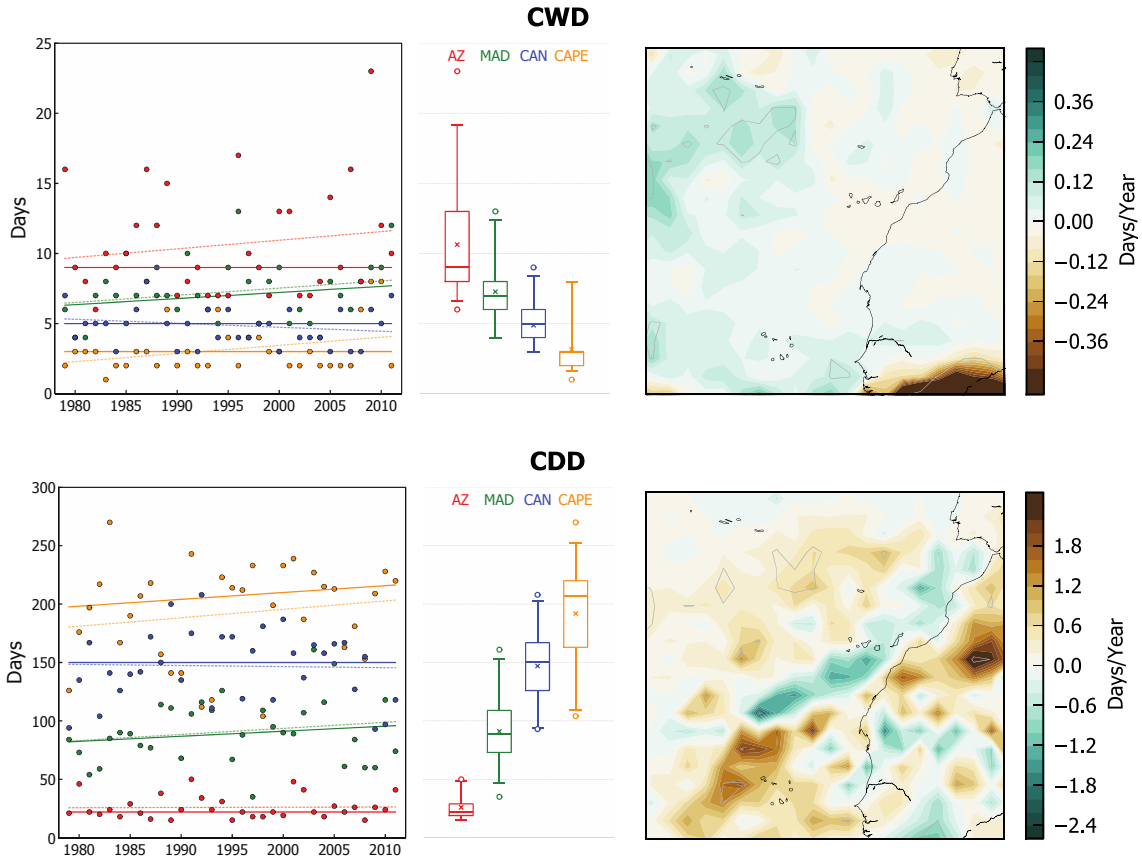

Figure 4.13. As for Figure 4.10 but for CWD and CDD.

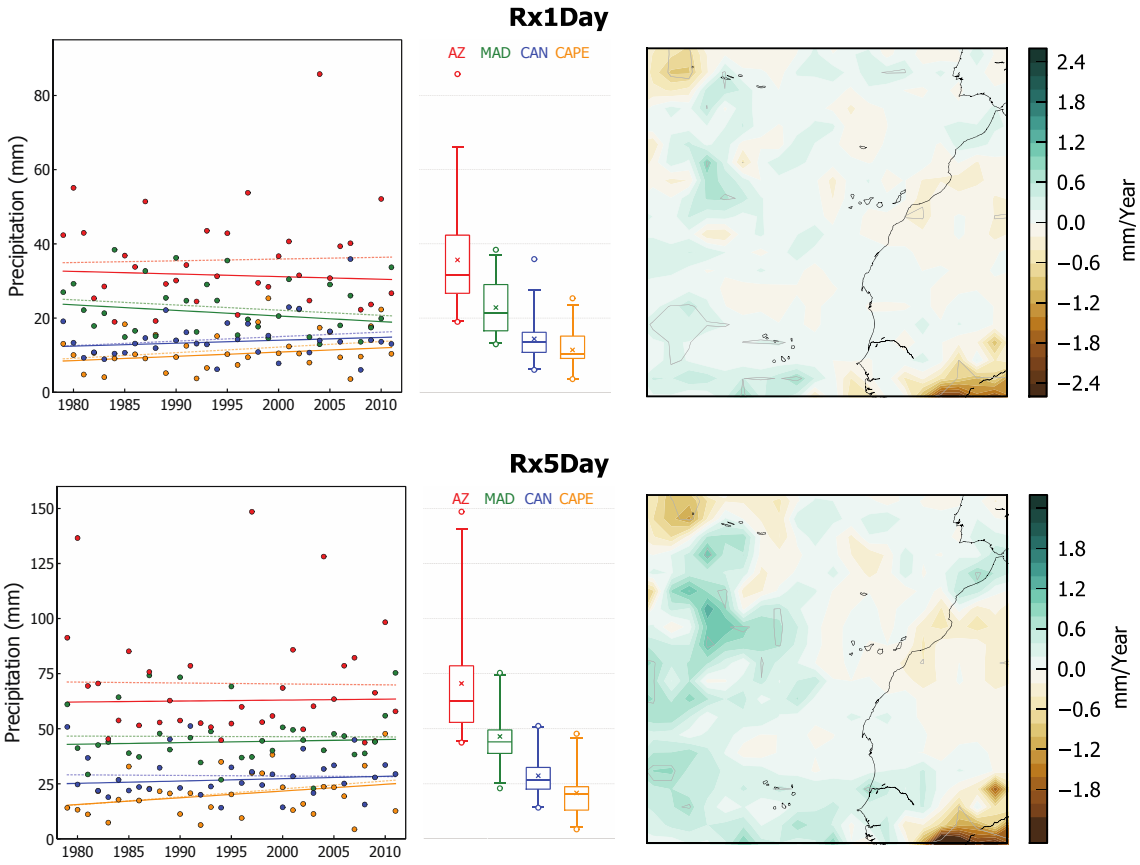

Figure 4.14. As for Figure 4.10 but for Rx1Day and Rx5Day.

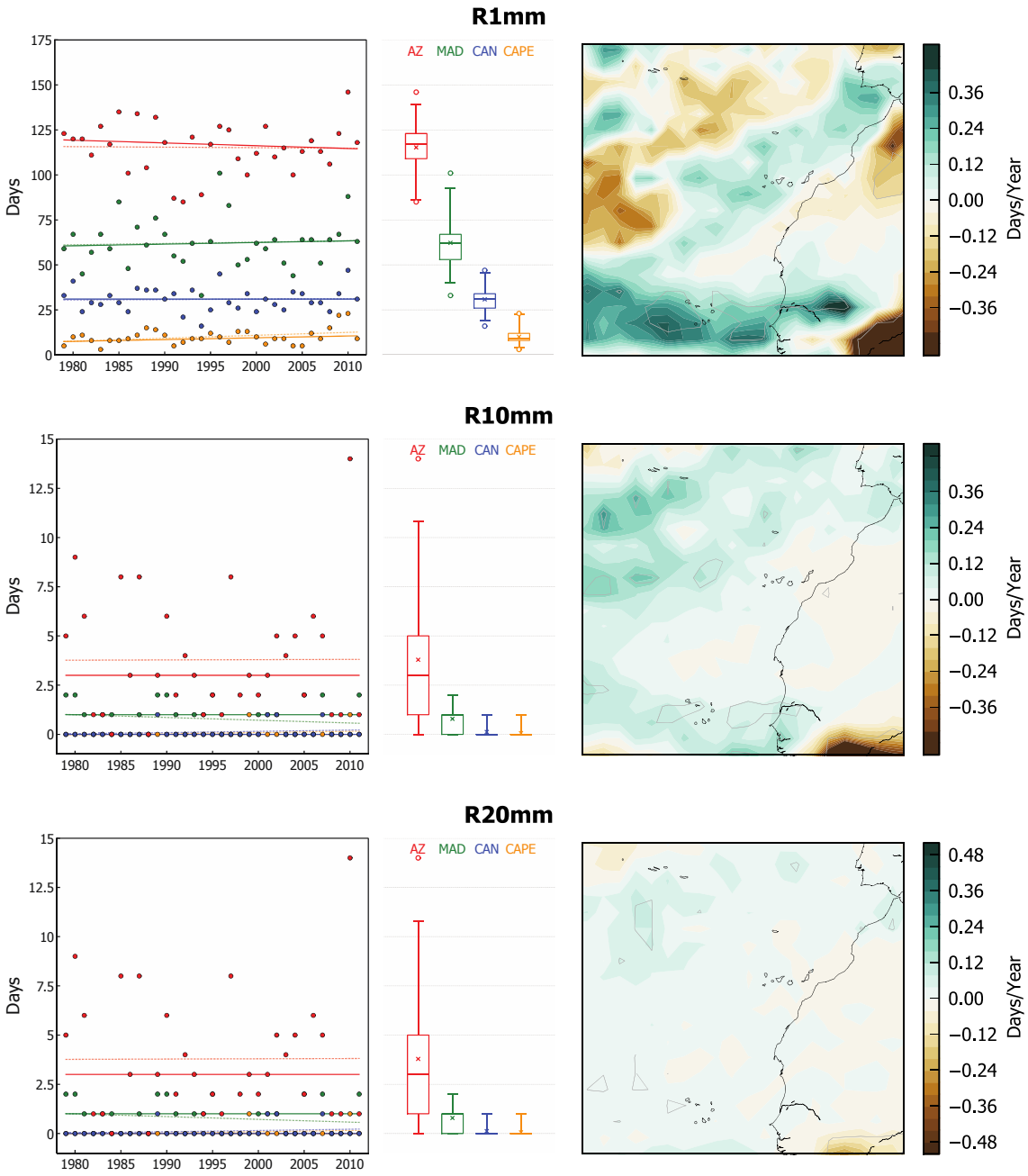

Figure 4.15. As for Figure 4.10 but for R1mm, R10mm and R20mm.

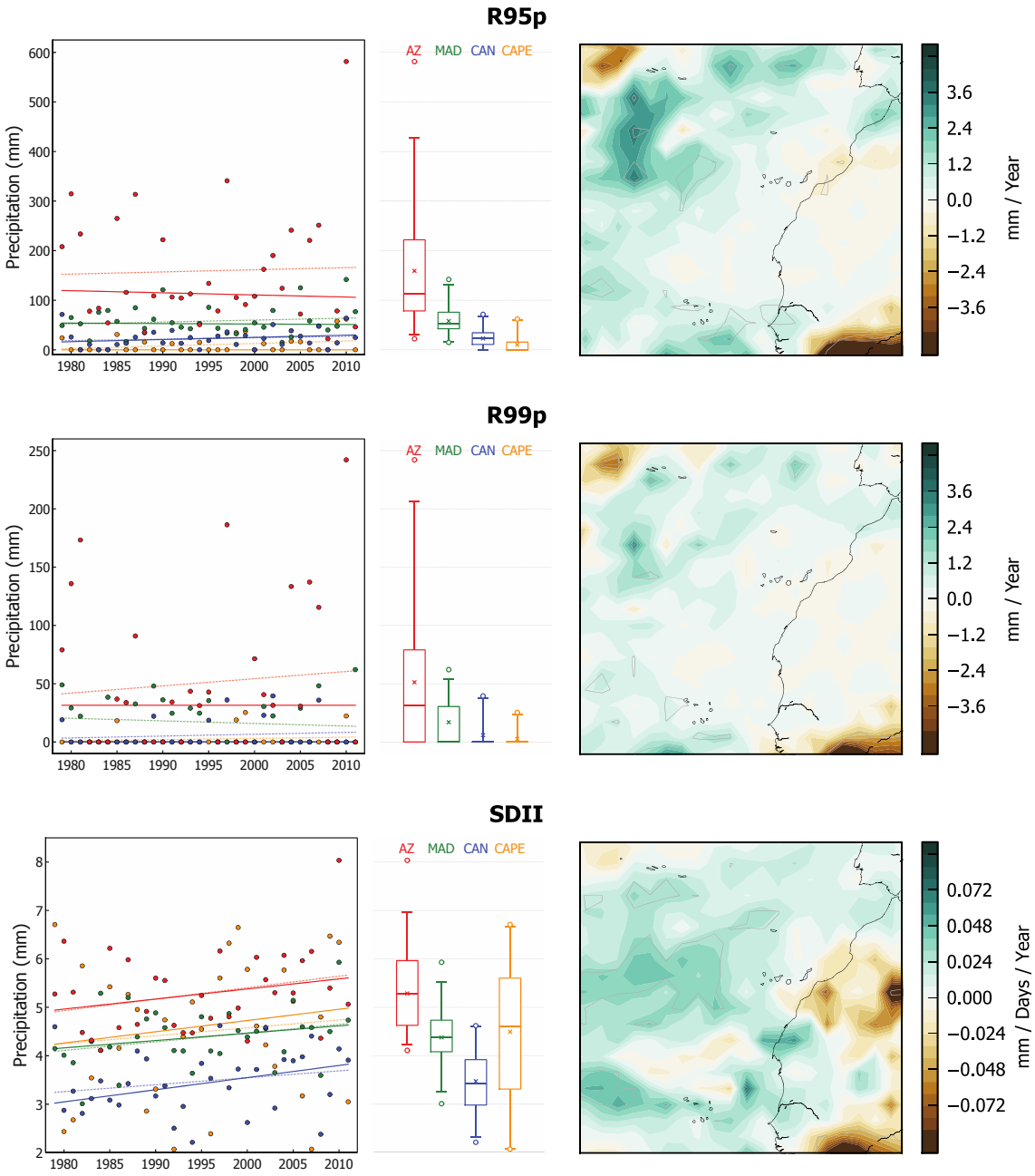

Figure 4.16. As for Figure 4.10 but for R95p, R99p and SDII.

Index	Units	Azores	Madeira	Canary Islands	Cape Verde
CSDI	Days	0	0	0	0
WSDI	Days	0	**3**	**3.33**	0
DTR	˚C	-0.01	0	0.01	0
TN10p	%	**-3.23**	**-2.46**	**-2.58**	-1.04
TN90p	%	1.37	**3.68**	**3.41**	**3.38**
TX10p	%	**-2.62**	**-2.76**	**-3.27**	-0.72
TX90p	%	**2.36**	**4.52**	**3.88**	**3.65**
TNN	˚C	0.06	0.15	**0.39**	-0.06
TNX	˚C	0.07	**0.26**	**0.28**	**0.36**
TXN	˚C	**0.34**	0.16	**0.25**	0.01
TXX	˚C	0.16	**0.25**	**0.36**	**0.34**
CDD	Days	0	4.33	0	5.86
CWD	Days	0	0.43	0	0
R1mm	Days	-1.54	0.91	0	1
R10mm	Days	1.11	0	0	0
R20mm	Days	0	0	0	0
R95p	mm	-4.28	-0.94	4.34	0
R99p	mm	0	0	0	0
Rx1Day	mm	-0.7	-1.51	0.78	1.14
Rx5Day	mm	0.43	0.71	1.07	3.05
SDII	mm	0.21	0.15	0.25	0.23

Table 4.9. Decadal trend rates (TS regression) in ETCCDI indices across Macaronesia from the ERA-I reanalysis. Significant (< 0.05) trends are highlighted.

4.4 Macaronesian Climate Change in Context

The 1981–2010 (mean) temperature increase is the most substantial, coherent trend observed across the four records from the Macaronesian Islands (Table 4.3). Comparisons with previously reported trends (Section 1.4) indicate that the Azores, Canary Islands and Cape Verde (0.33, 0.30 and 0.38°C dec^{-1}, relative to published rates of 0.30, 0.17 and 0.14°C dec^{-1} respectively) annual warming exceeds previously published values, mainly due to more up-to-date records presented here, which include more recent warm years, although the magnitude of warming at Madeira (0.33°C dec^{-1} rise, relative to 0.50°C dec^{-1}) appears to be less. This is most probably due to a combination of previous authors' use of OLS with an algorithm designed to find the maximum trends (Tomé and Miranda, 2004) as opposed to the TS regression trend rates presented in Table 4.3 (as OLS is more susceptible to outliers and may potentially overestimate trends), and also, the different time periods considered. The small range between the trends across the four island chains and the similar pattern of seasonal trends between the island groups provides a degree of confidence in the warming magnitudes. In terms of precipitation, trends in the Cape Verde wet season (ASO) were the only statistically significant increases during the 1981-2010 period, which falls in line with the recent recovery in African Sahel precipitation, after significant drought conditions in the 1970s-80s (Nicholson, 2013).

The NAO strongly correlates with precipitation throughout the Azores across all seasons and with Madeira in winter (also during spring and autumn, but only for the more mountainous main island station at Funchal, Table D1). The significant zone of winter negative correlation (Figure 3.10, 3.12) extends southwards to the Canary Islands, but is not shown in the station-based records (Table D1). Cape Verde precipitation trends display the strongest centennial-scale variability through time, with a marked drought during the 1970s–1990s and a recent recovery (Figure 4.8, 4.9, 4.17). This is concurrent with the major droughts across the Sahel and is strongly related to changing SST patterns (Shanahan *et al.*, 2009). The WAM (Section 1.3.5, Figure 4.17) also plays an important role as it is responsible for much precipitation across the Sahel (and Cape Verde) and is modified by the aforementioned SST changes, and also land-use changes. The WAM became more negative from the mid-1960s, with a sharp drop in the index around 1967 which continued until the late 1980s. The index appears to be recovering now, but is still at much lower levels than pre-1967. The WAM index and Cape Verde precipitation from Figure 4.17 indicate similar trends, and shown to be positively correlated ($r = 0.46$, $p < 0.05$, August to October (ASO) seasonal values, 1948–2012). Therefore, whilst the Azores High and associated storm tracks may be important in precipitation amounts further north across Macaronesia, the WAM is more important further south.

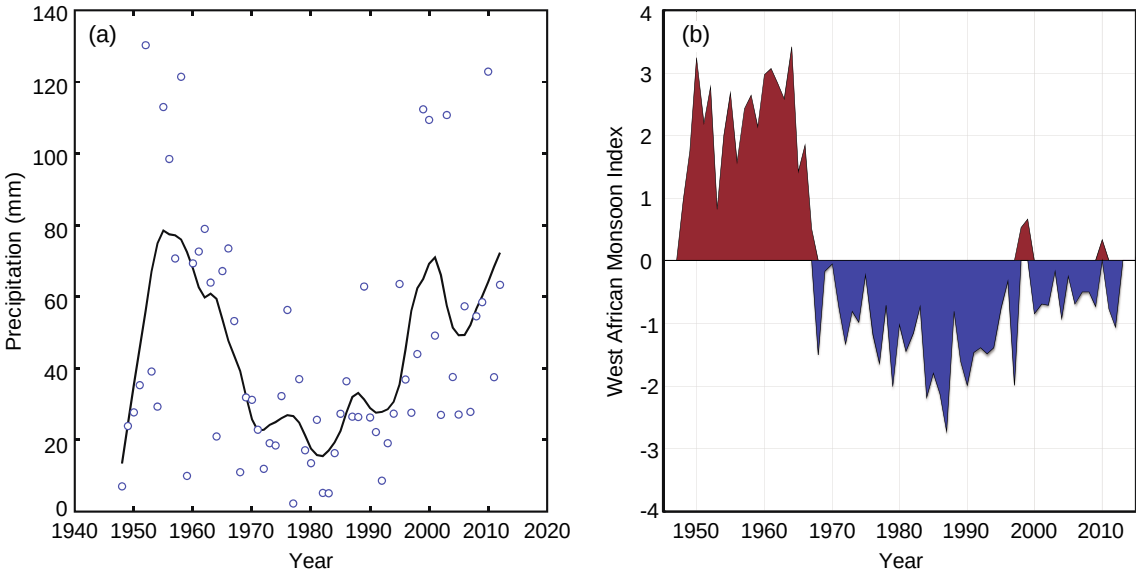

Figure 4.17. (a) Precipitation from Sal (Table 4.6) and (b) the WAM index (925 hPa meridional wind-speed anomalies – 200 hPa zonal wind-speed anomalies, standardised, data from NCEP/NCAR reanalysis) for August-October.

Spectral and wavelet analysis of the detrended winter NAOI and TWI (not shown here) yields very similar results. For winter, significant peaks at 7.7, 21 and 73 years were found in the extended NAOI series, with 6 to 8- and 20-year peaks in the TWI. For summer, a 6.6-year NAOI peak and a 5.5-year TWI peak were identified. The similarity of spectral peaks for both indices, which have the semi-permanent Azores High as a centre of action, emphasize the importance of inter-annual variations in the Azores High in the pacing of low-frequency climate variations across Macaronesia and the wider European climate. Wavelet coherence analysis (Veleda *et al.*, 2012) between the Macaronesia SAT time series described in Section 4.1 and leading modes of variability (Solar output, ENSO and the AMO) yields no striking significant output. It is possible to smooth the SAT time series and also the AMO, apply a lag and realise an almost 'perfect' fit between the time series due to their common low-frequency evolution, but treating the data this way artificially enhances the (initially weak) correlation.

Whilst geographically unique, it is of interest to compare the Macaronesian Islands to broadly similar sites (i.e. volcanic islands and atolls of similar latitude) and the recent general regional and global temperature trends. Therefore, Table 4.10 highlights the 1981–2010 annual and seasonal decadal trends for selected island stations. All these stations were from the GHCN and treated for homogeneity and quality as in Section 4.1, but no gap-filling methods were applied to these stations and only stations between the latitudes of 10-40° N/S with >85% data during 1981–2010 were considered. Also shown are the area-averaged global and European trends from the Goddard Institute for Space Sciences (GISS) dataset (these are based on GHCN v3 data (Hansen *et al.*, 2010)).

Regardless of the global dataset considered, Macaronesian stations display higher–magnitude warming across all seasons (Table 4.3). When compared with the European trends from the GISS record (Table 4.10), Macaronesian stations show largely comparable trends across all seasons. A common trait amongst the GISS Europe and the Macaronesian stations appears to be enhanced trends during the heating portions (i.e. spring and summer) of the year, the only exception being Cape Verde during SON, which is double (0.38°C dec^{-1}) the European average (September to November are still some of the warmest months of the year at the lower latitudes compared to what is autumn for Europe).

Table 4.10 illustrates that out of the selection of fourteen mid-latitude island/atoll stations, nine of these display no significant or negative temperature trends. Three stations from Mauritius all display positive warming trends, two of which (Plaisance and Saint Brandon, Table 4.10) display seasonally significant warming trends (0.30–0.36°C dec^{-1}) comparable to the trends displayed in the Macaronesia records (Table 4.3). Also, the station at Nassau, Bahamas, displays a slightly greater annual trend (0.40°C dec^{-1}) than the Macaronesian records, but comparable seasonal trends. A full comparison of global island temperature records would make an ideal comparison to place recent Macaronesian warming in context. However, without this, from the limited observations shown here, indications are that the warming across Macaronesia is strong for island locations, although the trends from the stations across Mauritius suggest it is potentially a comparable analogue. However, direct comparisons are potentially hazardous because of the variable influences of island size, station location and regional climate variability, such as ocean currents and atmospheric teleconnections. Similar trend magnitudes to the Macaronesian Islands in the temperature-extreme indices were observed across the Caribbean Islands and for the west African Sahel by Stephenson *et al.* (2014) and Ly *et al.* (2014). Precipitation trends were less certain in both studies, with trends rarely significant, although Ly *et al.* (2014) noted an increase in precipitation across the west African Sahel due to increased precipitation from extreme events since the turn of the century. Cape Verde precipitation during the wet season also shows a post-2000 increase (Figure 4.17a). The slight recovery in the WAM index (Figure 4.17b) is a potential explanation for both these trends.

Station	Country/Region	Latitude	Longitude	Altitude (m)	ANN	DJF	MAM	JJA	SON
GISS	Global	90°S-90°N	0-360°E	~2	**0.14**	**0.12**	**0.15**	**0.14**	**0.17**
GISS	Europe	35°N-65°N	10°W-30°E	~2	**0.32**	0.25	**0.34**	**0.47**	0.19
Nassau	Bahamas	25.05N	77.47W	7	**0.40**	0.39	0.42	**0.47**	**0.35**
Minamitorishima	Japan	24.29N	153.97E	9	-0.04	0.13	-0.08	-0.12	-0.07
Honolulu	Hawaii	21.35N	157.93W	5	-0.07	0.05	0.11	-0.04	-0.26
Wake Island	U.S.A.	19.28N	166.65E	4	**-0.37**	-0.49	-0.35	-0.23	**-0.36**
San Juan	Puerto Rico	18.43N	66.00W	19	-0.05	-0.08	-0.06	0.02	-0.04
Kingston	Jamaica	17.93N	76.46W	14	0.21	0.13	0.10	0.11	0.18
Hato	Curaçao	12.19N	68.97W	67	0.10	0.04	0.10	0.15	0.08
Cocos (Keeling) Island	Australia	12.18S	96.82E	3	0.03	0.10	0.03	0.09	-0.06
Saint Helena	British Overseas Territory	16.00S	05.70W	627	0.02	0.13	0.08	0.00	-0.12
Saint Brandon	Mauritius	16.80S	59.55E	4	**0.31**	**0.33**	**0.35**	**0.30**	**0.31**
Rodrigues	Mauritius	19.68S	63.42E	59	**0.19**	0.24	0.21	0.12	0.17
Plaisance	Mauritius	20.43S	57.67E	57	**0.35**	**0.35**	**0.36**	**0.31**	**0.33**
Easter Island	Chile	27.15S	109.42W	51	0.09	0.11	0.08	0.18	0.14
Robinson Crusoe Island	Chile	33.67S	78.97W	30	-0.15	-0.22	-0.16	-0.17	-0.05

Table 4.10. Seasonal and annual temperature trends (1981-2010) for the GISS Global and European average and fourteen mid-latitude island/atoll stations from the GHCN database. All trends are reported in degrees Celsius per decade (°C dec^{-1}). Bold indicates significant trends ($p < 0.1$) where the data passed both the standard and modified MK tests for significance.

4.5 Chapter Summary

Using multiple sources of archived data, four long term, continuous, gap-free, monthly temperature time series for the Azores (1865-2012), Madeira (1865-2012), Canary Islands (1885-2012) and Cape Verde (1895-2012) have been created. The temperature rise from 1981-2010, based on these four time series, ranges from 0.30 to 0.38 °C dec^{-1} (annually), with summer trends ubiquitously greater (and significant) than winter (not significant). A supporting analysis of independent stations reinforces the recent temperature trend, with a range of 0.26-0.50°C dec^{-1} from 1973-2012.

There was a significant increase in Cape Verde wet season (ASO) precipitation during 1981-2010; likely related to a recent 'recovery' of Sahel precipitation. Precipitation has been increasing across the Azores during all seasons except autumn (decreasing), but the trends were not significant. There has been little long-term precipitation change across the Canary Islands and Madeira. Azores precipitation is strongly influenced by the NAO, as is Madeira during winter. Precipitation is typically under 200 mm/year across Cape Verde and for the near-sea level Canary Island meteorological-stations, ~600-700 mm/year for Madeira (although this is halved for the flatter island, Porto Santo) and above 700 mm/year across the Azores. Contributions to the annual hydrological budget from fog-precipitation are starting to be monitored at Izaña (Mount Teide, Tenerife) and indicate that extra 'hidden' precipitation due to fog droplet condensation and/or capture may be very important at high-altitudes, contributing four to seven times more water than collected from standard precipitation observations during typical hydrometeorological years.

Changes in temperature extremes (1979-2011) typically follow the same pattern as mean temperature trends towards a warming climate and there were no significant trends in extreme precipitation indices across the Macaronesian Islands. However this analysis was conducted with reanalysis output, rather than meteorological station data, due to the difficulty of gap-filling daily precipitation data. It is hoped that a station-based analysis of extreme indices could take place in the future, as more complete weather and climate records are made publically available in time, following digitisation efforts such as the ERA-CLIM project (Valente *et al.*, 2013).

5. The Future Of Macaronesian Climate

The fourth scientific objective of this thesis was to *'Deliver estimates of future climate change at the end of the Twenty-first Century across Macaronesia'*. Realistically, this would be possible either by running a regional climate model across the Macaronesian region or using output from pre-existing model runs. The state of the art in assessing future climate change is from the CMIP5 suite of models as part of the IPCC AR5. Several hundred Global Climate Models (GCM) were produced by different modelling centres from around the world, which run historically from 1861-2005, and then predict the future climate from 2006 up to 2100, based on potential future emission scenarios. These are RCP2.6, RCP4.5, RCP6.0 and RCP8.5 which correspond to equivalent numerical amounts in the radiative forcing imbalance by 2100, in watts per square metre (2.6 W/m^2 for RCP2.6, up to 8.5 W/m^2 for RCP8.5). The radiative forcing imbalance (i.e. less longwave radiation is lost to space) arises due to hypothesised continued future emissions and land-use changes (Taylor *et al.*, 2012). The effective amount of CO_2 in the atmosphere in parts per million can be seen in Figure 5.1a. In this thesis, CMIP5 output is used to assess potential future temperature and precipitation changes across the Macaronesian region. The output was downloaded from the Earth System Grid (http://cmip-pcmdi.llnl.gov/cmip5/data_portal.html), the Climate Explorer website (http://climexp.knmi.nl) and the Environment Canada website (http://www.cccma.ec.gc.ca/data/climdex/).

The GCMs have arguably overestimated the short term (2006-2013), decadal scale temperature rise as global temperatures in the 2000s have risen at a slightly slower rate than the preceding two decades (mainly due to a perpetual La-Nina ENSO state, a low solar maximum, contribution from small-medium volcanic eruptions and coverage bias issues) (Stocker *et al.*, 2013). However, the long-term predictive properties of the models are still expected to be reasonably accurate, given that climate sensitivity estimates derived from the palaeo-record and inferred from observational data have not changed from a median value of ~2.5-3°C in about 30 years of research (IPCC AR1-5, Stocker *et al.*, 2013). The sensitivity is not purely related to just CO_2, but other GHGs and their non-linear feedbacks and influences on the climate system.

As with atmospheric reanalysis, the GCM output was provided across latitude/longitude grids of set resolution, so model output could be analysed from desired regions and individual grid-boxes and compared against atmospheric reanalysis. For each RCP scenario, many future model runs have been created from various modelling centres

around the world (Appendix E). Spatial analyses involving the GCM output has been re-gridded at the 2.5 x 2.5° resolution so that the multi-model mean statistic was easier to calculate. The initial analysis in Section 5.1, which discusses the mean future response of temperature and precipitation, uses almost every model with monthly temporal-resolution that was available at the time of the analysis. In Section 5.2, which analyses the distribution of climate extreme indices, all models with a daily resolution from the CMIP5 archive that were used in Sillmann *et al.* (2013a, b) are analysed here. For any spatial plots, the model-mean is the mean calculated from one run of each model from each modelling centre. Section 5.3 indicates the model future trajectories for the NAO and TWI. Section 5.4 discusses the physical controls on potential future changes and Section 5.5 summaries the chapter.

5.1 Mean Future Response

Information and analysis present in Section 5.1 is taken from C13.

5.1.1 Surface air temperature

Monthly mean SATs were extracted from each model run for each RCP scenario from the individual grids that cover the four Macaronesian Island chains. Figure 5.1 illustrates the evolution of the separate RCP paths (2.6 being the most conservative in the long-term and 8.5 the most severe) along with the future mean temperature evolution of the Macaronesian Islands. The station-based SAT time series for each island chain from Chapter 4 are displayed (thin black lines from ~1865-2012) in addition to the historical model mean (the thick black line that runs from 1861-2005) and the model predictions up to 2100 (thin coloured lines indicate individual model runs and the thick coloured line is the model mean for that scenario). There is a generally good agreement between the historical model runs and observations; the short-term variability of the models are supressed as they are the average of many runs, but the long-term trends closely match.

The temperature increase of the four scenarios is similar until ~2030 when the different scenarios begin to diverge. The difference in temperature between the model mean across 2071-2100 compared to the mean temperature across 1976-2005 is displayed for each scenario for each island (Figure 5.1). Generally, across the four islands, a warming of ~1.0°C is expected under scenario RCP2.6, which is the scenario which assumes a peak in GHG emissions around 2050. Temperature changes appear reasonably similar for all four island chains across all the scenarios, with a mean temperature increase of, respectively, ~1.5, ~1.8 and ~2.8 °C associated with the RCP4.5, 6 and 8.5 scenarios

across the four island chains, with the Azores and Cape Verde warming slightly more under the most severe RCP8.5 scenario. As a general statement for the Macaronesian bio-geographical zone in general, the temperature increase for the period 2071-2100, relative to the period 1976-2005, which has already warmed at a strong rate (Table 4.3), appears to be constrained between 0.6-3.2°C (when the upper and lower confidence intervals are considered) by 2100.

Globally, for 2081-2100, relative to 1986-2005, the change in global average SAT is expected to be between 0.3-4.8°C (Collins *et al.*, 2013). It is also expected that land regions will warm at a rate ~1.4-1.7 times greater than ocean regions. Applying this scaling to the upper limits of the global CMIP5 predictions assumes an upper warming limit of 2.8-3.4°C for the global oceans. The upper limit for Macaronesia of 3.2°C falls within this range, so it can be assumed that, in the CMIP5 suite of models, the maritime influence of the North Atlantic Ocean tempers some warming across the Macaronesian islands.

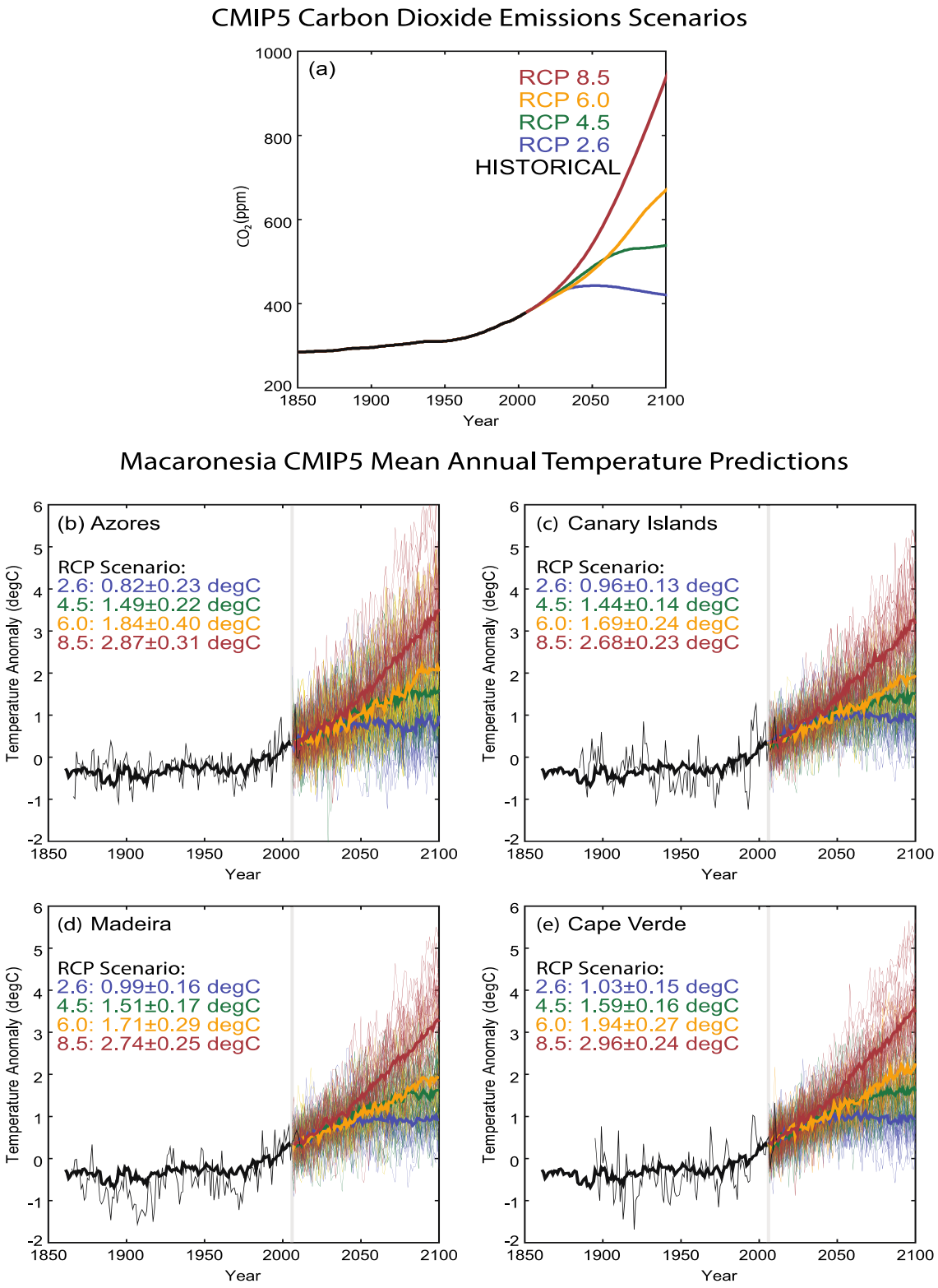

Figure 5.1. (a) The CMIP5 RCP emission scenarios and (b–e) the annual mean temperature anomaly relative to 1976–2005 for the Azores, Madeira, Canary Islands and Cape Verde (thin black line), CMIP5 historical multi-model ensemble (1861–2005, thick black line) and future predictions (2006–2100) for the Macaronesian Islands. Thin coloured lines represent individual model runs for their respective scenario whilst the thick coloured lines are the scenario model means. The RCP scenario changes are the difference in mean (with 95% confidence intervals) between 2071–2100 and 1976–2005.

5.1.2 Precipitation

Future precipitation changes during winter (DJF, Figure 5.2) and summer (JJA, Figure 5.3) are presented. ASO is used instead of JJA for Cape Verde in Figure 5.3 to better capture the wet season. Changes are displayed in percentage of seasonal precipitation total for 2071-2100 relative to 1976-2005 rather than actual precipitation amounts. From the winter predictions (using the same model ensemble as the temperature predictions in Figure 5.1) it is shown that Madeira (-22.1±5.2%), Canary Island (-36.7±5.6%), and Cape Verde (-26.6±9.8%) precipitation amounts are expected to decrease under the three most severe RCP scenarios. The decrease outweighs model variability. However, Madeira precipitation may increase during the mid-Twenty-first Century under scenario RCP2.6. The Cape Verde error margins exceed the expected change across the three lower emission scenarios, but Cape Verde precipitation is already generally low across these months. For the Azores, it appears that there is a slight tendency toward a small (~3%) precipitation increase but the error margins outweigh the decrease in the two more severe RCP scenarios.

Across summer (Figure 5.3), RCP2.6 leads to increased Azores precipitation by 2100 (although the error margin is greater than the potential gain) but the other scenarios indicate a potential decrease. Summer precipitation is limited across Madeira and the Canary Islands so the small changes displayed here are of little relevance. The model output during the wet season (ASO) for Cape Verde indicates an apparent increase across all scenarios, but again the error margins typically outweigh the expected response. The winter and summer changes are depicted spatially in Figure 5.4.

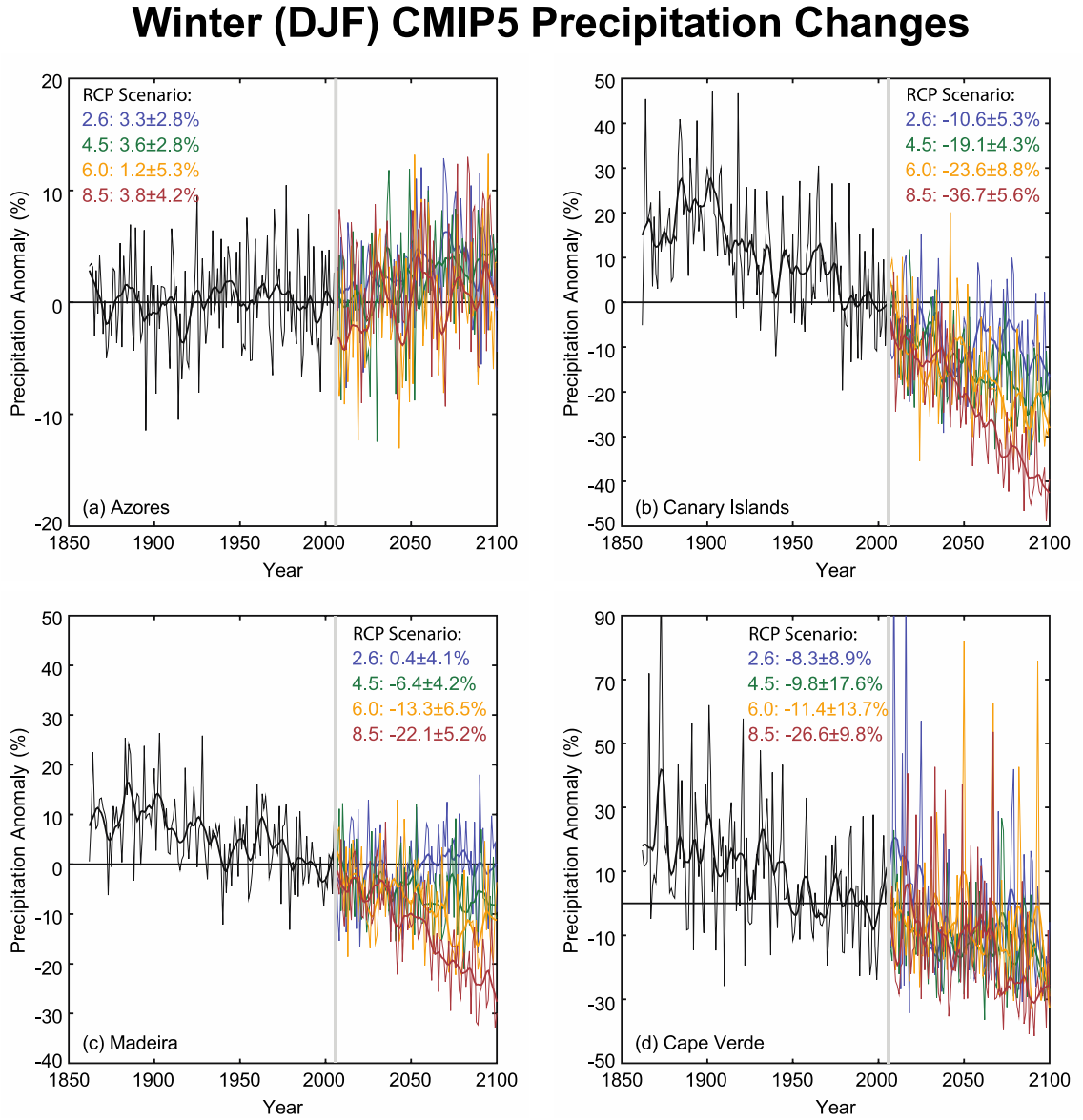

Figure 5.2. The CMIP5 multi-model mean historical (black line) and predicted winter (DJF) precipitation anomaly (colour lines), expressed as a percentage change relative to the 1976–2005 base period) for the Azores, Madeira, Canary Islands and Cape Verde. Thick, smooth lines indicate 11-year LOESS trends. The RCP scenario changes are the difference in mean (with 95% confidence intervals) between 2071–2100 and 1976–2005.

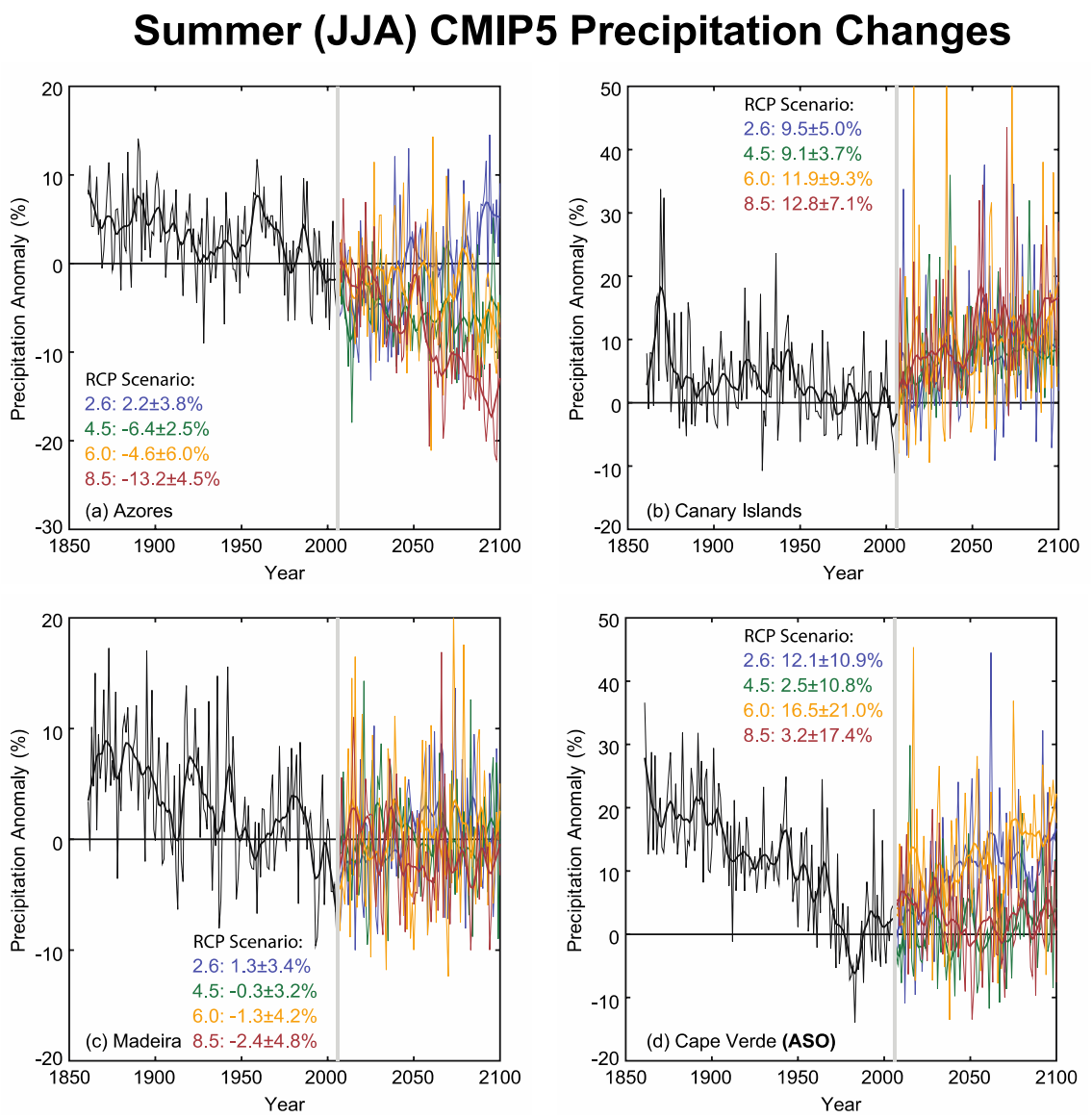

Figure 5.3. As for Figure 5.2 but for summer, or ASO for Cape Verde.

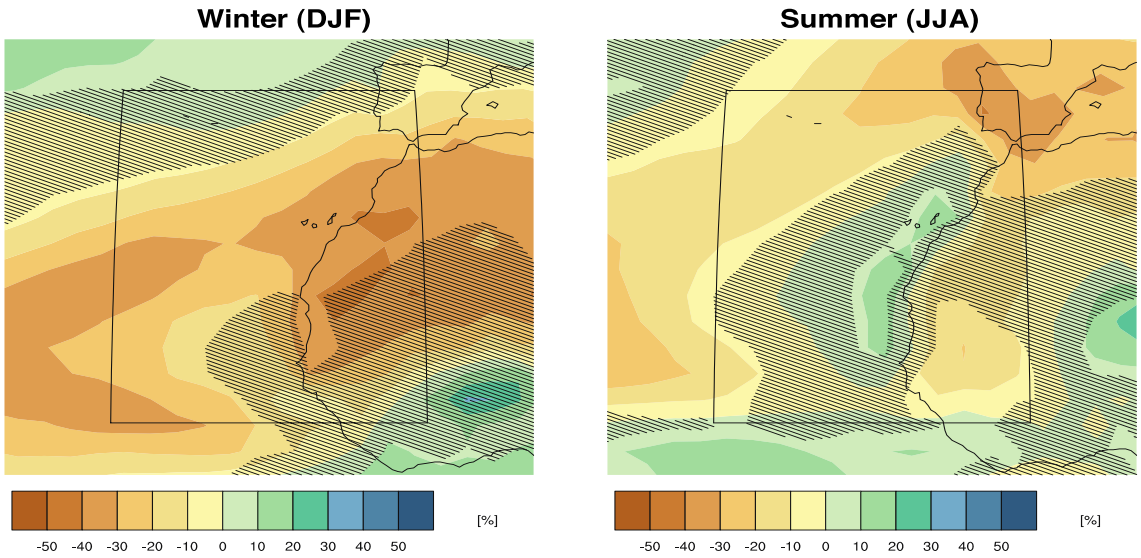

Figure 5.4. The relative changes (%) in DJF and JJA surface precipitation between 2081-2100 and 1976-2005 from the CMIP5 archive. Hatching indicates where the changes are less than ±1 SD.

5.2 Future Response in Extreme Conditions

5.2.1 Temperature Extremes

Figures 5.5 – 5.9 illustrate the historical and future output of the CMIP5 archive for the four Macaronesian Island chains for the nine temperature-based extreme indices as defined in Table B2 (or Table 4.8 for a shorter version). A clear trend emerges: extreme based temperature measures show a very similar increase to the mean temperature increase depicted in Section 5.1. The different RCP scenarios emerge and separate around 2030 for the 90th percentile-based indices (Tn90p and Tx90p, Figure 5.8) but more slowly (~2050) in the absolute indices (TXn, TXx, TN and TNx, Figure 5.5, 5.6). Across all four island chains, the model mean response for the 'cold' percentile-based indices (Tx10p and Tn10p, Figure 5.9), which would normally occur across 10% of days during the year (during the 1961-1990 period) appears to drop close to 0% by as early as the 2010s, regardless of which RCP path is followed. Individual years, when the Tn10p or Tx10p value can rise above 10% of days in the year, can still occur, but they will be much more infrequent than during the Twentieth Century.

Any realistic changes in DTR appear hard to constrain as the absolute DTR in the models varies a considerable amount (so the ensemble mean has low value here). Across the ocean around the Macaronesian region, the annual DTR climatology is 0.3-0.5°C from the HadDTR dataset (base period 1990-2004 and on a 5x5° resolution, Kennedy *et al.* (2007)). Such a wide spread in model DTRs (Figure 5.7) might reflect the balance towards whether the grid-box in each model was predominantly a 'land' or 'ocean' cell, which presumably would be resolution-based, given the size of the Macaronesia Islands. Although the grids were all re-interpolated to a 2.5° resolution, a 'land' DTR signal could still be observed (Figure 5.7 shows that this seems to affect the Canary Islands the most). Either way, changes in annual minimum and maximum temperatures appear reasonably consistent and linear, so no large changes were expected. How DTR changes will be dependent on the effect of AGW on daytime maximum temperatures and night-time minimum temperatures. A DTR decrease has been observed in data and models (Bragaza *et al.*, 2004); however Rohde *et al.* (2013) note that since 1987, globally, DTR has been increasing. Changes in cloud cover, that are potentially independent of global warming signals, can also impact the DTR. In addition, how AGW will affect patterns of maximum and minimum temperatures spatially and seasonally will also be important.

The most conservative estimates (RCP2.6) of changes across the Azores in the warm percentile indices TN90p and TX90p, suggests that by 2081-2100, approximately 40% (20%) of days according to the model mean (lowest individual model run) would be days that were previously classified as the warmest 10%, with respect to the 1961-1990 period

(Figure 5.8, 5.9). These values were similar for the Canary Islands, higher for Madeira (55% model mean) and much higher for Cape Verde (65% model mean / 40% lowest model run). In contrast, under scenario RCP8.5, for the period 2081-2100, there is the potential for nearly every day in the year (i.e. 80-100% of days) to be at a temperature that would have fallen in the top 10% percentile of days during the period 1961-1990 (TN90p/TX90p, Figure 5.8, 5.9). The model ensembles indicate that this is most likely for Cape Verde, shown by the lower range on the box and whisker plots. Interestingly, under RCP8.5, some of the lowest model runs for the Canary Islands and Madeira have some model runs where the changes were not as pronounced - i.e. as low as ~40-50% of days in what would have been the top 10% previously. This is perhaps due to the proximity of the islands to the northwest African upwelling zone and influence of the Canary Current or the location of these two island chains within the main Trade Wind belt.

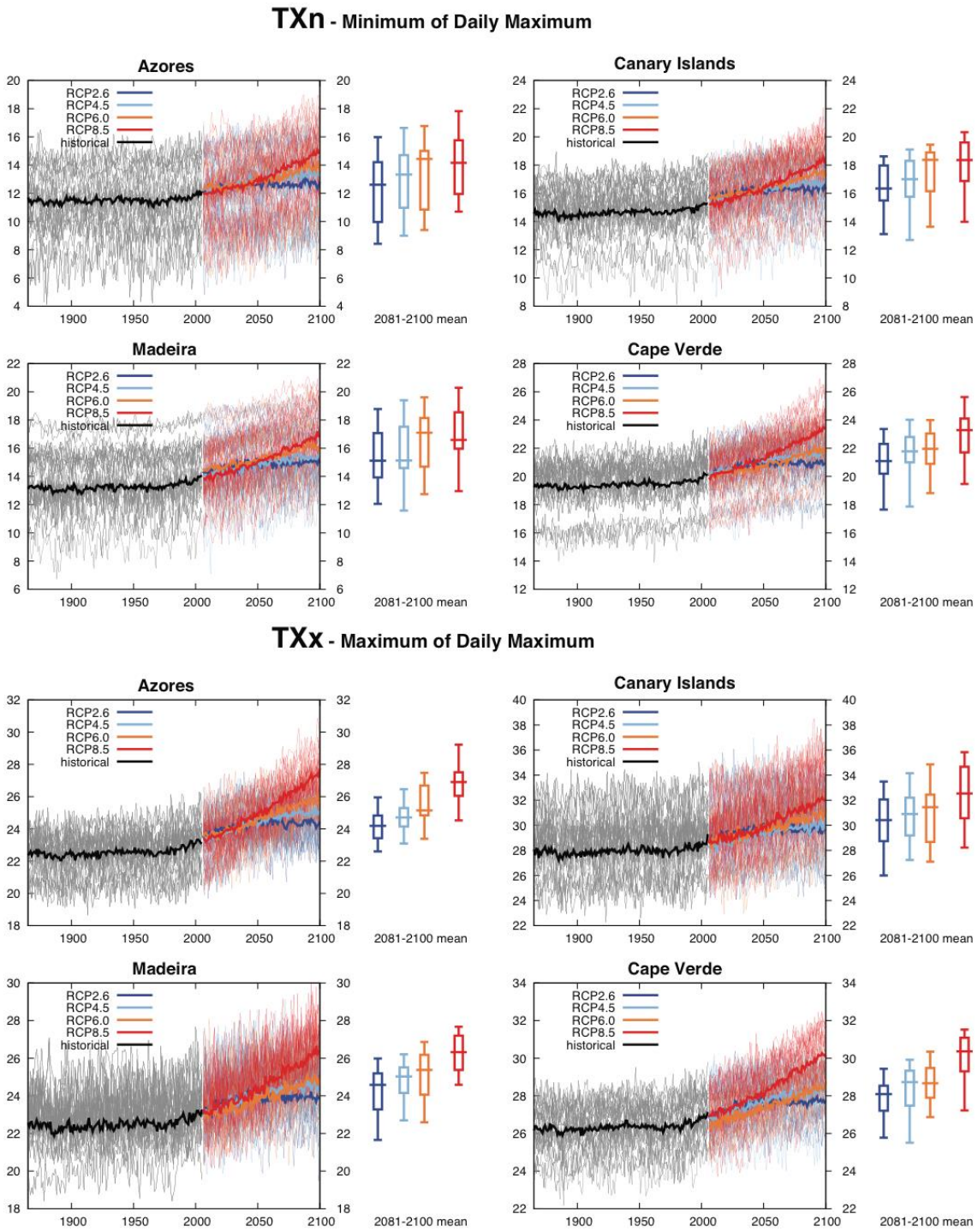

Figure 5.5. The CMIP5 model mean (thick lines) and individual model runs for the historical (1861-2005) and future (2006-2100) periods across the four Macaronesian Islands for TXn and TXx (Table B2). Also shown are Box-Whisker plots for the 2081-2100 period for each RCP scenario. Graph Units: °C.

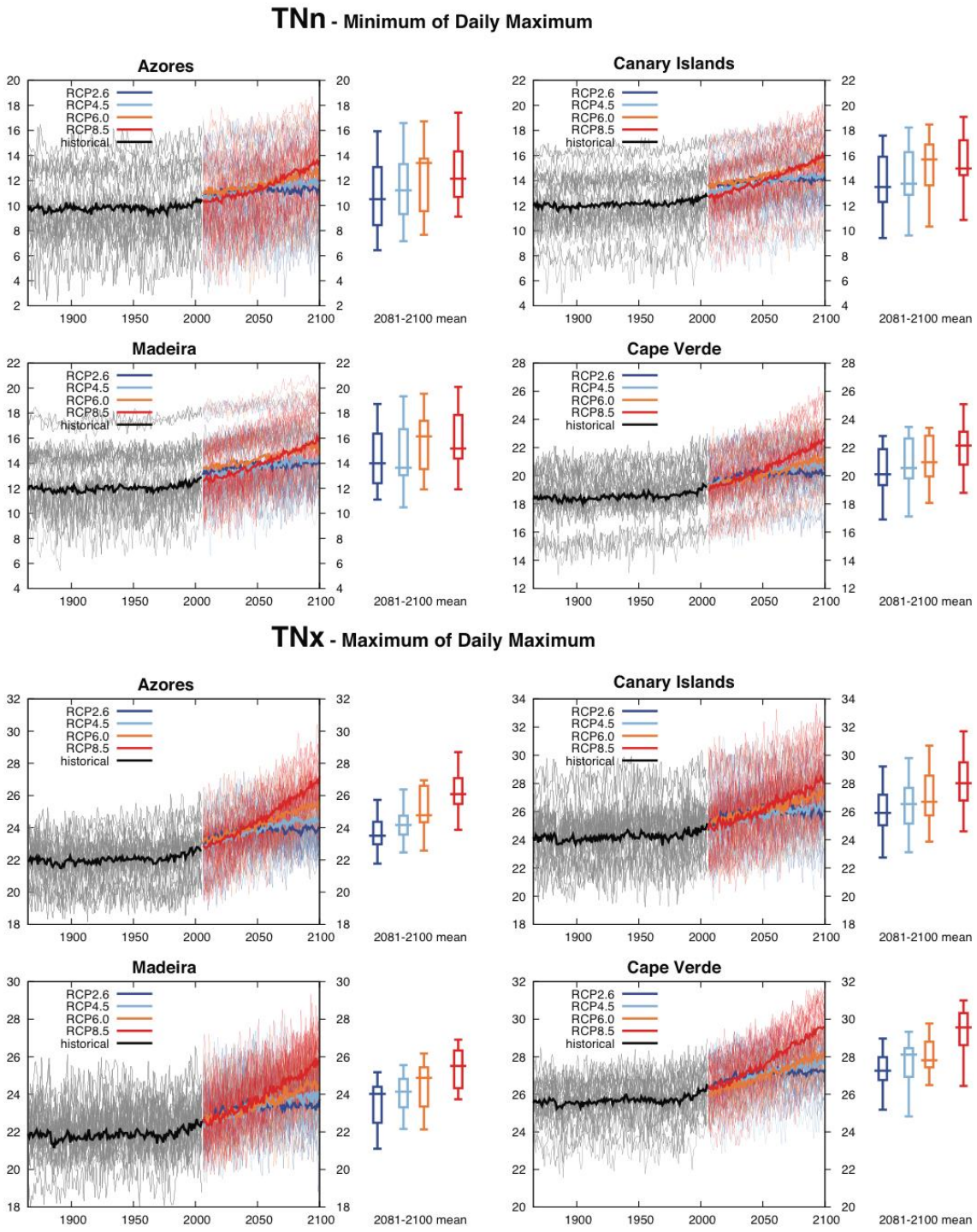

Figure 5.6. The CMIP5 model mean (thick lines) and individual model runs for the historical (1861-2005) and future (2006-2100) periods across the four Macaronesian Islands for TNn and TNx (Table B2). Also shown are Box-Whisker plots for the 2081-2100 period for each RCP scenario. Graph Units: °C.

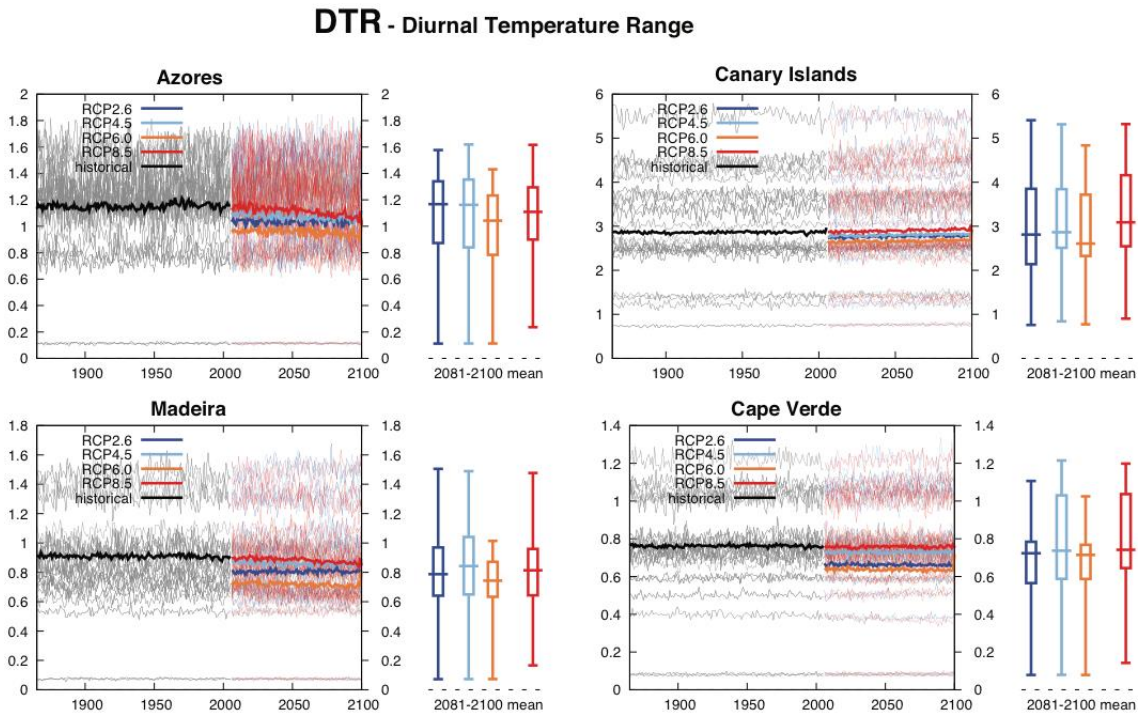

Figure 5.7. The CMIP5 model mean (thick lines) and individual model runs for the historical (1861-2005) and future (2006-2100) periods across the four Macaronesian Islands for DTR (Table B2). Also shown are Box-Whisker plots for the 2081-2100 period for each RCP scenario. Graph Units: °C.

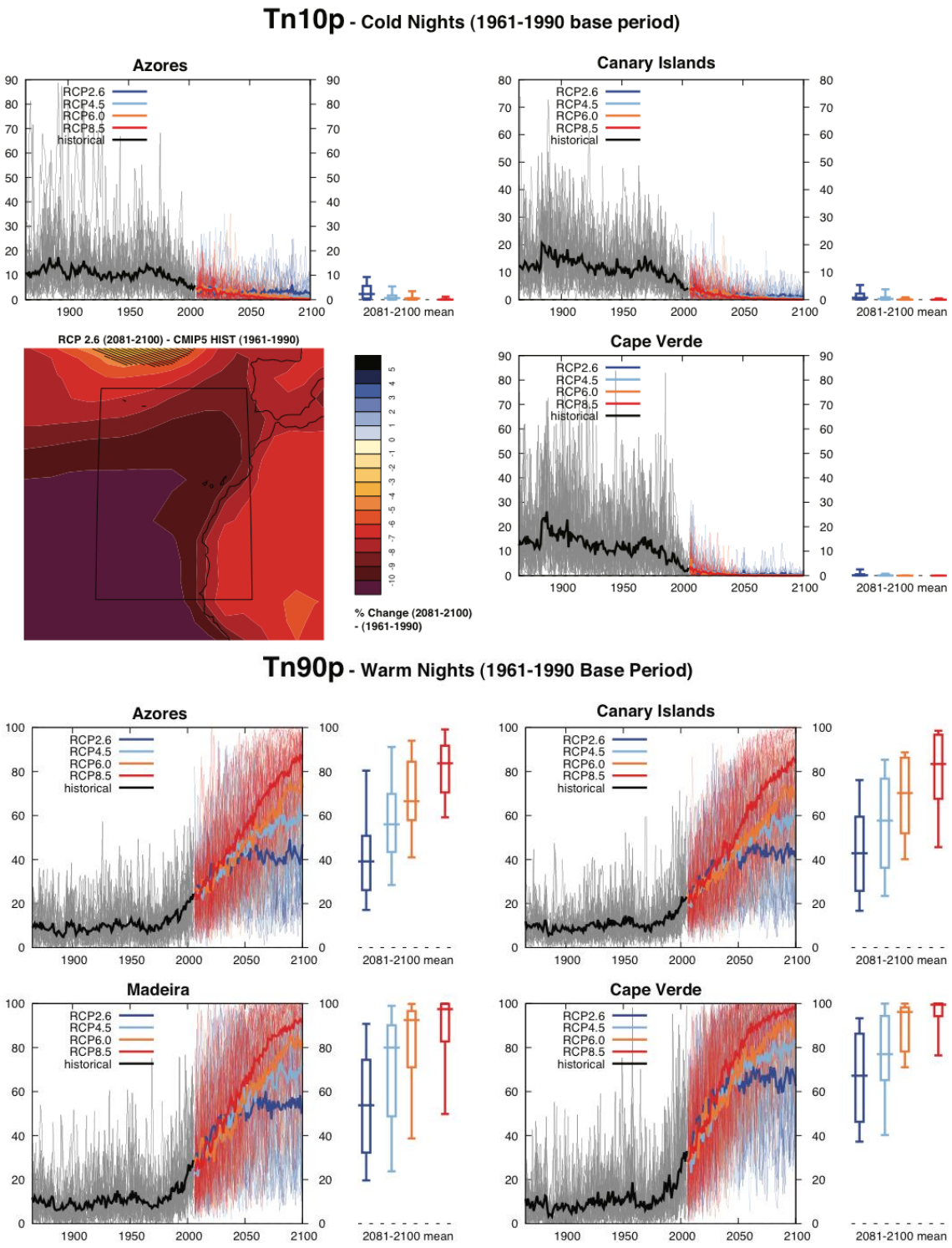

Figure 5.8. The CMIP5 model mean (thick lines) and individual model runs for the historical (1861-2005) and future (2006-2100) periods across the four Macaronesian Islands (with 2081-2100 Box-Whisker plots) for Tn10p and Tn90p. Also shown instead of the Madeira Tn10p plot (as the plot is exceptionally similar to the Canary Islands) is the spatial pattern of change for the period 2081-2100 relative to 1961-1990 (hatching indicates the magnitude of change is less than ±1 SD). Graph Units: %.

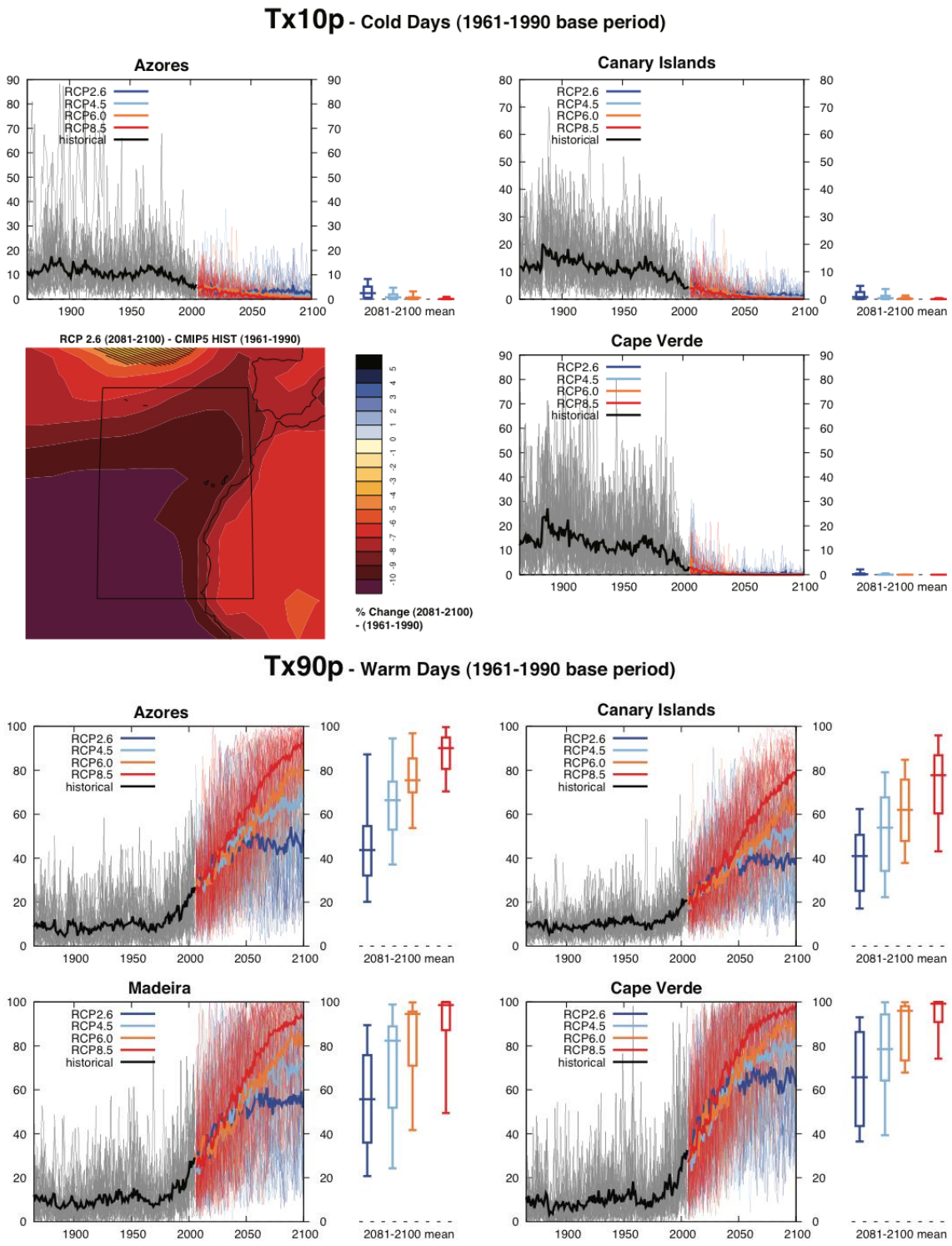

Figure 5.9. The CMIP5 model mean (thick lines) and individual model runs for the historical (1861-2005) and future (2006-2100) periods across the four Macaronesian Islands (with 2081-2100 Box-Whisker plots) for Tn10p and Tn90p. Also shown instead of the Madeira Tn10p plot (as the plot is exceptionally similar to the Canary Islands) is the spatial pattern of change for the period 2081-2100 relative to 1961-1990 (hatching indicates the magnitude of change is less than ±1 SD). Graph Units: %.

Arguably the most important extreme temperature measure is the Warm Spell Duration Indicator (WSDI, Table 4.8, B2) as it is the closest analogue to a 'heatwave index', although factors other than maximum daytime temperature, such as humidity, soil moisture content and cloud cover, can regulate the impact of heatwaves. Figure 5.10 indicates the WSDI index for the historical (1961-1990) period and the RCP2.6 and 8.5 model mean response for the period 2071-2100 across Macaronesia (note the different scales for the future scenarios). During the historical period, the average number of days per year where a series of >6 days total exceed the 90th percentile for that day varies between about 6-15 days of the year. Under RCP2.6, the minimum number of days that fall into the WSDI category (i.e. consistently >6 days higher than the 1961-1990 90th percentile) is ~50 days across northwest Africa and Iberia. The most severe RCP8.5 scenario has almost the entire year under 'heatwave' conditions relative to 1961-1990 across the Atlantic Ocean. This is likely due to the lower diurnal variability of the ocean. Arid land surface conditions, particular across the northwest African continent can have significant diurnal variability and also, temperatures are already much higher across land, so the distribution of average daily temperatures around the year might not shift as dramatically across the ocean. Regardless of the scenario, a lower latitude and oceanic setting appear to show more severe WSDI conditions than higher latitudes and proximity to land. The eastern Canary Islands appear the least affected under both future scenarios (proximity to the cool Canary Current and upwelling region off northwest Africa is the likely cause for this).

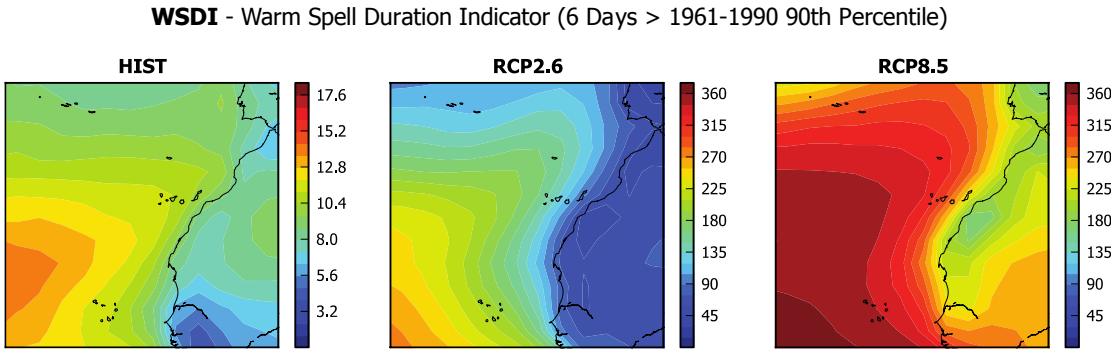

Figure 5.10. The number of days per year where the 90th temperature percentile (1961-1990 base period) is consistently (>6 days) exceeded for the CMIP5 Historical model mean (1961-1990) and the RCP2.6 and 8.5 model mean for 2071-2100.

5.2.2 Precipitation Extremes

The relative changes between the RCP8.5 model mean (2071-2100) and the historical model mean (1979-2005) in eleven precipitation extreme indices are displayed in Figure 5.11. A common feature amongst the indices appears to be a wetting of the region surrounding the Azores, a slight increase in precipitation near Cape Verde and a drying across the Madeira/Canary Islands 'trade-wind-axis', Iberia and Sahara regions.

Beginning with the Azores, a reduction in the number of days with >1 mm of precipitation is shown along with an increase in the number of days where >20 mm is expected (this increase is reflected in the percentile based R95/99p indices). The Consecutive Wet Day index shows a small decrease, whereas maximum precipitation across 1 and 5 day intervals (Rx1/5Day) shows a small increase. These factors all contribute towards a higher Simple Daily Intensity Index (i.e. more rainfall, less frequently) but without a significant change in total precipitation.

The Trade Wind region, encompassing Madeira and the Canary Islands is predicted to undergo a large-scale drying. A positive increase in CDD is mirrored by a general decrease in precipitation total and the Rx1/5Day precipitation and R1/10mm indices. Changes across Cape Verde appear to be relatively minor, although the likely discrepancies in-between models are large (as highlighted in Section 5.1.2).

How reliable might the CMIP5-based precipitation extreme estimates be? As a simple test, the CMIP5 output over the 'historical period', 1979-2005, can be compared against reanalysis output from the ERA-I dataset (Dee *et al.*, 2011), which also had the ETCCDI extreme indices computed by Sillmann *et al.* (2013a) which were also analysed in Chapter 4.3. A spatial comparison between the CMIP5 model mean and the ERA-I reanalysis for the ten precipitation extreme indices is shown (Figure 5.12) along with a comparison between the monthly precipitation mean from the 16 Macaronesian meteorological stations, the NCEP-NCAR and ERA-I grid-boxes that override the island locations and three selected CMIP5 models (Figure 5.13).

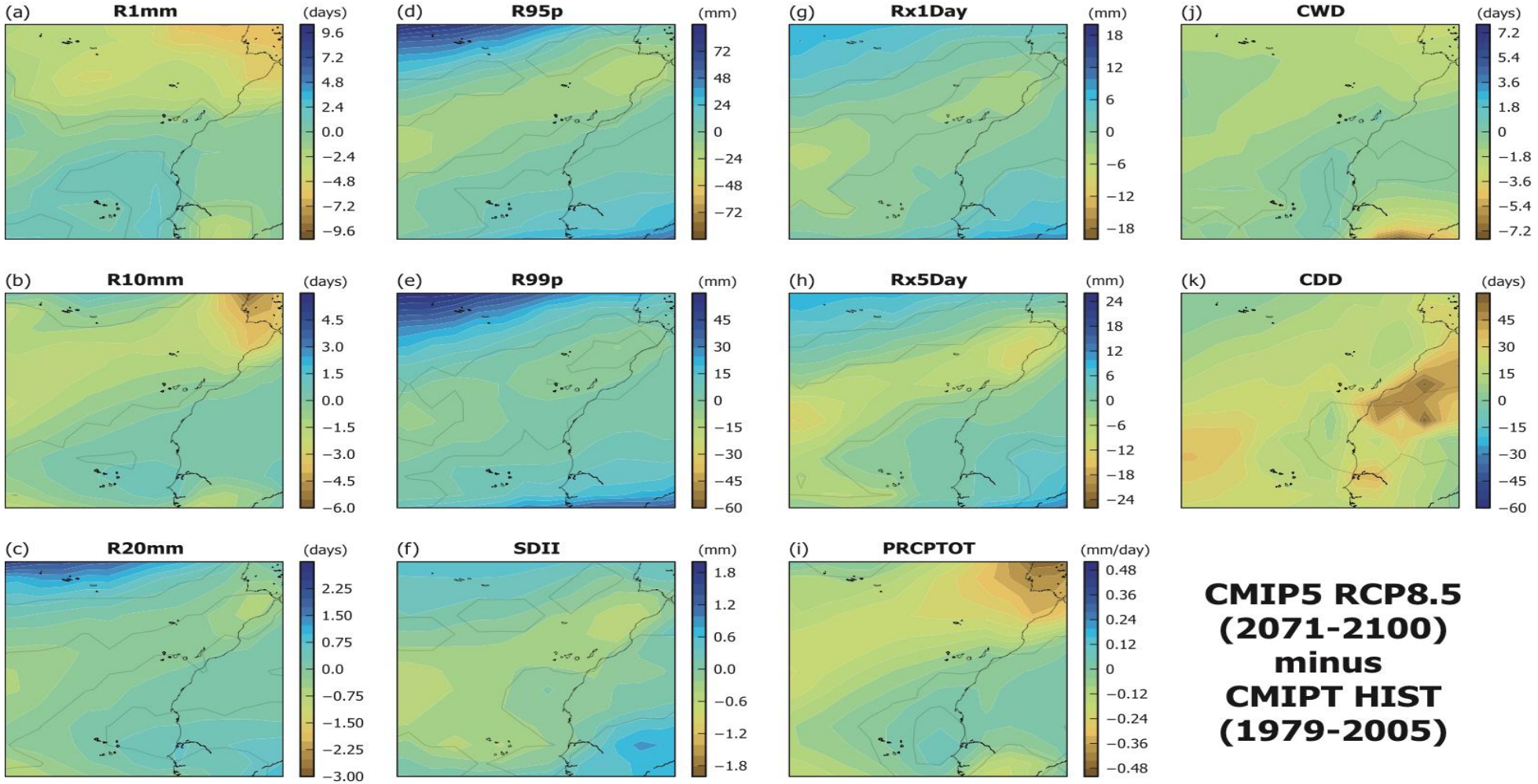

Figure 5.11. The difference between the (a) R1mm, (b) R10mm, (c) R20mm, (d) R95p, (e) R99p, (f) SDII, (g) Rx1Day, (h) Rx5Day, (i) CWD and (j) CDD precipitation-based extreme indices (Table B1) as calculated for the CMIP5 historical model mean (1979-2005) and the future period 2071-2100 (RCP 8.5). Grey lines denote regions that are significantly different according to a two-sample T-Test.

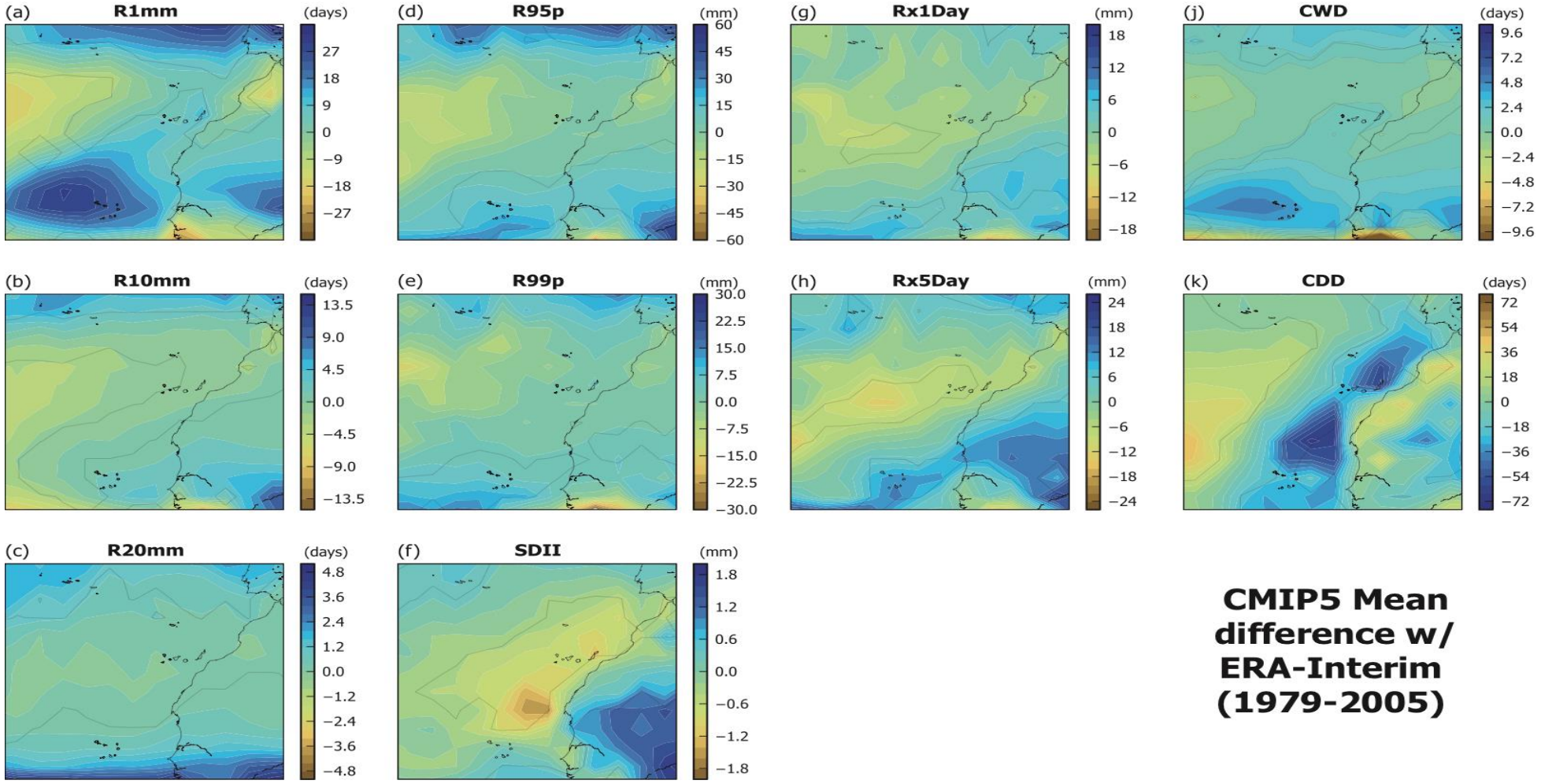

Figure 5.12. The difference between the (a) R1mm, (b) R10mm, (c) R20mm, (d) R95p, (e) R99p, (f) SDII, (g) Rx1Day, (h) Rx5Day, (i) CWD and (j) CDD precipitation-based extreme indices (Table B1) as calculated for the CMIP5 model mean and the ERA-I reanalysis for the period 1979-2005. Grey lines denote regions that are significantly different according to a two-sample T-Test.

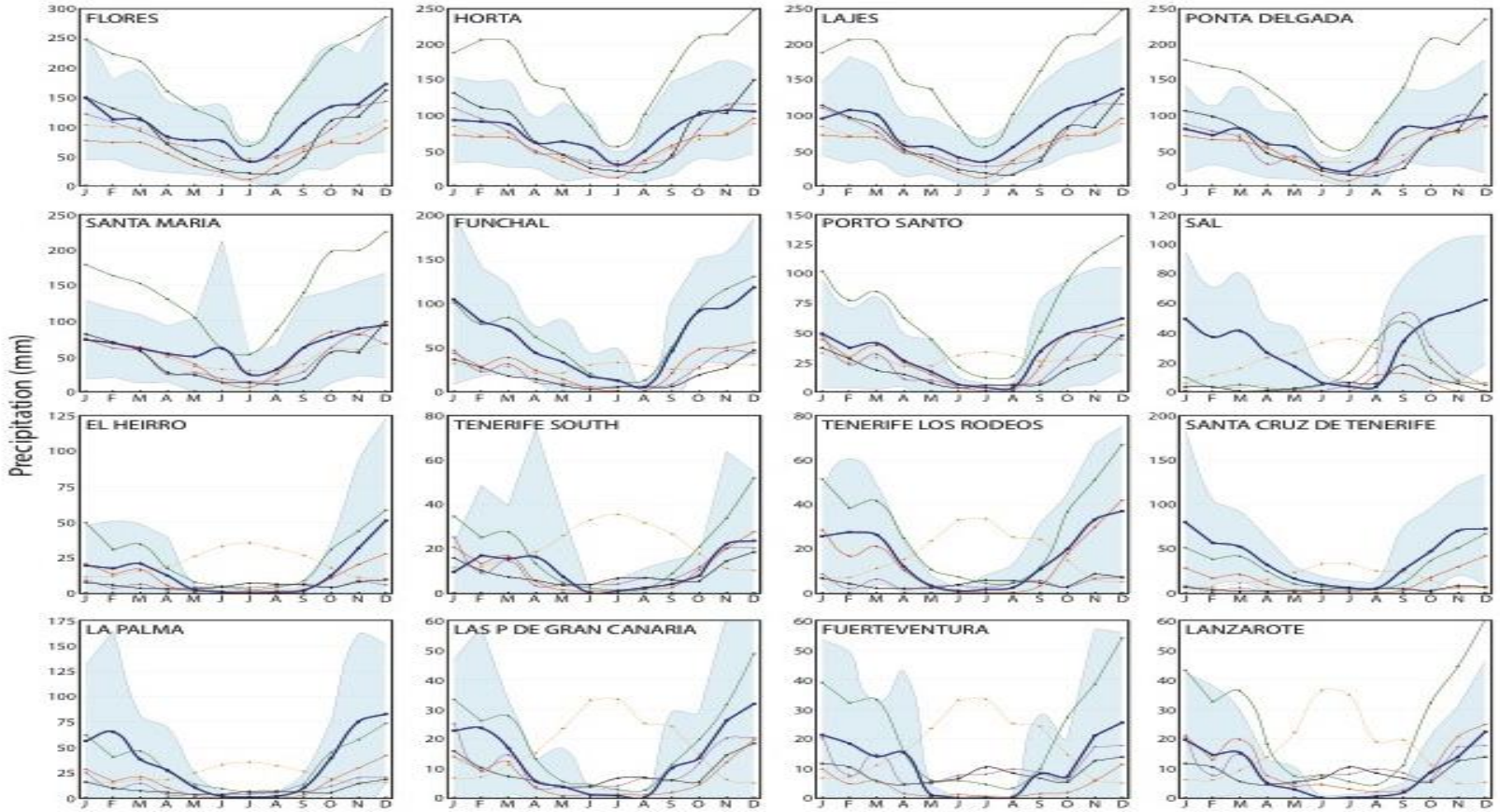

Figure 5.13. The monthly precipitation climatology (Blue line, 1979-2005) for the sixteen meteorological-stations from Table 4.7. Only months with full data were considered in calculation of the station mean. The shaded blue region indicates ±1SD variability around the mean. The red and green lines represent the NCEP/NCAR and ERA-I reanalysis values for the grid-box closest to each island respectively. The black, yellow and magenta lines represent the CMCC-CMS, IPSL-CM5A-MR and MPI-ESM-MR r1i1p1 CMIP5 climate models.

Figure 5.12 illustrates that perhaps the most striking difference between 'near-reality' (ERA-I) and the 'model-world' (CMIP5) is the difference in CDD, with the CMIP5 model mean being significantly 'wetter'. The storm track regions surrounding the Azores sometimes were classed as significantly different but generally seem to be reasonably consistent between CMIP5 and ERA-I. A significant bias over Cape Verde appears in the R1mm, RX5Day and CWD indices. A positive bias in the CMIP5 precipitation regimes across west Africa has been reported by Siongco *et al.* (2014). They found a bias towards high precipitation across west Africa that starts in spring and is sustained through summer in high horizontal resolution climate models. This may explain the 'wetter' conditions in CMIP5 around Cape Verde (less CDD / more CWD, more days with precipitation >R1mm and more precipitation over 5 day periods). The feature appears to be a dipole, with a precipitation bias across northeastern Brazil being the opposite centre of action that negatively correlates with the sign of the bias over west Africa (Siongco *et al.*, 2014).

When monthly mean precipitation values were considered (Figure 5.13) the annual cycle of the bias under a CMIP5 model becomes obvious. The climatology of precipitation from the sixteen precipitation stations from Table 4.7 (no gap filling measures applied to missing data), the nearest grid-box to each island from the NCEP/NCAR and ERA-I reanalysis and from three models from the CMIP5 archive are shown. It can be seen that the IPSL CMIP5 model (Figure 5.13) displays the traits described by Siongco *et al.* (2014) of an over-simulation of precipitation, most clearly displayed across the Canary Islands and Cape Verde (although it is also apparent across Madeira). However the IPSL model correctly simulates the annual cycle across the Azores (i.e. storm track regions). The two other CMIP5 models appear to achieve the correct annual cycle across the Macaronesia Islands well. In fact they better represent Azores precipitation (compared to the meteorological-station climatology) than the ERA-I reanalysis, which markedly exceeds the station precipitation values by over ±1SD in the wetter months (but gets the annual cycle correct).

5.3 Changes in Climate Indices

5.3.1 North Atlantic Oscillation

Using monthly SLP output from 77 different RCP8.5 realisations, proxies for the station-based NAO were created by subtracting the normalised (1901-2000 base period) SLP from the grid-box overriding Iceland from the grid overriding the Azores. No evidence of the increasing variability documented in Section 3.3.2 could be found in the winter or December index during the historical CMIP5 period (1861-2005) and into the future. A weak trend emerges towards more positive winter and December NAO conditions by the end of the Twenty-first Century (Figure 5.14). To rigorously analyse the NAO in the CMIP5 models, it is suggested that each individual run would have to be analysed as any ensemble statistics suppress the actual 'NAO' from each model run.

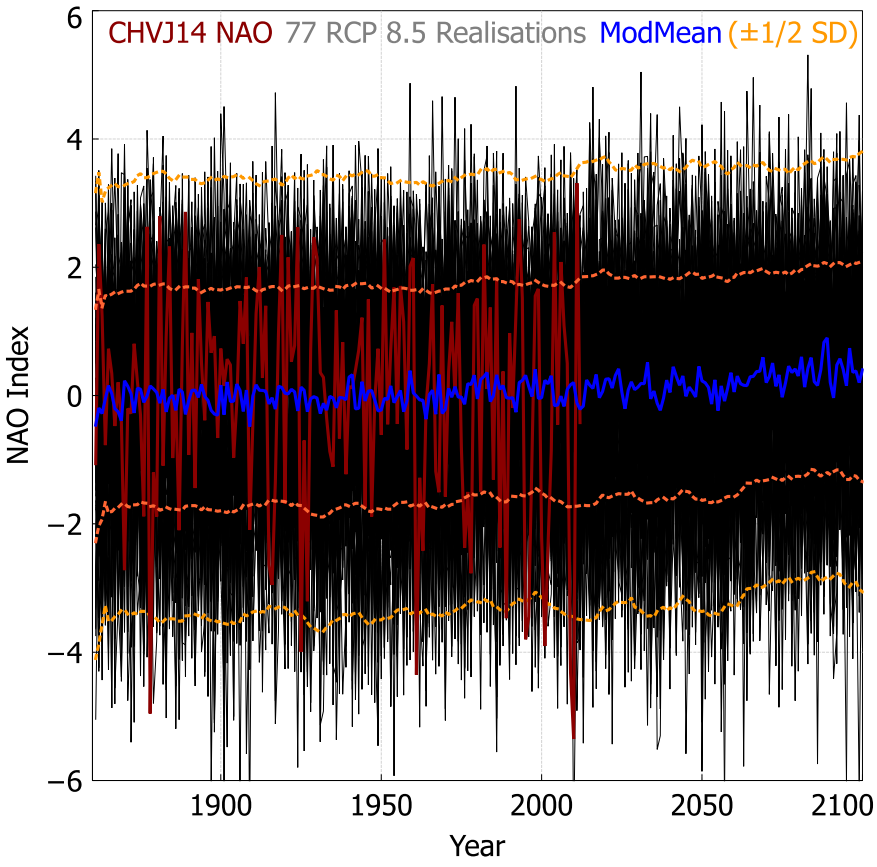

Figure 5.14. The December NAO, taken from each CMIP5 model (77 Historical + RC8.5 simulations) as the difference between the normalised monthly SLP between the grid-box overriding the Azores and Iceland. The model mean and the (11-year running mean) ±1/2 SD about the mean (based on the spread of all model runs) is indicated along with the CHVJ15 NAO index (values doubled so the scales match).

5.3.2. Trade Wind Index

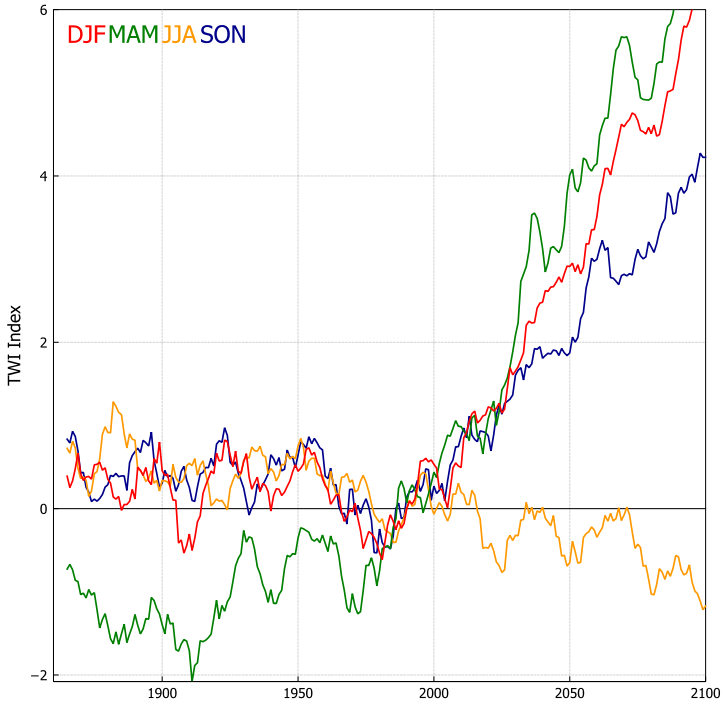

Figure 5.15. The (11-year running mean) seasonal TWI, defined as the difference between the RCP8.5 model mean between the grid-box overriding the Azores and Cape Verde.

The same principle is applied to creating a seasonal TWI from the CMIP5 archive, although the exception here is that only the model-mean from each RCP run is taken (Figure 5.15). A clear positive shift is evident in all seasons but summer. The summer TWI from the CMIP5 archive exhibits a long-term negative trend from the historical period to the end of the Twenty-first Century. There is an increase in the index, superimposed on the long-term decline that is reasonably consistent with the positive trend in the observed index during 1973-2012.

5.4 Physical Controls on Future Changes

The section discusses the physical basis behind the potential future changes documented in Section 5.1-5.3. Essentially, how the regional climate across Macaronesia will respond is a function of thermodynamic and dynamical/circulation changes. The expected increase in radiative forcing due to AGW will increase temperatures globally, this is a thermodynamic response. In Figure 5.1, we see that the end of the Twenty-first Century temperature response across Macaronesia is always positive and all the models agree on the sign of change – warmer temperatures. The differences in the various future scenarios are seen to diverge around 2030-2040. At this point in time it should be clear which future temperature destination is apparent for the Islands.

What is more uncertain are dynamics and circulation changes, essentially the 'weather'. Figure 5.14 shows that for the NAO, the models, whilst showing a weak mean response, are typically inconsistent in their yearly (i.e. specific years) NAO predictions. For example, for 2100, it can be reasonably certain most models will have a warmer year than any year in the Twentieth Century, but for the NAO, it would be a roughly 50/50 split of whether or not the model predicts a positive or negative NAO. This is the difference between thermodynamics and circulation. Temperature responses are thermodynamically-based, so the predictions from the CMIP5 archive can be taken with a high degree of confidence. Precipitation, in the mid-latitudes, is predominantly influenced by the atmospheric circulation, which is a circulation-based mechanism and can't be predicted with the same amount of confidence as temperature changes.

Typically, AGW is expected to increase precipitation amounts in 'wet' regions and decrease precipitation amounts in 'dry' regions (Liu and Allen, 2013). A further effect of AGW is the expected expansion of the subtropical arid regions towards the poles (i.e. a poleward shift of the Storm Tracks, Lu *et al.*, 2007). Also, the maximum water vapour holding capacity of the atmosphere scales with temperature at a rate of ~7-8%°C^{-1} (Held and Soden, 2006), so extreme precipitation amounts are expected to increase. The islands of Macaronesia essentially fit into three, large-scale precipitation regimes: the Azores along the southern edge of the mid-latitude storm tracks (wet region), the Canary Islands and Madeira in a subtropical Trade Wind zone (dry region) and Cape Verde in a position where influences stem from monsoonal rains and from African Easterly Wave activity.

The increase in extreme Azores precipitation can be identified by clear increases in the R20mm and R95/99p indices in Figure 5.11 without a great change in the state of mean total precipitation (Figure 5.2-3). This fits the 'wet get wetter' and increase in extreme precipitation aspect. The location of the Azores on the southern flank of the storm tracks,

in a modern climatological setting, may also help explain why the mean precipitation stays somewhat consistent – if the storm tracks do shift pole wards, there would be a reduced frequency in the amount of precipitation events. This can be inferred by a slight decrease in the R1mm indices around the Azores and generally lower R1mm values along the same latitude in Figure 5.11, which shows the difference in the CMIP5 models between 2071-2100 and 1976-2005, and implies a reduction in the amount of precipitation days.

Drying across Madeira, the Canary Islands and Cape Verde, particularly in winter (Figure 5.2) fits the 'dry gets drier' aspect. This occurs because in regions of the globe where evaporation is greater than precipitation, the existing pattern is expected to intensify, assuming no significant circulation changes (Stocker *et al.*, 2013). The winter reduction in Madeira and Canary Island precipitation is an important finding, which needs to be prepared for, as winter precipitation accounts for over half of the annual rainfall amounts across these Island regions (Table 4.7).

If the NAO mean winter state shifts towards more positive conditions, it might first be expected that a discrepancy between winter and summer temperature trends becomes pronounced across (at least the three northernmost) Macaronesian Islands, as NAO+ conditions generally equate to cooler winter temperatures across these islands (Figure 3.9). If the summer Trade Winds were to decrease, as shown in Figure 5.15, the temperature disparity (lower winter warming rates, higher summer warming rates) might further increase, as increased summer Trade Wind strength generally equates to cooler temperatures across the Trade Wind belt (Figure 3.12). The northward migration of the storm tracks, associated with the positive NAO, would contribute to lower precipitation amounts across the Canary Islands and Madeira. This would be a circulation-induced deficit, with the enhancement of the natural water cycle across the Trade Wind belt (where evaporation $>$ precipitation) being a thermodynamic component. The shift towards an NAO+ state arises due to a general increase of SLP in mid-latitudes and decrease across high latitudes (Collins *et al.*, 2013) and has also been found in the CMIP5 archive by Gillett and Fyfe (2013), reinforcing the small positive change projected in the NAO that is apparent under a warmer climate in Figure 5.14 here.

Cape Verde precipitation will be most likely controlled by changes in the WAM and in AEW propagation. There is less certainty in the sign of Cape Verde precipitation (Figure 5.3), which reflects an uncertainty in the models of the future direction of WAM changes and bias in the position of the ITCZ (Christensen *et al.*, 2013). Additionally the nature of certain models in the CMIP5 ensemble to incorrectly simulate west African precipitation (positive bias) likely adds to the uncertainty.

Will the topographic influence of the islands affect future precipitation? The large scale thermodynamic and circulation patterns discussed place no consideration with regards to the influence of topographic barriers and orographically induced rainfall. Logically, if the warming of the lower troposphere is reasonably coherent (across vertical levels), the height at which condensation occurs will increase, this would result in less precipitation at lower latitudes on the windward side of mountains and perhaps greater precipitation in the lee slopes of mountains (assuming the prevailing wind patterns remain constant). This 'downwind' modification of precipitation has been modelled by Siler and Roe (2014).

Changes in temperature extremes appear relatively synchronous across the islands. An apparent exception is a greater tendency towards 'warmer' conditions across the lower latitudes / oceanic zones, reflected by greater trends in TN90p/TX90p for Cape Verde (Figure 5.8, 5.9) and the spatial pattern of WSDI (Figure 5.10). Rather than this reflecting a significantly greater tropical warming, it is more likely that because of the lower day-to-day variability, a uniform absolute shift in the magnitude of temperatures will appear as greater, relative to a percentile based threshold.

Interestingly, when the absolute maximum and minimum trends in SAT and precipitation (across the Azores) from across the model ensemble (using RCP8.5) for a 55-year period (2006-2060) were taken, stark contrasts could be seen in SAT and precipitation trends (Figure 5.16). Under 'realisation 2', continental warming across Africa dominates and there is a cooling trend poleward of the Azores. A general wetting trend across Macaronesia is seen that is strongest across the Azores and south of Cape Verde (hurricane track region). Whereas under 'realisation 1', warming and wetting trends north/northeast of the Azores suggests a future where it could be assumed that NAO+ conditions contribute most to the observed trends and Macaronesia experiences an overall drying trend. Uncertainty in future climate projections essentially comes down to emissions-scenario uncertainty, model-response uncertainty and natural variability (Deser *et al.*, 2012). Here the emissions-scenario uncertainty does not apply (as RCP8.5 only is used) and Figure 5.1 indicates that for temperature, all of the models follow a reasonably consistent final path (i.e. up to 2100) so the changes in Figure 5.16 highlight the potential for natural variability to significantly influence the climate far into the Twenty-first Century. Under the two scenarios depicted (that were selected based on the two most extreme responses across the Azores) temperatures across Cape Verde would hypothetically evolve at a very similar rate, but the precipitation trend is of opposite sign. This highlights the potential differences in future model responses at the regional scale (for Macaronesia) and why the model mean and/or median is generally taken as the best informative metric, but could also be misleading as the spatial patterns of climate variables show great variability. It might be expected that by 2100 under RCP8.5 anthropogenic forcing would have a significantly greater influence and trends between

(at least temperature, but maybe not for precipitation) might not diverge as much by then. Either way, natural variability across Macaronesia will serve to either augment or temper any potential AGW influence.

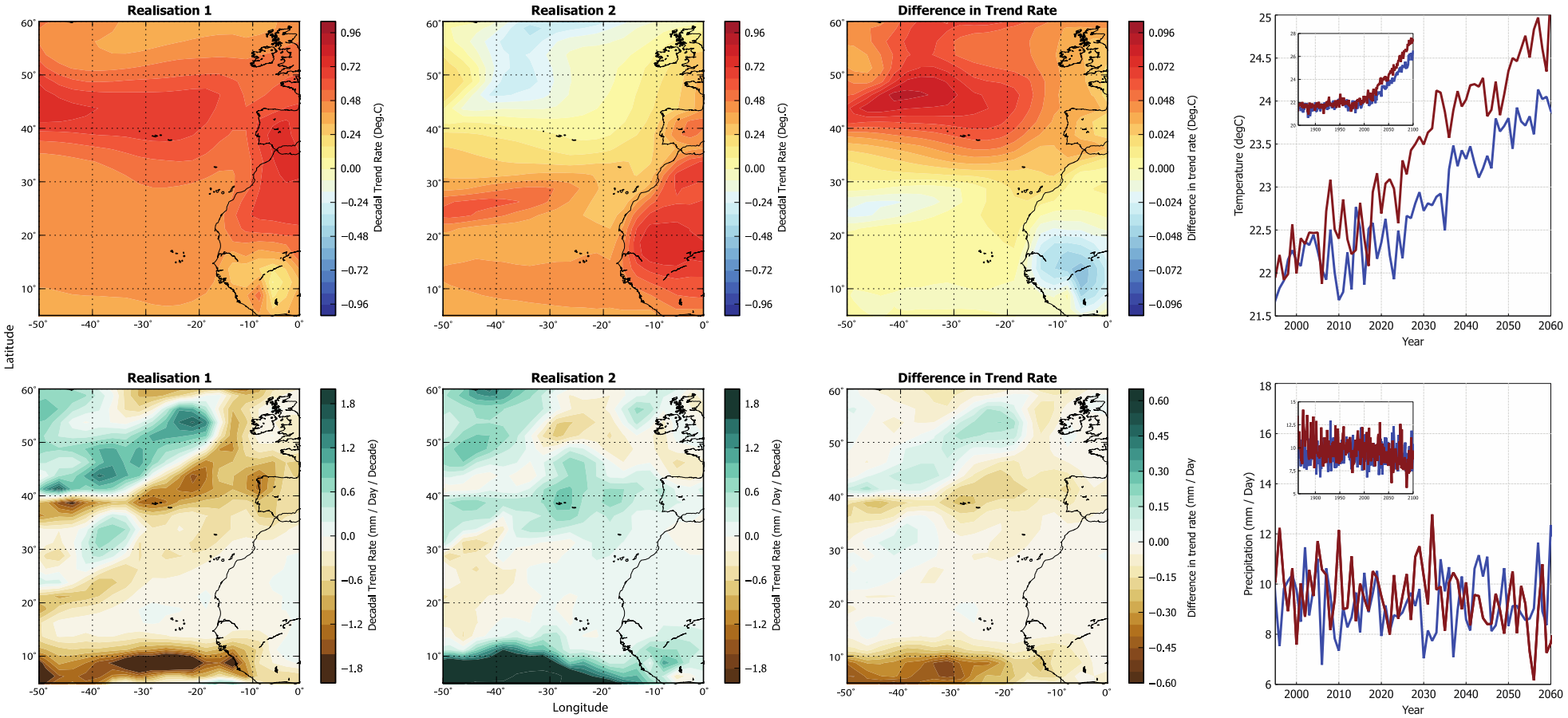

Figure 5.16. The difference between the CMIP5 models where the individually strongest warming/drying trends (Realisation 1) and weakest warming/strongest wetting trends (Realisation 2) across the Azores are shown along with the spatial difference between the trend rates and the temporal evolution of the Macaronesian (defined as the area-weighted average across 10-40°N, 325-355°E) time series for each model.

5.5 Chapter Summary

The CMIP5 model archive forms the basis of the conclusions of the IPCC. Here the CMIP5 models were analysed to determine the likely future evolution of climate across Macaronesia. SAT is expected to increase due to AGW, with predicted increases in mean SAT across the islands of ~0.8-3.0°C for the period 2071-2100 relative to 1976-2005. The more severe RCP scenarios lead to greater warming rates. Total precipitation changes are less certain. During winter, the Azores response is expected to be a slightly positive ~3% increase, but the ensemble is highly variable. Across Madeira, the Canary Islands and Cape Verde, a significant precipitation decrease (20-40%) is expected by the end of the Twenty-first Century. During summer, a small increase in precipitation is expected for the Azores under RCP2.6, but decreases under the more severe scenarios. Cape Verde precipitation could potentially increase during the wet season (ASO), although the ensemble is highly variable, and some CMIP5 models incorrectly simulate precipitation across the west African Sahel region. On the other hand, it was shown that some CMIP5 models more accurately simulate the annual precipitation cycle across the Azores than the ERA-I reanalysis for 1979-2005. Such variations in the models from simulating the recent past further clouds judgement and reduces uncertainty regarding future predictions.

Temperature-based extreme indices are expected to increase across all four island chains. As a warmer atmosphere can hold more moisture, extreme precipitation events are expected to increase in their yield/intensity. This signal emerges strongly across the Azores in the CMIP5 archive, but not for the other island chains. Natural variability in the climate system will continue to play a strong role throughout the Twenty-first Century, and serve to augment and/or reduce anthropogenically-driven global warming.

6. Northwest African Coastal Upwelling

6.1 Coastal Upwelling Overview

In Section 1.5, it was stated that the fifth and final research hypothesis of this thesis was to '*Test whether the Upwelling Intensification hypothesis can be verified across northwest Africa*'. A brief introduction to the coastal upwelling mechanism was also given in Section 1.3.8. Coastal upwelling is the phenomenon whereby wind-driven transport of water is directed offshore and replaced by cooler water from depth. There are four major coastal upwelling zones which are the Canary Upwelling Ecosystem (CUE) and the Benguela (Hagen *et al.*, 2001), Humboldt (Thiel *et al.*, 2007) and California (Pérez-Brunius *et al.*, 2007) eastern boundary upwelling ecosystems (Figure 6.1). Macaronesia hosts the CUE, which is situated off northwest Africa (11-35°N, Figure 6.2). The CUE, along with the other upwelling ecosystems, is an important socio-economic, oceanographic and biologically-active region. These coastal upwelling regions cover approximately 1% of the world's oceans, but account for over 20% of the global fisheries catch and a fisheries response to global warming has already been identified (Pauly and Christensen, 1995, Cheung *et al.*, 2013, Payne, 2013), so monitoring these regions is of high economic and environmental value. The Canary Current itself is the eastern, southward flowing component of the North Atlantic Subtropical Gyre (Figure 1.10).

In 1990, it was hypothesised that during the heating portions of the year (mainly summer) the effects of AGW would lead to an increase in daytime heating and reduction in nighttime cooling across the (sub-)tropical continental regions (Bakun, 1990). This would lead to enhanced continental thermal lows (i.e. lower SLP) adjacent to the oceanic subtropical highs, the greater SLP difference between these two centres of action would then drive stronger along-shore, coastal wind-speeds, which would lead to an increase in coastal upwelling. Since the original hypothesis in 1990, there has been a large body of research concerning the four major upwelling regions and whether or not an AGW response has been realised. Sydeman *et al.* (2014) conducted a meta-analysis of the published literature and discovered that across the Benguela, California and Humboldt regions, there was a clearly defined wind-speed increase – verifying the upwelling intensification hypothesis, but not across the CUE, where the trend was uncertain. Such a study reaffirms the need for a close examination of upwelling trends across the CUE. The literature review in Section 6.2 that follows hereafter clearly confirms this 'uncertain trend direction', and was the motivation for the published CHB14 paper, on which this

chapter is primarily-based. A key finding of the Sydeman *et al.* (2014) study was a disparity in the methods used, temporal scales analysed, data sources, and how each upwelling region itself was considered. The analysis in CHB14 and this chapter attempts to solve the often conflicting nature of published results regarding the recent evolution of upwelling across the region by analysis of several widely-, and some under-used data sources.

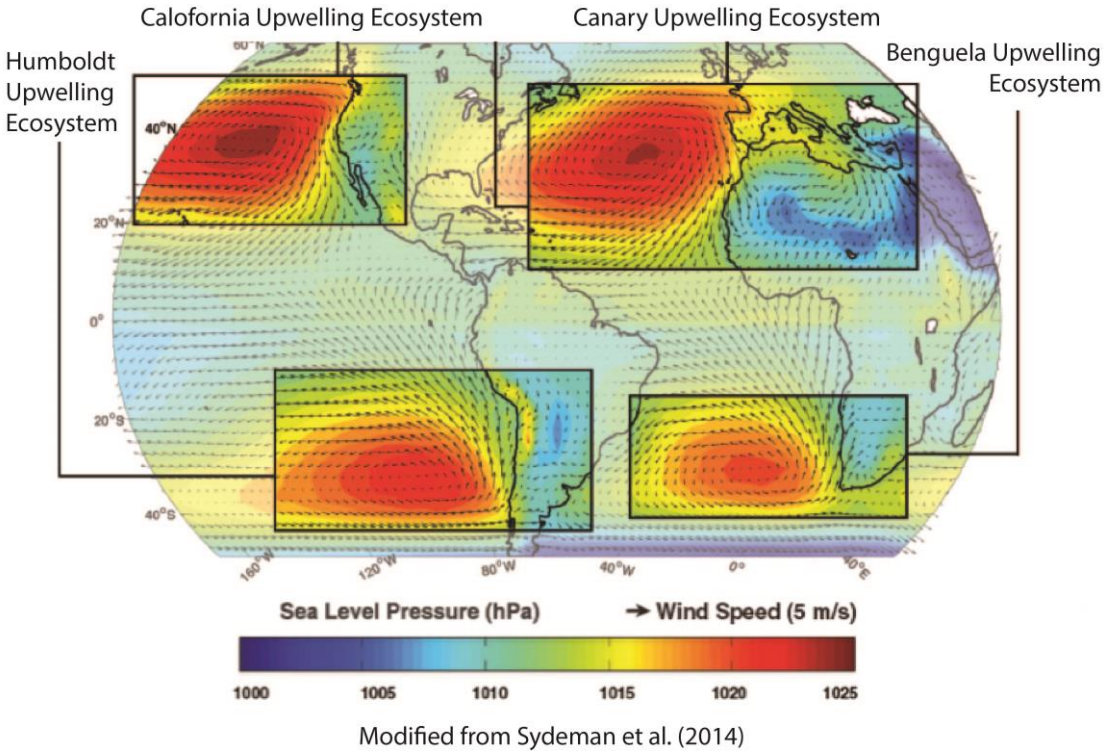

Figure 6.1. Adapted from Sydeman *et al.* (2014). The four major global coastal upwelling regions. SLP and wind data are taken from the NCEP/NCAR reanalysis (Kalnay *et al.*, 1996) and represent the warm season climatology - austral summer in the Southern Hemisphere and boreal summer in the Northern Hemisphere (Sydeman *et al.*, 2014).

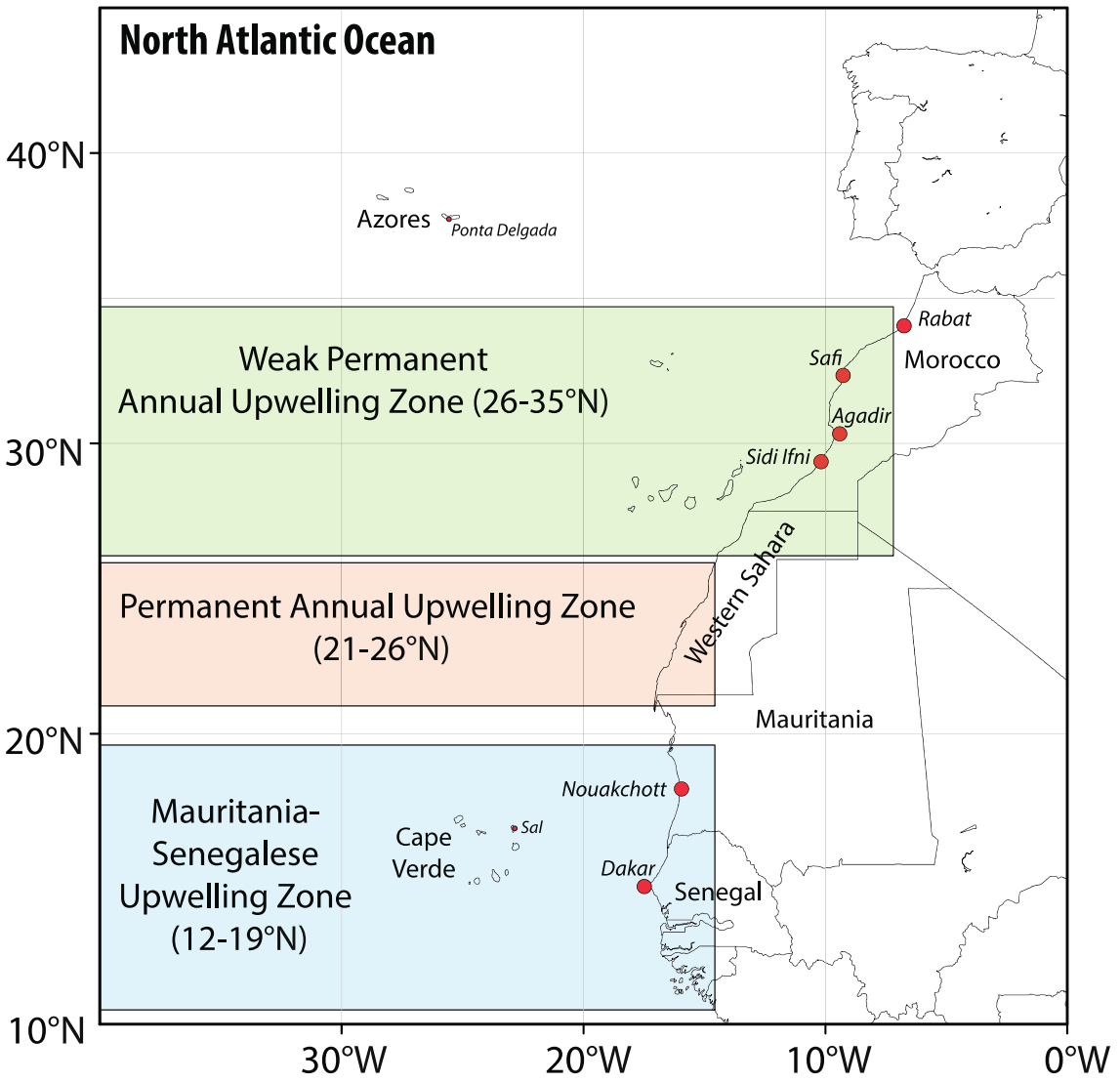

Figure 6.2. The northwest African upwelling region with the three upwelling zones (as described in Section 6.3.3.1) depicted. Also shown are the locations of Ponta Delgada, Azores and Sal, Cape Verde, which serve as the two nodes of the TWI and the location of six coastal meteorological-stations that were used for wind-speed analysis (Section 6.3.3.3).

6.2 The Upwelling Intensification Hypothesis across northwest Africa

The following Sections (6.2-6.3) were taken from CHB14. Phrase and tense were altered to fit in with the tone of the thesis, the scientific information and content is the same as the published article.

A considerable amount of literature has emerged since the original upwelling intensification hypothesis (Bakun, 1990; Diffenbaugh *et al.*, 2004; Bakun *et al.*, 2010), showing data and analysis for and against the upwelling intensification mechanism across the four main coastal upwelling regions and around the northwest African coastline and CUE in particular: these contrasting findings are examined below.

Maritime wind-speed observations suffer from the unfortunate bias (usually towards stronger winds) of artificially increasing trends due to temporal inconsistencies in recording and archiving methods (Ramage, 1987; Cardone *et al.*, 1990; Tokinaga and Xie, 2011a). To remove this problem, Bakun (1992) separately analysed wind-speed trends (during spring-summer) around the periphery of the North Atlantic Gyre in locations adjacent to, and away from, the areas where continental thermal lows develop. He concluded that the consistent positive trends in wind-speed found near the continental thermal low areas and decreasing trends away from these areas were indicative of the upwelling intensification mechanism (but also realised the difficulty in separating the 'real' wind-speed trend from the artificial one, as both were long-term trends). Subsequently, several authors sought to analyse the spatial and temporal variations in upwelling via computer model approaches, SSTs and wind-stress from satellite data, gridded datasets and palaeo-sedimentary studies.

Hsieh and Boer (1992) ran the first model experiments (300-400 km grid resolution) under the explicit guise of determining future climate change impacts on coastal upwelling regions. A doubling of atmospheric CO_2 in their study led to a decrease in coastal upwelling, primarily due to a relaxation of the Trade Winds because of a reduced equator-pole temperature gradient as a result of global warming. Mote and Mantua (2002) found little change in the magnitude and seasonality of upwelling across the four main EBUEs when comparing the 2080-2089 HadCM3 (300 km resolution) output to 1990-1999 observational wind-stress. Conversely, it would appear that when a significantly higher spatial resolution is applied, model predictions of upwelling conform to the upwelling intensification hypothesis. Snyder *et al.* (2003) used a regional climate model at 40 km resolution and identified an increase in upwelling under double CO_2 scenarios across the California Current. Examining a combination of global (fifteen models at ~2° resolution)

and regional climate models (25 km resolution) under the IPCC A2 and B2 scenarios, Falvey and Garreaud (2009) discovered an intensification of upwelling (roughly a 15% increase for 2071-2100 relative to 1961-1990) across the Humboldt Current region, because of a 2-3 hPa increase in the Southern Hemisphere mid-latitude high-pressure systems. Additionally, across the same time period under scenario A2, Miranda *et al.* (2012) used the Regional Ocean Modelling System (1/12° resolution) to identify an increase in upwelling frequency and magnitude across the western Iberian Shelf, locally reducing the effect of global warming under this scenario. Thus, the current state of the literature suggests a strong scale-dependence in the modelling approach to quantifying upwelling that yields very contrasting results.

Published results regarding trend directions in upwelling across the northwest African coastline show conflicting results. Using Advanced Very High Resolution Radiometer (AVHRR) SST data from 1982-2001, Santos *et al.* (2005) identified a decadal shift in upwelling regime intensity off northwest Africa (22-30°N) around 1995-1996 lasting until 1999. During this short period, coastal SSTs decreased by roughly 0.7°C and the meridional wind-speed anomaly from the NCEP/NCAR reanalysis (Kalnay *et al.*, 1996) across the same time period was enhanced by -0.7 ms^{-1} (a more negative value implies stronger equatorward meridional winds in the Northern Hemisphere). This relatively short 'shift' in conditions may represent the beginning of a regime change towards upwelling intensification, but could also have been due to natural inter-annual variability. Subsequently, a palaeo-sedimentary approach using two gravity cores from the Moroccan coastline (30.5°N, (McGregor *et al.*, 2007)), found negative trends in alkenone-derived SST (-1°C overall change). This suggested that Twentieth Century upwelling underwent a 'rapid' increase, consistent with meridional wind-speed increases (-1 ms^{-1} during 1950-1992) in the ICOADS dataset (Woodruff *et al.*, 2011) and positive trends in the Bakun (80 $m^3s^{-1}100m^{-1}$ across 1946-1981) and Pacific Fisheries Environment Laboratory (PFEL, 40 $m^3s^{-1}100m^{-1}$ across 1967-early 2000s) wind-stress-derived upwelling indices (Schwing *et al.*, 1996). Although the authors present a pertinent case for the upwelling intensification mechanism, there is the aforementioned caveat of the wind-speed sampling (Bakun *et al.*, 2010; Tokinaga and Xie, 2011b) present in the ICOADS dataset and the potential for significant errors in the alkenone record (Herbert, 2001). Marcello *et al.* (2011) extended the SST analysis with AVHRR data up to 2006 (from 1987, across 13-32.5°N) and identified warming trends across the northwest African coastline ranging from 1.0-3.3°C for the 20-year period. However, relative to the warming rates across the open ocean along the same latitude, the values were much lower (greater) across 20-32.5°N (13-19°N): thus the authors surmised a relative increase (decrease) in coastal upwelling. A corresponding analysis (by the same authors) of scatterometer wind-stress data (1992-2006) identified an increasing equatorward wind-stress at Cape Ghir (30.4°N) and Cape Juby (27.5°N), again hinting at an increase in upwelling favourable conditions.

Narayan *et al.* (2010) highlighted a significant increase in the ICOADS and ERA-40 reanalysis (Uppala *et al.*, 2005) meridional wind-stress across 28.5-33.5°N from 1960-2001 and 1958-2002 respectively in addition to a temperature reduction in their HadISST upwelling index (Rayner *et al.*, 2003) from 1870-2001. However, the same authors identified a positive temperature trend in the latter part of the HadISST record (1960-2001) and a reduction in meridional wind-stress from the NCEP/NCAR reanalysis (1960-2001) indicating a reduction in coastal upwelling. The study also considered basin-scale oscillations such as the NAO and AMO but relationships with upwelling were ambiguous. Pardo *et al.* (2011) studied the CUE in detail using the NCEP/NCAR reanalysis and found a decrease in upwelling intensity from 1970-2009 in both wind-stress and SST upwelling indices as well as discovering significant correlations with the NAO and the AMO (an r^2 value of approximately 0.3, dependent on latitude). Additionally, using the PFEL index, Gómez-Gesteria *et al.* (2008) discovered a decreasing trend in upwelling strength (a 45% (20%) decrease for April-September (October-March)) across 20-32°N from 1967-2006. Finally, Santos *et al.* (2012), using AVHRR data, (1982-2010) demonstrated the prominence of coastal upwelling across 22-33°N by showing the regular lower magnitude of coastal, compared to open ocean, warming (except across 28-31°N). However, they acknowledged a lack of significant positive trend in summer (MJJAS) upwelling (using the NCEP/NCAR dataset) and found a significant correlation at a 1-year lag with the extended winter EA pattern.

The SST and wind-stress derived methods of quantifying upwelling, mentioned above, are not without their caveats. SST derived estimates (hereafter, $UI^{\Delta SST}$) are typically the difference between SST at the coast and SST in the open ocean (usually a distance of 5° latitude). The main disadvantage of using this method is that changes in SST gradient between both the coast and the open ocean cannot be directly attributed to coastal upwelling. External factors such as freshwater input from local river discharge, macroscopic air-sea interactions, synoptic-scale weather systems and the variable oceanic mixed-layer depth can all influence SSTs. For example, a reduction in surface mixing across the open ocean could result in a shallower mixed layer that is readily susceptible to solar warming (Narayan *et al.*, 2010). The increased ocean temperature in this scenario would impact the SST gradient and indicate an upwelling increase in $UI^{\Delta SST}$. Nevertheless, $UI^{\Delta SST}$ has widespread application and has been shown to correspond spatially and temporally well with wind-stress-derived estimates, although usually with a time lag of 0-3 months (Nykjaer and Van Camp, 1994; Santos *et al.*, 2012).

Wind-stress derived upwelling (hereafter, UI^{W}), as found in numerous upwelling studies (Gómez-Gesteria *et al.*, 2006, 2008; Santos *et al.*, 2012), represents the (estimated) potential effects of wind-stress on the ocean surface. At the coastal grid-box scale, the UI^{W} effectively integrates the coastal boundary-associated Ekman divergence and the

Ekman divergence due to cyclonic wind-stress curl (Bakun and Nelson, 1991; Bakun and Agostini, 2001). Cyclonic wind-stress curl commonly occurs at the periphery of the major subtropical high-pressures close to land, where the typically stronger open ocean wind-speeds and weaker continental/coastal wind-speeds merge. A strong wind shear is generated between these winds, which leads to cyclonic wind-stress curl, divergence of surface waters and upwelling of subsurface waters. A graphical example is presented in the appendices (Figure F1) which indicates the differences in the location of upwelling due to the two different mechanisms. Some studies, given sufficiently high spatial resolution datasets, have separated Ekman divergence components into the wind-stress-derived 'Ekman transport' and the wind-stress curl derived 'Ekman pumping' (Picket and Paduan, 2003; Castelao and Barth, 2006). However, given the variable scales of grid-box size from the numerous datasets that were used in this thesis, the UI^{W} alone is sufficient for the spatial-temporal trend analysis goals of this thesis. Finally, the UI^{W} is parameterised and makes certain assumptions, but still, based on current understanding, represents a good approximation of Ekman transport (Schwing *et al.*, 1996).

Previous studies have naturally combined the various methods of quantifying upwelling in an attempt to elucidate spatial and temporal changes. However, there is still a degree of conflicting evidence regarding current changes across the CUE that mainly correspond to: (1) the way in which SST or wind data were obtained, via either in situ observations, satellites or reanalysis; (2) the exact spatial regions and temporal periods (intra- and inter-annual) considered; and (3) how upwelling estimates were analysed on an intra-annual basis, given that the intensification mechanism is not expected to operate all year round.

Bakun *et al.* (2010) recognised the need for further useful supporting time series in quantifying upwelling trends and demonstrated the use of atmospheric water vapour as a beneficial proxy variable in relation to upwelling trends off the coast of Peru. Their two water vapour time series (precipitable water and total column water vapour from the NCEP/NCAR and ERA-40 reanalysis respectively) correlated significantly with their upwelling estimates (typical r values in the range of 0.3-0.5 ($p < 0.05$) across most seasons). Their theory was that as the most important greenhouse gas, water vapour enhances the local radiative heating cycle and serves to augment the upwelling intensification mechanism even if the mesoscale winds slacken. Across the Humboldt region, the main driver of inter-annual climate variability, ENSO, is traditionally associated (during the El Niño phase) with a reduction of coastal wind-speeds (Huyer *et al.*, 1987), but also, with increases in atmospheric water vapour. As such, coastal wind-speeds could increase even if the synoptic conditions favour a decrease. This highlights a potential scale-dependence on coastal upwelling wind-speeds between large-scale and local

processes, which could both significantly change under global warming (Miranda *et al.*, 2012).

6.3 Upwelling: Increase, Decrease or No Change?

6.3.1 Research Approach

Following the same logic as Bakun *et al.* (2010), upwelling signals should also be detectable in previously lesser-considered, yet widely available, atmosphere and ocean datasets. Here, in addition to comparing a wide range of datasets using the $UI^{\Delta SST}$ and UI^{W} methods (Section 2.9), wind-speed from coastal land-based meteorological-stations were analysed, sea surface height variability from satellite altimetry and ocean reanalysis were considered (SSH), and vertical water column velocity was examined (VWCV). The influences of large scale atmosphere/ocean teleconnections were also considered.

The overriding aim was to test if the upwelling intensification hypothesis was evident in current records across the CUE. Additionally, the purpose of this chapter was to:

1. Examine the variability between various UI^{W} indices to determine if there were any significant differences between the datasets;

2. Determine if lesser-used indicators of upwelling agreed with these indices, to further elucidate any temporal and spatial trends;

3. Place an emphasis on seasonal trends (the intensification hypothesis should mainly apply during boreal summer (JJA)) and the importance of basin-scale oscillations on interannual variability.

6.3.2 Data & Methods

The CUE is defined here as 11-35°N (Figure 6.1, 6.2). Table F1 lists all the data and sources used in this chapter. All time series were created as, or aggregated to, monthly temporal-resolution, then converted to seasonal resolution for analysis. Spatial resolutions were dependent on the original datasets, and only the common temporal period of 1981-2012 is considered.

To adequately cover the range of previously used UI^{W} indices by other authors and compare different observational and reanalysis sources across the selected time period,

seven different sources were used to calculate the UI^{W}. These were: (1) the National Centre for Environmental Prediction reanalysis v2 (NCEP-DOE, Kanamitsu *et al.*, 2002); (2) the ERA-I reanalysis (Dee *et al.*, 2011); (3) the PFEL upwelling index (http://las.pfeg.noaa.gov); (4) the 20CR project (Compo *et al.*, 2011); (5) the ICOADS archive (Woodruff *et al.*, 2011); (6) the Modern-Era Retrospective Analysis For Research and Applications reanalysis (MERRA, (Rienecker *et al.*, 2011)); and (7) the Climate Forecast System reanalysis (CFSR, (Saha *et al.*, 2010)). Wave and Anemometer based Sea-Surface Wind (WASWind, (Tokinaga and Xie, 2011b)) and scatterometer-derived winds (SeaWinds, (Lungu *et al.*, 2006) were used later in the analysis and presented as supporting indices. Monthly zonal and meridional wind-speeds were extracted from all sources at 10 m height.

The UI^{W} was calculated using the equations 2.9.1-2.9.3. Using this index, positive (negative) values correspond to upwelling (downwelling) favourable conditions. Whilst highly irregular on smaller scales, the northwest African coastline angle can macroscopically be classed as 55° from 21-36°N, 90° from 12-21°N and 120° from 10-12°N relative to the equator. The data points for the UI^{W} transects along the northwest African coastline were selected as the closest full ocean grid-box to the coast (so as not to influence the drag coefficient). Due to the reduced Coriolis effect closer to the equator, upwelling estimates for the lower latitudes (below ~20°N) were probably biased slightly high.

Three different datasets were used to calculate the $UI^{\Delta SST}$: (1) the Hadley Centre Sea Ice and Sea Surface Temperature dataset (HadISST1, (Rayner *et al.*, 2003)); (2) the ICOADS SST; and (3) the Reynolds SST v2 dataset (OISST, (Reynolds *et al.*, 2007)). The $UI^{\Delta SST}$ at each latitudinal point was defined as the difference in SST between the coast and the ocean as in Section 2.9. An increase (decrease) in the $UI^{\Delta SST}$ is equivalent to a decrease (increase) in upwelling intensity (opposite the UI^{W}).

To supplement the traditional UI methodologies, further supporting data were used. Firstly, wind-speed data from six meteorological-stations situated along the northwest African coastline (Table 6.1, Figure 6.2) were taken from the GSOD network. The TWI from Section 3.4 was also used. An advantage of the TWI is that the index does not suffer from the sampling bias that affects maritime wind-speed observations. All of the wind-speed stations were tested for homogeneity (Section 2.5) using the Pettitt (Pettitt, 1979), Buishand and SNHT methods (Buishand, 1982; Alexanderson, 1986). Station metadata were not available, however identification of breaks was relatively straightforward when the test results corresponded to, or near-to, gaps in the time series that were accompanied by clear shifts in the mean (for times of adjustments, see Table 6.1).

Under upwelling conditions, along-shore winds transport water offshore. As such, the SSH near the coast should experience a detectable reduction (the greater density of upwelled water from depth should further augment the SSH reduction). There were no continuous long-term tide-gauge data along the northwest African coastline, from either the Permanent Mean Service for Sea Level (http://www.psmsl.org) or the Joint Archive for Sea Level (http://ilikai.soest.hawaii.edu/UHSLC/jasl.html). Therefore, the mean sea level anomaly obtained via satellite altimetry from the TOPEX/Poseidon, Jason-1, ERS and Envisat missions, was analysed. Three realisations of this data were used: (1) the Church and White (2011) dataset (with the inverse barometer and glacial isostatic correction applied); (2) the delayed time Ssalto/Duacs product directly from the Archiving, Validation and Interpretation of Satellite Oceanographic Data (AVISO) homepage (similar corrections applied); and (3) the Aviso/Niiler Climatology dataset (Table F1). Additionally, several ocean reanalysis datasets (which assimilate the altimetry data) were analysed: (1) the Global Ocean Data Assimilation System (GODAS, (Behringer and Xue, 2004)); (2) the Simple Ocean Data Analysis v2.1.6 (SODA, (Carton and Giese, 2008)); and (3) the Operational Ocean System reanalysis 4 (ORSA4, (Balmaseda *et al.* 2013)). The reason for this latter analysis was that, as the altimetry signal close to the coast deteriorates within approximately 40 km of the coastline (e.g. Saraceno *et al.* 2008), the SSH values in the closest coastal grid-box may not necessarily be an entirely accurate representation of the coastal SSH. Therefore, the effect on SSH due to upwelling (or other influences) may be lost. The fine resolution of the SODA, GODAS and AVISO datasets, may, however, allow coastal SSH changes to be captured.

Geometric vertical velocity was taken from the GODAS dataset at 50 m depth. This variable is used as a direct upwelling estimate across the northwest American coastline by the CPC (http://www.cpc.ncep.noaa.gov/products/GODAS/-coastal_upwelling.shtml) and measures the Ekman pumping/suction 'component' of the upwelling process, effectively integrating both the coastal-boundary wind-stress and open ocean wind-stress curl Ekman divergence effects.

Meteorological Wind-speed Stations

Station	Country	Temporal Extent	Latitude (N)	Longitude (W)	Distance from coast (km)	Homogeneity Adjustments
Rabat	Morocco	1973-2013	34.05	06.75	4	October 1986, November 1992
Safi	Morocco	1973-2013	32.34	09.27	1	June 1989, October 2004
Agadir	Morocco	1992-2013	30.33	09.41	20	
Sidi Ifni	Morocco	1973-2013	29.37	10.18	1	April 1992, October 2000
Nouakchott	Mauritania	1973-2013	18.10	15.95	5	July 1989
Dakar	Senegal	1973-2013	14.74	17.49	2	December 1987, May, June 1992

Table 6.1. Coastal meteorological-station data used in Chapter 6.

The following climate indices were used in this chapter (Table 6.2):

1. Two versions of the NAO; the station-based index from CH14 and the first PC of the leading EOF of SLP throughout all months across 25°-75°N, 90°W-30°E (using data from the NCEP-NCAR reanalysis). The latter is more suited to capturing the variability of the oscillation across the summer months, whereas the former is a better general indicator of changes in the Azores High
2. The EA pattern (Barnston and Livezey, 1987), a 'southward-shifted' NAO pattern representing the second mode of low-frequency SLP variability across the North Atlantic.
3. The AMO, defined here as the area-averaged, detrended, North Atlantic (25°N-60°N, 7°W-75°W) SST anomalies minus the regression of the SST on the global mean temperature after the methodology of van Oldenborgh *et al.* (2009) (using data from the Second Hadley Centre Sea Surface Temperature dataset (Rayner *et al.*, 2006));
4. The Multivariate Niño Index (Wolter and Timlin, 2011);
5. The TWI as discussed in Section 3.4 (Cropper and Hanna, 2014).

Lagged correlations - intra-annually (at a monthly and seasonal resolution) up to one year and inter-annually (yearly resolution of seasonal values) up to 10 years - were considered as well as standard correlation analysis between the climate oscillations and the various measures of upwelling.

Seasonal averages of the various upwelling indices were used from 1981-2012. The focus was primarily on summer (JJA), as this is the season where an oceanic-continental pressure gradient should be strongest. There is no realistic physical mechanism by which upwelling values from one season could influence the same season the year after, however some of the upwelling time series display traits of statistical dependence, i.e. autocorrelation, which spuriously affects significance estimates of the trendline (Santer *et al.*, 2000). As such, for determining trend rates, OLS and modified significance testing were used (Section 2.2.2). Almost identical trend magnitudes and significances were found with the TS slope and MK trend tests. It was found that the $UI^{\Delta SST}$ time series display traits of autocorrelation more frequently than the other upwelling (proxy) indices. This is most likely due to the persistence of seasonal anomalies for wind and SSTs. SSTs are more likely to display characteristics of slowly evolving time series due to the large thermal capacity of sea water, whereas wind speed can change direction and strength in seconds, so seasonal anomaly values may display more rapid year-to-year transitions, and therefore, no traits of autocorrelation.

Climate Variability Indices

Index	Description	Reference	Source
NAOI – North Atlantic Oscillation Index	1. Station based pressure difference between Iceland and Azores 2. EOF of North Atlantic (25°-75°N, 90°W-30°E) SLP, PC1 of the analysis constitutes the NAO index (NCEP/NCAR reanalysis data used)	1. (CH14) 2. (This Thesis)	
AMO – Atlantic Multidecadal Oscillation	Area-averaged SST across North Atlantic Ocean (25-60°N, 75-7°W) minus the regression of the SST on global mean temperature (using the Second Hadley Centre Sea Surface Temperature dataset)	(van Oldenborgh *et al.* 2009)	Climate Explorer (http://climexp.knmi.nl/)
EA – East Atlantic Pattern	Second leading mode of large-scale variability across the North Atlantic after the NAOI	(Barnston and Livezy, 1987)	(http://www.cpc.ncep.noaa.gov/data/teledoc/ea.shtml)
ENSO – Multivariate El Niño Southern Oscillation Index	Most complete characterisation of ENSO, based on SLP, U and V winds, SST, SAT and cloudiness	(Wolter and Timlin, 2011)	(http://www.esrl.noaa.gov/psd/enso/mei/)
TWI – Trade Wind Index	Station-based pressure difference between the Azores and Cape Verde - a proxy for northeast Atlantic Trade Winds	(CH14)	

Table 6.2. Climate Teleconnections/Oscillation indices used in this Chapter.

6.3.3 Results

6.3.3.1 Seasonal Upwelling Cycle

Figure 6.3 illustrates the mean annual cycle of upwelling for the seven UI^{W} and three $UI^{\Delta SST}$ indices. The general pattern is reflected well in all ten UI (note the reversed colour scheme for the $UI^{\Delta SST}$). The area of intense, permanent annual upwelling (21-26°N) is well captured by all ten indices. Upwelling appears to be a permanent annual phenomenon up to ~33°N – although a small zone around ~30°N near Cape Ghir (where the coastline inverts relative to its macroscopic orientation) appears to have much weaker upwelling compared to the surrounding latitudes. The seasonal pattern of upwelling differs slightly between the UI^{W} and the $UI^{\Delta SST}$, with the $UI^{\Delta SST}$ generally lagging the UI^{W} signal by 0-2 months, as previously found for this region by Nykjær and Van Camp (1994). South of 20°N, a downwelling regime is present between March and October (UI^{W}) or May and November ($UI^{\Delta SST}$). Based on the obvious latitudinal divides, and reinforced by covariance analysis between the upwelling grid-boxes (not shown), the CUE upwelling is characterised into three meridionally averaged zones (weighted by latitude, and shown on Figure 6.2):

1. 12-19°N – Mauritania-Senegalese upwelling zone. Upwelling occurs during the winter months and fades during the summer months, related to the seasonal migration of the Trade Winds;
2. 21-26°N – Strong permanent annual upwelling zone;
3. 26-35°N – Weak permanent annual upwelling zone. Upwelling is typically a year-round occurrence, but its magnitude is weaker than in the permanent upwelling zone. Stronger upwelling is present in summer, associated with the trade-wind migration.

Figure 6.4 illustrates the mean annual cycle and monthly SD of each of these three zones for each UI, allowing a more direct comparison between the UI magnitudes. Across the strong permanent upwelling zone (21-26°N), the annual range is much lower than that of the lower latitudes (12-19°N); however, monthly variability (signified by the 1σ bars) is generally higher. Across the weak permanent upwelling zone (26-35°N), upwelling averages around 50 $m^3s^{-1}100m^{-1}$ under the UI^{W} or -1°C under the $UI^{\Delta SST}$ with a modest seasonal cycle that peaks in summer. A similar pattern is evident across the strong permanent upwelling zone (21-26°N), with winter values ranging between 75-130 $m^3s^{-1}100m^{-1}$ and summer values between 130-200 $m^3s^{-1}100m^{-1}$. Across the Mauritania-Senegalese upwelling zone (12-19°N) downwelling during the summer months typically averages around -50 $m^3s^{-1}100m^{-1}$ or 1°C respectively and the winter upwelling varies in

strength (~200 and ~150 $m^3s^{-1}100m^{-1}$ for the PFEL and NCEP-DOE data respectively, compared to an average of around 50-75 $m^3s^{-1}100m^{-1}$ for the other five UI^W).

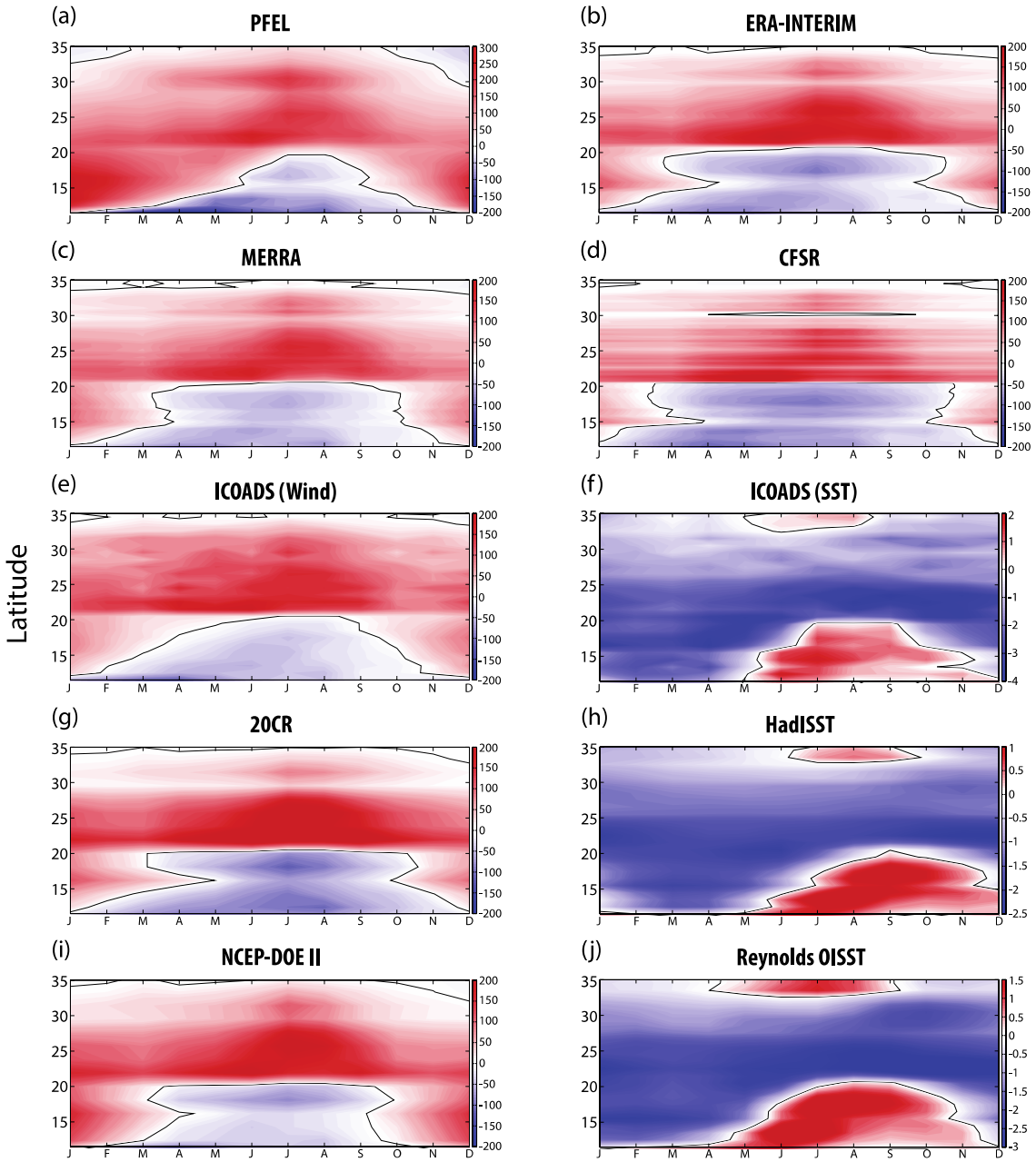

Figure 6.3. The 1981–2012 climatology of (a-e, g, i) the seven UI^W (units: $m^3s^{-1}100m^{-1}$) and (f, h, j) the three $UI^{\Delta SST}$ (units: °C) indices. Black contours indicate the divide between upwelling and downwelling favourable conditions. For the UI^W, red (blue) corresponds to upwelling (downwelling) conditions and the opposite applies for the $UI^{\Delta SST}$.

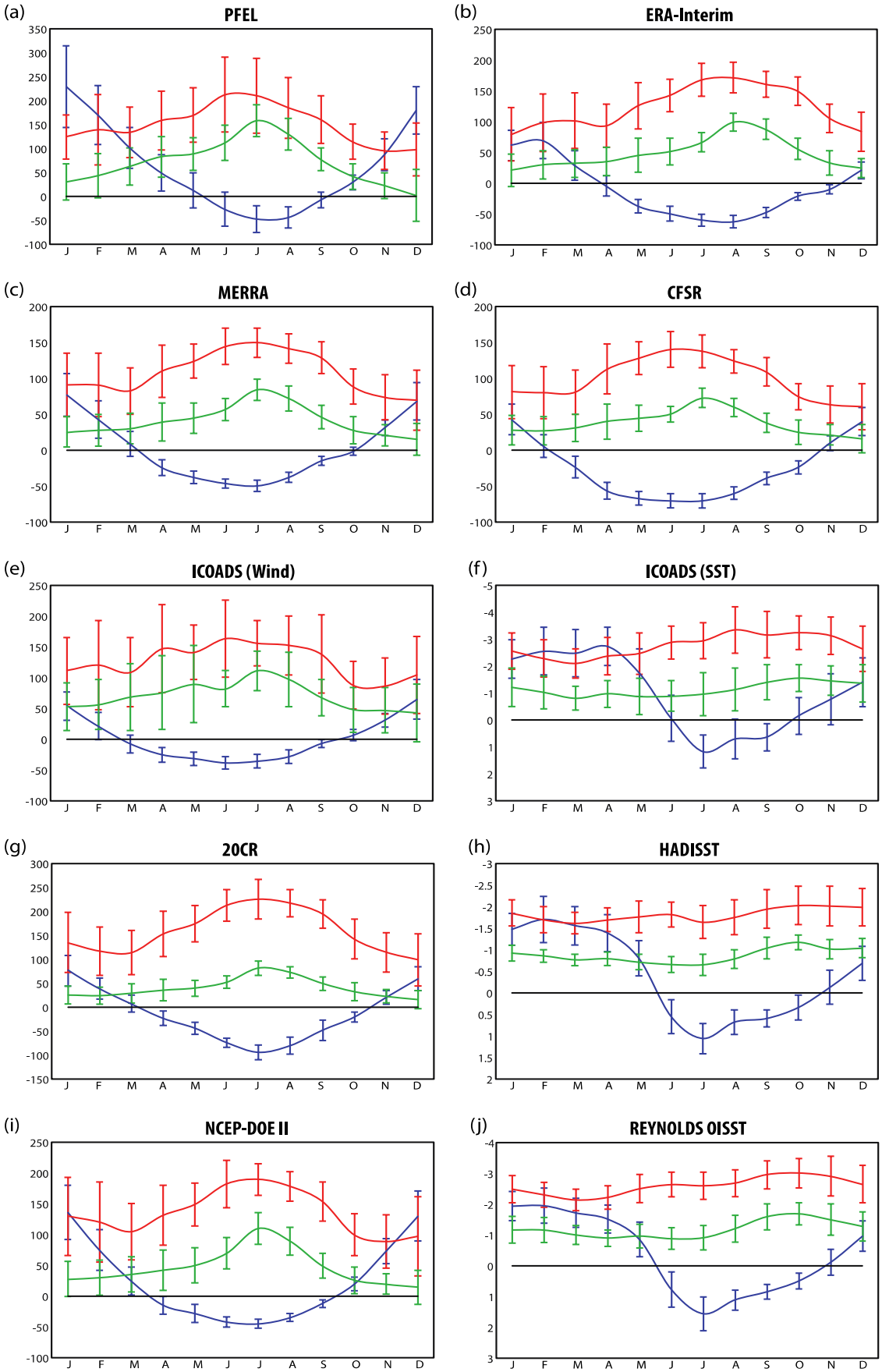

Figure 6.4. The monthly climatology (1981–2010) for the Mauritania–Senegalese upwelling zone (12–19°N, blue line), permanent upwelling zone (21–26°N, red line) and the weak permanent upwelling zone (26–35°N, green line) for the seven UI^{W} (units: units: $m^3s^{-1}100m^{-1}$) and three $UI^{\Delta SST}$ (units: °C) indices. Error bars on the individual months highlight the (1σ) monthly variability.

The three $UI^{\Delta SST}$ indices were strongly correlated with each other across their latitudinal zones with typical r-values of 0.8-1.0, with a similar trait shared by the six UI^{W} indices (r = 0.7-1.0, the correlations were applied to detrended, annual data). However, correlations between the $UI^{\Delta SST}$ and UI^{W} indices were generally ambiguous, unless, as in Nykjær and Van Camp (1994) time lags were applied (which latitudinally vary and were strongest when UI^{W} leads by between 0 and 2 months).

6.3.3.2 Interannual Upwelling Evolution

Figure 6.5 displays the evolution of summer upwelling from 1981-2012 for all ten UI spread across the three spatially defined upwelling zones. A prominent feature of the two higher-latitude zones (21-35°N) is a progressive increase during the 1990s, followed by a short-lived negative trend which lasts from 2000 until around 2004/5 which is followed in turn by a strong positive increase across most indices (the reanalysis-derived UI^{W} stay constant whereas the observationally derived UI^{W} (PFEL and ICOADS) rise across 21-26°N). Additionally, the PFEL and ICOADS UI^{W} experience a decrease in upwelling across the Mauritania-Senegalese Zone whereas the reanalysis UI appear to exhibit little change. Table 6.3 illustrates the seasonal trends in upwelling for the main seven UI^{W} (and WASWind) and three $UI^{\Delta SST}$ from 1981-2012 for the three specific latitudinal zones (a few indices don't fully extend to 2012, Table F1). Focusing again on summer trends first - a general tendency towards a decrease in upwelling is found across the Mauritania-Senegalese (12-19°N) upwelling zone, indicated by statistically significant reductions in the PFEL, ICOADS and CFSR UI^{W} indices and a significant increase in the OISST $UI^{\Delta SST}$. Confidence intervals for the other indices exceed the trend values and were not significant except the NCEP-DOE UI^{W}, which suggests a small positive upwelling increase (Table 6.3). Across the permanent upwelling zone (21-26°N), significant increases in upwelling are identified in the PFEL, ICOADS UI^{W}, NCEP-DOE, OISST and HadISST indices. Across the weak permanent upwelling zone (26-35°N), there was a positive tendency towards enhanced upwelling in every UI (except ICOADS $UI^{\Delta SST}$), although these trends were only significant for the ICOADS UI^{W}, NCEP-DOE and OISST indices.

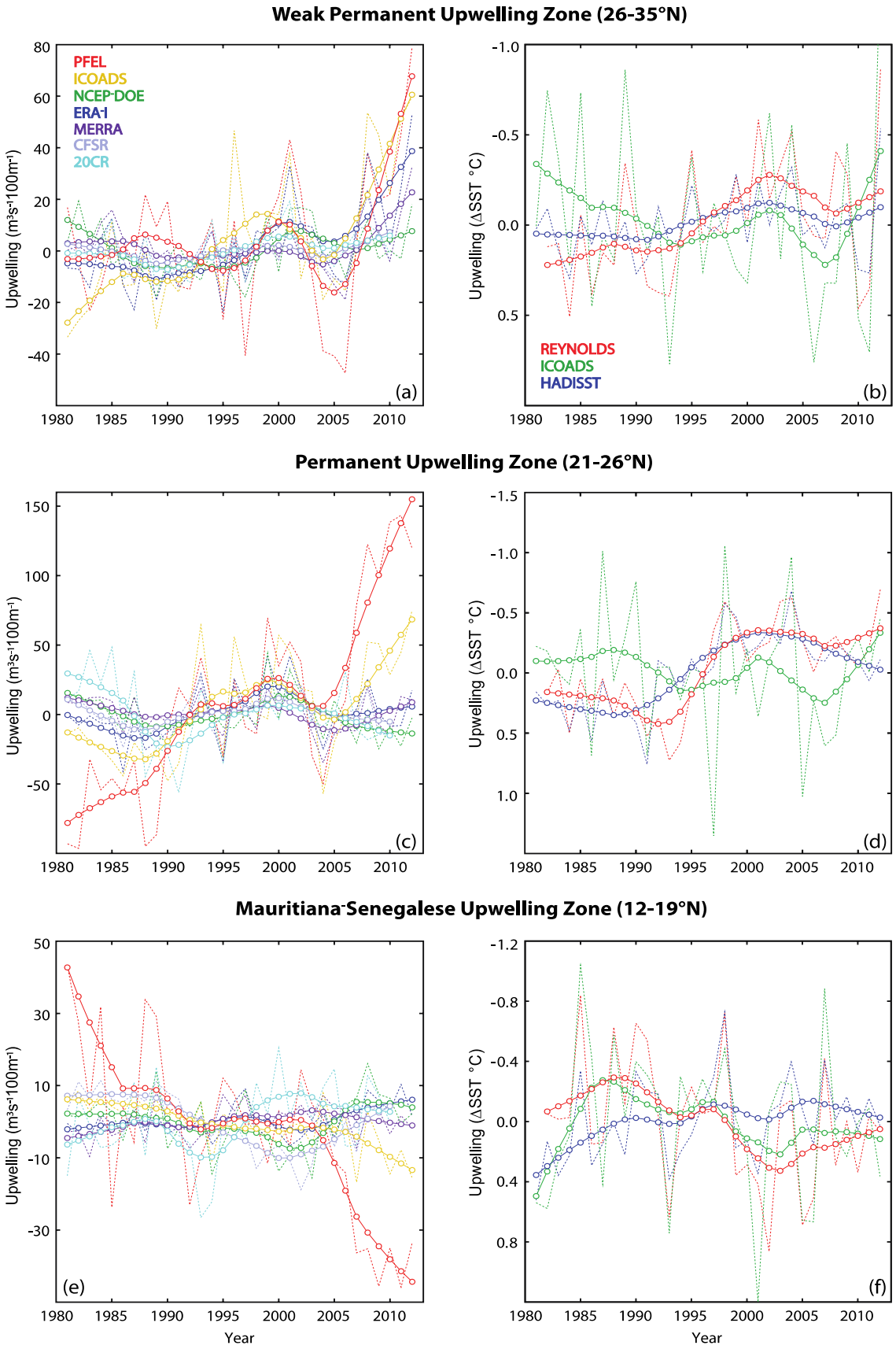

Figure 6.5. Temporal evolution of the (a, c, and e) seven UI^{W} and (b, d, and f) three $UI^{\Delta SST}$ for summer (JJA) from 1981 to 2012 (anomalies relative to the 1981–2010 base period). Thin dotted lines indicate yearly values and circled bold lines are the 9-year LOESS trend for each individual UI.

The general tendency across summer appears to be one of an increase in upwelling-favourable winds north of 21°N and increase in downwelling-favourable winds south of 20°N. The $UI^{\Delta SST}$ trends show support for this observation (Figure 6.5), although the strong interannual variability of SST affects the signal. When the widespread spatial patterns in meridional wind-speed and SST trends were considered (Figure 6.6b-h), further support was found for the latitudinal divide. Typically, increased negative trends in meridional wind-speed (that vary in their spatial significance dependent on the dataset) can be identified across the northwest African coastline from around 35°N down to ~20-25°N and positive trends from around the equator (but always west of the Gulf of Guinea) to 20°N. Additionally, isolated sections of negative SST trends adjacent to western Sahara and southern Morocco (21-30°N, Figure 6.6g-h) were surrounded by statistically significant open ocean warming regions.

Variable	Indices	Units	Season											
			DJF			MAM			JJA			SON		
			12–19°N	*21–26°N*	*21–26°N*	*12–19°N*	*21–26°N*	*26–35°N*	*12–19°N*	*21–26°N*	*26–35°N*	*12–19°N*	*21–26°N*	*26–35°N*
UI^{W}	ICOADS	$m^3\ s^{-1}\ 100\ m^{-1}\ dec^{-1}$	5.5 ± 6.6	***24.8*** $\pm$ ***14.9***[a]	9.9 ± 10.7	-0.6 ± 2.9	***25.0*** $\pm$ ***11.6***[a]	14.1 ± 13.4[a]	***−5.0*** $\pm$ ***2.9***[a]	***22.4*** $\pm$ ***11.5***[a]	***17.9*** $\pm$ ***7.5***[a]	1.8 ± 1.9	***27.4*** $\pm$ ***11.6***[a]	7.7 ± 7.1[a]
UI^{W}	PFEL	$m^3\ s^{-1}\ 100\ m^{-1}\ dec^{-1}$	**−18.9** $\pm$ **16.8**[a]	14.1 ± 15.1	-3.0 ± 11.1	***−18.0*** $\pm$ ***7.7***[a]	***33.2*** $\pm$ ***12.7***[a]	2.2 ± 7.9	***−19.8*** $\pm$ ***6.7***[a]	***59.1*** $\pm$ ***27.5***[a]	7.9 ± 16.4	**−6.0** $\pm$ **5.6**[a]	***26.8*** $\pm$ ***9.7***[a]	-2.7 ± 6.2
UI^{W}	NCEP-DOE II	$m^3\ s^{-1}\ 100\ m^{-1}\ dec^{-1}$	-0.9 ± 10.0	2.8 ± 15.0	-2.7 ± 6.8	-0.4 ± 4.4	3.2 ± 9.5	2.7 ± 5.8	**1.8** $\pm$ **1.5**[a]	*6.3* $\pm$ *7.1*[a]	***11.0*** $\pm$ ***5.4***[a]	-0.3 ± 3.5	7.2 ± 9.7	-0.1 ± 4.2
UI^{W}	ERA-I	$m^3\ s^{-1}\ 100\ m^{-1}\ dec^{-1}$	-1.6 ± 5.5	-0.6 ± 9.2	0.8 ± 5.0	2.1 ± 4.3	-2.3 ± 8.4	0.2 ± 4.5	0.3 ± 2.9	-3.5 ± 5.8	1.4 ± 3.9	1.4 ± 1.9	-1.8 ± 5.2	-2.8 ± 3.8
UI^{W}	MERRA	$m^3\ s^{-1}\ 100\ m^{-1}\ dec^{-1}$	-6.1 ± 7.0	-4.7 ± 10.4	-1.5 ± 5.5	-0.1 ± 3.1	-2.4 ± 6.7	-0.3 ± 4.6	1.4 ± 1.7	-3.0 ± 5.1	1.9 ± 4.1	0.4 ± 2.0	2.7 ± 7.0	-0.8 ± 4.0
UI^{W}	CFSR	$m^3\ s^{-1}\ 100\ m^{-1}\ dec^{-1}$	-7.4 ± 4.6	-5.3 ± 8.7	-3.1 ± 5.4	***−6.2*** $\pm$ ***3.0***[a]	4.5 ± 6.8	1.8 ± 4.0	*−4.9* $\pm$ *4.6*[a]	0.8 ± 6.2	1.2 ± 3.2	-2.5 ± 4.5	4.7 ± 6.2	0.4 ± 3.7
UI^{W}	20CR	$m^3\ s^{-1}\ 100\ m^{-1}\ dec^{-1}$	-4.0 ± 7.2	**−14.7** $\pm$ **14.1**[a]	-3.3 ± 4.8	**−4.2** $\pm$ **3.8**[a]	1.7 ± 10.8	3.7 ± 4.3	3.9 ± 4.3	-5.7 ± 10.2	3.1 ± 3.5	***6.7*** $\pm$ ***3.7***[a]	-6.4 ± 9.8	-1.3 ± 4.0
UI^{W}	WASWind	$m^3\ s^{-1}\ 100\ m^{-1}\ dec^{-1}$	-1.2 ± 4.6	**−8.9** $\pm$ **7.9**[a]	-3.1 ± 6.2	2.4 ± 2.4	0.2 ± 5.3	1.2 ± 5.6	0.9 ± 2.4	-2.0 ± 4.9	2.5 ± 3.7	2.0 ± 1.8	1.0 ± 5.1	2.6 ± 4.4
$UI^{\Delta SST}$	OISST	$°C\ dec^{-1}$	**−0.15** $\pm$ **0.13**[a]	**−0.32** $\pm$ **0.23**[a]	***−0.25*** $\pm$ ***0.12***[a]	*0.14* $\pm$ *0.14*[a]	***−0.24*** $\pm$ ***0.15***[a]	***−0.13*** $\pm$ ***0.09***[a]	**0.16** $\pm$ **0.15**[a]	**−0.26** $\pm$ **0.20**[a]	**−0.15** $\pm$ **0.12**[a]	0.03 ± 0.09	***−0.37*** $\pm$ ***0.19***[a]	**−0.30** $\pm$ **0.18**[a]
$UI^{\Delta SST}$	HadISST	$°C\ dec^{-1}$	-0.06 ± 0.11	*−0.16* $\pm$ *0.15*[a]	-0.01 ± 0.06	**−0.15** $\pm$ **0.11**[a]	**−0.16** $\pm$ **0.12**[a]	0.01 ± 0.05	-0.10 ± 0.10	***−0.22*** $\pm$ ***0.10***[a]	-0.05 ± 0.07	***−0.16*** $\pm$ ***0.07***[a]	***−0.27*** $\pm$ ***0.12***[a]	**−0.08** $\pm$ **0.06**[a]
$UI^{\Delta SST}$	ICOADS	$°C\ dec^{-1}$	0.02 ± 0.24	-0.06 ± 0.26	0.02 ± 0.18	0.04 ± 0.20	-0.05 ± 0.19	*0.11* $\pm$ *0.11*[a]	0.04 ± 0.18	0.06 ± 0.21	0.06 ± 0.19	0.13 ± 0.19	0.08 ± 0.19	0.02 ± 0.11
SSH	AVISO (1)	$cm\ dec^{-1}$	3.1 ± 12.5	1.3 ± 15.4	-3.3 ± 12.7	-1.2 ± 8.6	-0.6 ± 9.9	-1.3 ± 11.6	-1.7 ± 14.5	3.8 ± 7.1	5.56 ± 7.69	1.7 ± 11.5	-1.0 ± 8.1	-0.3 ± 8.5
SSH	AVISO (2)	$cm\ dec^{-1}$	2.8 ± 8.2	5.2 ± 13.4	1.8 ± 13.1	0.4 ± 9.2	-0.2 ± 7.5	2.5 ± 9.8	5.6 ± 7.1	4.7 ± 8.6	5.9 ± 5.5	4.0 ± 7.5	5.9 ± 9	4.7 ± 6.3
SSH	AVISO (3)	$cm\ dec^{-1}$	6.6 ± 11.9	8.8 ± 18.4	6.9 ± 17.6	-0.6 ± 13.4	-0.8 ± 11.2	0.8 ± 14.3	5.6 ± 13.5	4.7 ± 12.4	5.5 ± 10.1	10.1 ± 11.6	8.0 ± 10.1	5.7 ± 9.9
SSH	ORSA4	$cm\ dec^{-1}$	-13.6 ± 22.6	-9.3 ± 15.3	-3.9 ± 18.8	***−21.1*** $\pm$ ***11.9***[a]	**−19.4** $\pm$ **9.4**[a]	*−13.4* $\pm$ *13.5*[a]	-1.7 ± 17.8	-1.1 ± 9.2	-4.9 ± 7.5	4.9 ± 11.6	4.1 ± 11.4	2.1 ± 10.2
SSH	GODAS	$cm\ dec^{-1}$	***10.6*** $\pm$ ***6.9***[a]	0.8 ± 5.9	0.6 ± 7.0	0.0 ± 5.8	-3.4 ± 4.9	0.1 ± 5.8	15.7 ± 19.3	-1.6 ± 6.2	-1.7 ± 7.7	***21.7*** $\pm$ ***7.7***[a]	3.7 ± 6.2	-0.3 ± 4.8
SSH	SODA	$cm\ dec^{-1}$	5.2 ± 11.5	2.5 ± 9.7	-1.6 ± 12.7	3.5 ± 11.9	-5.2 ± 9.3	-6.5 ± 10.0	0.8 ± 13.0	-1.3 ± 9.9	-4.5 ± 9.8	0.2 ± 9.7	-1.4 ± 8.6	-4.0 ± 9.8
VWCV	GODAS	$m\ mon^{-1}\ dec^{-1}$	***10.7*** $\pm$ ***5.8***[a]	-2.3 ± 5.8	-2.8 ± 6.5	***14.6*** $\pm$ ***5.5***[a]	***5.6*** $\pm$ ***3.5***[a]	1.8 ± 3.8	**−4.0** $\pm$ **3.6**[a]	3.5 ± 4.2	**4.5** $\pm$ **3.6**[a]	2.6 ± 3.9	-0.3 ± 5.0	2.2 ± 3.7

Table 6.3. Seasonal decadal trend rates during 1981-2012 (or the longest temporal period available, see Table F1) for multiple Upwelling Index estimates and 'proxy' variables (SSH – sea surface height and VWCV – 50 m depth vertical water column motion). * Indicates a statistically significant trend (Section 2.2), italicized text, bold and bold italics correspond to significance levels of $p < 0.1$, 0.05 and 0.01 respectively.

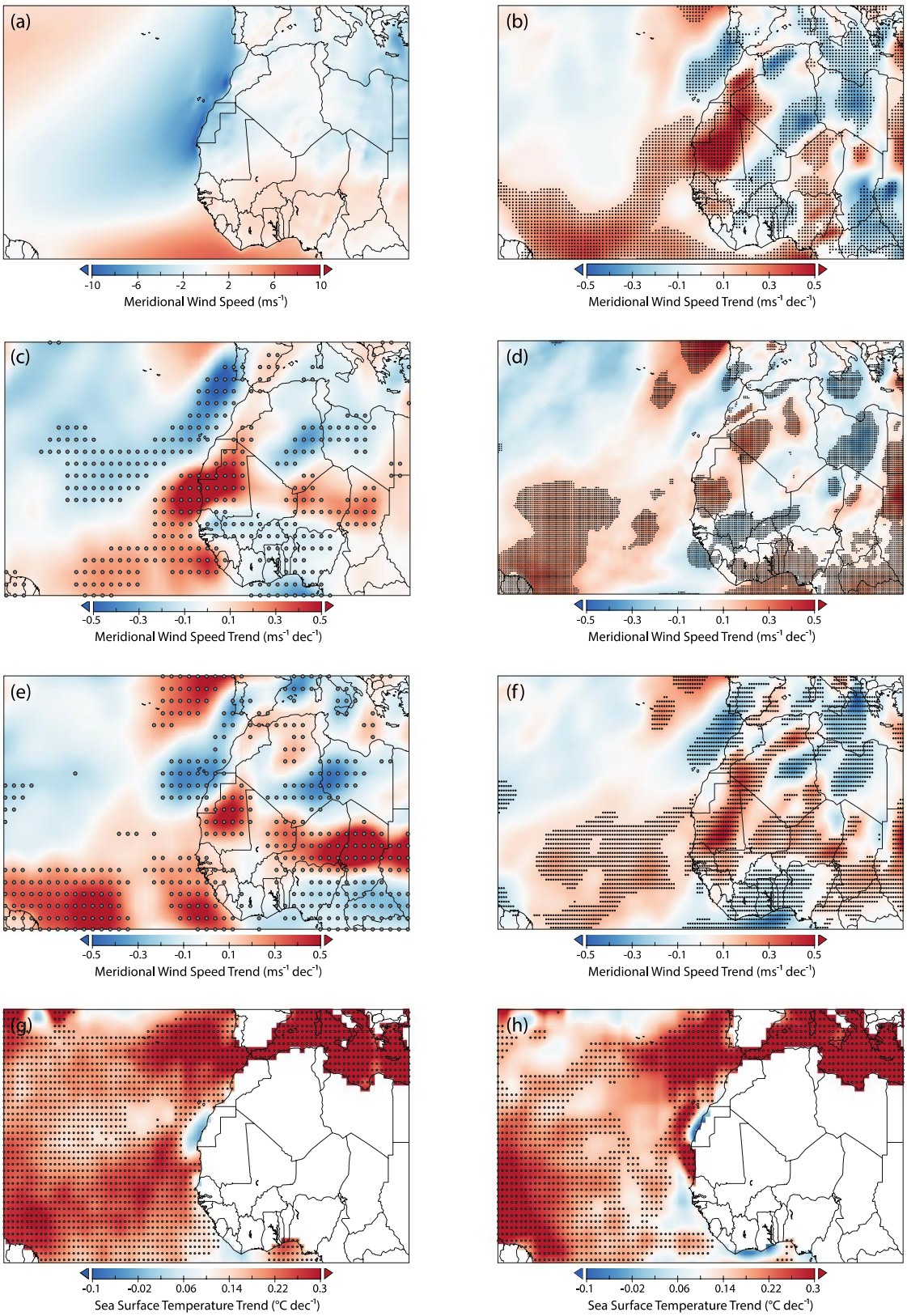

Figure 6.6. (a) Climatological summer (JJA) mean of meridional wind-speed from the CFSR reanalysis (1981–2010) and the linear trend (1981–2012) of summer meridional wind-speed for the (b) MERRA, (c) 20CR, (d) CFSR, (e) NCEP-DOE and (f) ERA-I reanalysis datasets. A negative (positive) trend is associated with an equatorward (poleward) meridional wind anomaly. Also shown are the summer linear trends (1981–2012) in SST from the (g) HadISST and (h) OISST datasets. Stippling indicates significant trends ($p < 0.1$).

Trends in winter upwelling variability appeared strongly correlated with the NAO (Figure 6.7, Table F2). The correlations between the winter NAO and the various UI^W indices were significant for nearly every UI^W, even as far south as the Mauritania-Senegalese upwelling zone, but the relationship is weaker than across the more northerly upwelling zones. The average correlation coefficient between the station-based winter NAO and the three latitudinal zones ranges from 0.50 (12-19°N) to 0.59 (21-26°N), to 0.74 (26-35°N). The NAO/UI^W relationship remains strong during autumn (Table F5). During spring (Table F3), the NAO/UI^W relationship also remains strong (except across the permanent upwelling zone); however, for 21-35°N the EA pattern emerges as an important variable, significantly correlating with the NCEP-DOE, MERRA, CFSR, 20CR and WASWind UI^W. During summer (Table F4), only the EA pattern across 26-35°N consistently appears as a significant correlation (with the PFEL, NCEP-DOE, CFSR and 20CR UI^W), although its realistic summer impact is likely to be very limited (Barston and Livezey, 1987).

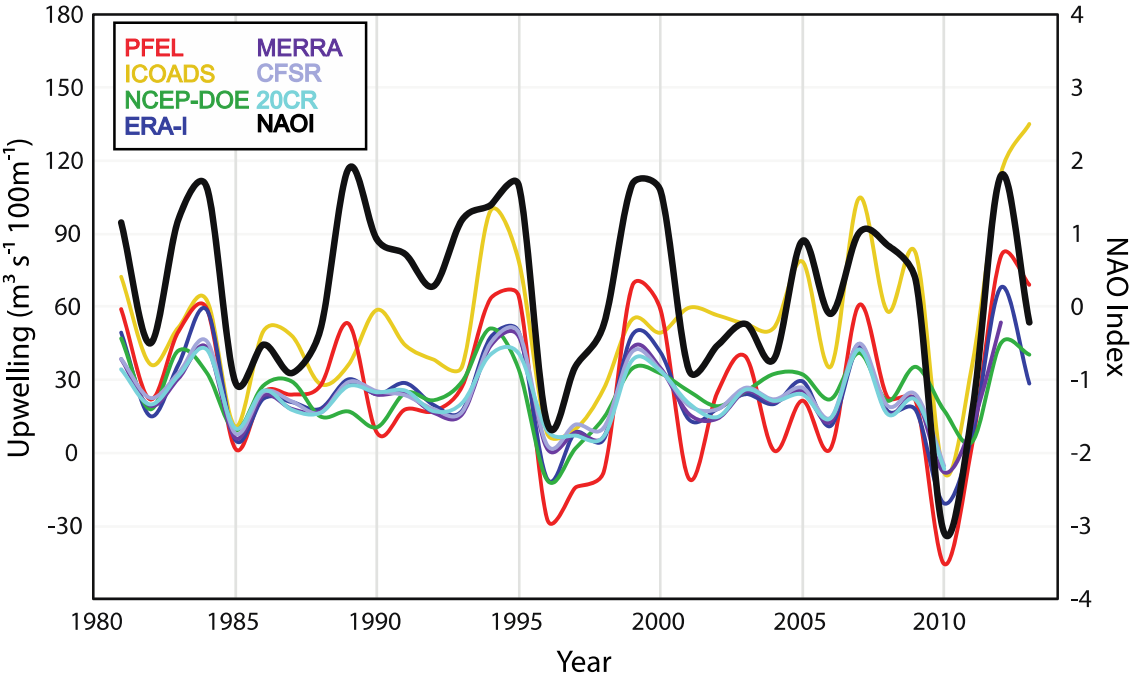

Figure 6.7. Temporal evolution of winter (DJF) NAOI and winter UI^W indices across the Moroccan (26–35°N) upwelling zone.

Direct correlations between the (linearly detrended) seasonal upwelling indices and the seasonal AMO and ENSO were generally ambiguous, although the correlation tables do not display the effect of lag times or account for the potential low-frequency response of the oscillations. Generally, it would be expected that the NAO and EA will have an instantaneous/short lag effect on upwelling (when considering monthly/seasonal temporal scales), and no evidence is found of temporal lags increasing the correlation

strength (except for the $UI^{\Delta SST}$, which is known to generally lag the wind based indices by 0-2 months). Of particular interest were the lagged correlations (on the order of 0-9 months) between ENSO and the UI indices, seen as the ENSO mode typically initiates around April-June, and peaks during the autumn/winter months, with potential lags around the eastern Atlantic/African sector varying from 0-9 months (An and Wang, 2001; Wang and Enfield, 2003). However, no evidence for a significant ENSO contribution is found across all the various UI indices at either monthly or seasonal timescales. The potential influence of the AMO on upwelling variability is discussed in Section 6.3.4.

6.3.3.3 Upwelling Proxy Variables

This section discusses the findings from land-based meteorological-station data and the TWI index, SSH data and VWCV data. Unfortunately, there was a lack of quality station-based wind-speed data along the northwest African coastline. The large gap in the location of (coastal) meteorological-stations was between 21°N and 29°N (Figure 6.2) which covers most of the major summer upwelling region. Regardless of this, summer trends in wind-speed from six available coastal stations were analysed (Figure 6.8). A positive trend was identified at four out of the six stations, but this was only significant at Safi (32.3°N). However, the trends at Agadir and Nouakchott also became significant ($p < 0.1$) when outlier values (1992 and 1995 for Agadir, 1986 for Nouakchott) were removed.

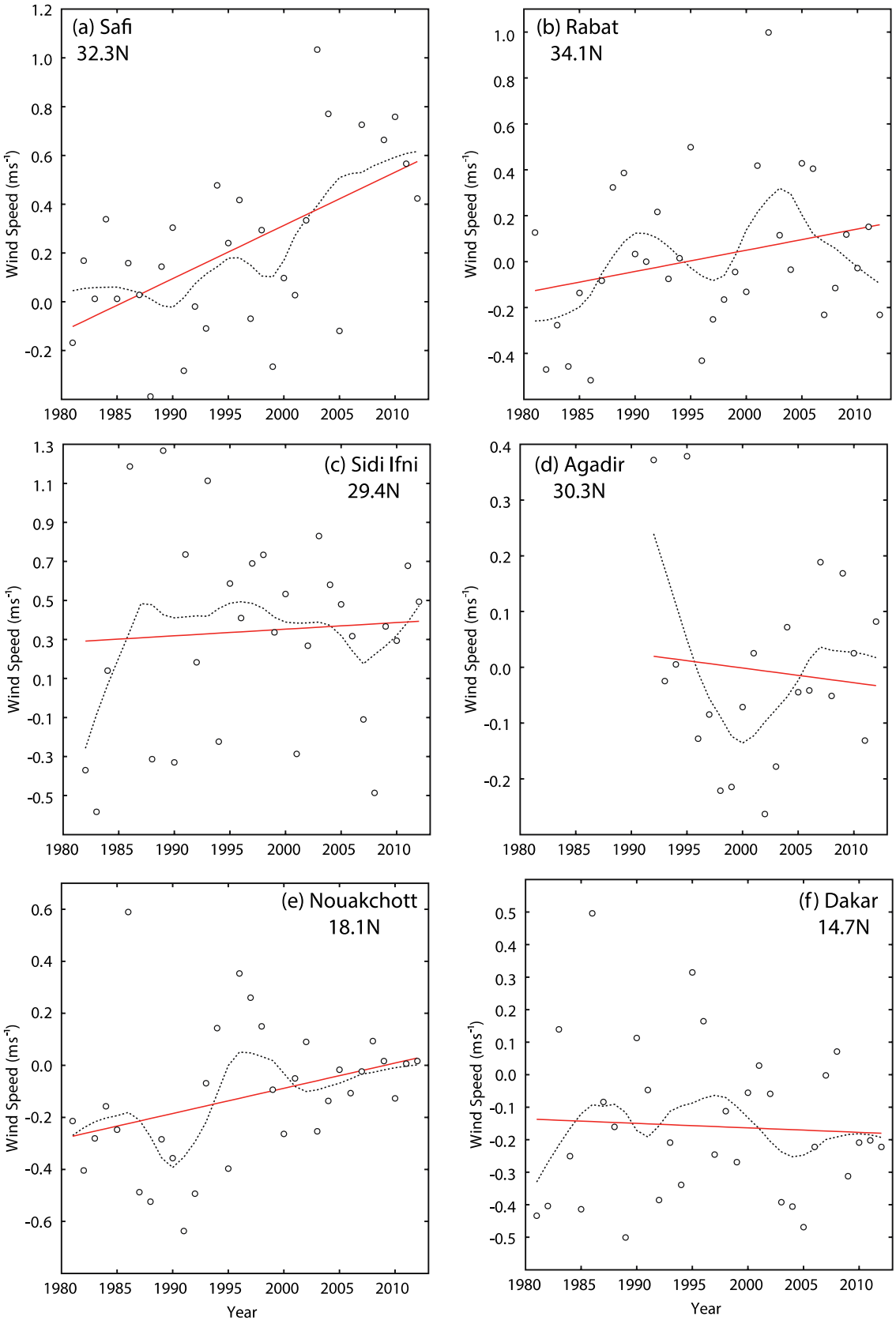

Figure 6.8. Temporal evolution of summer wind-speed anomalies (relative to the 1981–2010 base period) across six coastal meteorological-stations situated along the northwest African coastline (Fig. 1). Red lines indicate the linear trend across the entire period and dotted lines the 9-year LOESS trend.

An alternative method exists to characterise meridional/Trade Wind strength across the northeast Atlantic sector based on the normalised SLP difference between the Azores and Cape Verde. Theoretically, an increased pressure difference between these two locations (the semi-permanent Azores High and the relatively lower pressure across Cape Verde) would result in greater wind-speeds. Correspondingly, the TWI has been shown to display a strong relationship with wind-speeds across northwest Africa (CH14) and has been increasing since 1973 (Figure 6.9). The regression of the index onto the meridional wind-speed field from the CFSR reanalysis highlights an equatorward (poleward) meridional wind-speed relationship north of (south of) ~21°N, although this isn't significant across the entire coastal region (just the permanent annual upwelling zone). However, the positive trend in the TWI would seem to point to stronger large-scale meridional wind-speeds across the upwelling regions (Figure 6.9b).

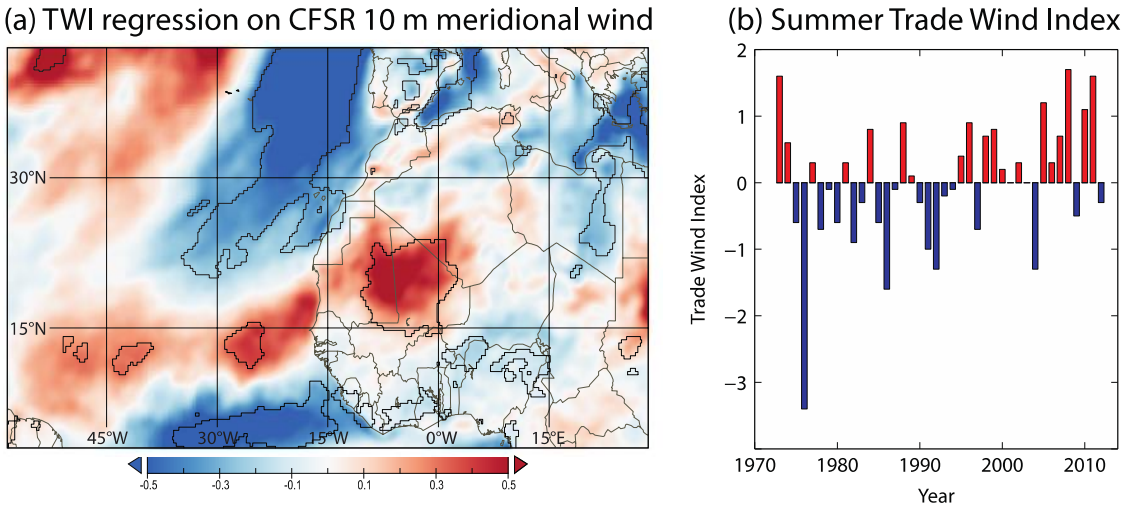

Figure 6.9. (a) OLS regression of the summer TWI on 10 m meridional wind-speed from the CFSR reanalysis (1981–2010), significant ($p < 0.1$) areas bounded by solid black lines and (b) the evolution of the summer TWI (based on the normalised SLP difference between the Azores and Cape Verde) from 1973 to 2012.

The VWCV variable from the GODAS reanalysis shows a strong divide between upwelling and downwelling around 21°N for its summer climatology (Figure 6.10a). Once more, the slightly weaker upwelling area around 30°N is readily identified. Summer trends across the three upwelling zones (Table 6.3) indicate a significant decline across the Mauritania-Senegalese Zone and an increase across the two higher latitude zones. A more detailed spatial and temporal picture of the summer trend since 1981 is shown in Figures 6.10b-d. Vertical velocity is shown to be increasing (i.e. water is more readily transported up to towards the surface) within a few grid points from the coastline north of 21°N and is decreasing (i.e. an increase in downward water column motion) southwards (Figure

6.10b). This is reflected as well in Figure 6.10c, which depicts the summer trends from the grid-box closest to the coast, showing a significant increase from 22-30°N (with a gap around 25°N) and a negative trend south of 17°N. The Hovmöller diagram of annual summer anomalies (3-year running mean; Figure 6.10d) highlights 1996-2004 and 2007-2012 as periods of generally enhanced vertical velocity transport (agreeing with stronger periods in the UI records), but for the equatorward region below 17°N, positive anomalies were most pronounced during 1980-1989, with strong negative anomalies during the post-2006 period.

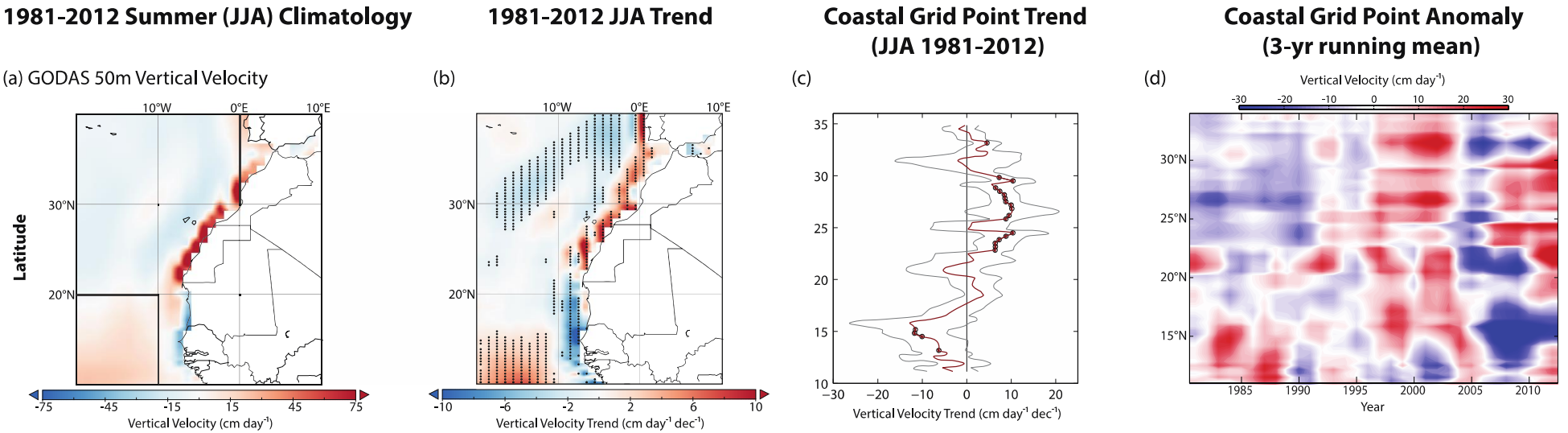

Figure 6.10. (a) The summer (JJA) climatology and (b) linear trend of GODAS 50m vertical water column velocity across 1981–2012, stippling indicates significant trends ($p < 0.1$). Figure (c) displays the linear trend (by latitude) of the nearest available grid-box adjacent to the coastline with circles indicating significant trends and grey lines the confidence intervals. Also shown (d) are the summer anomalies (3-year running average) of the coastal grid-boxes.

Prior to trend analysis in Table 6.3, the seasonal cycle from all the SSH data was removed and the regression of the global mean SSH on the SSH fields was subtracted to serve as a crude removal of the general global SSH signal. Unfortunately, in addition to this crude removal potentially not fully removing the global signal, a trait shared across all six SSH measures is that the variability typically outweighed any trend estimates (Table 6.3) so significant trends are rare. However, it is noted for summer that the reanalysis trends north of 21°N (Table 6.3) are mostly negative (i.e. fitting in with the upwelling intensification hypothesis) but not significant, whereas altimetry trends are positive but also not significant.

6.3.4 Discussion

On the one hand, there is ample evidence for a summer upwelling increase north of 21°N for the 1981-2012 period, with significant trends in the ICOADS (wind), PFEL, NCEP-DOE, HadISST, OISST and GODAS VWCV upwelling indices, as well as the TWI, and meteorological-station wind-speeds from Safi (and potentially Agadir and Nouakchott). There were supporting trends across the various UI's (more so across 26-35°N), including 10 m meridional wind-speed (Figure 6.6), SST and the GODAS and SODA SSH ocean reanalysis products (Table 6.3). The observations show a statistically significant increase north of 21°N and a generally significant decrease in upwelling-favourable winds south of 19°N (Table 6.3, Figure 6.5). Such observations can be explained by invoking Bakun's (1990) upwelling intensification hypothesis, discussed in Section 6.2. During summer, under a warming climate, a more rapidly warming African continent relative to the eastern North Atlantic Ocean will intensify the gradient between the continental low and the oceanic high-pressures, enhancing onshore wind strength. Due to the Coriolis deflection, these winds will enhance equatorward along-shore wind strength, generally in the region around 21-35°N (i.e. the permanent annual upwelling regions), driving greater Ekman transport and upwelling. South of ~19°N poleward meridional winds are strengthened, favouring downwelling. This latitudinal divide is a function of the summer position of the Azores High / ITCZ, which makes the average along-shore/meridional wind component equatorward (poleward) across the permanent upwelling zones (Mauritania-Senegalese upwelling zone, (Figure 6.6a)). A similar latitudinal divide has also been noticed in SST trends by Marcello *et al.* (2011). This along-shore wind-speed intensification mechanism is augmented by the large scale northeasterly Trade Winds and southwesterly WAM winds which again, reach a summer latitudinal divide at around ~20°N.

Contrary to the supporting evidence for an upwelling intensification across the northwest African coastline are differing lines of evidence that raise sufficient doubt as to whether

or not the supporting results can positively support a real trend. The main source of doubt is the general lack of a supporting reanalysis UI^W trend (Table 6.3, Figure 6.5). Discrepancies between reanalysis and maritime and continental wind-speed trends have been demonstrated by several authors, with the common consensus appearing to be that reanalysis wind-speeds are biased low (Smith *et al.* 2001; Wu and Xie, 2003; Vautard *et al.* 2010). Recently, Kent *et al.* (2013) highlighted how wind-speeds in several datasets (including NCEP and ERA-I) suffer from a low wind-speed bias (~1-2 ms^{-1}) at coastal locations when compared to the open ocean, offering further support for this idea. Thomas *et al.* (2008) attempted to remove the spurious positive bias in ICOADS wind-speed trends due to observational influences and identified that, since 1982, a real wind-speed trend is still likely, although they may not have accounted for every inhomogeneity. Narayan *et al.* (2010) encountered similar conflicting trends between reanalysis datasets and ICOADS when examining meridional wind-speeds across the four eastern boundary currents, and gave greater credibility to the conclusions from the ICOADS dataset (but without an attempt to correct for bias). The PFEL indices offer another data source that is somewhat independent of ICOADS, as they are derived from the US Navy Fleet Numerical Meteorology and Oceanography operational forecast model (Goerss and Phoebus, 1992). The PFEL UI^W trends often exceed the ICOADS values (Table 6.3), highlighting the consistency of significant trends that were seen from the 'observational' indices as opposed to reanalysis. Figure 6.6 illustrates that the trends in the observational UI^W (i.e. enhanced equatorward (poleward) meridional wind north of (south of) ~21°N) are, in essence, represented in meridional reanalysis summer trends. However, reanalyses indicate a latitudinal divide in meridional trends around ~25°N which is slightly further poleward than the approximate climatological meridional 10 m wind-speed direction change (Figure 6.6a). This disagreement arises because of the inclusion of the zonal wind component and coastline rotation in the UI^W calculation (meridional wind-speed on its own serves as a good indicator but the UI^W will be more accurate).

An attempt was made to validate the ICOADS trends by analysing the WASWind dataset (Tokinaga and Xie, 2011b) and by comparing ICOADS data to SeaWinds data derived from scatterometry (Lungu *et al.*, (2006). The WASWind dataset adjusts the ICOADS observations by correcting wind-speeds for anemometer height changes, removing spurious Beaufort estimates and estimating wind-speeds from wave height data and it was found that across the CUE, the summer UI^W calculated from WASWind (not shown) across all latitudes displays a monotonic trend, suggesting that the ICOADS trend from 1981-2012 is positively biased. However the lack of a significant WASWind trend is probably due to the course spatial resolution (4°), which makes it unlikely that coastal wind intensification would be picked up by the dataset. A comparison of ICOADS and SeaWinds summer evolution (UI^W) across the three upwelling zones is shown in Figure 6.11. The SeaWinds magnitudes are generally weaker north of (stronger

southwards) 21°N, probably due to the ICOADS observations having a variable height but generally in the region of around ~25 m (Kent *et al.*, 2007) compared to the 10 m SeaWinds. Figure 6.11 shows that the SeaWinds results match ICOADS with reasonable agreement across 21-35°N but poorly across 12-19°N; however, with such a short temporal record the fit is partly subjective. Potential errors in the SeaWinds include signal degradation near the coast, due to rather variable surface roughness near the coastline and the land boundary and the (low) wind-speed bias due to precipitation and clouds; yet the fit with ICOADS is encouraging and adds further support towards a coastal wind intensification.

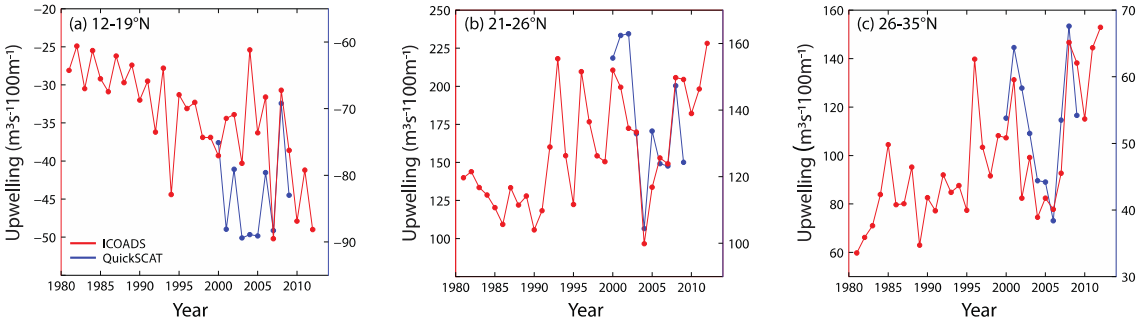

Figure 6.11. A comparison of ICOADS and QUICKSCAT calculated summer (JJA) UI^W values across the (a) Mauritania–Senegalese upwelling zone (12–19°N), (b) permanent upwelling zone (21–26°N) and (c) weak permanent upwelling zone (26–35°N).

Further evidence, which is potentially contrary to the upwelling intensification hypothesis, is a lack of significant wind-speed increase from near-coastal meteorological-stations except at Safi (Figure 6.8). However, land-based stations worldwide have a documented decrease in wind-speed during the past four decades (Vautard *et al.*, 2010) - attributed mainly to increasing surface roughness. It is possible such a signal contaminates the analysed meteorological-stations (and that being airport stations – are potentially poorly sited). However, the summer 1981-2012 wind-speed trends were positive at four out of six stations and the trend at Agadir and Nouakchott are positive and significant when the anomalously high values (section 3.3.1) early in the record are removed, leaving only Dakar (less than ideally sited on the Cape Vert Peninsula) displaying no long-term positive trend.

One final uncertainty was the discrepancy between altimetry and reanalysis SSH (Table F1). The summer climatological SSH means of the GODAS and SODA reanalyses and the altimetry data show a clear match. All three reflect the reduced SSH near the northwest African coastline (Figure 6.12); however trend directions vastly differ. The two reanalyses indicate a summer reduction in SSH between ~23-31°N whereas the altimetry shows a ubiquitous increase across all latitudes. This may be due to the global SSH signal overriding any coastal process at a monthly scale in the altimetry data, hence why the

global signal from SSH trends was crudely removed before analysis in Table 6.3. However, given the variability in the data, no significant trend emerges. As the ocean reanalyses all assimilate SSH, it is speculated that the difference is due to how the reanalyses incorporate altimetry observations and close the global freshwater budget. With ocean reanalysis, Boussinesq approximations are made (i.e. global ocean volume has to remain constant) which makes assimilation of a steric (changes from temperature and salinity) global trend problematic. The different models overcome this problem in different ways (Behringer, 2007; Carton and Giese, 2008; Balmaseda *et al.*, 2013) and generally show good agreement (via root mean square error) with altimetry SSH in the Pacific, but not as good in the Atlantic. It is possible the reanalyses trends (which fit the upwelling intensification hypothesis) may be an artefact of less than perfect model SSH calculation/resolution in the Atlantic (or the discrepancies in temporal period analysed, (Figure 6.12)); this requires future investigation. However given the large variability of seasonal SSH trends and the relatively short time periods that SSH data are available across the northwest African coastline (along with a lack of quality tide-gauge data and uncertainty of SSH at the coastal boundary), it is suggested that this variable is not currently ideal for analysing northwest African upwelling.

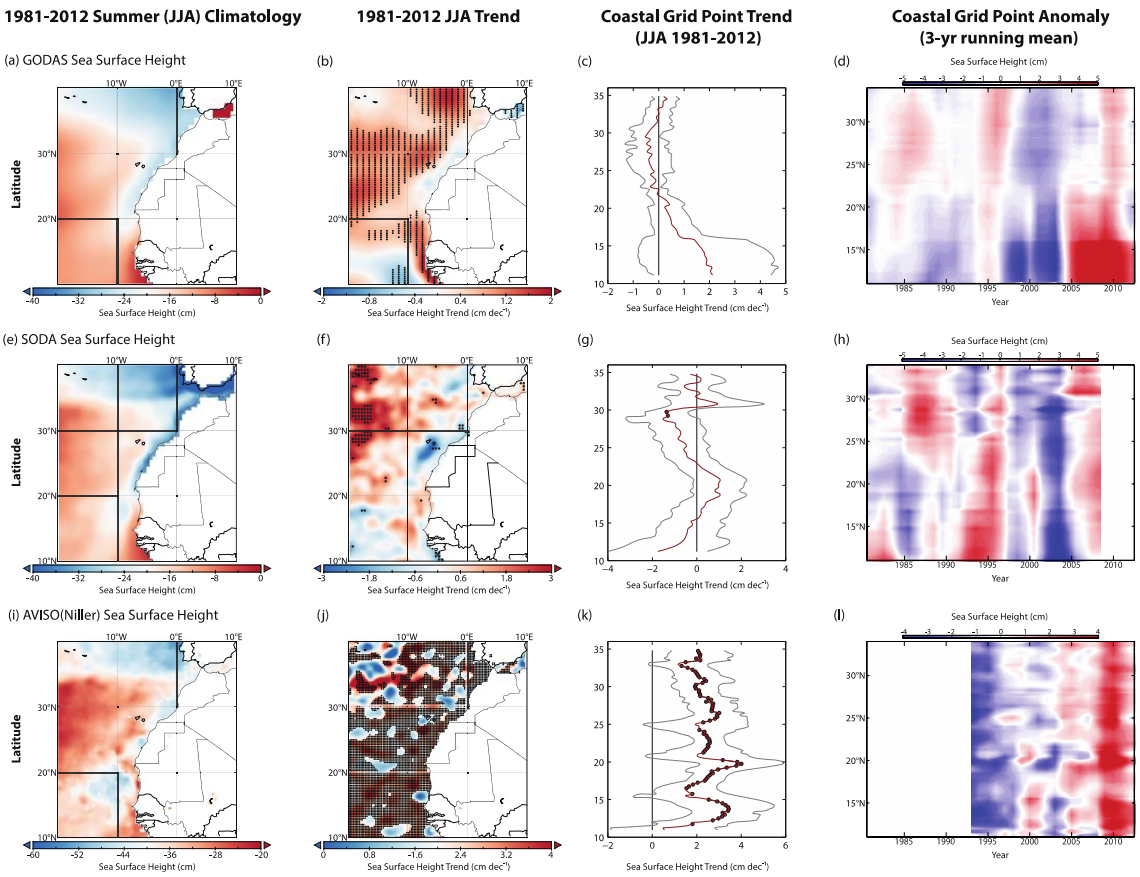

Figure 6.12. As for Figure 6.10 but for SSH. (a, e, i) The summer (JJA) climatology and (b, f, j) linear trend of GODAS, SODA and AVISO SSH across 1981-2012 (1981-2008 for SODA, 1993-2012 for AVISO), stippling indicates significant trends ($p < 0.1$). Figure (c, g, k) displays the linear trend (by latitude) of the nearest available grid-box adjacent to the coastline with circles indicating significant trends and grey lines the confidence intervals. Also shown (d, h, l) are the summer anomalies (3-year running average) of the coastal grid-boxes.

Outside of summer, spring is the other season in which, intuitively, one would expect a potential UI increase (across all latitudes), but find generally insignificant/conflicting trends (Table 6.3). The NAO correlations with the various UI indices are strong in spring and autumn (Table F3, F5), but exceptionally strong in winter (Figure 6.7, Table F2). This relationship is due to the strength of the Azores semi-permanent high-pressure system, which modifies Trade Wind strengths, and so the wind-speed fields across the northwest African upwelling zone. This is why the fixed NAO Azores-Iceland station based index displays generally stronger relationships than the PC-based version (Table F2-5). The EA pattern, which is a southward-shifted NAO-like oscillation, becomes prominent in spring and correlates with several of the weak upwelling zone indices in summer. Rather than this being an alternative pattern potentially explaining the variability in the UI, it generally (during these seasons) better serves as a reflection of the state/strength of the Azores High, which itself is most persistent during autumn-spring. As such, the main mode of variability across the Atlantic sector, which directly

relates to the Azores High (represented by either the NAO/EA) can generally explain about 20-40% of the seasonal variability in the spring and autumn UI, 30-60% during winter and a likely insignificant amount of seasonal variability during summer (Table F2-5). A recently published study, which used ICOADS, WASWIND, NCEP, PFEL and ERA-40 winds, identified a weakening in upwelling across the CUE from 1967-2007 (Barton *et al.*, 2013). However, the authors present only annual trends (and in this thesis it is identified that the seasonal variation is strongly dependent on the NAO/EA) and truncate the time series to 2007 (the past five years significantly enhance the UI^{W} trends), potentially explaining a lack of summer intensification in their findings.

The AMO, which has been in its positive phase from ~1995 (Wang, 2012), may potentially have an effect on coastal upwelling by modifying SSTs around the northwest African coastline (associated with its typical 'tri-pole' SST signal across the Atlantic Ocean). Generally, raw correlations between the AMO and the UI are ambiguous (Table F2-5); however, as the main time cycle of the AMO is roughly ~70 years, it cannot be guaranteed that the AMO has no effect based solely on the correlations in Table F2-5. Additionally, the effects of ENSO are also likely limited, as direct correlations are rarely significant (Table F2-5).

Figure 6.13 depicts the potential effect on summer upwelling across the northwest African coastline in a globally warming world based on the patterns found in the various UI. The mechanism in Figure 6.13 applies to the selected period of study (1981-2012), but one would also expect, if global warming continues unabated, that this mechanism will intensify (i.e. Figure 6.13b). The findings in this chapter reinforce the upwelling intensification hypothesis of Bakun (1990), whilst modifying the idea for the northwest African coastline, across which a ubiquitous upwelling increase has not occurred due to the latitudinal divide in summer wind-speed regimes. Generally, a consistent increase in wind-speed brought about by the land-ocean pressure gradient results in an increase in coastal upwelling across 21-35°N (near-surface offshore winds) and increase in downwelling-favourable winds south of 19°N (near-surface onshore winds). The latter may be related to the 'recovery' in Sahel precipitation since the droughts of the 1970-80s (Nicholson, 2013), as increased onshore winds are consistent with a strengthening WAM, although this is one of many potential explanations. Additionally, under enhanced upwelling conditions, impacts on marine life can vary (Bakun *et al.*, 2010; Chavez *et al.*, 2011), as a direct upwelling increase does not necessarily equate to an increase in chlorophyll/primary production. In addition to biological constraints (mainly iron availability (Capone and Hutchins, 2013)), physical constraints such as the depth/size/slope of the continental shelf result in different upwelling regimes across the northwest African coastline as the shelf properties can control how nutrients are recycled between periods of more intense upwelling and relaxation periods (Arístegui *et al.*, 2009).

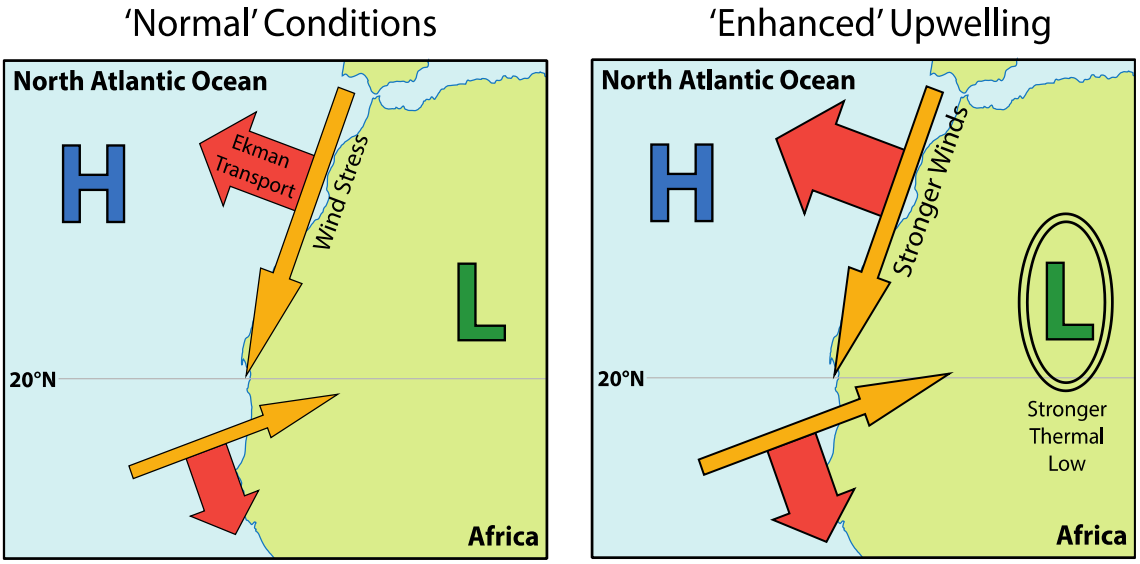

Figure 6.13. The upwelling intensification hypothesis (for summer, JJA), modified for the CUE after Bakun *et al.* (2010). A thermal low surface pressure cell develops across the African continent as a result of the continent heating faster than the ocean. The comparatively higher pressures across the ocean results in airflow towards the continent which is deflected by the Coriolis effect to the right, resulting in enhanced equatorward (poleward) along-shore winds across ~45–20°N (below 20°N). This latitudinal divide is a function of the mean position of the Intertropical Convergence Zone during summer, as such, the general wind patterns are from the northeast above 20°N (the Trade Winds) and southwest below 20°N. Figure (b) depicts the upwelling region in a globally warming world, with (assumed) more greenhouse gas emissions and water vapour across the region, which increases daytime heating and inhibits night-time cooling – driving a stronger pressure gradient between atmosphere and ocean. This results in stronger winds across the region, which drives stronger than normal Ekman transport and increases coastal upwelling north of 20°N, and downwelling south of 20°N.

6.4 The Future of Coastal Upwelling

Determining the future evolution of coastal upwelling systems is a complex and important issue to attempt to resolve. It cannot be certain that the hypothesis presented in Figure 6.13 will continue to enhance upwelling-favourable winds unabated. Upper ocean stratification has increased in the second half of the Twentieth Century due to Twentieth Century warming (Capotondi *et al.*, 2012), which implies a larger wind-stress needed to bring deeper ocean waters to the surface. Whether enhanced wind-stress would override changes in stratification is uncertain, as is whether upwelling-favourable winds are actually increasing and will continue to increase in the future. The CHB14 study would suggest that, at least across the CUE, upwelling-favourable winds have increased. Figure 6.14 is taken from Chapter 22 of the IPCC AR5 report and illustrates the complex issues

in determining the impacts of future upwelling. Delineating trend direction does not necessary equate to enhanced fisheries due to negative biological feedbacks.

A further potential negative feedback on upwelling-favourable wind-stress is water vapour, which could increase much more over the oceans than over land and reduce the continental-oceanic induced pressured gradient required for the intensification hypothesis in Figure 6.13. Section 7.2 discusses the potential future direction studies of (the physical aspects of) coastal upwelling regions should take.

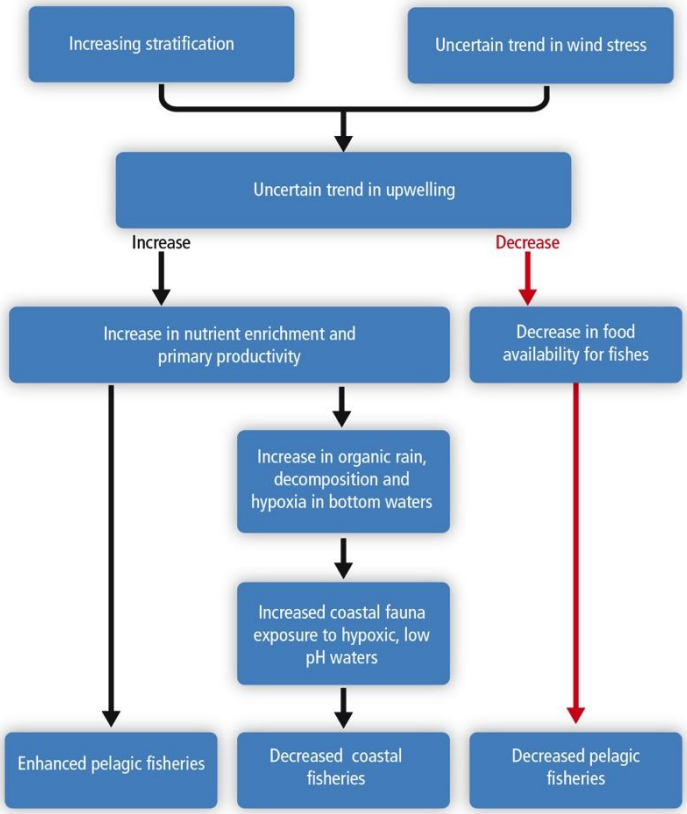

Figure 6.14. Taken from Niang *et al.* (2013), indicating the potential future impacts across coastal upwelling regions.

6.5 Chapter Summary

Trends in seasonal values of coastal upwelling across the northwest African coastline were analysed from 1981-2012. The different data sources used to characterise UI^{W} and $UI^{\Delta SST}$ provide very similar results for the mean fields (Figure 6.3), and show the previously described spatial and temporal patterns of upwelling well – a permanent annual upwelling regime north of 21°N (which sometimes weakens/reverses around 30°N) and a seasonal regime south of 19°N (where downwelling conditions dominate during the summer months). However, trend directions often differ between observational and reanalysis datasets (Table 6.3). Focusing on summer (JJA), it was found that the observational UI^{W} and $UI^{\Delta SST}$ favour an increase in upwelling across 21-35°N and increase in downwelling south of 19°N, a pattern generally supported by a separate analysis of 10 m meridional wind-speed trends. Reanalysis-derived UI^{W} support the trend increase across 26-35°N (the weak permanent upwelling zone) but appear mainly monotonic across the lower latitudes. Additionally, supporting proxy indices, which include wind-speed data from six meteorological-stations, the TWI (judged by its regression pattern on 10- m meridional wind-speeds and its positive trend from 1973 onwards), vertical water column motion and SSH trends from ocean reanalyses, all offer further indication that the observational datasets generalised wind-speed increase across all latitudes (11-35°N) is real. Negative trends in summer coastal SST across the permanent upwelling zone (21-26°N) suggest that the impact of stronger winds is already clear across this part of the coastline.

The NAO is an extremely strong influence on non-summer upwelling magnitudes and inter-annual variability, especially in winter, where significant correlations are displayed across all latitudes (Table F2-5). The EA pattern (which reflects the Azores High strength as it is a southward-shifted NAO like dipole) correlates strongly with the UI^{W} in spring, illustrating the strong influence of the Azores High in all seasons but summer. An ENSO and AMO signal are absent in the analysis, but the latter's low frequency component may have a strong effect on northwest Africa upwelling – a longer temporal UI^{W} record will help elucidate this in the future.

A modification of the Bakun upwelling intensification hypothesis based on the latitudinal divide between the northeasterly Trade Winds and southwesterly monsoon winds around 20°N (just for summer and for northwest Africa) has been presented. As global warming intensifies, it would be expected that more favourable conditions for enhanced summer upwelling north of 20°N and an increase in downwelling-favourable winds equatorward will prevail. This will likely result in coastal SSTs displaying a reduced warming rate in comparison to the open ocean across the northern upwelling zones (21-35°N). The increase

in onshore favourable winds across 12-19°N is possibly related to the minor recovery of the WAM (compared to low values during the 1970s-1980s), which may have assisted in a recent, partial recovery of rainfall for the Sahel region.

7. Syntheses & Outlook

7.1 Thesis Summary & Conclusions

This thesis has presented one of the most complete modern characterisations of the physical climate of the Macaronesian bio-geographical region. The following paragraphs qualitatively summarise the content and work done in each chapter. Section 7.1.1 (quantitatively) summarises the major findings of the thesis and Section 7.2 offers thoughts on the potential future direction of research one interested in the Macaronesian region might pursue.

Chapter 1 provided a brief overview of the physical influences across the region and a complete review of the published literature concerning the direct influences and effects of climate change across Macaronesia. For locations along the same latitude, the islands represent a much more habitable climate, due to the tempering maritime influence and the reliable nature of orographically generated precipitation. The effect of altitude on some of the islands with larger mountains gives rise to different climate zones that would normally span anywhere between 30-50° latitude. Finally, the islands and climate of the wider region are further influenced by large-scale atmosphere-ocean modes of variability. Chapter 2 summarises the major methodologies and datasets used throughout the thesis.

Chapter 3 documented the production of a daily NAO index that can be extended back to 1850. This index extends the length of the longest-term, widely-available daily NAO index - the CPC daily NAO - by 100 years. Chapter 3 also presents an analysis of the temporal evolution of the NAO (by using many different characterisations of the index). This identified a significant long-term increase in winter NAO variability and a significant negative trend in the summer NAO index. Potential reasons behind these changes were discussed; the winter variability increase is uncertain as many factors are at play, but the long-term summer negative trend is largely related to an increase in atmospheric blocking across Greenland. The time-variant spatial nature of the NAO is also explored. The NAO index is strongly correlated with precipitation and temperature patterns across Macaronesia, but the centres of action of the index and its resultant spatial correlation patterns across Macaronesia have changed in time. A northeast Atlantic Trade Wind Index was also developed, which has shown a significant trend in increasing Trade Wind-speeds since 1973.

Chapter 4 presents the construction of a SAT time series from 1865/1885/1895-present for the Azores and Madeira/Canary Islands/Cape Verde respectively. These time series

are the first long-term, continuous, instrumental records for these island chains and highlight how the recent (post 1976) temperature rise is the most pronounced change across all four island chains in these >160 year-long records. Additional analysis of complementary meteorological records from independent stations corroborates the recent temperature trends. Precipitation variability was analysed from several stations across the islands and it was found that there were no striking long-term changes. There appears to be a significant increase in Cape Verde precipitation during the wet season for some meteorological stations that appears coherent with changes in the WAM index. Several temperature and precipitation 'extreme' indices were analysed and it was found that current trends in these indices mirrored the trends in the mean state of temperature and precipitation (a temperature increase and no significant precipitation trends). Temperature trends across Macaronesia exceed most other rates from 'island locations' within 10-40°N/S globally, but similar warming rates in Mauritius (an Indian Ocean archipelago) point towards this location being a potential analogue.

Chapter 5 considers the potential future changes across the region based on the same suite of global climate models as the IPCC AR5. A robust response in temperature is found, with expected increases across the islands ranging between 0.8-3.0°C above the 1976-2005 average, dependent on island and forcing scenario. Precipitation responses generally point towards a drying across Madeira and the Canary Islands, wetter conditions across the Azores and variable (if slightly favouring wetting) conditions across Cape Verde. Trends in percentile-based temperature extremes indicate that by the period 2081-2100, anywhere between 40-90% of days during the year will have temperatures that would be classified in the top 10% of days based on recent (1961-1990) climatology. This is, of course, strongly dependent on the RCP scenario followed. The CMIP5 model mean indicates that a greater proportion of precipitation over the Azores will fall as heavy (>R20mm/R95/99p) events without the total amount drastically changing, with more limited changes across the other islands.

Chapter 6 presents a thorough reconciliation of the literature and combines numerous data sources to address the question of whether coastal upwelling across the northwest African coastline has been increasing (or not) in line with the Bakun hypothesis. The main conclusion is that coastal upwelling during the summer season has significantly increased from 1981-2012 and that the large-scale mode of meridional atmospheric circulation (represented by the NAO/EA pattern) exerts a strong control during other seasons. The upwelling intensification is reflected in SST fields, which exhibit cooling trends across limited regions of the northwest African coastline. The initial intensification hypothesis is modified to reflect the transition of the northeast Trade Winds and southwesterly monsoon winds; as such, upwelling is expected to increase above (decrease below) 20°N if the continental-oceanic temperature gradient remains the most influential

mechanism. The upwelling intensification may be disrupted in the future if ocean stratification increases and/or water vapour feedbacks serve to reduce the land-sea pressure gradients.

7.1.1 Highlights

- **Temperatures across the Macaronesian archipelagos warmed at a rate from 0.30-0.38°C dec^{-1} from 1981-2010.** This is based on analysis of the four major temperature time series reconstructed in Chapter 4. The consistent temperature rise across all four islands is the most pronounced, coherent change in the Macaronesian instrumental record, with anthropogenically-induced climate forcing the most likely cause. The 2001-2010 decade was the warmest decade for all four Macaronesian Islands. A separate analysis of sixteen meteorological-stations across the archipelagos indicates an absolute range of surface air temperature trend between 0.26-0.50°C dec^{-1} from 1973-2012. The 1981-2010 annual warming rates (0.30°C dec^{-1} for the Canary Islands, 0.33°C dec^{-1} for the Azores and Madeira and 0.38°C dec^{-1} for Cape Verde) are greater than the global average temperature trend (0.14°C dec^{-1}) and very similar to continental Europe (0.32°C dec^{-1}). Ocean Heat content (0-700 m) has also shown to be strongly increasing across the Macaronesian region since the early 1980s.

- **Precipitation changes across the islands are generally experiencing no change in mean conditions, except Cape Verde, where a positive trend (15-39 mm dec^{-1}, 1981-2010) during ASO is documented.** This trend is significant for the NCEP-NCAR grid-boxes over the Cape Verde Islands used in Chapter 4 and CH14. There is a positive trend at the end (1981-2010) of the Azores records through DJF to JJA and a negative trend during SON, but none of these trends were significant. There were no significant long-term changes in Canary Island or Madeira precipitation.

- **Changes in climatological extreme conditions generally mirror the changes displayed in the mean state of temperature and precipitation variables.** Widespread significant increases were displayed in the highest minimum and highest maximum temperatures (TNx and TXx) across the Canary Islands, Cape Verde and Madeira, with rates comparable to the increases in mean temperature of 0.25-0.36° dec^{-1} (1979-2011). Trends in the lowest minimum and lowest maximum temperatures (TNn and TXn) were not ubiquitously significant. Trends in percentile based indices (TN10p, TN90p, TX10p and TX90p) all point in the direction of significant warming

and there is an increasing trend in the warm-spell duration indicator across Madeira and the Canary Islands.

- **A daily North Atlantic Oscillation index that extends back to 1850 has been produced.** This extends the length of the previously only-available, widely used daily NAO from the CPC by 100 years, and is the first station-based version. Initial analysis of the monthly average of the index shows that it compares well with existing measures. A normalised and un-normalised version of the index has been created. The work has been published as a data paper and it is hoped the index will be of widespread use to researchers across multiple disciplines.

- **The NAO has been identified to have undergone centennial scale changes in its variability, culminating in a period since 2004 of rapid variability, leading to extremely variable Atlantic Sector weather.** The (winter) NAO was strongly negative in the 1960s and positive in the 1980s/early 1990s. Recently, the winter trend from 1991-2013 has been strongly negative, which is partly due to the recent winters of 2009/10 and 2010/11, where extremely negative NAO conditions prevailed. The winter (especially December) NAO index shows signs of a long-term shift towards more variable conditions. This characteristic is restricted to winter, and shows up clearly in all versions of the NAO. Five out of the ten most extremely positive/negative December NAO values have been since 2004, suggesting that the long-term trend in variability is potentially being amplified. The summer NAO index shows a negative trend following a peak in positive values in the 1930s. The period 1991-2013 is also significantly negative in the summer NAO index.

- **A novel characterisation of the Trade Winds across the eastern North Atlantic has been produced, highlighting a linear increase in wind-speeds since 1973.** Corresponding analysis of changes in Ocean Heat Content across Macaronesia implies that this trend is robust. It is likely that stronger Trade Winds have offset a small amount of warming across the Canary Islands/Madeira region (based on TWI-SAT correlation maps).

- **The mean temperature across the Macaronesian Islands could increase between 0.8-3.0°C for the period 2071-2100, relative to 1976-2005.** This is based on analysis of several hundred models from the CMIP5 archive. Warming is progressively greater under the more severe RCP scenarios. RCP2.6 equates to a warming of ~1°C across all four islands. RCP4.5-6.0 implies a warming of 1.5-1.9°C and RCP 8.5 between 2.7-3°C (with confidence intervals of ~±0.15-2°C). These statistics summarise the model mean response, internal variability within the climate

systems is likely to play a large role in how the spatial and temporal climate evolves. 55-year trends (2006-2060) in temperature and precipitation from the individual CMIP5 model runs can show drastically different spatial patterns (i.e. opposite signs over certain regions), which serve as a broad indicator of potential future variability (in the model domain).

- **Future precipitation changes (by 2071-2100) are variable), although a generalised trend towards 'Wet gets Wetter, Dry gets Drier' is found.** Mean winter precipitation increases under future climate scenarios for the Azores and decreases for Madeira, the Canary Islands and Cape Verde. The drying trend across the lower latitude island appears more robust than the wetting trend for the Azores (based on model confidence intervals). The largest magnitudes under RCP8.5 were a 22% to 37% winter decrease for Madeira, the Canary Islands and Cape Verde. During summer, the Azores and Madeira display a weak drying trend where the magnitudes do not exceed the model ranges. summer precipitation appears to increase by 10% across the Canary Islands across all scenarios, with a similar magnitude for Cape Verde during the wet (ASO) season, although the model ranges were wider than the projected changes (and for the Canary Islands summer precipitation is already very low). Extreme precipitation events would be expected to increase in their intensity, as a warmer atmosphere holds more moisture.

- **Future changes in the NAO hint at a small shift towards positive conditions, while the TWI is expected to increase during autumn-spring but decrease during summer.** The NAO increase does not appear to be highly significant and the CMIP5 models fail to pick up the increasing Twentieth Century variability that was identified in the observational record. A more positive NAO in winter and reduced TWI in summer could allow a large seasonal discrepancy in warming rates to develop, as NAO+ winter conditions favour generally lower temperatures across Macaronesia and weaker Trade Winds in summer may favour higher temperatures.

- **Coastal upwelling across the northwest African coastline is found to have undergone a significant increase during summer (1981-2012).** A modification of the Bakun Upwelling Intensification hypothesis to account for changing seasonal wind regimes across northwest Africa is also presented. Identifying the summer upwelling increase was dependent on analysis of numerous, often-conflicting variables, but the general consensus from the more reliable sources strongly supports the upwelling intensification. The NAO (winter, autumn) and the EA pattern (spring) were found to be important controls on upwelling magnitudes by their influence on

large-scale wind fields. The upwelling increase has led to a localised SST cooling around areas of the northwest African coastline. The basic properties of the upwelling intensification mechanism (land-sea pressure gradient) may also help explain precipitation trends across northwest Africa. The future trend magnitude and direction of upwelling is uncertain as water vapour and ocean stratification feedbacks could enhance or slow the intensification mechanism.

At the end of Chapter 1, it was stated that the five major objectives of this thesis were:

1. *Create a climate record that will allow analysis of long-term changes in Macaronesian Climate.*
2. *Determine if additional climate data support the conclusions drawn from the main climate records.*
3. *Conduct a detailed analysis of the North Atlantic Oscillation, including extending the daily-resolution index back to 1850.*
4. *Deliver estimates of future climate change at the end of the Twenty-first Century across Macaronesia.*
5. *Test whether the Upwelling Intensification hypothesis can be verified across northwest Africa.*

Additionally, it was stated that the contribution of this thesis to the wider scientific literature was to:

1. *Create a daily-resolution NAO back to 1850, available to researchers across multiple disciplines.*
2. *Analyse the temporal variability of the winter NAO, presenting recent dramatic changes.*
3. *Present an analysis of the spatial relationship of NAO and Macaronesian climate.*
4. *Create a long-term monthly-resolution Macaronesian time series and analyse the current and historical climate of the Macaronesian Islands.*
5. *Summarise the potential future climate change scenarios across the Macaronesian Islands.*
6. *Characterise the spatial-temporal trends in coastal upwelling across the northwest African coastline to verify the upwelling intensification hypothesis.*

These objectives and contributions have been achieved through the realisation of the direct content of this thesis and also as five peer-reviewed, published articles at the time of submission, with plans to write up the work done with the climate extreme indices as a final paper.

7.2 Future Work Direction & Suggestions

Daily NAO

The production of the daily NAO index in Chapter 3 was conducted near the end of the thesis. Therefore an obvious direction for future work is to analyse its evolution in more detail. An immediate interest would be if any significant findings are present in the 'weather' time period of days to a few weeks. Yan *et al.* (2001) identified strong power in the 16-day timescale for selected temperature and westerly indices across Europe, so intuitively, the daily NAO should be useful for similar analyses. There has been a recent increase in literature regarding potential changes in the sub-polar jet stream and mid-latitude blocking (e.g. Overland *et al.* 2012; Francis and Vavrus, 2012) that may arise as a result of Arctic amplification. Given the close relationship of the NAO to the jet stream and mid-latitude circulation, it will be interesting to see if any links can be found. It is hoped that presentation of the work as a data paper (CHVJ15), where the datasets are provided with the paper, will stimulate research interest in the index.

The index could be potentially further developed by use of data from Gibraltar as initially used in the characterisation of the NAO by Jones *et al.* (1997). Daily data are believed to exist back to the 1820s with minimal gaps except during the 1850s. This would allow a daily index to be created spanning almost 200 years as the southwest Iceland SLP series also goes back to the 1820s. More data from the Azores are likely to become available as the result of digitisation efforts during the ERA-CLIM2 project (Stickler *et al.*, 2014), which may allow replacement of periods in the Azores SLP time series that are currently filled in with reanalysis.

The time-variant NAO-Macaronesia relationship

The changing nature of the NAO relationship with SAT across Macaronesia through time was identified in Chapter 4 and has been noticed in spatial fields of numerous climate variables by Polyakova *et al.* (2006) and Wang *et al.* (2014) who have identified the changing position of the nodes of the centres of action of the NAO throughout the Twentieth Century. How the NAO will change in the future will have significant impacts across the Macaronesian region, so a greater knowledge of its past and potential future variability will be advantageous. Recent research has highlighted the potential high skill for pre-winter forecasting of the state of the index (Garcia-Serrano and Frankignoul, 2014; Scaife *et al.*, 2014), which could be useful for the three northern-most Macaronesian Island chains, where the NAO-relationship is currently most evident.

Macaronesian station data

Additional data sources for the Macaronesian region are likely to increase in number as digitisation of historical records (e.g. Bethke and Valente, 2012; Valente *et al.*, 2008; 2013; Stickler *et al.*, 2014) and production of new reanalysis/observational datasets continues. A new temperature record from Cape Verde with (non-continuous) data as far back as the 1860s has been archived in the Berkeley SAT dataset (Rohde *et al.*, 2013) and a forthcoming version of the 20CR dataset will begin in 1816 (~2018 release). Revisiting the approach of CH14 (i.e. building on all the available historical archives with Macaronesian data) would be an interesting study in the future. The Trade Wind Index and North Atlantic Oscillation indices will be periodically updated and further improved as more data become available, especially when gaps filled via reanalysis can be replaced with real station data.

Climate Extreme Indices

Efforts will be made in the future to perform the same analysis using the ETCCDI extreme indices on fully homogenised, gap-filled data from the Macaronesian Islands when a suitable approach to sufficiently gap fill daily-precipitation data across island locations has been identified. This is difficult for island locations because of the intra- and inter-island variability, which reduces the decorrelation scale for climatic variables making nearest-neighbour and regression-based approaches often sub-optimal/misleading. How well the island-station indices relate to the ERA-I and CMIP5 fields can be used to determine if such large-scale datasets are of use in simulating island climate extremes. So far there does not appear to have been a study that has dedicated application of the indices across island locations, so future work in this regard would be of great value.

Coastal Upwelling

The analysis in Chapter 6 used data at a monthly scale. If the analysis were repeated using daily data, it would be possible obtain more information about the wind fields favourable for upwelling (although daily data would only be available from reanalysis, where the coastal values were suspect, or from satellites, where there is a limited temporal-resolution). The extra analysis could include a cumulative upwelling index (sum of daily values across the year) and changes in the annual cycle (onset dates and transitions between regimes), which would offer more information into the physical evolution of upwelling (Bograd *et al.*, 2009). This could be applied not just across the CUE, but also to other regions where upwelling occurs.

Furthermore, no assessment (as far as the author is aware) of coastal upwelling has been carried out with the CMIP5 archive. Such an analysis could compare future upwelling potential to present day values, or compare the wind / ocean fields in the mid-Holocene simulations to those of the present day. Such assessments would be helpful in validating information found in sediment-core proxies taken from upwelling regions that span the Holocene (McGregor *et al.*, 2007). The future scenarios could be evaluated at daily and monthly resolutions but would require a long time to comprehensively undertake. It is suggested that after wind-speed fields are analysed, a 'detection and attribution' approach could be followed by analysing oceanic stratification and atmospheric water vapour to test potential contradictory mechanisms (i.e. the stratification 'stalling' and negative water vapour feedbacks) to the upwelling intensification hypothesis.

8. REFERENCES

Abe-Ouchi A, Saito F, Kawamura K, Raymo ME, Okuno J, Takaashi K and Blatter H, (2013), Insolation-drive 100,000-year glacial cycles and hysteresis of ice-sheet volume, *Nature*, **500**, 190-193

AEMET, Agencia Estatal de Meteorología, (2014a), *Hydrometeorological year 2011-2012 has been the driest in the Izaña Observatory record*, http://izana.aemet.es/index.php?option=com_content&view=article&id=290%3Ahydrometeorological-year-2011-2012-has-been-the-driest-in-the-izana-observatory-record&catid=10%3Anews&Itemid=49&lang=en, Accessed 2014

AEMET, Agencia Estatal de Meteorología, (2014b), The Izaña Observatory, Battered by a Strong winter Storm, (15th-18th February, 2014), http://izana.aemet.es/index.php?option=com_content&view=article&id=356%3Awinter-storm-feb-14&catid=10%3Anews&Itemid=49&lang=en, Accessed 2014

AEMET, Agencia Estatal de Meteorología, (2014c), Rainfall during the hydrometeorological year 2012-2013 was below average in Izaña, http://izana.aemet.es/index.php?option=com_content&view=article&id=346%3Arainfall-during-the-hydrometeorological-year-2012-2013-was-below-average-in-izana&catid=10%3Anews&Itemid=49&lang=en, Accessed 2014

Aguilar E, Auer I, Brunet M, Peterson TC, Wieringa J, (2003), WCDMP 53, *WMD/TD No, 1186: Guidelines on Climate Metadata and Homogenization*, World Meteorological Organization, Geneva, Switzerland

Alcoforado MJ, Vaquero JM, Trigo RM and Taborda JP, (2012), Early Portuguese meteorological measurements (18th century), *Climate of the Past*, **8**, 353-371

Alexander LV, Zhang X, Peterson TC, Caesar J, Gleason B, Klein Tank AMG, Haylock M, Collins D, Trewin B, Rahimzdeh F, Tagipour A, Kumar Kolli R, Revadekar JV, Griffiths G, Vincent L, Stephenson DB, Burn J, Aguilar E, Brunet M, Taylor M, New M, Zhai P, Rusticucci M, Vazquez Aguirre JL, (2006), Global observed changes in daily climate extremes of temperature and precipitation, *Journal of Geophysical Research: Atmospheres*, **111**, D05109

Alexanderson H, (1986), A homogeneity test applied to precipitation data, *Journal of Climatology*, **6**, 661–675

Allen R and Ansell T, (2006), A New Global Complete Monthly Historical Gridded Mean Sea Level Pressure Dataset (HadSLP2): 1850-2004, *Journal of Climate*, **19**, 5816-5842

An S-I and Wang B, (2001), Mechanisms of locking the El Nino and La Nina mature phases to boreal winter, *Journal of Climate*, **14**, 2164-2176

Ansell TJ, Jones PD, Allan RJ, Lister D, Parker DE, Brunet M, Moberg A, Jacobeit J, Brohan P, Rayner NA, Aguilar E, Alexandersson H, Barriendos M, Brandsma T, Cox NJ, Della-Marta PM, Drebs A, Founda D, Gerstengarbe F, Hickey K, Jonsson T, Luterbacher J, Nordli Ø, Oesterle H, Petrakis M, Philipp A, Rodwell MJ, Saladie O, Sigro J, Slonosky V, Srnec L, Swail V, Garcia-Suarez AM, Tuomenvirta H, Wang X, Wanner H, Werner P, Wheeler D and Xoplaki E, (2006), Daily mean sea level pressure reconstructions for the European – North Atlantic region for the period 1850 – 2003, *Journal of* Climate, **19**, 2717–2742

Anstey JA and Shepherd TG, (2014), High-latitude influence of the quasi-biennial oscillation, *Quarterly Journal of the Royal Meteorological Society*, **140**, 1-21

Arístegui J, Barton ED, Álvarez-Salgado XA, Santos AMP, Figueiras FG, Kifani S, Hernández-León S, Mason E, Machú E and Demarcq H, (2009), Sub-regional ecosystem variability in the Canary Current upwelling, *Progress in Oceanography*, **83**, 33-48

Ba J, Keenlyside NS, Park W, Latif M, Hawkins E and Ding H, (2013), A mechanism for Atlantic multidecadal variability in the Kiel Climate Model, *Climate Dynamics*, **41**, 2133-2144

Baines PG and Folland CK, (2007), Evidence for a rapid global climate shift across the late 1960s, *Journal of Climate*, **20**, 2721–2744

Bakun A, (1973), Coastal upwelling indices, west coast of North America, 1946-71, U.S. Dep. Commer., NOAA Tech. Rep., NMFS SSRF-671, 103p

Bakun A, (1990), Global climate change and intensification of coastal upwelling, *Science*, **247**, 198−201

Bakun A, (1992), Global greenhouse effects, multi-decadal wind trends and potential impacts on coastal pelagic fish populations, *ICES Marine Science Symposia*, **195**, 316-325

Bakun A and Agnostini VN, (2001), Seasonal patterns of wind-induced upwelling/downwelling in the Mediterranean Sea, *Scientia Marina*, **65**, 243-257

Bakun A and Nelson CS, (1991), The Seasonal Cycle of Wind-Stress Curl in Subtropical Eastern Boundary Current Regions, *Journal of Physical Oceanography*, **21**, 1815-1834

Bakun A, Field DB, Redondo-Rodriguez A and Weeks SJ, (2010), Greenhouse gas, upwelling-favorable winds, and the future of coastal ocean upwelling ecosystems, *Global Change Biology*, **16**, 1213–1228

Baldwin MP, Gray LJ, Dunkerton TJ, Hamilton K, Haynes PH, Randel WJ, Holton JR, Alexander MJ, Hirota, I, Horinouchi T, Jones DBA, Kinnersley JS, Marquardt C, Sato K, and Takahashi M, (2001), The quasi-biennial oscillation, *Reviews of Geophysics*, **39**, 179-229

Ball S, (2011), Exceptional rainfall in Gibraltar during winter 2009/10, *Weather*, **66**, 22–25

Balmaseda MA, Mogensen K and Weaver AT, (2013), Evaluation of the ECMWF ocean reanalysis system ORAS4, *Quarterly Journal of the Royal Meteorological Society*, **139**, 1132-1161

Barnston AG and Livezey RE, (1987), Classification, seasonality and persistence of low-frequency atmospheric circulation patterns, *Monthly Weather Review*, **115**, 1083-1126

Barry RG, (1992), Mountain Climatology and Past and Potential Future Climatic Changes in Mountain Regions: A Review, *Mountain Research and Development*, **12**, 71-86

Barry RG, (2008), *Mountain Weather and Climate 3rd Edition*, Cambridge University Press, Cambridge, United Kingdom and New York, NY, USA

Barton ED, (2001), *Ocean currents: Atlantic Eastern Boundary – Canary Current/ Portugal Current*, in Encyclopaedia of Ocean Sciences, Volume 1, Steele J, Thorpe S and Turekian K (eds), Academic Press, London, 380–389

Behringer DW, (2007), *The Global Ocean Data Assimilation System at NCEP*, 11th Symposium on Integrated Observing and Assimilation Systems for Atmosphere, Oceans and Land Surface, American Meteorological Society, San Antonio, Texas

Behinger DW, and Xue Y, (2004), *Evaluation of the global ocean data assimilation system at NCEP The Pacific Ocean*, Eighth Symposium on Integrated Observing and Assimilation Systems for Atmosphere, Oceans, and Land Surface, AMS 84th Annual Meeting, Washington State Convention and Trade Centre, Seattle, Washington, 11-15

Bellflamme A, Fettweis X and Erpicum M, (2015), Recent summer Arctic atmospheric circulation anomalies in a historical perspective, *The Cryosphere*, **9**, 53-64

Bergametti G, Gomes L, Coudé-Gaussen G, Rognon P and Le Coustumer M-N, (1989), African dust observed over Canary Islands: Source-regions identification and transport pattern for some summer situations, *Journal of Geophysical Research*, **94(D12)**, 14855–14864

Bethke J and Valente MA, (2012), *Homogeneity tests applied to FFCUL surface data*, Poster presentation, 5th ACRE Workshop, Toulouse, France, 28-30 November 2012

Bevan J, (2006), Tropical Cyclone Report, *Tropical Storm Delta*, National Hurricane Centre, http://www.nhc.noaa.gov/pdf/TCR-AL292005_Delta.pdf (accessed 7 February 2014)

Bielli S, Douville H and Pohl B, (2010), Understanding the West African monsoon variability and its remote effects: an illustration of the grid point nudging methodology, *Climate Dynamics*, **35**, 159–174

Björnsson H, (2013), *The seasonal cycle of just about everything*, Northern Hemisphere Polar Jet Stream and Links with Arctic Climate Change Workshop, Icelandic Meteorological Office, Reykjavik, Iceland, 13-15 November 2013

Björnsson H and Venegas SA, (1997), *A Manual of EOF and SVD Analysis of Climatic Data*, C2GCR Report, 97-1, McGill University

Björnsson H, Olason EO, Jónsson T and Henriksen S, (2007), Analysis of a smooth seasonal cycle with daily resolution and degree day maps for Iceland *Meteorologische Zeitschrift*, **16**, 57-69

Blake ES, Landsea CW, Gibney EJ, (2011), *The deadliest, costliest and most intense United States tropical cyclones from 1851 to 2010 (and other frequently requested hurricane facts)*, NOAA Technical Memorandum, NWS NHC-6

Blessing S, Fraedrich K, Junge M, Kunz T and Lunkeit F, (2005), Daily North-Atlantic Oscillation (NAO) index: Statistics and its stratospheric polar vortex dependence, *Meteorologische Zeitschrift*, **14**, 763-769

Bližňák V, Valente MA and Bethke JA, (2014), Homogenzation of time series from Portugal and its former colonies for the period from the late 19th to the early 21st century, *International Journal of Climatology*, Early Online View

Bograd SJ, Schroder I, Sarkar N, Qiu X, Sydeman WJ and Schwing FB, (2009), Phenology of coastal upwelling in the California Current, *Geophysical Research Letters*, **36**, L01602

Borja A, Uriarte A, Valencia V, Motos L and Uriarte A, (1996), Relationships between anchovy (Engraulis encrasicolus) recruitment and the environment in the Bay of Biscay, *Scientifica Marina*, **60(2)**, 179-192

Boucher O, Randall D, Artaxo P, Bretherton C, Feingold G, Forster P, Kerminen V-M, Kondo Y, Liao H, Lohmann U, Rasch P, Satheesh SK, Sherwood S, Stevens B and Zhang XY, (2013), *Clouds and Aerosols. In: Climate Change 2013: The Physical Science Basis. Contribution of Working Group I to the Fifth Assessment Report of the Intergovernmental Panel on Climate Change*, Cambridge University Press, Cambridge, United Kingdom and New York, NY, USA

Braganza K, Karoly DJ and Arblaster JM, (2004), Diurnal temperature range as an index of global climate change during the Twentieth Century, *Geophysical Research Letters*, **31**, L13217

Braun H, Christl M, Rahmstorf S, Ganopolski A, Mangini A, Kubatzki C, Roth K and Kromer B, (2005), Possible solar origin of the 1,470-year glacial climate cycle demonstrated in a coupled mode, *Nature*, **438**, 208-211

Brohan P, Kennedy JJ, Harris I, Tett SF and Jones PD, (2006), Uncertainty estimates in regional and global observed temperature changes: A new data set from 1850, *Journal of Geophysical Research: Atmospheres*, **111**, D12106

Brown DP, (2013), Tropical Cyclone Report, *Hurricane Nadine*, National Hurricane Centre, http://www.nhc.noaa.gov/data/tcr/AL142012_Nadine.pdf (accessed 1 March 2013)

Buishand TA, (1982), Some methods for testing the homogeneity of rainfall records, *Journal of Hydrology*, **58**, 11–27

Capone DG and Hutchins DA, (2013), Microbial biogeochemistry of coastal upwelling regimes in a changing ocean, *Nature Geoscience*, **6**, 711-717

Capotondi A, Alexander AM, Bond NA, Curchitser EN and Scott JD, (2012), Enhanced upper ocean stratification with climate change in the CMIP3 models, Journal of Geophysical Research – Oceans, 117, C04031

Cardone VJ, Greenwood JG and Cane MA, (1990), On trends in historical wind data, *Journal of Climate*, **3**, 113-127

Carton JA and Giese BS, (2008), A Reanalysis of Ocean Climate Using Simple Ocean Data Assimilation (SODA), *Monthly Weather Review*, **136**, 2999–3017

Cassou C, (2008), Intraseasonal interaction between the Madden–Julian Oscillation and the North Atlantic Oscillation, *Nature*, **455**, 523-527

Castelao RM and Barth JA, (2006), Upwelling around Cabo Frio, Brazil: The importance of wind-stress curl, *Geophysical Research Letters*, **33**, LO3602

Chavez FP, Messié M and Pennington JT. (2011), Marine primary production in relation to climate variability and change, *Annual Reviews of Marine Science*, **3**, 227-260

Cheung WWL, Watson, R and Pauly D, (2013), Signature of ocean warming in global fishers catch, *Nature*, **497**, 365-368

Christensen JH, Krishna Kumar K, Aldrian E, An SI, Cavalcanti IFA, de Castro M, Dong W, Goswami P, Hall A, Kanyanga JK, Kitoh A, Kossin J, Lau NC, Renwick J, Stephenson DB, Xie S-P and Zhou T, (2013), *Climate Phenomena and their Relevance for Future Regional Climate Change. In: Climate Change 2013: The Physical Science Basis. Contribution of Working Group I to the Fifth Assessment Report of the Intergovernmental Panel on Climate Change*, Cambridge University Press, Cambridge, United Kingdom and New York, NY, USA

Church JA and White NJ, (2011), Sea-level rise from the late 19th to the early 21st Century, *Surveys in Geophysics*, **32**, 585-602

Chylek P, Klett J, Lesins G, Dubey MK and Hengartner N, (2014), The Atlantic Multi-decadal Oscillation as a dominant factor of oceanic influence on climate, *Geophysical Research Letters*, Early Online View

Climate Atlas, (2012), *Climate atlas of the archipelagos of the Canary Islands, Madeira and the Azores*, The Meteorological State Agency of Spain and the Institute of Meteorology, Portugal, http://goo.gl/eAA1ta

Cohen JL, Furtado JC, Barlow M, Alexeev VA and Cherry JE, (2012), Asymmetric Seasonal Temperature trends, *Geophysical Research Letters*, **39**, L04705

Collins M, Knutti R, Arblaster J, Dufresne J-L, Fichefet T, Friedlingstein P, Gao X, Gutowski WJ, Johns T, Krinner G, Shongwe M, Tebaldi C, Weaver AJ and Wehner M, (2013), *Long-term Climate Change: Projections, Commitments and Irreversibility*, In: Climate Change 2013: The Physical Science Basis, Cambridge University Press, Cambridge, United Kingdom and New York, NY, USA.

Compo GP, Whitaker JS, Sardeshmukh PD, Matsui N, Allan RJ, Yin X, Gleason BE, Vose RS, Rutledge G, Bessemoulin P, Brönnimann S, Brunet M, Crouthamel RI, Grant AN, Groisman PY, Jones PD, Kruk MC, Kruger AC, Marshall GJ, Maugeri M, Mok HY, Nordli Ø, Ross TF, Trigo RM, Wang XL, Woodruff SD and Worley SJ, (2011), The Twentieth Century Reanalysis Project, *Quarterly Journal of the Royal Meteorological Society*, **137**, 1–28

Conover WL, (1980), *Practical nonparametric statistics 2nd Edition*, New York, John Wiley and Sons

Conrad V and Pollack C, (1962), *Methods in Climatology*, Harvard University Press

Cornes RC, (2010), *Early meteorological data from London and Paris: extending the North Atlantic Oscillation Series*, PhD thesis, University of East Anglia, https://ueaeprints.uea.ac.uk/10590/

Cornes RC, Jones PD, Briffa KR and Osborn TJ, (2013), Estimates of the North Atlantic Oscillation back to 1692 using a Paris-London westerly index, *International Journal of Climatology*, **33**, 228-248

Costa A and Soares A, (2009), Homogenization of climate data: review and new perspectives using geostatistics, *Mathematical Geosciences*, **41**, 291–305

Cowtan K and Way RG, (2014), Coverage bias in the HadCRUT4 temperature series and its impact on recent temperature trends, *Quarterly Journal of the Royal Meteorological Society*, In press

Cropper TE, (2013), The weather and climate of Macaronesia: past, present and future, *Weather*, **68**, 300-307

Cropper TE and Hanna E, (2014), An analysis of the climate of Macaronesia, 1865-2012, *International Journal of Climatology*, **34**, 604-622

Cropper TE, Hanna E and Bigg, GR, (2014), Spatial and temporal seasonal trends in coastal upwelling off northwest Africa, 1981–2012, *Deep-Sea Research I*, **86**, 94-111

Cropper TE, Hanna E, Valente MA and Jonsson T, (2015), A Daily Azores-Iceland North Atlantic Oscillation Index back to 1850, *Early Online View at Geoscience Data Journal*

Cullen HM, D'Arrigo RD, Cook ER and Mann ME, (2001), Multiproxy reconstructions of the North Atlantic Oscillation, *Palaeoceanography*, **16**, 27-39

Dai A and Wang J, (1999), Diurnal and Semidiurnal Tides in Global Surface Pressure Fields, *Journal of the Atmospheric Sciences*, **56**, 3874–3891

De La Torre L, Gimeno L, Añel JA and Nieto R, (2007), The role of the solar cycle in the relationship between the North Atlantic Oscillation and Northern Hemisphere surface temperatures, *Advances in Atmospheric Sciences*, **24**, 191-198

Dee DP, Uppala SM, Simmons AJ, Berrisford P, Poli P, Kobayashi S, Andrae U, Balmaseda MA, Balsamo G, Bauer P, Bechtold P, Beljaars ACM, van de Berg L, Bidlot J, Bormann N, Delsol C, Dragani R, Fuentes M, Geer AJ, Haimberger L, Healy SB, Hersbach H, Hólm EV, Isaksen L, Kållberg P, Köhler M, Matricardi M, McNally AP, Monge-Sanz BM, Morcrette J-J, Park B.K, Peubey C, de Rosnay P, Tavolato C, Thépaut J-N and Vitart F, (2011), The ERA-Interim reanalysis: configuration and performance of the data assimilation system, *Quarterly Journal of the Royal Meteorological Society*, **137**, 553–597

Delworth TL, Manabe S and Stouffer RJ, (1993), Interdecadal variations of the thermohaline circulation in a coupled ocean-atmosphere model, *Journal of Climate*, 6, 1993–2011

Deser C, Knutti R, Solomon S and Phillips A, (2012), Communication of the role of natural variability in future North American climate, *Nature Climate Change*, **2**, 775-779

Diaz HF, Giambelluca TW and Eischeid JK, (2011), Changes in the vertical profiles of mean temperature and humidity in the Hawaiian Islands, *Global and Planetary Change*, **77**, 21-25

Diffenbaugh NS, Snyder MA and Sloan LC, (2004), Could CO_2-induced land-cover feedbacks alter near-shore upwelling regimes? *Proceedings of the National Academy of Sciences*, **101**, 27–32.

Dima M and Lohmann G, (2007), A Hemispheric Mechanism for the Atlantic Multidecadal Oscillation, *Journal of Climate*, **20**, 2706-2719

Dippner JW, Möller C and Kröncke I, (2014), Loss of persistence of the North Atlantic Oscillation and its biological implication, *Frontiers in Ecology and Evolution*, **2**, 57

Donat MG Alexander LV, Yang H., Durre I, Vose R, Dunn RJH, Willett KM, Aguilar E, Brunet M, Caesar J, Hewitson B, Jack C, Klein Tank AMG, Kruger AC, Marengo J, Peterson TC, Renom M, Oria Rojas C, Rusticucci M, Salinger J, Elrayah AS, Sekele SS, Srivastava AK, Trewin B, Villarroel C, Vincent LA, Zhai P, Zhang X, and Kitching S, (2013) Updated analyses of temperature and precipitation extreme indices since the beginning of the twentieth century: The HadEX2 dataset, *Journal of Geophysical Research: Atmospheres*, **118**, 2098–2118

Eden C and Jung T, (2001), North Atlantic Interdecadal Variability: Oceanic Response to the North Atlantic Oscillation (1865–1997), *Journal of Climate*, **14**, 676-691

Elison-Timm O, Takahashi M, Giambelluca TW and Diaz HF, (2013), On the relation between large-scale circulation pattern and heavy rain events over the Hawaiian Islands: Recent trends and future changes, *Journal of Geophysical Research: Atmospheres*, **118**, 4129-4141

Enfield DB and Mayer DA, (1997), Tropical Atlantic sea surface temperature variability and its relation to El Niño-Southern Oscillation, *Journal of Geophysical Research: Oceans*, **102**, 929-945

England MH, McGregor S, Spence P, Meehl GA, Timmerman A, Cai W, Sen Gupta A, McPhaden MJ, Purich A and Santosa A, (2014), Recent intensification of wind-driven circulation in the Pacific and the ongoing warming hiatus, *Nature Climate Change*, **4**, 222-227

Falvey M and Garreaud RD, (2009), Regional cooling in a warming world: Recent temperature trends in the southeast Pacific and along the west coast of subtropical South America (1979-2006), *Journal of Geophysical Research*, **114**, D04102

Fereday DR, Maidens A, Arribas A, Scaife AA and Knight JR, (2012) Seasonal forecasts of Northern Hemisphere winter 2009/10, *Environmental Research Letters*, **7**, 034031

Fernández-Palacios JM, de Nascimento L, Otto R, Delgado D, García-del-Rey E, Arévalo JR and Whittaker RJ, (2011), A reconstruction of Palaeo-Macaronesia, with particular reference to the long-term biogeography of the Atlantic island laurel forests, *Journal of Biogeography*, **38**, 226-246

Fettweis X, Hanna E, Lang C, Bellflamme A, Erpicum M and H Gallée, (2012), Important role of the mid-tropospheric atmospheric circulation in the recent surface melt increase over the Greenland ice sheet, *The Cryosphere*, **7**, 241-248

Folland CK, Knight J, Linderholm HW, Fereday D, Ineson S and Hurrell JW, (2009), The summer North Atlantic Oscillation: past, present, and future. *Journal of Climate*, **22**, 1082–1103

Foster G and Rahmstorf S, (2011), Global temperature evolution 1979–2010, *Environmental Research Letters,* **6**, 044022

Fragoso M, Trigo RM, Pinto JG, Lopes S, Lopes A, Ulbrich S and Magro C, (2012), The 20 February 2010 Madeira flash-floods: synoptic analysis and extreme rainfall assessment, *Natural Hazards and Earth System Sciences*, **12**, 715-730

Francis JA and Vavrus SJ, (2012), Evidence linking Arctic amplification to extreme weather in mid-latitudes, *Geophysical Research Letters*, **39**, L06801

Frölich C, (2000), Observations of Irradiance Variations, *Space Science Reviews*, **00**, 1-10

Fründt B, Müller TJ, Schulz-Bull DE and Waniek JJ, (2013), Long-term changes in the thermocline of the subtropical Northeast Atlantic (33°N, 22°W), *Progress in Oceanography*, **116**, 246-260

Gallego D, García-Herrera R, Ribera P and Jones PD, (2005), Seasonal mean pressure reconstruction for the North Atlantic (1750–1850) based on early marine data, *Climate of the Past*, **1**, 19-33

Galvin JFP, (2007), The weather and climate of the tropics Part 2: The subtropical jet streams, *Weather*, **62**, 295-299

García-Herrera R, Gallego D, Hernandez E, Gimeno L and Ribera P, (2001), Influence of the North Atlantic oscillation on the Canary Islands precipitation, *Journal of Climate*, **14**, 3889–3903

García-Herrera R, Gallego D, Hernandez E, Gimeno L and Ribera P, (2003), Precipitation trends in the Canary Islands, *International Journal of Climatology,* **23**, 235–241

García-Herrera R, Können GP, Wheeler DA, Prieto MR, Jones PD and Koek FB, (2005), CLIWOC: A Climatological Database for the World's Oceans 1750-1854, *Climatic Change*, **73**, 1-12

García-Serrano J and Frankignoul C, (2014), High predictability of the winter Euro–Atlantic climate from cryospheric variability, *Nature Geoscience*, Early Online View

Garzón-Machado V, del Arco Aguilar MJ, González FV and Pérez-de-Paz, (2012), Fire as a threatening factor for endemic plants of the Canary Islands, *Biodiversity and Conservation*, **21**, 2621-2632

Gillett NP, Graf HF, Osborn TJ, (2003), Climate Change and the North Atlantic Oscillation, *Geophysical Monograph*, **134**, 193-209

Gillett NP and Fyfe JC, (2013), Annular mode changes in the CMIP5 simulations, *Geophysical Research Letters*, **40**, 1189-1193

Glickman TS, (2000), *Glossary of Meteorology, 2nd Edition*, American Meteorological Society, Boston, MA

Goerss J and Phoebus P, (1992), The Navy's operational atmospheric analysis, *Weather Forecasting*, **7**, 232-249

Gómez-Gesteira M, Moreira C, Álvarez I and deCastro M, (2006), Ekman transport along the Galician coast (NW, Spain) calculated from forecasted winds, *Journal of Geophysical Research*, **111**, C10005

Gómez-Gesteira M, deCastro M, Álvarez I and Gómez-Gesteira JL, (2008), Coastal sea surface temperature warming trend along the continental part of the Atlantic Arc (1985–2005). *Journal of Geophysical Research*, **113**, C04010

Gouirand I, Jury MR and Sing B, (2012), An Analysis of Low- and High-Frequency summer Climate Variability around the Caribbean Antilles, *Journal of Climate*, **25**, 3942-3952

Granato GE, (2006), *Kendall-Theil Robust Line (KTRLine—version 1.0)-A Visual Basic Program for Calculating and Graphing Robust Nonparametric Estimates of Linear-Regression Coefficients between Two Continuous Variables*, Techniques and Methods of the U.S. Geological Survey, **4(7)**, U.S. Geological Survey

Gray LJ, Crooks S, Pascoe C, Sparrow S and Palmer M, (2004), Solar and QBO Influences on the Timing of Stratospheric Sudden Warmings, *Journal of the Atmospheric Sciences*, **61**, 2777-2796

Gray LJ, Scaife AA, Mitchell DM, Osprey S, Ineson S, Hardiman S, Butchart N, Knight J, Sutton R and Kodera K, (2013), A lagged response to the 11 year solar cycle in observed winter Atlantic/European weather patterns, *Journal of Geophysical Research: Atmospheres*, **118**, 13,405–13,420

Gyory J, Mariano AJ and Ryan RH, (2014), *Ocean Surface Currents*, http://oceancurrents.rsmas.miami.edu/atlantic/canary.html http://oceancurrents.rsmas.miami.edu/atlantic/azores.html

Hagen E, Feistel R, Agenbag JJ and Ohde T, (2001), Seasonal and interannual changes in intense Benguela upwelling (1982-1999), *Oceanologica Acta*, **24**, 557-568

Hamed KH and Rao AR, (1998), A modified Mann-Kendall trend test for autocorrelated data, *Journal of Hydrology*, **204**, 182–196

Hanna E, Jonsson T, Olafsson J and Valdimarsson H, (2006), Icelandic coastal sea-surface temperature records constructed: putting the pulse on air-sea-climate interactions in the northern North Atlantic, Part 1: comparison with HadISST1 open ocean surface temperatures and preliminary analysis of long-term patterns and anomalies of SSTs around Iceland, *Journal of Climate*, **19(21)**, 5652–5666

Hanna E, Jones J, Cappelen J, Mernild SH, Wood L, Steffen K and Huybrechts P, (2012), The influence of North Atlantic atmospheric and oceanic forcing effects

on 1900–2010 Greenland summer climate and ice melt/runoff, *International Journal of Climatology*, **33**, 862-880

Hanna E, Jones JM, Cappelen J, Mernild SH, Wood L, Steffen K and Huybrechts P, (2013), The influence of North Atlantic atmospheric and oceanic forcing effects on 1900–2010 Greenland summer climate and ice melt/runoff, *International Journal of Climatology*, **33**, 862–880

Hanna E, Cappelen J, Fettweis X, Mernild SH, Mote T, Steffen K and Wood L, (2014), Atmospheric and oceanic climatic forcing of the exceptional Greenland Ice Sheet surface melt in summer 2012, *International Journal of Climatology*, **34**, 1022–1037

Hanna E, Cropper TE, Jones PD, Scaife AA and Allan R, (2015), Recent seasonal asymmetric changes in the NAO: a marked summer decline and increased winter variability, Early Online View at *International Journal of Climatology*

Hannachi A, Jolliffe IT and Stevenson DB, (2007), Empirical orthogonal functions and related techniques in atmospheric science: A review, *International Journal of Climatology*, **27**, 1119-1152

Hansen J, Ruedy R, Sato M and Lo K, (2010), Global surface temperature change, *Reviews of Geophysics*, **48(4)**, RG4004

Hansen J, Sato M, Russell G and Kharecha P, (2013a), Climate sensitivity, sea level and atmospheric carbon dioxide, *Philosophical Transactions of the Royal Society A*, **371**, 20120294

Hansen J, Kharecha P, Sato M, Masson-Delmotte V, Ackerman F, Beerling DJ, Hearty PJ, Hoegh-Guldberg O, Hsu S-L, Parmesan C, Rockstrom J, Rohling EJ, Sachs J, Smith P, Steffen K, Van Susteren L, von Schuckmann K, Zachos JC, (2013b), Assessing "Dangerous Climate Change": Required Reduction of Carbon Emissions to Protect Young People, Future Generations and Nature, *PLoS One*, **8(12)**, e81648

Harris MF, Finger FG and Teweles S, (1962), Diurnal variation of wind, pressure, and temperature in the troposphere and stratosphere over the Azores, *Journal of the Atmospheric Sciences*, **19(2)**, 136–149

Hartmann DL, Klein Tank AMG, Rusticucci M, Alexander LV, Brönnimann S, Charabi Y, Dentener FJ, Dlugokencky EJ, Easterling DR, Kaplan A, Soden BJ, Thorne PW, Wild M and Zhai PM, (2013), *Observations: Atmosphere and Surface. In: Climate Change 2013: The Physical Science Basis. Contribution of Working Group I to the Fifth Assessment Report of the Intergovernmental Panel on Climate Change*, Cambridge University Press, Cambridge, United Kingdom and New York, NY, USA

Held IM and Soden BJ, (2006), Robust Responses of the Hydrological Cycle to Global Warming, *Journal of Climate*, **19**, 5686-5699

Henriksen S, (2003), *Report on the approximation of the annual cycle of temperature in Iceland*, Technical Report 03006, Icelandic Meteorological Office, Reykjavik, Iceland, 16 pp

Herbert TD, (2001), Review of alkenone calibrations (culture, water column, and sediments), *Geochemistry Geophysics Geosystems*, **2**, 2000GC000055

Hewitt NC and Jackson AV, (2009), *Atmospheric Science for Environmental Scientists*, Wiley-Blackwell, Malaysia

Hoerling MP, Eischeid J and Perlwitz J, (2010), Regional precipitation trends: distinguishing natural variability from anthropogenic forcing, *Journal of Climate*, **23(8)**, 2131–2145

Hoogakker BAA, Chapman M, McCave N, Hillaire-Marcel C, Ellison C, Hall IR and Telford RJ, (2011), Dynamics of North Atlantic deep water masses during the Holocene, *Palaeoceanography*, **26(4)**, PA4214

Hsieh WW and Boer GJ, (1992), Global climate change and ocean upwelling, *Fisheries Oceanography*, **1**, 333-338

Hurrell JW, (1995), Decadal trends in the North Atlantic oscillation: regional temperatures and precipitation, *Science*, **269**, 676–679

Hurrell JW and van Loon H, (1997), *Decadal variations in climate associated with the North Atlantic Oscillation*, In Climatic Change at High Elevation Sites, 69-94, springer Netherlands

Huyer A, Smith R and Paluszkiewicz T, (1987), Coastal upwelling off Peru during normal and El Niño times, 1981–1984, *Journal of Geophysical Research*, **92**, 14297–14307

Ineson S, Scaife AA, Knight JR, Manners JC, Dunstone NJ, Gray LJ and Haigh JD, (2011), Solar forcing of winter climate variability in the Northern Hemisphere, *Nature Geoscience*, **4**, 753-757

Jain SK and Kumar V, (2012), Trend analysis of rainfall and temperature data for India, *Current Science India*, **102(1)**, 37–49

Johanson CM and Fu Q, (2009), Hadley Cell Widening: Model Simulations versus Observations, *Journal of Climate*, **22**, 2713-2725

Joly M and Voldoire A, (2009), Influence of ENSO on the West African Monsoon: Temporal Aspects and Atmospheric Processes, *Journal of Climate*, **22** 3193-3210

Jones PD, Jónsson T and Wheeler D, (1997), Extension to the North Atlantic Oscillation using early instrumental pressure observations from Gibraltar and south-west Iceland. *International Journal of Climatology*, **17**, 1433-1450

Jones PD, New M, Parker DE, Martin S and Rigor IG, (1999a), Surface air temperature and its changes over the past 150 years, *Reviews of Geophysics*, **37(2)**, 173-199

Jones PD, Davies TD, Lister DH, Slonosky V, Jónsson T, Bärring L, Jönsson P, Maheras P, Kolyva-Machera F, Barriendos M, Martin-Vide J, Rodriguez R, Alcoforado MJ, Wanner H, Pfister C, Luterbacher J, Rickli R, Schuepbach E, Kaas E, Schmith T, Jacobeit J and Beck C, (1999b), Monthly mean pressure reconstructions for Europe for the 1780-1995 period, *International Journal of Climatology*, **19**, 347–264

Jónsson T and Miles MW, (2001), Anomalies in the seasonal cycle of sea level pressure in Iceland and the North Atlantic Oscillation, *Geophysical Research Letters*, **22**, 4231-4234

Jónsson T and Garđarsson H, (2001), *Early Instrumental Meteorological Observations in Iceland*, In The Iceberg in the Mist: Northern Research in pursuit of a "Little Ice Age", 169-187

Jónsson T and Hanna E, (2007), A new day-to-day pressure variability index as a proxy of Icelandic storminess and complement to the North Atlantic Oscillation index 1823-2005, *Meteorologische Zeitschrift*, **16**, 25-36

Kalnay E, Kanamitsu M, Kistler R, Collins W, Deaven D, Gandin L, Iredell M, Saha S, Woollen J, Zhu Y, Chelliah M, Ebisuzaki W, Higgins W, Janowiak J, Mo KC, Ropelewski C, Wang J, Leetmaa A, Reynolds R, Jenne R and Joseph D, (1996), The NCEP/NCAR 40-year reanalysis project, *Bulletins of the American Meteorological Society*, **77**, 437ñ471

Kanamitsu M, Ebisuzaki W Woollen J, Yang S-K, Hnilo JJ, Fiorino M and Potter GL, (2002), NCEP–DOE AMIP-II Reanalysis (R-2). *Bulletin of the American Meteorological Society*, **83**, 1631–1643

Kang HM and Yusof F, (2012), Homogeneity Tests on Daily Rainfall Series in Peninsular Malaysia, *International Journal of Contemporary Mathematical Sciences*, **7**, 9-22

Kendall MG, (1938), A new measure of rank correlation, *Biometrika*, **30**, 81–93

Kennedy JJ, Brohan P and Tett SFB, (2007), A global climatology of the diurnal variations in 1 sea-surface temperature and implications for MSU 2 temperature trends, *Geophysial Research Letters*, **34**, L05712

Kent EC, Woodruff SD and Berry DI, (2007), Metadata from WMO Publication No. 47 and an Assessment of Voluntary Observing Ship Observation Heights in ICOADS, *Journal of Atmospheric and Oceanic Technology*, **24**, 214–234

Kent EC, Fangohr S and Berry DI, (2013), A Comparative assessment of monthly mean wind-speed products over the global ocean, *International Journal of Climatology,* **33**, 2520-2541

Klein Tank AMG, Wijngaard JB, Können GP, Böhm R, Demarée G, Gocheva A, Mileta M, Pashiardis S, Hejkrlik L, Kern-Hansen C, Heino R, Bessemoulin P, Müller-Westermeier G, Tzanakou M, Szalai S, Pálsdóttir T, Fitzgerald D, Rubin S, Capaldo M, Maugeri M, Leitass A, Bukantis A, Aberfeld R, van Engelen AFV, Forland E, Mietus M, Coelho F, Mares C, Razuvaev V, Nieplova E, Cegnar T, Antonio López J, Dahlström B, Moberg A, Kirchhofer W, Ceylan A, Pachaliuk O, Alexander LV and Petrovic P, (2002), Daily dataset of 20th century surface air temperature and precipitation series for the European climate assessment, *International Journal of Climatology*, **22**, 1444–1453

Knight JR, Allan RJ, Folland CK, Vellinga M and Mann ME, (2005), A signature of persistent natural themohaline circulation cycles in observed climate, *Geophysical Research Letters*, **32**, L20708

Knudsen MF, Seidenkrantz M, Jacobsen BH and Kuijpers A, (2011), Tracking the Atlantic Multidecadal Oscillation through the last 8,000 years, *Nature Communications*, 2, 178

Kondrashov D and Ghil M, (2006), Spatio-temporal filling of missing points in geophysical data sets, *Nonlinear Processes in Geophysics*, **13**, 151-159

Laing A and Evans J-L, (2014), *Introduction to Tropical Meteorology 2nd Edition*, http://www.goes-r.gov/users/comet/tropical/textbook_2nd_edition/index.htm "The source of this material is the COMET® Website at http://meted.ucar.edu/ of the University Corporation for Atmospheric Research (UCAR), sponsored in part through cooperative agreement(s) with the National Oceanic and Atmospheric Administration (NOAA), U.S. Department of Commerce (DOC). ©1997-2015 University Corporation for Atmospheric Research. All Rights Reserved."

Lau KM and Kim KM, (2007), Cooling of the Atlantic by Saharan dust, *Geophysical Research Letters*, **34**, L23811

Lawrimore JH, Menne MJ, Gleason BE, Williams CN, Wuertz DB, Vose RS and Rennie J, (2011), An overview of the Global Historical Climatology Network monthly mean temperature data set, version 3, *Journal of Geophysical Research*, **116**, D19121

Lean JL and Rind DH, (2008), How natural and anthropogenic influences alter global and regional surface temperatures: 1889 to 2006, *Geophysical Research Letters*, **35**, L18701

Lehner F, Raible CC and Stocker TF, (2012), Testing the robustness of a precipitation proxy-based North Atlantic Oscillation reconstruction, *Quaternary Science Reviews*, **45**, 85-94

Levitus S, Antonov JI, Boyer TP, Baranova OK, Garcia HE, Locarninil RA, Mishonovl AV, Reagan JR, Seidov D, Yarosh ES and Zweng MM, (2012),

World ocean heat content and thermosteric sea level change (0–2000 m), 1955–2010, *Geophysical Research Letters*, **39**, L10603

Levizzani V, Laviola S, Cattani E and Costa MJ, (2013), Extreme precipitation on the Island of Madeira on 20 February 2010 as seen by satellite passive microwave sounders, *Internatinoal Journal of Remote Sensing*, **46**, 475-489

Li J and Zeng Q, (2002), A unified monsoon index, *Geophysical Research Letters*, **29**, 115-1-115-4

Liu C and Allan RP, (2013), Observed and simulated precipitation responses in wet and dry regions 1850-2100, *Environmental Research Letters*, **8**, 034002

Lu J and Delworth TL, (2005), Oceanic forcing of the late 20th century Sahel drought, *Geophysical Research Letters*, **32**, L22706

Lu J, Vecchi GA and Reichler, (2007), Expansion of the Hadley cell under global warming, *Geophysical Research Letters*, **34**, L06805

Lu J, Hu A and Zeng Z, (2014), On the possible interaction between internal climate variability and forced climate change, *Geophysical Research Letters*, **41**, 2962ñ2970

Luna T, Rocha A, Carvalho AC, Ferreira JA and Sousa J, (2011), Modelling the extreme precipitation event over Madeira Island on 20 February 2010. Natural Hazards and Earth System Sciences, **11**, 2437-2452

Lungu, T, Callahan PS, Dunbar S, Weiss B, Stiles B, Huddleston J, Shirtcliffe G, Perry KL, Hsu C, Mears C, Wentz F, Smith D, (2006), *QuikSCAT Science Data Product User's Manual. Version 3.0.* ftp://podaac.jpl.nasa.gov/ocean_wind/quikscat/L2B/doc/QSUG_v3.pdf

Luterbacher J, Schmutz C, Gyalistras D, Xoplaki E and Wanner H, (1999), Reconstruction of monthly NAO and EU indices back to AD 1675, *Geophysical Research Letters*, **26**, 2745-2748

Ly M, Traore SB, Alhassane A and Sarr B, (2013), Evolution of some observed climate extremes in the West African Sahel, *Weather and Climate Extremes*, **1**, 19-25

Mann HB, (1945), Nonparametric tests against trend, *Econometrica*, **13**, 245-259

Mannaerts CM and Gabriels D, (2000), Rainfall erosivity in Cape Verde, *Soil and Tillage Research*, **55**, 207–212

Manola I, Haarsma RJ and Hazeleger W, (2013), Drivers of North Atlantic Oscillation Events, *Tellus A*, **65**, 19741

Marcello J, Hernandez-Guerra A, Eugenio F and Fonte A, (2011), Seasonal and temporal study of the northwest African upwelling system, *International Journal of Remote Sensing*, **32**, 1843-1859

Marcott SA, Shakun JD, Clark PU and Mix AC, (2013), A reconstruction of Regional and Global Temperature for the Past 11,300 Years, *Science*, **339**, 1198-1201

Martin ER and Thorncroft C, (2014), The impact of the AMO on the West African Monsoon Annual Cycle, *Quarterly Journal of the Royal Meteorological Society*, **140**, 31-46

Martín JL, Bethencourt J and Cuevas-Agullo E, (2012), Assessment of global warming on the island of Tenerife, Canary Islands (Spain), Trends in minimum, maximum and mean temperatures since 1944, *Climatic Change*, **144**, 343–355

Masson-Delmotte V, Schulz M, Abe-Ouchi A, Beer J, Ganopolski A, Gonz·lez Rouco JF, Jansen E, Lambeck K, Luterbacher J, Naish T, Osborn T, Otto-Bliesner B, Quinn T, Ramesh R, Rojas M, Shao X and Timmermann A, (2013), *Information from Palaeoclimate Archives*. In: Climate Change 2013: The Physical Science Basis. Contribution of Working Group I to the Fifth Assessment Report of the Intergovernmental Panel on Climate Change, Cambridge University Press, Cambridge, United Kingdom and New York, NY, USA

McGregor HV, Dima M, Fischer HW and Militza S, (2007), Rapid 20th-Century Increase in Coastal Upwelling off northwest Africa, *Science*, **315**, 637-639

McSweeney C, Lizcano G, New M and Lu X, (2010), The UNDP climate change country profiles, *Bulletin of the American Meteorological Society*, **91**, 157–166

Miranda PMA, Alves JMR and Serra N, (2012), Climate change and upwelling: response of Iberian upwelling to atmospheric forcing in a regional climate scenario, *Climate Dynamics*, **40**, 2813-2824

Moody JA and Ebel BA, (2012), Hyper-dry conditions provide new insights into the cause of extreme floods after wildfire, *CATENA*, **93**, 58-63

Morice CP, Kennedy JJ, Rayner NA and Jones PD, (2012), Quantifying uncertainties in global and regional temperature change using an ensemble of observational estimates: The HadCRUT4 data set, *Journal of Geophysical Research*, **117(D8)**, D08101

Morozova AL and Valente MA, (2012), Homogenization of Portuguese long-term temperature data series: Lisbon, Coimbra and Porto, *Earth System Science Data*, **4**, 187-213

Mote PW and Mantua NJ, (2002), Coastal upwelling in a warmer future, *Geophysical Research Letters*, **29**, 2138

Narayan N, Paul A, Mulitza S and Schulz M, (2010), Trends in coastal upwelling intensity during the late 20th century, *Ocean Science*, **7**, 335-360

Niang I, Ruppel OC, Abdrabo M, Ama Essel A, Lennard C, Padgham J and Urquhart P, (2013), *Chapter 22: Africa*, IPCC AR5 WGII, Final Draft, Cambridge University Press, Cambridge, United Kingdom and New York, NY, USA

Nicholson SE, (2013), The West African Sahel: A Review of Recent Studies on the Rainfall Regime and Its Interannual Variability, *ISRN Meteorology*, 2013, 32p

Niiler PP, Maximenko NA and McWilliams JC, (2003), Dynamically balanced absolute sea level of the global ocean derived from near-surface velocity observations, Geophysical Research Letters, **30(22)**, 2164

Neris J, Tejedor M, Fuentes J and Jiménez C, (2013), Infiltration, runoff and soil loss in Andisols affected by forest fire (Canary Islands, Spain), *Hydrological Processes*, **27**, 2814-2824

Nykjaer L and Van Camp L, (1994), Seasonal and interannual variability of coastal upwelling along northwest Africa and Portugal from 1981 to 1991, *Journal of Geophysical Research*, **99**, 14197-14207

Oliver JE, (2005), *Encyclopaedia of World Climatology*, springer, The Netherlands

Olsen AD and Eggert P, (2013), *Internet Assigned Numbers Authority Time Zone Database*, ftp://ftp.iana.org/tz/data/europe, (Accessed on 21/12/2013)

Osborn TJ, (2011), winter 2009/10 temperatures and a record-breaking North Atlantic Oscillation index, *Weather*, **66**, 19-21

Ottersen G, Planque B, Belgrano A, Post E, Reid PC and Stenseth NC, (2001), Ecological effects of the North Atlantic Oscillation, *Oecologia*, **128**, 1-14

Overland JE, Rodionov S, Minobe S and Bond N, (2008), North Pacific regime shifts: definitions, issues and recent transitions, *Progress in Oceanography*, **77**, 92–102

Overland JE, Francis JA, Hanna E, and Wang M, (2012), The recent shift in early summer Arctic atmospheric circulation, *Geophysical Research Letters*, **39**, L19804

Pardo PC, Padin XA, Gilcoto M, Farina-Busto L and Pérez FF, (2011), Evolution of upwelling systems coupled to the long-term variability in sea surface temperature and Ekman transport, *Climate Research*, **48**, 231-246

Patricola CM and Cook KH, (2007), Dynamics of the West African Monsoon under Mid-Holocene Precessional Forcing: Regional Climate Model Simulations, *Journal of Climate*, **20**, 694-716

Pauly D and Christensen V, (1995), Primary production required to sustain global fisheries, *Nature*, **374**, 255-257

Payne MR, (2013), Fisheries: Climate change at the dinner table, *Nature*, **497**, 320-321

Peel MC, Finlayson BL and McMahon TA, (2007), Updated world map of the Köppen–Geiger climate classification, *Hydrology and Earth System Sciences*, **11**, 1633–1644

Pérez-Brunius P, Lopez M, Parés-Sierra A and Pineda J, (2007), Comparison of upwelling indices off Baja California derived from three different wind data sources, *CalCOFI Report*, **48**, 204-214

Peterson TC, Easterling DR, Karl TR, Groisman P, Nicholls N, Plummer N, Torok S, Auer I, Boehm R, Gullett D, Vincent L, Heino R, Tuomenvirta H, Mestre O, Szentimrey T, Salinger J, Førland EJ, Hanssen-Bauer I, Alexandersson H, Jones P and Parker D, (1998), Homogeneity adjustments of in situ atmospheric climate data: a review, *International Journal of Climatology*, **18**, 1493–1517

Pettitt AN, (1979), A nonparametric approach to the change-point problem, *Journal of the Royal Statistical Society, Series C (Applied Statistics)*, **28**, 126–135

Philipp A, Della-Marta PM, Jacobeit J, Fereday DR, Jones PD, Moberg A and Wanner H, (2007), Long-Term Variability of Daily North Atlantic–European Pressure Patterns since 1850 Classified by Simulated Annealing Clustering, *Journal of Climate*, **20**, 4065–4095

Pickett MH and Paduan JD, (2003), Ekman transport and pumping in the California Current based on the U.S. Navy's high-resolution atmospheric model (COAMPS), *Journal of Geophysical Research*, **108**, 3327

Planton S, (2013), *Annex III Glossary. In: Climate Change 2013: The Physical Science Basis. Contribution of Working Group I to the Fifth Assessment Report of the Intergovernmental Panel on Climate Change*, Cambridge University Press, Cambridge, United Kingdom and New York, NY, USA, p.1450-1451

Polyakova EI, Journel AG, Polyakov IG and Bhatt US, (2006), Changing relationship between the North Atlantic Oscillation and key North Atlantic climate parameters, *Geophysical Research Letters*, **33**, L03711

Pozo-Vázquez D, Esteban-Parra MJ, Rodrigo FS and Castro-Díez Y, (2000), An analysis of the variability of the North Atlantic Oscillation in the time and the frequency domains, *International Journal of Climatology*, **20**, 1675-1692

Prospero JM and Lamb PJ, (2003), African droughts and dust transport to the Caribbean: Climate change implications, *Science*, **302**, 1024– 1027

Ramage CS, (1987), Secular change in reported wind-speeds over the ocean, *Journal of Climate and Applied Meteorology*, **26**, 525-528

Rayner NA, Parker DE, Horton EB, Folland CK, Alexander LV, Rowell DP, Kent EC and Kaplan A, (2003), Global analyses of sea surface temperature, sea ice, and night marine air temperature since the late nineteenth century, *Journal of Geophysical Research,* **108**, 4407, D14

Rayner NA, Brohan P, Parker DE, Folland CK, Kennedy JJ, Vanicek M, Ansell TJ and Tett SFB, (2006), Improved Analyses of Changes and Uncertanties in Sea Surface Temperature Measured In Situ since the Mid-Nineteenth Century: The HadSST2 Dataset, *Journal of Climate*, **19**, 446-469

Reeves J, Chen J, Wang XL, Lund R and Lu Q, (2007), A Review and Comparison of Changepoint Detection Techniques for Climate Data, *Journal of Applied Meteorology and Climatology*, **46**, 900-915

Reynolds RW, Smith TM, Liu C, Chelton DB, Casy KS, and Schlax MG, (2007), Daily high Resolution-Blended Analysis for Sea Surface Temperatures, *Journal of Climate*, **20**, 5473-5496

Rienecker MM, Suarez MJ, Gelaro R, Todling R, Bacmeister J, Liu E, Bosilovich MG, Schubert SG, Takacs L, Kim GK, Bloom S, Chen J, Collins D, Conaty S, da Silva A, Gu W, Joiner J, Koster RD, Lucchesi R, Molod AM, Owens T, Pawson S, Pegion P, Redder CR, Reichle R, Robertson FR, Ruddick AG, Sienkiewicz M and Woollen J, (2011), MERRA – NASA's Modern-Era Retrospective Analysis for Research and Applications, *Journal of Climate*, **24**, 3624–3648

Rohde R, Muller RA, Jacobsen R, Muller E, Perlmutter S, Rosenfeld A, Wurtele J, Groom D and Wickham C, (2013), A New Estimate of the Average Earth Surface Land Temperature Spanning 1753 to 2011, *Geoinformation and Geostatistics: An Overview*, **1**, 1

Saha S, Moorthi S, Pan H-L, Wu X, Wang J, Nadiga S, Tripp P, Kistler R, Woollen J, Behringer D, Liu H, Stokes D, Grumbine R, Gayno G, Wang J, Hou Y-T, Chuang H-Y, Juang H-MH, Sela J, Iredell M, Treadon R, Kleist D, Van Delst P, Keyser D, Derber J, Ek M, Meng J, Wei H, Yang R, Lord S, van den Dool H, Kumar A, Wang W, Long C, Chelliah M, Xue Y, Huang B, Schemm J-K, Ebisuzaki W, Lin R, Xie P, Chen M, Zhou S, Higgins W, Zou C-Z, Liu Q, Chen Y, Han Y, Cucurull L, Reynolds RW, Rutledge G and Goldberg M, (2010), The NCEP Climate Forecast System Reanalysis, *Bulletin of the American Meteorological Society*, **91**, 1015–1057

Sanchez-Moreno JF, Mannaerts CM and Jetten V, (2014), Influence of topography on rainfall variability in Santiago Island, Cape Verde, *International Journal of Climatology*, Early Online View

Santer BD, Wigley TML, Boyle JS, Gaffen DJ, Hnilo JJ, Nychka D, Parker DE and Taylor KE, (2000), Statistical significance of trends and trend differences in layer average atmospheric temperature time series, *Journal of Geophysical Research*, **105(D6)**, 7337-7356

Santos C, Lima M, Montiel R, Angles N, Pires L, Abade A and Aluja MP, (2003), Genetic structure and origin of peopling in the Azores islands (Portugal): the view from mtDNA., *Annals of Human Genetics*, **67**, 433-56

Santos FD, Valente MA, Miranda PMA, Aguiar A, Azevedo EB, Tome AR and Coelho F, (2004), Climate Change Scenarios in the Azores and Madeira Islands, *World Resource Review*, **16**, 473-491

Santos AM, Kazmin AS and Peliz A, (2005), Decadal changes in the Canary upwelling system as revealed by satellite observations: their impact on productivity, *Journal of Marine Research,* **63**, 359–379

Santos F, Gómez-Gesteira M, deCastro M and Álvarez I, (2012), Differences in coastal and oceanic SST warming rates along the Canary upwelling ecosystem from 1982 to 2010, *Continental Shelf Research*, **47**, 1-6

Saraceno M, Strub PT and Kosro PM, (2008), Estimates of sea surface height and near-surface along-shore coastal currents from combinations of altimeters and tide gauges, *Journal of Geophysical Research*, **113**, C11013

Scaife AA, Ineson S, Knight JR, Gray L, Kodera K and Smith DM, (2013), A mechanism for lagged North Atlantic climate response to solar variability, *Geophysical Research Letters*, **40**, 434–439

Scaife AA, Arribas A, Blockley E, Brookshaw A, Clark R, Dunstone N, Eade R, Fereday D, Folland CK, Gordon M, Hermanson L, Knight JR, Lea DJ, MacLachlan C, Maidens A, Martin M, Peterson AK, Smith D, Vellinga M, Wallace E, Waters J and Williams A, (2014), Skilful Long Range Prediction of European and North American winters, Geophysical Research Letters, Early Online View

Schneider T, Bischoff T and Haug GH, (2014), Migrations and dynamics of the intertropical convergence zone, *Nature*, **513**, 45-53

Schöne BR, Oschmann W, Rössler J, Freyre Castro AD, Houk SD, Kröncke I, Dreyer W, Janssen R, Rumohr H and Dunca E, (2003), North Atlantic Oscillation dynamics recorded in shells of a long-lived bivalve mollusk, *Geology*, **31**, 1037-1040

Schwing FB, O'Farrell M, Steger JM and Baltz K, (1996), Coastal upwelling indices, West Coast of North America, 1946–1995, NOAA Tech. Memo, NOAA-TM-NMFS-SWFSC-231, 144 pp

Sen PK, (1968), Estimates of the regression coefficient based on Kendall's tau, *Journal of the American Statistical Association*, **63**, 1379–1389

Serreze MC, Carse F, Barry RG and Rogers JC, (1997), Icelandic Low Cyclone Activity: Climatological Features, Linkages with the NAO, and Relationships with Recent Changes in the Northern Hemisphere Circulation, *Journal of Climate*, **10**, 453-465

Shanahan TM, Overpeck JT, Anchukaitis KJ, Beck JW, Cole JE, Dettman DL, Peck JA, Scholz CA and Wing JW, (2009), Atlantic forcing of persistent drought in West Africa, *Science*, **324**, 377–380

Shepherd TG, (2014), Atmospheric circulation as a source of uncertainty in climate change projections, *Nature Geoscience*, **7**, 703-708

Siedler G, Armi L and Müller TJ, (2005), Meddies and decadal changes at the Azores Front from 1980 to 2000, *Deep-Sea Research II*, **52**, 583-604

Siler N and Roe G, (2014), How Will Orographic Precipitation Respond to Surface Warming?–An Idealized Thermodynamic Perspective, *Geophysical Research Letters*, **41**, Early Online View

Sillmann J, Kharin VV, Zwiers, FW, Zhang X and Bronaugh D, (2013a), Climate extremes indices in the CMIP5 multi-model ensemble. Part 1: Model evaluation in the present climate, *Journal of Geophysical Research – Atmospheres*, **4**, 1716-1733

Sillmann J, Kharin VV, Zwiers, FW, Zhang X and Bronaugh D, (2013b), Climate extremes indices in the CMIP5 multi-model ensemble. Part 2: Future projections, *Journal of Geophysical Research – Atmospheres*, **6**, 2473-2493

Siongco AC, Stevens B and Hohenegger C, (2014), Precipitation biases over the tropical Atlantic in low and high-resolution CMIP5 models, *Geophysical Research Abstracts*, EGU2014-1379

Smith SR, Legler DM and Verzone KV, (2001), Quantifying Uncertainties in NCEP Reanalyses Using High-Quality Research Vessel Observations, *Journal of Climate*, **14**, 4062–4072

Snyder MA, Sloan LC, Diffenbaugh NS and Bell JL, (2003), Future climate change and upwelling in the California Current, *Geophysical Research Letters*, **30**, 1823

Sperling FN, Wasingthon R and Wittaker RJ, (2004), Future climate change of the subtropical north Atlantic: implications for the cloud forests of Tenerife, *Climatic Change*, **65(1–2)**, 103–123

Stephenson TS, Vincent LA, Allen T, Van Meerbeeck CJ, McLean N, Peterson TC, Taylor MA, Aaron-Morrison AP, Auguste T, Bernard D, Boekhoudt JRI, Blenman RC, Braithwaite GC, Brown G, Butler M, Cumberbatch CJM, Etienne-Leblanc S, Lake DE, Martin DE, McDonald JL, Ozoria Zaruela M, Porter AO, Santana Ramirez M, Tamar GA, Roberts BA, Sallons Mitro S, Shaw A, Spence JM, winter A and Trotman AR, (2014), Changes in extreme temperature and precipitation in the Caribbean region, 1961–2010, *International Journal of Climatology*, Early Online View

Stern H and Davidson NE, (2015), Trends in the Skill of Weather Prediction at Lead Times of 1 to 14 Days, *Quarterly Journal of the Royal Meteorological Society*, Early Online View

Stickler A, Brönnimann S, Valente MA, Bethke J, Sterin A, Jourdain S, Roucaute E, Vasquez MV, Reyes DA, Allan R and Dee D, (2014), ERA-CLIM: Historical Surface and Upper-Air Data for Future Reanalyses, *Bulletin of the American Meteorological Society*, **95**, 1419-1430

Stocker TF, Qin D, Plattner GK, Alexander LV, Allen SK, Bindoff NL, Bréon FM, Church JA, Cubasch U, Emori S, Forster P, Friedlingstein P, Gillett N, Gregory JM, Hartmann DL, Jansen E, Kirtman B, Knutti R, Krishna Kumar K, Lemke P, Marotzke J, Masson-Delmotte V, Meehl GA, Mokhov II, Piao S, Ramaswamy V, Randall D, Rhein M, Rojas M, Sabine C, Shindell D, Talley LD, Vaughan DG and Xie S-P, (2013), *Technical Summary. In: Climate Change 2013: The Physical Science Basis. Contribution of Working Group I to the Fifth Assessment Report of the Intergovernmental Panel on Climate Change*, Cambridge University Press, Cambridge, United Kingdom and New York, NY, USA

Sutton RT and Dong B, (2012), Atlantic Ocean influence on a shift in European climate in the 1990s, *Nature Geoscience*, **5**, 788-792

Sverdrup HV, (1938), On the process of upwelling, *Journal of Marine Research*, **2**, 155-164

Sydeman WJ, Garcia-Reyes M, Schoeman DS, Rykaczewski RR, Thompson SA, Black BA and Bograd SJ, (2014), Climate change and wind intensification in coastal upwelling ecosystems, *Science*, **345**, 77-80

Taylor KE, Stouffer RJ and Meehl MA, (2012), An overview of the CMIP5 and the experimental design, *Bulletin of the American Meteorological Society*, **93**, 485-498

Thayer B, (2014), *Plutarch, The Parallel Lives: The Life of Sertorius*, Internet reproduction of the Loeb Classical Library Edition (1919), accessed online on 06/01/2014
http://penelope.uchicago.edu/Thayer/E/Roman/Texts/Plutarch/Lives/Sertorius*.html

Theil H, (1950), A rank-invariant method of linear and polynomial regression analysis, *Nederlandse Akademie Wetenchappen Series A*, **53**, 386-392

Thiel M, Macaya EC, Acuña E, Arntz WE, Bastias H, Brokordt K, Camus PA, Castilla JC, Castro LR, Cortés M, Dumont CP, Escribano R, Fernandez M, Fajardo JA, Gaymer CF, Gomez I, González AE, González HE, Haye PA, Illanes JE, Iriarte JL, Lancellotti DA, Luna-JorqueraG, Luxoro C, Manriquez PH, Marín V, Muñoz P, Navarrete SA, Perez E, Poulin E, Sellanes J, Sepúlveda HH, Stotz W, Tala F, Thomas A, Vargas CA, Vasquez JA and Alonso JM, (2007), The Humboldt Current System of Northern And Central Chile:

Oceanographic Processes, Ecological Interactions And Socioeconomic Feedback, *Oceanographic Marine Biology: An Annual Review,* **45**, 195-344

Thomas B, Kent EC, Swail VR and Berry DI, (2008), Analysis of monthly mean marine winds adjusted for observation method and height, *International Journal of Climatology*, **28**, 747–763

Thompson DWJ and Wallace JM, (1998), The Arctic oscillation signature in the wintertime geopotential height and temperature fields, *Journal of Geophysical Research*, **25**, 9, 1297-1300

Tokinaga H and Xie S-P, (2011a), Weakening of the equatorial Atlantic cold tongue over the past six decades, *Nature Geoscience*, **4**, 222–226

Tokinaga H and Xie S-P, (2011b), Wave- and Anemometer-Based Sea Surface Wind (WASWind) for Climate Change Analysis, *Journal of Climate,* **24**, 267-285

Tomczak M and Godfrey JS, (2003), *Regional Oceanography: An Introduction*, http://www.es.flinders.edu.au/~mattom/regoc/pdfversion.html

Tomé AR and Miranda PMA, (2004), Precise linear fitting and trend changing points of climate parameters, *Geophysical Research Letters*, **31**, L02207

Tveito OE, Førland EJ, Alexandersson H, Drebs A, Jónsson T, Tuomenvirta E and Vaarby-Laursen E, (2001), *Nordic Climate Maps*, DMNI Report 06/01 KLIMA, Oslo

Uppala SM, Kållberg PW, Simmons AJ, Andrae U, Da Costa Bechtold V, Fiorino M, Gibson JK, Haseler J, Hernandez A, Kelly GA, Li X, Onogi K, Saarinen S, Sokka N, Allan RP, Andersson E, Arpe K, Balmaseda MA, Beljaars ACM, Van De Berg L, Bidlot J, Bormann N, Caires S, Chevallier F, Dethof A, Dragosavac M, Fisher M, Fuentes M, Hagemann S, Hólm E, Hoskins BJ, Isaksen L, Janssen PAEM, Jenne R, McNally AP, Mahfouf JF, Morcrette J-J, Rayner NA, Saunders RW, Simon P, Sterl A, Trenberth KE, Untch A, Vasiljevic D, Viterbo P and Woollen J, (2005), The ERA-40 re-analysis, *Quarterly Journal of the Royal Meteorological Society,* **131**, 2961–3012

Valente MA, Barros RM, Nunes LF, Alves EI, Pinhal E, Coelho FES, Mendes M and Miranda JM, (2008), *Early stages of the recovery of Portuguese historical meteorological data*, In MEDARE - Proceedings of the International Workshop on Rescue and Digitization of Climate Records in the Mediterranean Basin, Editors: Brunet M and Kuglitsch FG, World Meteorological Organisation, WCDMP no. 67, WMO-TD No. 1432, June 2008, 95-102

Valente MA, Gomes P and Trigo RM, (2013), *Recovering Upper Air and Surface Atmospheric data from Portuguese FFCUL sources for ERA-CLIM - Work Package 1*, 13th European Meteorological Society Meeting, 9-13 September 2013, Reading, UK

Vallis GK and Gerber EP, (2008), Local and hemispheric dynamics of the North Atlantic Oscillation, annular patterns and the zonal index, *Dynamics of Atmospheres and Oceans*, **44**, 184-212

van Oldenborgh GJ, te Raa LA, Dijkstra HA and Phillip SY, (2009), Frequency- or amplitude-dependent effects of the Atlantic meridional overturning on the tropical Pacific Ocean, *Ocean Science*, **5**, 293-301

Vanlommel P, Cugnon P, Van Der Linden RAM, Berghmans and Clette F, (2004), The SIDC: World Data Centre for the Sunspot Index, *Solar Physics*, **224**, 113-120

Vannest KJ, Parker RI and Gonen O, (2011), *Single Case Research: web based calculators for SCR analysis, (Version 1.0) (Web-based application)*, College Station, TX, Texas A&M University. - accessed online on 16/1/2014

Vautard R, Cattiaux J, Yiou P, Thépaut J-N and Cials P, (2010), Northern Hemisphere atmospheric stilling partly attributed to an increase in surface roughness, *Nature Geoscience,* **3**, 756-761

Vautard R, Gobiet A, Sobolowski S, Kjellström E, Stegehuis A, Watkiss P, Mendlik T, Landgren O, Nikulin G, Teichmann C and Jacob D, (2014), The European climate under a 2 °C global warming, *Environmental Research Letters*, **9**, 034006

Veleda D, Montagne R and Araujo M, (2012), Cross-Wavelet Bias Corrected by Normalizing Scales, *Journal of Atmospheric and Oceanic Technology*, **29**, 1401-1408

Visbeck MH, Hurrell JW, Polvani L and Cullen HM, (2001), The North Atlantic Oscillation: Past, present, and future, *Proceedings of the National Academy of Sciences*, **98**, 12876-12877

Walter K and Graf H-F, (2002), On the changing nature of the regional connection between the North Atlantic Oscillation and sea surface temperature, *Journal of Geophysical Research: Atmospheres*, **107(D17)**, 4338

Wang C, (2012), Atlantic multidecadal oscillation, in "State of the Climate in 2011", *Bulletin of the American Meteorological Society*, **93(7)**, S119-S122

Wang C and Enfield DB, (2003), A further study of the tropical Western Hemisphere warm pool, *Journal of Climate*, **16**, 1476-1493

Wang XL, (2008a), Penalized Maximal F Test for Detecting Undocumented Mean Shift without Trend Change, *Journal of Atmospheric and Oceanic Technology*, **25(3)**, 368-384

Wang XL, (2008b), Accounting for autocorrelation in detecting mean-shifts in climate data series using the penalized maximal t or F test, *Journal of Applied Meteorology and Climatology*, **47**, 2423-2444

Wang XL and Feng Y, (2013), *RHtestsV4 User Manual*, Climate Research Division Atmospheric Science and Technology Directorate Science and Technology Branch, Environment Canada Toronto, Ontario, Canada, http://goo.gl/viDuL9, accessed online 02/02/2014

Wang XL, Chen H, Wu Y, Feng Y and Pu Q, (2010), New Techniques for the Detection and Adjustment of Shifts in Daily Precipitation Data Series, *Journal of Applied Meteorology and Climatology*, **49**, 2416–2436

Wang Y-H, Magnusdottir G, Stern H, Tian X and Yu Y, (2014), Uncertainty Estimates of the EOF-derived North Atlantic Oscillation, *Journal of Climate*, In print Online

Wanner H, Brönnimann S Casty C, Gyalistras D, Luterbacher J, Schmultz C, Stephenson DB and E. Xoplaki, (2001), North Atlantic Oscillation - concepts and studies, *Surveys in Geophysics*, **22**, 321–382

Westgarth-Smith AR, Roy DB, Scholze M, Tucker A and Sumpter JP, (2012), The role of the North Atlantic Oscillation in controlling U.K. butterfly population size and phenology, *Ecological Entomology*, **37(3)**, 221-232

Wigley TML and Jones PD, (1987), England and Wales Precipitation: a discussion of recent changes in variability and an update to 1985, *Journal of Climatology*, **7**, 231-246

Wijngaard JB, Klein-Tank AMG and Konnen GP, (2003), Homogeneity of 20th century European daily temperature and precipitation series, *International Journal of Climatology*, **23**, 679–692

Wilks D, (2011), *Statistical Methods in the Atmospheric Sciences 3rd Edition*, International Geophysics Series Volume 100, Academic Press, San Diego

Wolter K and Timlin MS, (2011), El Niño/Southern Oscillation behaviour since 1871 as diagnosed in an extended multivariate ENSO index (MEI.ext), *International Journal of Climatology*, **31**, 1074-1087

Woodruff SD, Worley SJ, Lubker SJ, Ji Z, Freeman JE, Berry DI, Brohan P, Kent EC, Reynolds RW, Smith SR and Wilkinson C, (2011), ICOADS Release 2.5: extensions and enhancements to the surface marine meteorological archive, *International Journal of Climatology*, **31**, 951-967

Woollings T and Blackburn M, (2012), The North Atlantic Jet Stream under Climate Change and Its Relation to the NAO and EA Patterns, *Journal of Climate*, **25**, 886-902

Woollings T, Hannachi A, Hoskins B and Turner A, (2010), A regime view of the North Atlantic Oscillation and its response to anthropogenic forcing, *Journal of Climate*, **23**, 1291-1307

Woollings T, Gregory JM, Pinto JG, Reyers M and Brayshaw DJ, (2012), Response of the North Atlantic storm track to climate change shaped by ocean-atmosphere coupling, *Nature Geoscience*, **5**, 313-317

Wu R and Xie S-P, (2003), On Equatorial Pacific Surface Wind Changes around 1977: NCEP-NCAR Reanalysis versus COADS Observations, *Journal of Climate*, **16**, 167–173

Wyatt MG and Curry JA, (2014), Role for Eurasian Arctic shelf sea ice in a secularly varying hemispheric climate signal during the 20th century, *Climate Dynamics*, **42**, 2763-2782

Yan Z, Jones PD, Moberg A, Bergstorm H, Davis TD and Yang C, (2001), Recent trends in weather and seasonal cycles: An analysis of daily data from Europe and China, *Journal of Geophysical Research*, **106**, 5123-5138

Yin X, Gleason BE, Compo GP, Matsui N and Vose RS, (2008), *The International Surface Pressure Databank (ISPD) land component version 2.2*, National Climatic Data Centre, Asheville, NC

Yue S and Wang CY, (2002), Applicability of prewhitening to eliminate the influence of serial correlation on the Mann-Kendall test, *Water Resources Research*, **38(6)**, 1068

Zhang Q, Xu CY, Chen X, and Zhang Z, (2011a), Statistical behaviours of precipitation regimes in China and theirs links with atmospheric circulation 1960-2005, *International Journal of Climatology*, **31**, 1665-1678

Zhang Q, Singh VP, Li J and Xiaohong C, (2011b), Analysis of the periods of maximum consecutive wet days in China, *Journal of Geophysical Research*, **116**, D23106

9. APPENDICES

The appendices consists of seven sections. Section A-F contain supplementary material to Chapters 1-6 of the thesis. Section G lists the Digitial Object Identifiers for the journal articles that were published as a result of this thesis.

A. Supplementary Material to Chapter 1

Contains four tables, A1-A4, which describe the basic geography of the Macaronesian Islands.

Island	Major City/ Municipality	Location		Area (km^2)	Highest Peak (m)	Island Group	Information
		North	West				
					AZORES		
Flores	*Santa Cruz das Flores*	39°27'	31°8'	143	914 (Morro Alto)	western Azores	
Corvo	*Vila do Corvo*	39°40'	31°6'	17	718 (Morro dos Homens)	western Azores	
Faial	*Horta*	38°32'	28°38'	173	1,043 (Cabeço Gordo)	central Azores	Horta serves as the 'legislative' Capital of the Azores.
Pico	*Madalena*	38°32'	28°31'	447	2,351 (Montanha do Pico)	central Azores	Mount Pico is the highest peak in Portugal.
Säo Jorge	*Velas*	38°41'	28°12'	244	1,053 (Pico de Esperança)	central Azores	
Graciosa	*Santa Cruz da Graciosa*	39°05'	28°00'	61	402 (Caldeira)	central Azores	
Terceira	*Angra do Heroismo*	38°39'	27°13'	401	1,021 (Serra de Santa Bárbara)	central Azores	Angra do Heroismo serves as the 'judicial' Capital of the Azores.

Table A1. The major islands of the Azores. The location column is the approximate central location of the major city/municipality of the island. Emboldened Island names indicate islands with at least one 'long-term;' (i.e. $>$ 25 years of data) meteorological-station with data freely available to download from publically accessible archives.

Table A1 continued.

São Miguel	*Ponta Delgada*	37°44'	25°40'	745	1,103 (Pico da Vara)	eastern Azores	Ponta Delgada serves as the 'executive' Capital of the Azores.
Santa Maria	*Vila do Porto*	36°57'	25°08'	97	587 (Pico Alto)	eastern Azores	

Island	**Major City/ Municipality**	**Location**		**Area (km²)**	**Highest Peak (m)**	**Island Group**	**Information**
		North	**West**				
					MADEIRA		
Madeira	*Funchal*	32°39'	16°55'	741	1,862 (Pico Ruivo)		Funchal is the Capital of Madeira.
Porto Santo	*Vila Baleira*	33°03'	16°20'	46	437 (Pico do Castelo)		
Desertas	*Deserta Grande*	32°31'	16°30'	14	442 (Boqueirão Norte)		

Table A2. As for Table A1 but for the major islands of Madeira.

Island	Major City/ Municipality	Location		Area (km^2)	Highest Peak (m)	Island Group	Information
		North	West				
					CANARY ISLANDS		
El Heirro	*Valverde*	27°49'	17°55'	278	1,501 (Pico de Malpaso)	western Canary Islands	
La Palma	*Los Llanos de Aridane*	28°39'	17°54'	706	2,423 (Roque de los Muchachos)	western	
La Gomera	*San Sebastián de La Gomera*	28°05'	17°06'	370	1,487 (Garajonay)	western	
Tenerife	*Santa Cruz de Tenerife*	28°27'	16°17'	2,034	3,718 (Pico del Teide)	central Canary Islands	Santa Cruz is the co-capital of the Canary Islands. Mount Teide is the highest peak in Spain.
Gran Canaria	*Las Palmas*	28°06'	15°26'	1,560	1,949 (Pico de las Nieves)	central	Las Palmas is the co-capital of the Canary Islands.
Fuerteventura	*Puerto del Rosario*	28°29'	13°52'	1,660	807 (Pico de Jandía)	eastern Canary Islands	
Lanzarote	*Arrecife*	28°58'	13°33'	846	670 (Peñas del Chache)	eastern	

Table A3. As for Table A1 but for the major islands of the Canary Islands.

Island	Major City/ Municipality	Location*		Area (km^2)	Highest Peak (m)	Island Group	Information
		North	West				
					CAPE VERDE		
Santo Antão	*Ribeira Grande*	17°11'	25°04'	779	1,979 (Topa da Coroa)	Barlavento	Barlavento = Windward Islands
São Vicente	*Mindelo*	16°53'	24°59'	227	750 (Monte Verde)	Barlavento	
Santa Luzia	*Uninhabited*	16°45'	24°44'	34	395 (Topona/Monte Grande)	Barlavento	
São Nicolau	*Ribeira Brava*	16°38'	24°17'	388	1,312 (Monte Gordo)	Barlavento	
Sal	*Santa Maria*	16°36'	22°54'	216	406 (Monte Vermelho)	Barlavento	
Boa Vista	*Sal Rei*	16°11'	22°55'	620	387 (Monte Estância)	Barlavento	
Maio	*Vila Do Maio*	15°08'	23°12'	269	431 (Monte Penoso)	Sotavento	Sotavento = Leeward Islands
Santiago	*Praia*	14°55'	23°31'	991	1,394 (Pico da Antónia)	Sotavento	Praia is the Capital of Cape Verde.
Fogo	*São Filipe*	15°08'	23°12'	476	2,829 (Pico do Fogo)	Sotavento	Mount Fogo is the highest peak in Cape Verde.
Brava	*Nova Sintra*	15°08'	23°12'	67	976 (Monte Fontainhas)	Sotavento	

Table A4. As for Table A1 but for the major islands of the Cape Verde.

B. Supplementary Material to Chapter 2

Contains one figure and six tables. Figure B1 shows the the code for the tension spline that was introduced in Section 2.6. Tables B1-B2 describe the climate extreme indices as defined by the ETCCDI. Table B3-B6 lists the meteorological station archives, climate indices, and reanalysis/observationally-derived gridded data sources used in this thesis.

tensionspline.R

Save Print <functions> Functions Help search Search

```
1  # Tension Spline R Code written by Thomas Cropper Dec 2013 (modified from H.
   Bjornsson)
2  # Please cite as Cropper et al. (2014) (Under review at Dataset Papers in Science)
3  # Please also cite the original developers Tveito et al. (2001); Henriksen (2003);
   Bjornsson et al. (2008) and Bjornsson (2013)
4  # Lines 5-20 do the Calculation, 22-26 plot output and write csv file
5  {
6  if (length(mondata)!=12) stop("the variable mondata is your monthly mean series and
   must have exactly twelve monthly values")
7  monlen = c(31, 29, 31, 30, 31, 30, 31, 31, 30, 31, 30, 31) # number of days in each
   month
8  numdays = c(1:367) # number of days in year add one
9
10 montoyear = rep(mondata,monlen) # creates a series where all of one months daily
   values equal the monthly mean
11 cumyear = cumsum(c(0,montoyear)) # cumulative daily total
12 endyear = c(0,cumsum(monlen))+1 # marks the end of each month during the year
13
14 ltrend = seq(from=0, to=cumyear[length(cumyear)], length.out =length(cumyear))
15 cumyearanom = cumyear-ltrend
16
17 tensionspline = spline(y = cumyearanom[endyear], x = endyear, xout=numdays, method
   ="periodic")
18
19 AnnualSpline = diff(tensionspline$y)+diff(ltrend) # annual cycle of daily data that
   retains the monthly average as estimated by the tension spline method
20
21 # basic plot of spline and is written to a csv file
22
23 plot(AnnualSpline, col="2", xlab="Julian Day")
24 lines(montoyear)
25 write.csv(AnnualSpline, file="tensionspline.csv")
26 }
```

Figure B1. R-code to implement the tension spline method from Section 2.6.

Index	Description	Abbreviation	Units
Maximum 1 Day Precipitation	Let PR_{ij} be the daily precipitation amount on day i in period j. The maximum 1 day value for period j are: RX1dayj = max (PR_{ij})	RX1day	mm
Maximum 5 Day Precipitation	Let PR_{kj} be the precipitation amount for the 5 day interval ending k, period j. Then maximum 5 day values for period j are: RX5dayj = max (PR_{kj})	RX5day	mm
Simple Daily Intensity Index	Let PR_{wj} be the daily precipitation amount on wet days, PR ≥ 1 mm in period j. If w represents number of wet days in j, then: $SDII_j = (\sum_{w=1}^{w} PR_{wj})/w$	SDII	mm
Wet Days	Let $PRij$ be the daily precipitation amount on day i in period j. Count the number of days where $PR_{ij} \geq 1$ mm	R1mm	Days
Heavy Precipitation Days	As above but $PR_{ij} \geq 10$ mm	R10mm	Days
Very Heavy Precipitation Days	As above but $PR_{ij} \geq 20$ mm	R20mm	Days
Consecutive Dry Days	Let PR_{ij} be the daily precipitation amount on day i in period j. Count the largest number of consecutive days where $PR_{ij} < 1$ mm	CDD	Days
Consecutive Wet Days	As above but where $PR_{ij} > 1$ mm	CWD	Days
Very Wet Days	Let PR_{wj} be the daily precipitation amount on a wet day w ($PR \geq 1$ mm) in period i and let $PR_{wn}95$ be the 95th percentile of precipitation on wet days in the 1981–2010 period. If w represents the number of wet days in the period, then: $R95p_j = \sum_{w=1}^{w} PR_{wj}$, where $PR_{wj} > PR_{wn}95$	R95p	mm
Extremely Wet Days	As above but for the 99th percentile, $PR_{wn}99$, where $R99p_j = \sum_{w=1}^{w} PR_{wj}$, where $PR_{wj} > PR_{wn}99$	R99p	mm
Precipitation Total	Let PR_{ij} be the daily precipitation amount on day i in period j. If i represents the number of days in j, then: $PRCPTOT_j = \sum_{n=l}^{j} PR_{ij}$	PRCPTOT	mm

Table B1. The precipitation-based extreme indices as defined by the ETCCDI.

Index	Description	Abbreviation	Units
Cold Nights	Let TN_{ij} be the daily minimum temperature on day i in period j and let $TN_{in}10$ be the calendar day 10^{th} percentile centred on a 5 day window. The percentage of days in a year is determined where $TN_{ij} < TN_{in}10$	TN10p	%
Warm Nights	As above but for the 90^{th} percentile $TN_{in}90$, and where $TN_{ij} > TN_{in}90$	TN90p	%
Cold Days	Let TX_{ij} be the daily maximum temperature on day i in period j and let $TX_{in}10$ be the calendar day 10th percentile centred on a 5 day window. The percentage of days is determined where $TX_{ij} < TX_{in}10$	TX10p	%
Warm Days	As above but for the 90^{th} percentile $TX_{in}90$, and where $TX_{ij} > TX_{in}90$	TX90p	%
Cold Spell Duration Indicator	Let TN_{ij} be the daily minimum temperature on day i in period j and let $TN_{in}10$ be the calendar day 10th percentile centred on a 5 day window for the base period 1981–2010. Then the number of days per period is summed where, in intervals of at least 6 consecutive days: $TN_{ij} < TN_{in}10$	CSDI	Days
Warm Spell Duration Indicator	As above but for TX_{ij} where $TX_{in}90$ is the calendar day 90^{th} percentile centred on a 5 day running window for the base period 1981-2010 and $TX_{ij} > TX_{in}90$	WSDI	days
Minimum Daily Minimum Temperature	Let TNn be the daily minimum temperatures in month k, period j. The minimum daily minimum temperature each month is then: $TNn_{kj} = \min(TNn_{kj})$	TNn	°C
Maximum Daily Minimum Temperature	As above but for the maximum daily minimum temperature, where $TNx_{kj} = \max(TNx_{kj})$	TNx	°C
Minimum Daily Maximum Temperature	Let TXn be the daily maximum temperatures in month k, period j. The minimum daily maximum temperature each month is then: $TXn_{kj} = \min(TXn_{kj})$	TXn	°C

Table B2. The temperature-based extreme indices as defined by the ETCCDI. Some of the 'core' indices are excluded (Frost Days, Ice Days and Growing Season Length, as they are not suited for use across the Macaronesian climatic range).

Table B2 continued.

Index	Description	Abbreviation	Units
Maximum Daily Maximum Temperature	As above but for the maximum daily maximum temperature, where $TXx_{\mathrm{kj}} = \max(TXx_{kj})$	TXx	°C
Summer Days	Let TX be the daily maximum temperature on day i in period j. Count the number of days where $TXij > 25$°C	SU	Days
Tropical Nights	Let TN be the daily minimum temperature on day i in period j. Count the number of days where $TNij > 20$°C	TR	Days
Diurnal Temperature Range	Let TN and TX be the daily minimum and maximum temperature respectively on day i in period j. If i represents the number of days in j, then: $DTR_j = \sum_{n=1}^{i}(TX_{ij} - TN_{ij})/i$	DTR	Days

Abbreviation	Archive	Contains	Reference	Chapters
		Meteorological-station Archives		
GHCN	Global Historical Climatology Network v3 via http://climexp.knmi.nl/	Monthly Temperature and Precipitation data	Lawrimore *et al.* (2011)	4
ECA&D	European Climate Assessment and Dataset via http://climexp.knmi.nl/	Daily climatological data	Klein-Tank *et al.* (2002)	4
GSOD	Global Summary of the Day	Daily climatological data	www.ncdc.noaa.gov	3, 4, 6
ADVICE	http://climexp.knmi.nl/	Monthly SLP data	Jones *et al.* (1999b)	3, 4
ERA-CLIM, -SIGN and the Icelandic Meteorological Office	International Surface Pressure Data Bank and Hourly Surface Data from www.ncdc.noaa.gov	Historical STP/SLP data	Bethke and Valente (2012); Valente *et al.* (2013); Jones *et al.* (1997); www.ncdc.noaa.gov	3

Table B3. The meteorological-station archives used in this thesis.

Abbreviation	Index	Information	Reference	Chapters
		Climate Indices		
NAO	North Atlantic Oscillation	The leading pattern of (annual) SLP variability across the North Atlantic	Various, see Table C1	3, 5, 6
EA	East Atlantic Pattern	The second most dominant pattern of SLP variability across the North Atlantic, represents a southward shifted NAO. Present in all seasons but summer.	Barnston and Livezey (1987)	6
AMO	Atlantic Multidecadal Oscillation	Tripole oscillation of Atlantic Ocean SSTs with a potentially widespread influence. One cycle length is ~50-70 years.	Van Oldenborgh *et al.* (2009)	4, 6
ENSO	El Niño Southern Oscillation	Widespread oscillation (2-8 year period) across the tropical Pacific Ocean. Exerts strong control on global temperature variability and widespread regional climate impacts	Wolter and Timlin (2011)	4, 6
Solar	Solar Cycle / Sunspot numbers	Solar output varies across a number of cycles. Activity was strong during the early and late 20th century. The past 11-year cycle has been very low.	http://sidc.oma.be/sunspot-data/	4
TWI	Trade Wind Index	Difference of SLP between the Azores and Cape Verde, serving as a proxy for trade wind strength across the subtropical northeast Atlantic.	CH14	3, 6

Table B4. The climate indices used in this thesis.

Abbreviation	Data Product	Spatial Resolution	Temporal Resolution	Reference	Chapters
Atmosphere and Ocean Reanalyses					
ERA-I	ERA-Interim reanalysis	0.7° x 0.7°	1979-2013	Dee *et al.* (2011)	3, 4, 6
NCEP-NCAR	National Centre for Environmental Prediction reanalysis I	1.9° x 1.875°	1948-2013	Kalnay *et al.* (1996)	4, 6
NCEP-DOE	National Centre for Environmental Prediction reanalysis II	1.9° x 1.875°	1979-2013	Kanamitsu *et al.* (2002)	6
MERRA	Modern-Era Retrospective Analysis for Research and Applications	0.5° x 0.67°	1979-2013	Rienecker *et al.* (2011)	6
CFSR	Climate Forecast System reanalysis	0.31° x 0.31°	1979-2013	Saha *et al.* (2010)	6
20CR	Twentieth Century reanalysis	1.9° x 1.875°	1871-2011	Compo *et al.* (2011)	3, 6
ORAS4	Operational Ocean reanalysis System	1° x 1°	1958-2011	Balmaseda *et al.* (2013)	6
GODAS	Global Ocean Data Assimilation System	0.33° x 1°	1980-2013	Behringer and Zue (2004)	6
SODA	Simple Ocean Data reanalysis v2.1.6	0.5° x 0.5°	1958-2008	Carton and Giese (2008)	6
CMIP5	Coupled Model Intercomparison Project Phase 5	Various	1861-2100	Taylor *et al.* (2012)	5

Table B5. The atmospheric and oceanic reanalysis datasets and model output used in this thesis.

Additional Gridded Datasets

EMSLP	European–North Atlantic mean sea level pressure dataset	5° x 5°	1850-2003	Ansell *et al.* (2006)	3
HadISST	Hadley Centre Sea Ice and Sea Surface Temperature Dataset	1.9° x 1.875°	1948-2013	Kalnay *et al.* (1996)	4, 6
ICOADS	International Comprehensive Ocean- Atmosphere Data Set	1° x 1° and 2° x 2°	1960-2013 and 1800-2013	Woodruff *et al.* (2011)	1, 6
CLIWOC	Climatological Database for the world's oceans	-	1750-1854	García-Herrera *et al.* (2005)	1
OISST	NOAA Optimum Interpolation (OI) Sea Surface Temperature v2	1.9° x 1.875°	1979-2013	Reynolds *et al.* (2007)	6
WASWind	Wave and Anemometer adjusted Sea-Surface Wind	0.5° x 0.67°	1979-2013	Tokinaga and Xie (2011b)	6
SeaWinds	Scatterometer winds from QuickSCAT	0.31° x 0.31°	1979-2013	Lungu *et al.* (2006)	6
CMIP5	Coupled Model Intercomparison Project Phase 5	Various	1861-2100	Taylor *et al.* (2012)	5
AVISO 1	Archiving, Validation and Interpretation of Satellite Oceanographic Data – Altimetry Sea Surface Height	1° x 1°	1950-2013	Church and White (2011)	6
AVISO 2		0.25° x 0.25°	1992-2013	AVISO website (Table F1)	6
AVISO 3		0.25° x 0.25°	1992-2013	Niiler *et al.* (2003)	6

Table B6. The observationally-derived gridded datasets used in this thesis. Column structure is the same as Table B5.

C. Supplementary Material to Chapter 3

Contains two tables and one figure. Table C1 lists the different variations of the NAO index used in this thesis and C2 lists the data sources that contribute to the creation of the Azores SLP time series used in the CHVJ15 NAO. Figure C1 indicates the maximum and minimum possible daily SLP for the ERA-I reanalysis during each calender month for the period 1979-2013.

Index	Southern	Reference	Notes
Gibraltar-Jones	Gibraltar	Jones *et al.* 1997	Used in H15 and CHVJ15 (Section 3.3.2 and 3.2)
MOHC	Gibraltar	H15 (Met Office data)	Used in H15 (Section 3.3.2)
Hurrell Station	Lisbon	Hurrell, 1995. https://climatedataguide.ucar.edu/climate-data/hurrell-north-atlantic-oscillation-nao-index-station-based	Used in H15 and CHVJ2015 (Section 3.3.2)
CRU / Azores-Jones	Azores	http://www.cru.uea.ac.uk/cru/data/nao/	Used in H15 and CHVJ15 (Section 3.3.2 and 3.2)
CH14	Azores	CH14	Used in and H15, CH14 and CHB14 (Section 3.3.2, 3.2 and 6)

Index	Method	Reference	Notes
Hurrell PC	PC	https://climatedataguide.ucar.edu/climate-data/hurrell-north-atlantic-oscillation-nao-index-pc-based	Used in H15 and CHVJ15 (Section 3.3.2 and 3.2)
20CR	PC Projection	H15	Used in H15 (Section 3.3.2)
CPC	PC Projection	http://www.cpc.ncep.noaa.gov/products/precip/CWlink/pna/nao_index.html	Used in CHVJ15 (Section 3.2.4 and 3.3.2). Uses 500 hPa data rather than SLP.
NAO PC	PC	CH14	Used in Chapter 6

Table C1. All the versions of the NAO used in this thesis (excluding the CHVJ2015 index presented in Chapter 3). Southwest Iceland pressure series is used as the northern node exclusively in all station-based reconstructions. The PC Projection method slightly differs from the traditional PC approach in that the leading pattern of variability (i.e. 1st EOF for a selected base period) is regressed against the SLP fields then the resultant time series normalised. The CPC index is the only index produced at a native daily resolution.

ID	Location	Latitude	Longitude	Altitude (m)	Measurement Time (UTC/z)	Temporal Start	Temporal End	Source	Detail
Historical / 'Old' Azores SLP time series									
Old PD	Ponta Delgada (São Miguel)	37.74N	334.32E	20	09:00z	December 1872	December 1887	Valente *et al.* (2008)	
Old PD	Ponta Delgada	37.73N	334.33E	17	09:00z	January	December	Valente *et al.* (2013)	
Old PD	Ponta Delgada	37.73N	334.33E	22	09:00z	January	December	Valente *et al.* (2013)	
Old PD	Ponta Delgada	37.73N	334.33E	22	11:00z	January 1922	December 1935	Valente *et al.* (2013)	1 year gap during 1931
Old PD	Ponta Delgada	37.73N	334.33E	22	06:00z	January	December	Valente *et al.* (2013)	
Old PD	Ponta Delgada	37.73N	334.33E	22	07:00z	January	December	Valente *et al.* (2013)	
OPD(ISD) 0600	Ponta Delgada	37.73N	334.33E*	22	06:00 UTC	January 1931	November 1939	ISD	*Assumed based on Old PD location
		37.73N	334.33E**	22	06:00 UTC	April 1953	August 1961	ISD	** Pressure reading is only to nearest whole SLP
OPD(ISD) 1200		37.73N	334.33E*	22	12:00 UTC	January 1931	October 1939	ISD	*Assumed based on Old PD location
		37.73N	334.33E**	22	12:00 UTC	January 1948	April 1953	ISD	** Pressure reading is only to nearest whole SLP

Table C2. The various data sources used to create the daily (~09:00 UTC) Ponta Delgada SLP time series from 1850-2013. * / ** indicates when metadata assumptions were made or when precision issues were present in the source data.

Table C2 continued.

Modern Azores SLP time series

Modern PD	Ponta Delgada	37.74N	334.3E	71	09:00 UTC	January 1973	Present	ISD	Nordela Airport
NPD(ISD) 0600	Ponta Delgada	37.74N	334.3E	71	06:00 UTC	January 1973	Present	ISD	Nordela Airport
NPD(ISD) 1200	Ponta Delgada	37.74N	334.3E	71	12:00 UTC	January 1973	Present	ISD	Nordela Airport
Lajes (SLP/STP)	Lajes Air Base (Terceira)	38.76N	332.91E	55	09:00 UTC	January 1947	Present	ISD	
Santa Maria	(Santa Maria)	36.97N	334.83E	100	09:00 UTC	August 1944	Present	ISD	

Reanalysis-derived SLP time series

20CR	Ponta Delgada (São Miguel)	38N	334E	Sea Level	09:00 UTC	January 1871	December 2011	Compo *et al.* (2011)	09:00 UTC is average of 06:00 and 12:00 SLP data
EMSLP	Ponta Delgada (São Miguel)	35N	335E	Sea Level	Daily Average	January 1850	December 2003	Ansell *et al.* (2006)	SLP is a daily value, not 09:00 UTC

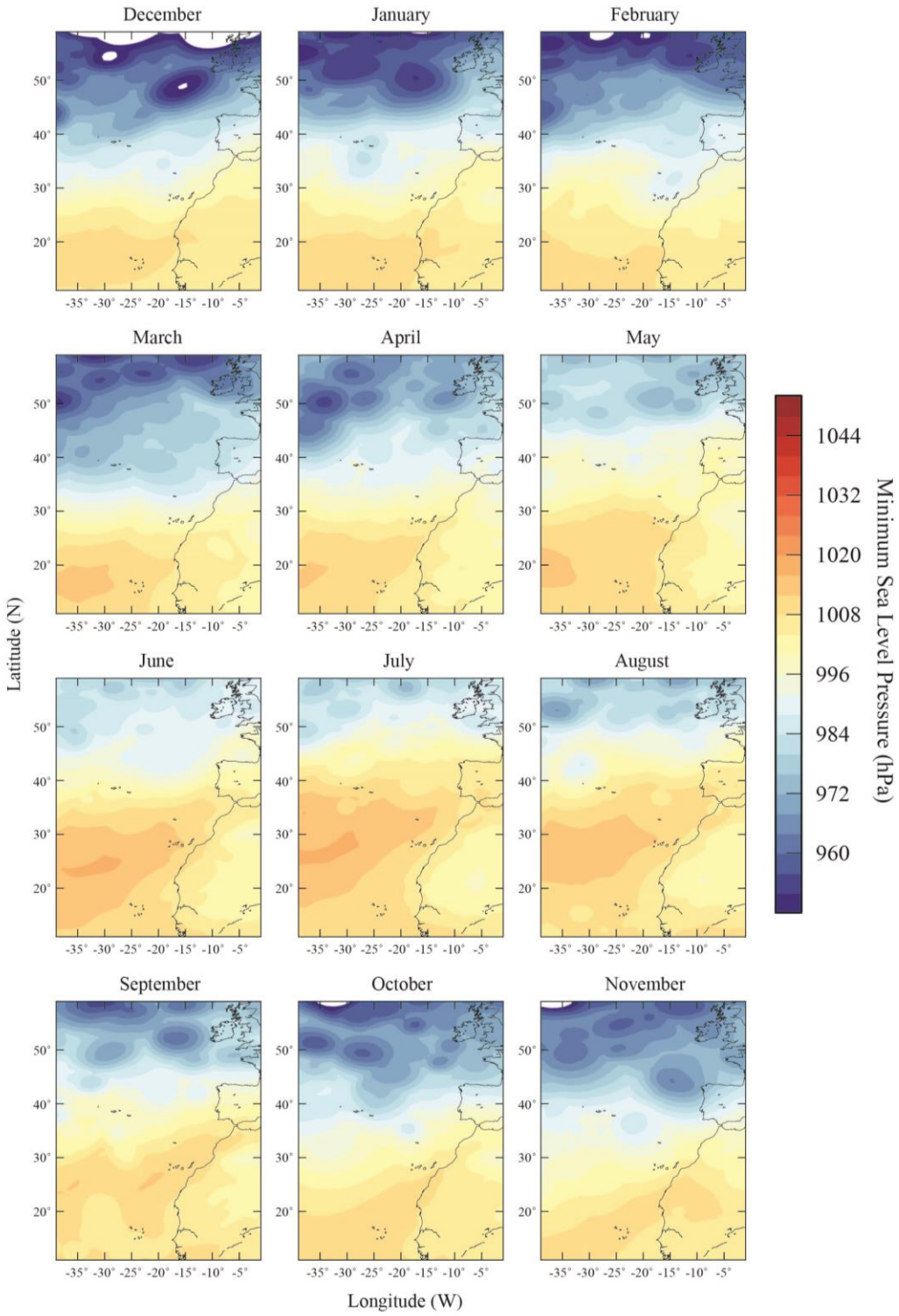

Figure C1a. The value of the lowest SLP reading found during each month using daily-resolution data from the ERA-I reanalysis (Dee *et al.*, 2011) between 1979-2013. Uncoloured (white) regions represent areas where the record lowest SLP was below 950 hPa.

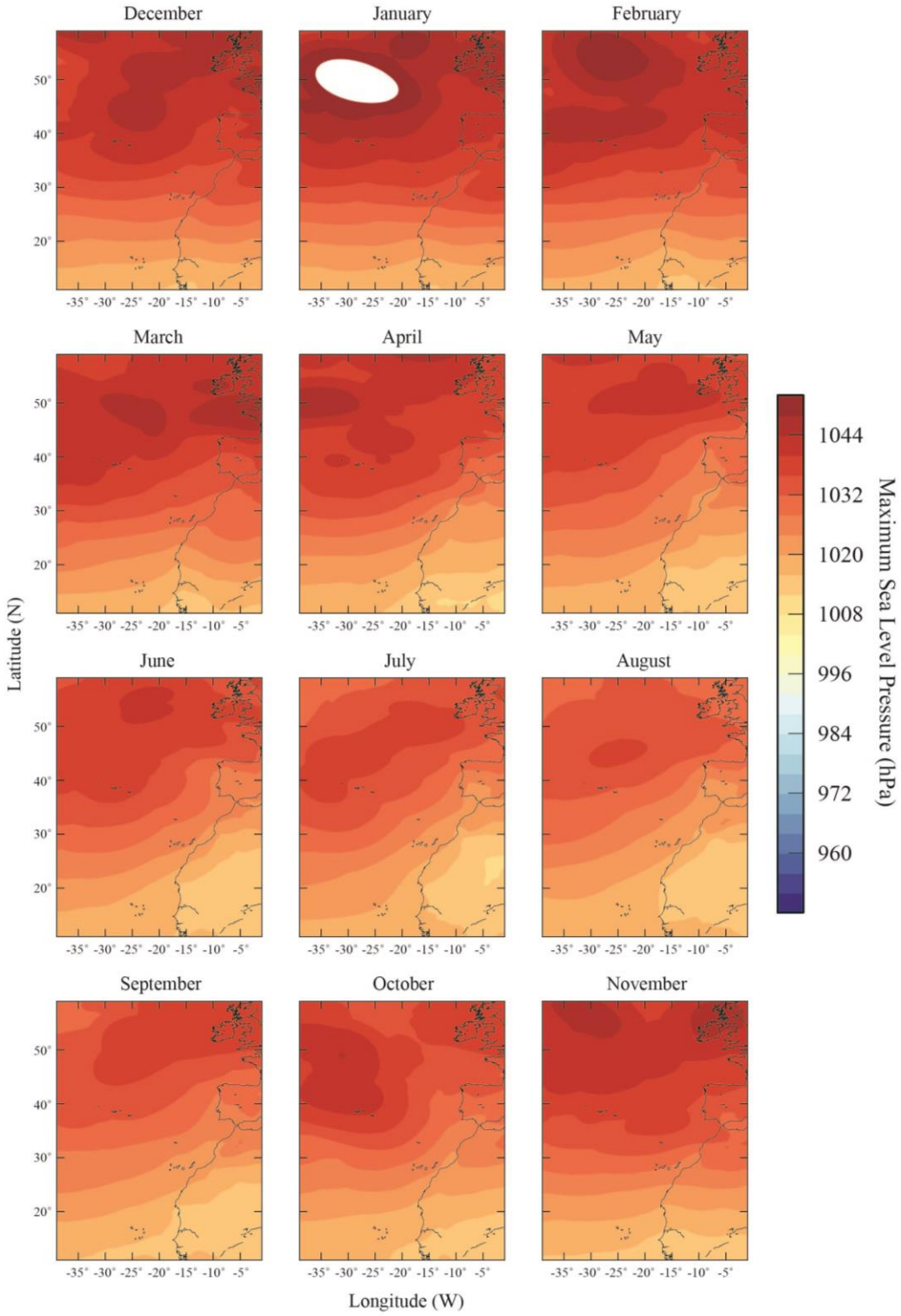

Figure C1b. The value of the highest SLP reading found during each month using daily-resolution data from the ERA-I reanalysis (Dee *et al.*, 2011) between 1979-2013. Uncoloured (white) regions represent areas where the record highest SLP was above 1050 hPa.

D. Supplementary Material to Chapter 4

Contains a table, D1, which displays precipitation means, trends and correlations with the NAO for selected Macaronesian stations.

Station	Temporal Coverage	Mean (Standard Deviation) (mm)					1981-2010 Trend (mm dec^{-1})				NAO Correlation			
		Annual	**DJF**	**MAM**	**JJA**	**SON***	**DJF**	**MAM**	**JJA**	**SON***	**DJF**	**MAM**	**JJA**	**SON***
						Azores								
Ponta Delgada	1865-2012	1044.2 (178.6)	343.5 (115.8)	252.6 (84.6)	135.1 (53.2)	313.6 (88.6)	29.1	24.7	14.3	-15.7	***-0.64***	***-0.60***	***-0.31***	***-0.40***
Santa Maria	1961-2012	753.6 (178.2)	273.5 (115.7)	164.9 (71.2)	81.3 (43.8)	233.7 (82.6)	14.4	7.6	7.7	-16.2	***-0.78***	***-0.70***	-0.25	***-0.40***
Horta	1902-2012	1017.5 (166.9)	328.1 (103.0)	236.5 (76.0)	143.8 (59.4)	307.6 (82.0)	22.8	17.0	1.6	-17.4	***-0.56***	***-0.58***	***-0.38***	***-0.43***
						Canary Islands								
Las Palmas	1941-2012	143.3 (74.8)	75.9 (58.5)	20.6 (19.1)	1.5 (3.3)	46.1 (41.5)	15.1	-4.1	0.0	1.9	0.03	0.15	**0.26**	0.11
Fuerteventura	1970-2012	103.6 (52.4)	61.0 (39.3)	18.6 (18.9)	0.3 (0.7)	24.6 (20.9)	-3.5	-1.0	0.0	1.6	0.02	0.10	-0.11	-0.27
Santa Cruz M	1925-2012	237.0 (95.8)	120.0 (71.5)	49.9 (42.9)	1.8 (5.0)	66.1 (49.3)	12.6	2.9	0.0	-5.0	-0.14	***0.28***	0.05	-0.06

Table D1. Macaronesia station precipitation long-term annual and seasonal means (SD in parenthesis), linear trends for the 1981-2010 period and correlation coefficients with the NAOI for the entire record. All trends are reported in millimetres per decade (mm dec^{-1}). Bold indicates significant trends ($p < 0.1$) where the data passed both the standard and modified MK tests for significance. For the correlation table, bold ($p < 0.05$) and emboldened italics ($p < 0.01$) highlight significant values. *For Cape Verde only, the three month autumn period is ASO rather than SON, to better capture the wet season.

Table D1 continued

						Cape Verde								
Saint Vincent	1883-1976	76.0 (80.6)	9.3 (11.3)	1.6 (4.2)	27.9 (33.0)	85.5 (69.5)	-	-	-	-	0.07	0.04	-0.08	0.10
Saint Vincent NCEP/NCAR Grid	1948-2012	58.5 (43.1)	2.0 (3.7)	0.6 (1.7)	16.9 (16.6)	52.9 (39.0)	0.0	0.0	4.2	**15.2**	***-0.36***	0.03	-0.11	-0.05
Praia	1885-1973	160.5 (173.5)	5.8 (10.0)	0.3 (1.5)	78.4 (91.8)	201.2 (160.4)	-	-	-	-	0.18	0.11	**-0.24**	-0.01
Praia NCEP/NCAR Grid	1948-2012	152.0 (83.4)	1.5 (4.2)	0.1 (0.5)	59.2 (40.4)	138.4 (73.7)	0.0	0.0	11.9	**38.7**	-0.22	-0.08	-0.06	0.08
Sal	1973-2012	293.0 (228.3)	97.9 (149.7)	36.0 (115.4)	47.3 (89.9)	126.8 (144.1)	0.0	0.0	2.1	17.5	0.12	0.07	-0.04	-0.17
						Madeira								
Funchal	1880-2012	629.3 (210.7)	261.7 (144.1)	136.1 (77.8)	15.1 (23.9)	215.0 (130.8)	6.1	-2.6	-1.3	-0.7	***-0.58***	***-0.32***	-0.13	***-0.43***
Porto Santo	1940-2012	367.2 (95.4)	153.1 (77.5)	78.4 (40.1)	15.5 (9.6)	118.2 (58.5)	11.2	-3.0	1.1	4.1	***-0.63***	-0.01	-0.05	-0.22

E. Supplementary Material to Chapter 5

The CMIP5 models used in Chapter 5 were: ACCESS1-0, ACCESS1-3, BCC-CSM-1-1, BCC-CSM-1-1m, BNU-ESM, CanESM2, CCSM4, CESM1-BGC, CESM1-CAM5, CMCC-CM, CMCC-CMS, CNRM-CM5, CSIRO-Mk3-6-0, EC-EARTH, FGOALS-s2, FIO-ESM, GFDL-CM3, GFDL-ESM2G, GFDL-ESM2M, GISS-E2-H, GISS-E2-H-CC, GISS-E2-R, GISS-E2-R-CC, HadGEM2-AO, HadGEM2-CC, HadGEM2-ES, INMCM4, IPSL-CM5A-LR, IPSL-CM5A-MR, IPSL-CM5B-LR, MIROC-ESM, MIROC-ESM-CHEM, MIROC5, MPI-ESM-LR, MPI-ESM-MR, MRI-CGCM3, NorESM1-M and NorESM1-ME. A description of the CMIP5 process is given by Taylor *et al.* (2012). When the term 'model mean' is used, this assumes one run of each separately named model contributes to the mean, unless otherwise stated. This means the most frequently used model from each centre is the 'r1i1p1' model – typically the first run to be archived from each individual modelling group.

F. Supplementary Material to Chapter 6

Contains five tables and one figure. Figure F1 illustrates the differences between the coastal upwelling that occurs at the physical ocean boundary and the wind-stress curl-induced upwelling that occurs in the open ocean. Table F1 lists the data sources for upwelling and upwelling proxy indices in Chapter 6. Table F2-F5 indicates seasonal correlation values between various upwelling indices and several large-scale modes of climate variability.

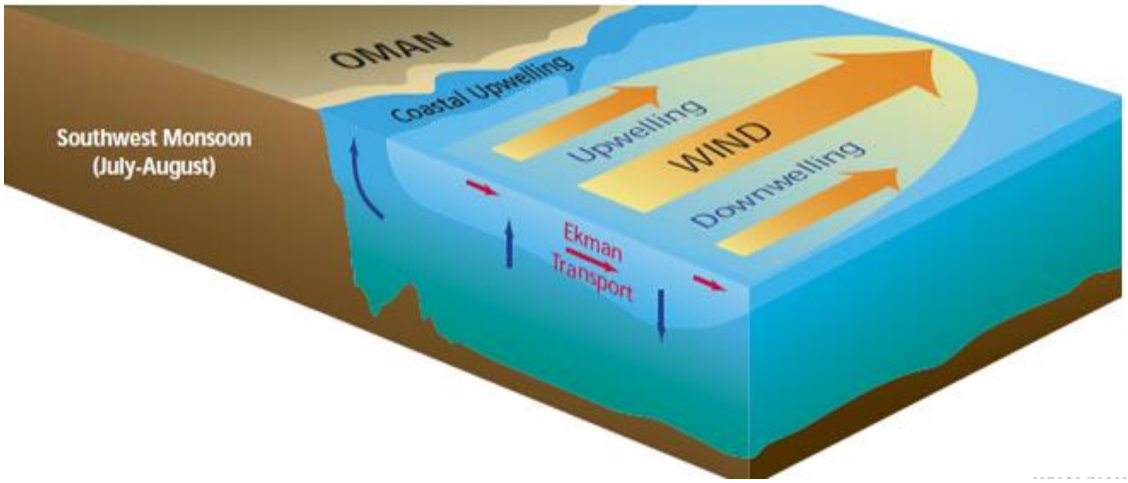

Figure F1. Diagram illustrating coastal and wind-stress curl-induced upwelling (for Oman, but applicable for all coastal upwelling regions). The alongshore wind-stress and physical coastal boundary lead to the direct coastal upwelling of subsurface water. Variations in the alongshore wind-stress field, which is typically strongest ~10^1-10^2 km offshore, leads to differences in the Ekman transport and ocean surface divergence and convergence in the open ocean. On the onshore side of the wind-stress maximum, the wind-stress curl is cyclonic (anticlockwise), leading to divergence of the water mass and upwelling of subsurface water. On the offshore side of the wind-stress maximum, the wind-stress curl is anticyclonic (clockwise), leading to convergence of the water mass and downwelling. Image reproduced from Laing and Evans (2014).

Upwelling Index Data

Data Set	Source	Resolution (Lat x Lon)	Temporal Extent	Reference	Variable
PFEL – Pacific Fisheries Environmental Laboratory Derived Upwelling Indices	(http://www.pfeg.noaa.gov/products/pfel/modeled/model_derived.html)	1° x 1°	1967-2012	(*Schwing et al.* 1996)	UI^W
ERA-I – Era-Interim reanalysis	(http://www.ecmwf.int/research/era/do/get/era-interim)	0.7° x 0.7°	1979-2012	(*Dee et al.* 2011)	10 m U,V Wind
NCEP-DOE – National Centre for Environmental Prediction reanalysis II	(http://www.esrl.noaa.gov/psd/data/gridded/data.ncep.reanalysis2.html)	1.9° x 1.875°	1979-2012	(Kanamitsu *et al.* 2002)	10 m U,V Wind
ICOADS – International Comprehensive Ocean-Atmosphere Data Set	(http://www.esrl.noaa.gov/psd/data/gridded/data.coads.1deg.html)	1° x 1°	1960-2012*	(*Woodruff et al.* 2011)	Near-surface U,V Wind, SST
CFSR – Climate Forecast System reanalysis	(http://rda.ucar.edu/pub/cfsr.html)	0.31° x 0.31°	1979-2010	(*Saha et al.* 2010)	10 m U,V Wind
MERRA – Modern-Era Retrospective Analysis for Research and Applications	(http://gmao.gsfc.nasa.gov/merra/)	0.5° x 0.67°	1979-2012	(*Rienecker et al.* 2011)	10 m U,V Wind
20CR – Twentieth Century reanalysis	(http://www.esrl.noaa.gov/psd/data/20thC_Rean/)	1.9° x 1.875°	1870-2010	(*Compo et al.* 2011)	10 m Wind
WASWind – Wave and Anemometer adjusted Sea-Surface Wind	(http://iprc.soest.hawaii.edu/users/tokinaga/waswind.html)	4° x 4°	1950-2011	(*Tokinaga and Xie*, 2011b)	10 m Wind

Table F1. Data sources used to calculate upwelling indices or 'proxy' upwelling indices in this study. *ICOADS data from 2007 are preliminary values. Occasional gaps in the ICOADS coastal grid-boxes were interpolated by the average of the surrounding four grid-boxes.

Table F1 continued

SeaWinds – Scatterometer winds from QuickSCAT	(http://coastwatch.pfeg.noaa.gov/erddap/griddap/erdQSwindmday.html)	0.125° x 0.125°	1999-2009	(*Lungu et al.*, 2006)	10 m Wind
HadISST – Hadley Centre Sea Ice and Sea Surface Temperature Dataset	(http://www.metoffice.gov.uk/hadobs/hadisst/)	1° x 1°	1871-2012	(*Rayner et al.* 2003)	SST
OISST – NOAA Optimum Interpolation (OI) Sea Surface Temperature v2	(http://www.esrl.noaa.gov/psd/data/gridded/data.ncep.oisst.v2.html)	1° x 1°	1981-2012	(*Reynolds et al.* 2002)	SST
	Upwelling Proxy Data				
ORAS4 – Operational Ocean reanalysis System 4	(http://www.ecmwf.int/products/forecasts/d/charts/oras4/reanalysis/)	1° x 1°	1958-2011	(*Balmaseda et al.* 2013)	SSH
SODA – Simple Ocean Data reanalysis v2.1.6	(http://iridl.ldeo.columbia.edu/SOURCES/.CARTON-GIESE/.SODA/.v2p1p6/)	0.5° x 0.5°	1958-2008	(*Carton and Giese*, 2008)	SSH
GODAS – Global Ocean Data Assimilation System	(http://www.esrl.noaa.gov/psd/data/gridded/data.godas.html)	0.33° x 1°	1980-2012	(*Behringer and Zue*, 2004)	SSH, 50 m Vertical Velocity
AVISO – Archiving, Validation and Interpretation of Satellite Oceanographic Data – Altimetry Sea Surface Height	**1.**(http://www.cmar.csiro.au/sealevel/sl_data_cmar.html) **2.**(http://www.aviso.oceanobs.com/en/data/data-access-services.html) **3.**(http://coastwatch.pfeg.noaa.gov/erddap/griddap/noaa_pifsc_dc75_b265_fef6.html)	1. 1° x 1° 2 & 3. 0.25° x 0.25°	**1.** 1950-2012 **2 & 3.** 1992-2012	1. (*Church and White*, 2011) 3. (*Niiler et al.*, 2003)	SSH

DJF	NAO (Station)	NAO (PC)	EA	AMO	ENSO
		12-19°N			
ICOADS (UI^{W})	***0.52***	**0.36**	0.04	0.07	0.00
PFEL (UI^{W})	***0.55***	**0.41**	-0.17	-0.02	-0.28
NCEP-DOE (UI^{W})	***0.47***	0.32	0.08	0.00	-0.20
ERA (UI^{W})	**0.43**	0.30	0.04	-0.09	-0.02
MERRA (UI^{W})	***0.53***	**0.43**	0.15	0.02	-0.18
CFSR (UI^{W})	***0.46***	**0.40**	0.24	0.02	-0.13
20CR (UI^{W})	**0.37**	0.34	0.28	0.00	-0.06
WASWIND (UI^{W})	***0.67***	***0.53***	-0.21	0.16	-0.16
OISST ($UI^{\Delta SST}$)	0.27	0.34	0.31	0.17	0.19
HADISST ($UI^{\Delta SST}$)	0.17	0.24	0.26	0.22	0.13
ICOADS ($UI^{\Delta SST}$)	0.09	0.08	0.24	0.08	-0.01
AVISO (SSH)	**-0.47**	-0.31	-0.05	-0.09	0.16
ORSA4 (SSH)	-0.21	-0.11	0.06	0.03	0.03
GODAS (SSH)	0.10	0.23	0.10	0.22	0.11
SODA (SSH)	0.06	0.06	0.02	0.26	0.08
GODAS (VWCV)	-0.28	**-0.35**	-0.29	-0.13	-0.30
		21-26°N			
ICOADS (UI^{W})	***0.44***	0.32	-0.21	-0.08	0.17
PFEL (UI^{W})	***0.73***	***0.65***	0.00	0.28	-0.18
NCEP-DOE (UI^{W})	***0.76***	***0.63***	0.02	0.23	-0.19
ERA (UI^{W})	***0.50***	0.32	0.03	-0.04	0.12
MERRA (UI^{W})	***0.71***	***0.57***	0.01	0.17	-0.20
CFSR (UI^{W})	**0.40**	0.29	0.28	0.14	-0.05
20CR (UI^{W})	**0.41**	0.31	0.27	0.08	-0.05
WASWIND (UI^{W})	***0.74***	***0.62***	-0.05	0.24	-0.18
OISST ($UI^{\Delta SST}$)	-0.15	-0.07	0.07	0.01	-0.16
HADISST ($UI^{\Delta SST}$)	***-0.46***	-0.33	-0.01	-0.19	-0.07
ICOADS ($UI^{\Delta SST}$)	-0.26	-0.19	0.06	-0.27	-0.10
AVISO (SSH)	***-0.84***	***-0.72***	0.25	**-0.38**	0.21
ORSA4 (SSH)	***-0.63***	**-0.49**	0.26	-0.16	0.18
GODAS (SSH)	***-0.49***	-0.33	0.06	-0.07	0.00
SODA (SSH)	**-0.43**	-0.24	0.10	0.30	-0.03
GODAS (VWCV)	**0.42**	0.24	-0.04	-0.06	-0.22
		26-34°N			
ICOADS (UI^{W})	***0.57***	***0.45***	-0.14	0.12	0.14
PFEL (UI^{W})	***0.81***	***0.70***	-0.12	0.30	-0.11
NCEP-DOE (UI^{W})	***0.86***	***0.75***	-0.19	0.32	-0.12
ERA (UI^{W})	***0.62***	***0.47***	-0.13	0.10	0.18
MERRA (UI^{W})	***0.84***	***0.73***	-0.12	0.27	-0.13
CFSR (UI^{W})	***0.70***	***0.61***	0.13	0.26	0.02
20CR (UI^{W})	***0.70***	***0.61***	0.10	0.26	-0.01
WASWIND (UI^{W})	***0.81***	***0.72***	-0.25	0.29	-0.08
OISST ($UI^{\Delta SST}$)	-0.25	-0.14	0.07	-0.07	-0.33
HADISST ($UI^{\Delta SST}$)	-0.14	-0.09	0.08	0.01	***-0.49***
ICOADS ($UI^{\Delta SST}$)	0.05	0.18	-0.04	0.15	**-0.41**
AVISO (SSH)	***-0.62***	**-0.48**	0.37	-0.13	0.17
ORSA4 (SSH)	***-0.69***	**-0.55**	0.19	-0.17	0.09
GODAS (SSH)	***-0.56***	**-0.43**	0.26	-0.27	0.03
SODA (SSH)	***-0.63***	**-0.45**	0.18	0.00	0.00
GODAS (VWCV)	***0.84***	***0.70***	-0.15	0.33	-0.08

Table F2. 1981-2012 (or the longest temporal period available - see Table F1 for temporal data availability) winter (DJF) correlations between latitudinally averaged upwelling indices/indicators and the NAO (station-based and PC based indices), EA Pattern, AMO and ENSO. All time series were linearly detrended beforehand. Values that are bold and bold italics correspond to significant correlations ($p < 0.05$ and 0.01 respectively).

MAM	NAO (Station)	NAO (PC)	EA	AMO	ENSO
		12-19°N			
ICOADS (UI^{W})	0.21	0.31	-0.06	0.07	-0.13
PFEL (UI^{W})	0.19	0.23	0.04	-0.18	0.24
NCEP-DOE (UI^{W})	**0.40**	***0.53***	-0.14	-0.26	0.16
ERA (UI^{W})	0.29	**0.40**	-0.18	0.06	-0.10
MERRA (UI^{W})	**0.36**	***0.46***	0.08	-0.28	0.05
CFSR (UI^{W})	***0.46***	***0.55***	0.00	**-0.36**	0.03
20CR (UI^{W})	**0.60**	***0.61***	0.23	-0.14	-0.01
WASWIND (UI^{W})	**0.36**	**0.43**	0.16	-0.15	0.01
OISST ($UI^{\Delta SST}$)	-0.19	**-0.36**	0.25	0.28	-0.16
HADISST ($UI^{\Delta SST}$)	-0.12	-0.18	-0.04	0.22	-0.12
ICOADS ($UI^{\Delta SST}$)	-0.16	**-0.36**	0.00	0.04	-0.11
AVISO (SSH)	**-0.52**	-0.38	0.17	-0.18	0.21
ORSA4 (SSH)	***-0.78***	***-0.70***	0.14	0.24	0.20
GODAS (SSH)	-0.29	-0.27	-0.04	0.10	**0.40**
SODA (SSH)	**-0.47**	***-0.49***	0.06	0.12	0.07
GODAS (VWCV)	**0.43**	**0.40**	-0.22	-0.23	**-0.36**
		21-26°N			
ICOADS (UI^{W})	0.28	0.23	0.15	0.26	-0.15
PFEL (UI^{W})	0.29	0.11	0.19	**0.36**	-0.11
NCEP-DOE (UI^{W})	0.27	0.01	***0.55***	0.20	0.14
ERA (UI^{W})	0.31	0.18	0.09	0.29	-0.18
MERRA (UI^{W})	0.21	-0.04	***0.48***	0.19	0.09
CFSR (UI^{W})	0.30	0.01	***0.50***	0.05	0.02
20CR (UI^{W})	0.29	0.02	***0.58***	-0.07	0.02
WASWIND (UI^{W})	0.26	0.06	***0.51***	0.24	0.17
OISST ($UI^{\Delta SST}$)	0.12	0.16	**-0.42**	0.03	-0.35
HADISST ($UI^{\Delta SST}$)	0.30	0.32	-0.13	**-0.36**	-0.31
ICOADS ($UI^{\Delta SST}$)	0.13	0.11	-0.27	-0.07	-0.21
AVISO (SSH)	**-0.46**	-0.38	-0.03	-0.31	0.38
ORSA4 (SSH)	***-0.68***	-0.43	-0.21	-0.01	0.33
GODAS (SSH)	**-0.39**	-0.28	-0.27	-0.18	0.26
SODA (SSH)	***-0.58***	***-0.48***	-0.13	-0.05	-0.10
GODAS (VWCV)	0.33	0.09	0.32	-0.26	-0.05
		26-34°N			
ICOADS (UI^{W})	**0.41**	0.23	0.24	0.14	-0.02
PFEL (UI^{W})	0.31	0.14	0.30	0.13	0.04
NCEP-DOE (UI^{W})	**0.35**	0.13	***0.48***	0.08	0.11
ERA (UI^{W})	0.22	0.15	0.10	**0.36**	-0.10
MERRA (UI^{W})	0.28	0.06	**0.50**	0.07	0.08
CFSR (UI^{W})	**0.39**	0.17	**0.45**	0.00	0.04
20CR (UI^{W})	***0.51***	0.23	**0.38**	-0.06	-0.02
WASWIND (UI^{W})	0.33	0.13	0.28	0.23	0.14
OISST ($UI^{\Delta SST}$)	-0.17	0.03	-0.32	-0.27	-0.01
HADISST ($UI^{\Delta SST}$)	0.34	0.35	-0.08	**-0.41**	**-0.42**
ICOADS ($UI^{\Delta SST}$)	-0.12	0.04	-0.31	0.17	-0.12
AVISO (SSH)	-0.29	-0.25	0.04	-0.34	0.21
ORSA4 (SSH)	**-0.50**	-0.20	-0.33	-0.16	0.20
GODAS (SSH)	-0.30	-0.15	**-0.37**	-0.32	0.20
SODA (SSH)	***-0.61***	***-0.48***	-0.06	-0.08	-0.10
GODAS (VWCV)	***0.46***	0.23	**0.39**	0.07	0.00

Table F3. As for Table F2, but for spring (MAM).

JJA	NAO (Station)	NAO (PC)	EA	AMO	ENSO
		12-19°N			
ICOADS (UI^{W})	-0.07	-0.30	-0.23	0.12	0.25
PFEL (UI^{W})	0.18	0.33	0.03	0.15	-0.12
NCEP-DOE (UI^{W})	-0.22	**-0.39**	-0.31	0.05	0.11
ERA (UI^{W})	-0.13	**-0.37**	-0.30	0.12	0.08
MERRA (UI^{W})	-0.10	0.18	**-0.35**	0.27	0.14
CFSR (UI^{W})	-0.35	-0.21	-0.27	0.29	-0.08
20CR (UI^{W})	-0.08	-0.06	-0.02	**0.38**	0.00
WASWIND (UI^{W})	0.02	-0.30	0.02	0.03	0.24
OISST ($UI^{\Delta SST}$)	0.16	0.29	-0.19	-0.05	0.25
HADISST ($UI^{\Delta SST}$)	-0.12	0.22	-0.15	0.22	-0.06
ICOADS ($UI^{\Delta SST}$)	-0.08	0.05	-0.22	0.20	0.33
AVISO (SSH)	-0.01	-0.08	-0.27	0.18	**-0.42**
ORSA4 (SSH)	-0.16	-0.06	-0.15	0.26	**-0.43**
GODAS (SSH)	-0.13	-0.01	**-0.36**	0.11	-0.13
SODA (SSH)	-0.20	0.05	**-0.42**	0.23	0.07
GODAS (VWCV)	0.05	0.11	-0.11	-0.03	0.04
		21-26°N			
ICOADS (UI^{W})	-0.04	-0.13	0.12	0.04	0.14
PFEL (UI^{W})	-0.04	-0.20	-0.03	-0.26	0.03
NCEP-DOE (UI^{W})	0.17	0.00	0.12	-0.01	0.14
ERA (UI^{W})	0.05	0.19	0.06	0.20	0.12
MERRA (UI^{W})	0.07	-0.18	-0.04	-0.01	0.10
CFSR (UI^{W})	0.25	-0.10	0.08	-0.14	0.26
20CR (UI^{W})	0.04	0.00	0.10	-0.04	0.24
WASWIND (UI^{W})	0.27	0.05	-0.11	-0.10	0.14
OISST ($UI^{\Delta SST}$)	0.15	0.11	-0.19	-0.33	-0.13
HADISST ($UI^{\Delta SST}$)	-0.07	0.02	-0.11	-0.18	-0.10
ICOADS ($UI^{\Delta SST}$)	0.11	0.22	-0.21	-0.31	0.17
AVISO (SSH)	-0.04	-0.01	-0.16	0.35	-0.36
ORSA4 (SSH)	-0.42	-0.21	-0.34	0.33	-0.32
GODAS (SSH)	-0.13	-0.01	**-0.37**	-0.04	-0.10
SODA (SSH)	-0.35	0.05	-0.32	**0.41**	-0.23
GODAS (VWCV)	0.09	**-0.41**	0.21	-0.37	0.13
		26-34°N			
ICOADS (UI^{W})	0.05	0.00	0.05	0.22	0.00
PFEL (UI^{W})	-0.02	-0.29	**0.44**	0.07	-0.33
NCEP-DOE (UI^{W})	-0.03	**-0.39**	**0.44**	-0.01	-0.17
ERA (UI^{W})	-0.08	-0.01	0.22	0.02	-0.02
MERRA (UI^{W})	-0.11	**-0.35**	0.32	0.03	-0.30
CFSR (UI^{W})	0.11	-0.29	**0.40**	-0.10	-0.26
20CR (UI^{W})	0.02	-0.08	**0.42**	0.07	**-0.41**
WASWIND (UI^{W})	0.12	-0.22	0.28	-0.07	-0.34
OISST ($UI^{\Delta SST}$)	0.24	-0.08	-0.06	***-0.54***	-0.09
HADISST ($UI^{\Delta SST}$)	**0.39**	0.14	-0.06	***-0.46***	-0.22
ICOADS ($UI^{\Delta SST}$)	0.19	0.08	-0.13	-0.20	-0.22
AVISO (SSH)	-0.01	-0.40	-0.10	0.03	-0.14
ORSA4 (SSH)	-0.22	-0.17	**-0.45**	0.05	0.03
GODAS (SSH)	-0.11	-0.15	-0.26	-0.11	-0.01
SODA (SSH)	**-0.39**	-0.12	-0.34	**0.37**	-0.08
GODAS (VWCV)	0.05	-0.31	**0.42**	-0.13	0.05

Table F4. As for Table F2, but for summer (JJA).

SON	NAO (Station)	NAO (PC)	EA	AMO	ENSO
		12-19°N			
ICOADS (UI^{W})	**0.37**	0.07	0.20	***-0.44***	0.29
PFEL (UI^{W})	**0.42**	0.16	-0.24	-0.28	0.12
NCEP-DOE (UI^{W})	***0.47***	0.16	-0.07	***-0.46***	0.02
ERA (UI^{W})	0.31	0.24	0.28	**-0.38**	0.05
MERRA (UI^{W})	0.28	0.14	0.07	***-0.51***	0.05
CFSR (UI^{W})	0.31	0.29	0.16	***-0.52***	-0.02
20CR (UI^{W})	0.31	0.20	-0.02	-0.05	0.04
WASWIND (UI^{W})	**0.52**	0.30	***0.48***	**-0.37**	0.30
OISST ($UI^{\Delta SST}$)	-0.16	-0.17	0.08	0.30	0.18
HADISST ($UI^{\Delta SST}$)	0.09	-0.06	***0.52***	0.27	0.03
ICOADS ($UI^{\Delta SST}$)	-0.13	-0.32	0.20	0.16	0.23
AVISO (SSH)	0.20	-0.14	0.27	0.08	-0.36
ORSA4 (SSH)	-0.06	-0.22	0.11	0.19	-0.30
GODAS (SSH)	-0.08	-0.23	0.16	-0.13	-0.07
SODA (SSH)	0.15	***-0.50***	0.12	0.08	-0.01
GODAS (VWCV)	**0.36**	**0.41**	0.03	-0.31	-0.06
		21-26°N			
ICOADS (UI^{W})	0.27	**0.40**	0.19	-0.27	0.05
PFEL (UI^{W})	**0.42**	**0.35**	0.04	-0.12	-0.06
NCEP-DOE (UI^{W})	***0.55***	0.31	0.07	-0.10	-0.03
ERA (UI^{W})	***0.46***	0.32	0.14	0.01	-0.08
MERRA (UI^{W})	***0.49***	**0.36**	0.01	-0.22	-0.03
CFSR (UI^{W})	**0.44**	0.22	0.07	0.00	0.19
20CR (UI^{W})	***0.55***	**0.44**	0.15	-0.14	0.02
WASWIND (UI^{W})	**0.39**	0.34	0.15	-0.20	0.15
OISST ($UI^{\Delta SST}$)	-0.11	-0.12	0.11	0.01	-0.02
HADISST ($UI^{\Delta SST}$)	0.01	0.00	0.15	-0.05	-0.01
ICOADS ($UI^{\Delta SST}$)	-0.12	**-0.39**	-0.09	0.19	0.03
AVISO (SSH)	-0.18	-0.27	0.24	0.23	-0.09
ORSA4 (SSH)	-0.25	-0.40	0.05	0.14	-0.29
GODAS (SSH)	-0.12	-0.17	0.11	-0.18	-0.15
SODA (SSH)	0.02	**-0.46**	0.12	0.06	-0.10
GODAS (VWCV)	0.14	**0.36**	-0.27	-0.18	0.26
		26-34°N			
ICOADS (UI^{W})	***0.50***	0.13	-0.05	-0.15	**-0.37**
PFEL (UI^{W})	***0.45***	0.15	0.18	-0.08	-0.16
NCEP-DOE (UI^{W})	***0.55***	0.23	0.21	-0.11	-0.18
ERA (UI^{W})	0.27	0.23	0.05	0.01	***-0.45***
MERRA (UI^{W})	***0.51***	0.21	0.16	-0.06	-0.19
CFSR (UI^{W})	***0.48***	0.15	0.22	0.10	-0.09
20CR (UI^{W})	***0.57***	0.16	0.27	0.05	-0.06
WASWIND (UI^{W})	***0.53***	0.02	0.23	-0.06	-0.23
OISST ($UI^{\Delta SST}$)	-0.32	-0.04	-0.03	-0.05	0.21
HADISST ($UI^{\Delta SST}$)	-0.05	0.18	-0.10	-0.07	-0.02
ICOADS ($UI^{\Delta SST}$)	-0.30	-0.15	0.00	0.01	-0.11
AVISO (SSH)	-0.30	-0.41	-0.03	0.41	-0.04
ORSA4 (SSH)	**-0.50**	-0.38	-0.31	0.01	-0.02
GODAS (SSH)	-0.27	0.10	-0.18	-0.20	0.05
SODA (SSH)	-0.14	-0.14	0.05	-0.17	0.09
GODAS (VWCV)	***0.58***	0.15	0.06	-0.10	0.01

Table F5. As for Table F2, but for autumn (SON).

G. Published Material from this Thesis.

The Digital Object Identifiers to material(s) stemming from this thesis are given below:

C13: doi:10.1002/wea.2155
CH14: doi:10.1002/joc.3710
CHB14: doi:10.1016/j.dsr.2014.01.007
H15: doi:10.1002/joc.4157
CHVJ15: doi:10.1002/gdj3.23 (paper) http://dx.doi.org/10.5281/zenodo.9979 (dataset)